Dissertation
submitted to the
Combined Faculties for the Natural Sciences and for Mathematics
of the Ruperto-Carola University of Heidelberg, Germany
for the degree of
Doctor of Natural Sciences

Put forward by
Sanam Noreen Vardag
Born in Regensburg, Germany
Date of oral examination: 04. May 2016

Greenhouse gas measurements with the Fourier Transform Infrared analyser – Our tool to study greenhouse gas fluxes

Referees: **Dr. Ingeborg Levin**
Prof. Dr. Werner Aeschbach

Abstract

This cumulative thesis assesses several ways of improving greenhouse gas flux estimates and consists of four main parts. Firstly, within the framework of a measurement campaign, CO_2, CH_4 and N_2O measurements of different instruments and between different measurement networks were compared and differences of 0.14 ppm (CO_2), 0.04 ppb (CH_4) and 0.37 ppb (N_2O) were found, respectively. The main result is that N_2O differences could partly be explained by a difference between the *WMO N_2O X2006a* reference scale and the *SIO-1998* scale. Secondly, $^{18}O(CO_2)$ retrievals were implemented in a Fourier Transform Infrared spectrometer, allowing for continuous CO_2 gross fluxes estimates. The measurements are compatible to mass spectrometer measurements and have a precision of about 0.3 ‰, which suffices to detect $\delta^{18}O(CO_2)$ variations in Heidelberg. Thirdly, in a model study, possible tracers for estimating continuous anthropogenic CO_2 were assessed. $\delta^{13}C(CO_2)$ and CO are well suited for this, but only in urban areas and if the isotopic signature and the emission ratio CO/CO_2 of the mean anthropogenic CO_2 source are known. Finally, a method to estimate the hourly $\delta^{13}C(CO_2)$ source signature accurately (median: 0.2 ‰) and precisely (interquartile range: 1.2 ‰) is proposed. Applying the method to Heidelberg data, a seasonal cycle is observed. It allows estimation of the isotopic signature of one source, but only if the contributions from other sources are small.

Zusammenfassung

Diese kumulative Dissertation untersucht verschiedene Ansätze zur verbesserten Abschätzung von kontinentalen Treibhausgasflüssen. Zuerst wurden im Rahmen einer Messkampagne CO_2-, CH_4- und N_2O- Messungen verschiedener Instrumente und Messnetzwerke verglichen und Unterschiede von 0.14 ppm (CO_2), 0.04 ppb (CH_4) und 0.37 ppb (N_2O) gefunden. Das zentrale Ergebnis ist, dass sich die N_2O-Unterschiede teilweise durch eine Differenz der *WMO N_2O X2006a* Referenzskala und der *SIO-1998* Referenzskala erklären lassen. Zweitens wurde eine $^{18}O(CO_2)$ Analyse in die Auswertung des Fourier Transform Infrarot Spektrometers implementiert. Diese Messungen ebnen den Weg für eine kontinuierlichen Abschätzung von CO_2 Bruttoflüssen. Sie sind kompatibel zu massenspektrometerischen Messungen und haben eine Präzision von ca. 0.3 ‰, was ausreicht um $\delta^{18}O(CO_2)$ Variationen in Heidelberg zu detektieren. Drittens wurden in einer Modellstudie mögliche Hilfstracer für die kontinuierliche Bestimmung des anthropogenen CO_2-Anteils untersucht. Dabei zeigt sich, dass $\delta^{13}C(CO_2)$ und CO geeignet sind, allerdings nur in städtischen Gebieten und sofern die isotopische Signatur und das CO/CO_2 Emissionsverhältnis der mittleren anthropogenen CO_2 Quelle bekannt ist. Schließlich wird eine Methode zur genauen (Median: 0.2 ‰) und präzisen (Interquartilbereich: 1.2 ‰) Bestimmung der stündlichen mittleren $\delta^{13}C(CO_2)$ Quellsignatur vorgestellt. Bei Anwendung der Methode auf Heidelberger Daten zeigt sich ein saisonaler Verlauf. Dieser ermöglicht eine Abschätzung der isotopischen Signatur einer Quelle, aber nur wenn andere Quellbeiträge gering sind.

Contents

Part 1

Introduction

1.1 Changes in the climate system and their causes

1.1.1 Increase of greenhouse gas concentration

In December 2015, 195 nations met in Paris, France, to negotiate a global agreement on the limitation of climate change. They agreed to the goal to hold the global temperature increase below 2 °C above pre-industrial times and therefore to restrict the emissions of man-made greenhouse gases significantly from 2020 to 2100 (United Framework Convention on Climate Change UNFCCC, 2015).

The scientific basis for the decisions reached in the "Paris agreement", is a strong consensus among climate scientists that the main reason for recent climate change is an increase of greenhouse gas concentration in the atmosphere due to man's act (Intergovernmental Panel of Climate Change IPCC, 2014a). Since the start of the Industrial Revolution, the atmospheric concentration of carbon dioxide (CO_2) increased by about 40%, of methane (CH_4) by about 150% and of nitrous oxide (N_2O) by about 20% relative to 1750 (IPCC, 2014a, see Fig. 1.1). The associated additional greenhouse effect contributed for the most part to global surface warming between 1880 and 2012 (IPCC, 2014a). In turn, warming has led to changes of the climate system (e.g. global mean sea level rise, reduction of the Arctic Sea Ice extent, see Sect. 1.1.2) and will continue to pose a great challenge for future generations (IPCC, 2014a).

1.1.2 Changes in the climate system

Many of the changes of the climate system since the mid-20th century are unprecedented over decades to millenia. From 1880 to 2012 the atmosphere warmed by about 0.85 [90% uncertainty intervals: 0.65 to 1.06] °C (entire paragraph based on IPCC, 2014a). The heat content of the upper ocean (0-700 m) increased from 1971 to 2010 by about 137 [120-154] $\cdot 10^{12}$ W. Glaciers as well as Greenland and Antarctic snow and sea ice sheets have decreased. The rate of decrease of Arctic sea-ice extend was about 3.5 to 4.1 % per decade (since 1979). The mean global sea level rose by 0.19 [0.17 to 0.21] cm within the last century. Further, global precipitation patterns as well as the distribution of ocean surface salinity have changed. Additional oceanic uptake of CO_2 has shifted the chemical balance of dissolved CO_2, bicarbonate and carbonate in the ocean towards a lower pH value, leading to ocean acidification.

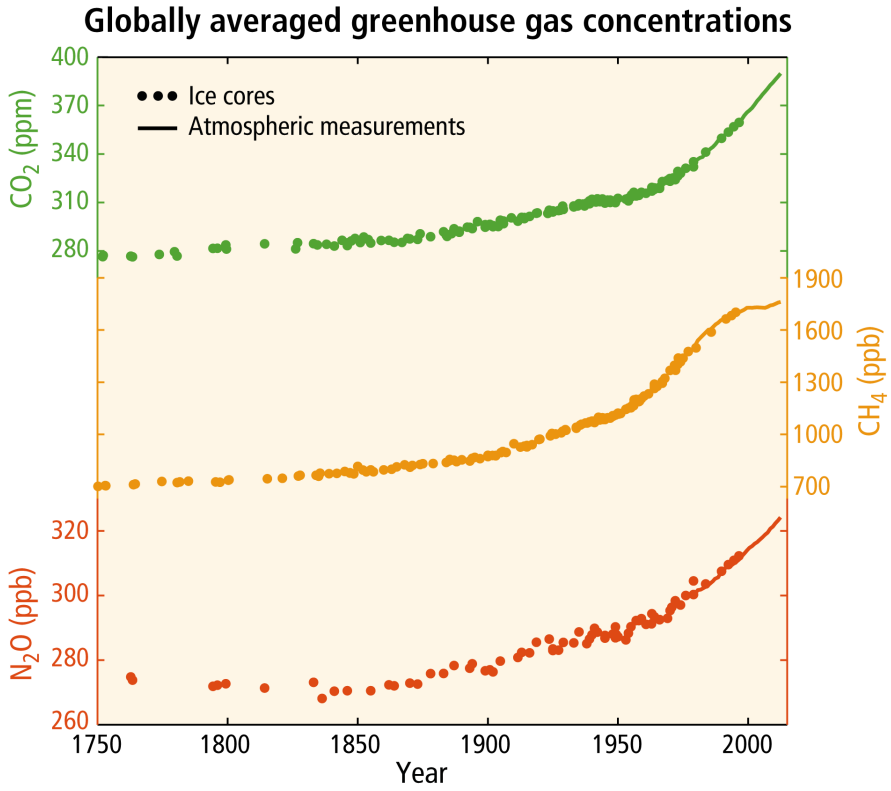

Fig. 1.1: Observed changes in atmospheric greenhouse gas concentrations. Atmospheric concentrations of carbon dioxide (CO_2, green), methane (CH_4, orange), and nitrous oxide (N_2O, red). Data from ice cores (symbols) and direct atmospheric measurements (lines) are overlaid. WGI 2.2, 6.2, 6.3, Figure 6.11, IPCC (2014a).

The pursued emission of anthropogenic greenhouse gases will lead to further warming of the climate system associated with further changes in the climate system (IPCC, 2014a). In order to limit the impact of climate change a limitation of greenhouse gas emissions is required. Within the framework of the IPCC (2014a), a range of realistic emission mitigation scenarios are assessed. In all emission mitigation scenarios the global surface temperature is expected to further rise at least until the mid of the 21st century, but the rate of increase depends strongly on the emission mitigation scenario. Associated changes of the climate system also depend on the underlying emission mitigation scenario and are often associated with large uncertainties. Especially feedback processes contribute to the uncertainty as they may amplify or diminish the effect of enhanced greenhouse gas emissions on climate change, but are subject of uncertainty themselves (IPCC, 2014a). One example for a negative feedback process is the so-called "CO_2 fertilization", which describes the increased CO_2 sequestration of the biosphere

as response to higher atmospheric CO_2 concentrations, thus counteracting rising atmospheric CO_2 levels. A variety of studies could, on average, confirm the CO_2 fertilization effect, but the study results are variable and also depend on other factors such as the availability of nutrients or organic substrate and on the time scale investigated (e.g. Cramer et al., 2001; Oren et al., 2001; Norby and Iversen, 2006; Körner et al., 2005). This highlights the complexity of the climate system.

Despite large uncertainties, the IPCC (2014a) states that is likely that observed changes of the climate system will intensify within the 21st century under all assessed emission mitigation scenarios, leading to e.g. more frequent extreme weather events, global ocean warming, ocean acidification, increased rate of sea level rise, decrease of the Arctic sea ice extend and of the permafrost extent at high northern latitudes (IPCC, 2014a). The risks due to a changing climate are various and include threat of food security, biodiversity reduction, local scarcity of water and may lead to displacement of people. Emission mitigation strategies and adaptation plans are already being developed in many regions, but are highly sensitive to the quantification and uncertainty assessment of climate change as response to greenhouse gas emissions (IPCC, 2014b).

Improving estimates of the impact of greenhouse gas emissions on climate change and assessing their uncertainties requires a fundamental understanding of the greenhouse gas cycles and their response to changes in enhanced greenhouse gas concentration, temperature, moisture, precipitation, salinity etc., which can then be fed to global carbon models.

1.2 Global greenhouse gas cycles

The atmosphere serves as integrating volume of all positive and negative greenhouse gas fluxes from different greenhouse gas reservoirs. In equilibrium, when the atmospheric concentration and the planetary boundary layer height are constant, positive and negative gross fluxes into and out of the atmosphere balance each other. Any increase of atmospheric greenhouse gas concentration must be due to an enhanced flux into the atmosphere or a reduced flux out of the atmosphere (assuming a constant planetary boundary layer height).

The focus of this thesis lies on assessing possible improvement of CO_2 flux estimates. Therefore, CO_2 is especially considered in this introduction. Nevertheless, as CH_4 and

N_2O concentrations are considered in this thesis as well, they are also introduced in the following.

CO_2

The ocean is the largest carbon reservoir with an inventory of mobile carbon of about 38000 petagram of Carbon (PgC=10^{15} gC) followed by the biosphere with a size of about 2500 PgC (see Fig. 1.2). The carbon cycle of the atmosphere nowadays holds about 800 PgC. In equilibrium, the net global biospheric uptake of CO_2 via photosynthesis of about 120 PgC per year is about balanced by the biogenic (autotrophic and heterotrophic) respiration of CO_2 while the ocean takes up and releases about 80 PgC CO_2 per year. However, emission of fossil fuel CO_2 as well as land use change disturb this equilibrium. In the last decade, about 9 PgC were emitted into the atmosphere per year from fossil fuel burning and additional ca. 0.9 PgC by land use change (Le Quéré et al., 2015). About half of it (4.4 PgC) remained in the atmosphere and the other part was taken up to about equal parts by the biosphere (3.0 PgC) and the ocean (2.6 PgC), corresponding to a net flux into the biosphere and the ocean. Note that CO_2 is the most important anthropogenic greenhouse gas as it is responsible for the largest change in radiative forcing (ca. 1.68 W m^{-2} on an emission basis since 1750, IPCC, 2013).

CH_4

Methane (CH_4) is the second most important anthropogenic greenhouse gas with additional radiative forcing of about 0.97 W m^{-2} (IPCC, 2013). Major natural CH_4 sources are wetlands, freshwater, terrestrial and marine seepage, mud volcanoes, wild animals, termites, ocean methane hydrates and geothermal and volcanic areas. Anthropogenic sources account for about 50-65 % of the total emissions and include oil and gas systems, ruminant livestock, rice cultivation, landfills, waste treatment as well as fossil fuel and biomass burning. OH radicals in the troposphere are the main sink of CH_4, followed by stratospheric OH and chlorine as well as oxidation in soils (IPCC, 2013).

N_2O

Nitrous oxide (N_2O) is the third most important anthropogenic greenhouse gas (additional radiative forcing ca. 0.17 W m^{-2}) after CO_2 and CH_4. Naturally, N_2O is

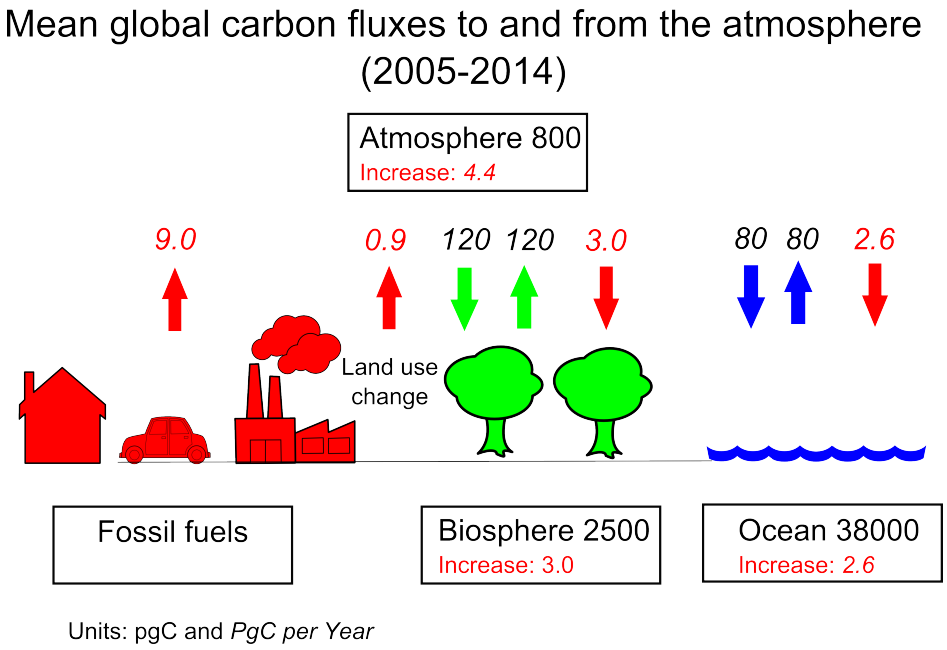

Fig. 1.2: The global carbon cycle from 2002 to 2012. Flux and inventory numbers are taken from the Le Quéré et al. (2015). The uncertainties of these fluxes are in the order of 5-30 %.

mainly emitted from soils and from the oceans during microbial nitrification and denitrification. The main sink of N_2O is dissociation and photo-oxidation of N_2O in the stratosphere. The balance of the natural nitrogen cycle is disturbed, mainly by intensification of the application of fertilizers used in agriculture, but also because of fossil fuel combustion, industrial processes and waste water management. Anthropogenic N_2O production is spatially and temporally highly variable. The concentration of N_2O in the atmosphere is about a factor 1000 smaller than that of CO_2, but due to the long atmospheric life-time of N_2O of about 114 years (IPCC, 2013), it is an important greenhouse gas. As stratospheric N_2O destruction can form NO radicals (during photo-oxidation), N_2O also plays an important role in destructing the ozone layer (IPCC, 2013).

1.3 Why study the greenhouse gas cycles in-depth?

In order to improve projections on the consequences of enhanced greenhouse gas emissions (Sect. 1.1.2), it is necessary to quantify the various fluxes of the greenhouse

gas cycles individually as the consequences differ depending on where the gases are currently stored and on carbon cycle feedbacks of the individual fluxes.

For example, CO_2 remaining in the atmosphere contributes to the additional greenhouse effect, but additional CO_2 in the ocean leads to ocean acidification and consequently threatens marine ecosystems (Roedel and Wagner, 2000; IPCC, 2014a). Also, depending on the mean residence time of carbon in the different reservoirs, the CO_2, which was taken up by a reservoir, will be released back into the atmosphere earlier or later. For carbon stored in biogenic ecosystems the mean turnover time is about 1-100 years, whereas for the deep sea it may be as large as a few thousand years (IPCC, 2013). Therefore, CO_2 stored in the biosphere will in average be released to the atmosphere much earlier than CO_2 stored in the ocean and therefore will contribute to a change in radiative forcing earlier.

Next, the gross fluxes of the ocean and biosphere respond differently to changes in the climate system. For example, in 2003, an extreme heat wave over Europe led to a net increase of biospheric CO_2 emissions over the continent due to a decrease of gross primary production as response to heat and drought (Ciais et al., 2005). Therefore, in order to predict the consequences of enhanced greenhouse gas emissions and of climate change, it is vital to quantify the different gross fluxes independently.

Further, to study the response of the biosphere to climatic variations, the change of greenhouse gas sources and sinks need to be attributed to specific changes in plant species, regional temperatures, regional droughts, regional changes in ocean stratification etc.. Therefore, climate scientist are not only interested in the global budget of greenhouse gas fluxes, but the spatial distribution of greenhouse gas fluxes is of interest as well. Also, monitoring of emissions of anthropogenic CO_2 and other long-lived greenhouse gases over specified regions is politically relevant (see Sect. 1.1.1) and it is therefore desirable to attribute fuel CO_2 emissions to specific regions and nations.

In summary, it is not sufficient to quantify total greenhouse gas fluxes to and from the atmosphere, but additionally a separation of greenhouse gas net fluxes to and from different reservoirs and between gross fluxes (e.g. photosynthesis and respiration) is desirable on high spatial resolution.

1.4 How to estimate greenhouse gas fluxes

Different approaches to estimate greenhouse gas fluxes over a specified region exist. Here, the "bottom-up" approach and the "top-down" approach are briefly introduced.

1.4.1 Bottom-up approach

In bottom-up approaches, greenhouse gas fluxes of ecosystems are measured in the field at one point e.g. via eddy-covariance measurements (Running et al., 1999; Canadell et al., 2000) and/or flux chamber measurements (e.g. Norman et al., 1997). The uncertainties of these point measurements are rather small and typically less than 20%, but the spatial representativeness of these measurements is typically less than 1 km^2 as the biosphere is spatially heterogeneous (Schulze et al., 2009; illustrated as black square in Fig. 1.3). Further, the biospheric fluxes vary with changing climatic parameters calling for repeated measurements under different climatic conditions. Typically one is interested in estimating the biopsheric fluxes on a regional to continental scale. In this case, the point measurements of biospheric fluxes need to be scaled up to the larger region of interest using economic data, e.g. on agricultural and forest fields, ecosystem models and airborne observations of carbon stocks, which all exhibit large uncertainties.

Information on anthropogenic greenhouse gas fluxes and biomass burning usually stem from national energy data, data on agricultural activities, fossil fuel suppliers, emission data from individual facilities etc.. They are summarized in emission inventories. When distributing the total national emissions correctly in space and time, infrastructure data such as the distribution of population, which is correlated to the emissions of domestic heating or the distribution of streets, which is correlated to traffic emissions, are utilized. However, the correlation is not perfect, varies in time and is associated with uncertainties. Further, self-reported emissions (e.g. by individual facilities) are not independent from the emitters' interests and may therefore be biased (Ciais et al., 2015). Altogether, an immense effort is necessary to correctly distribute and extrapolate the anthropogenic emissions correctly. Therefore, biases of up to 70-100 % for highly resolved bottom-up emission inventories (0.1° x 0.1°) have been detected (Wang et al., 2013).

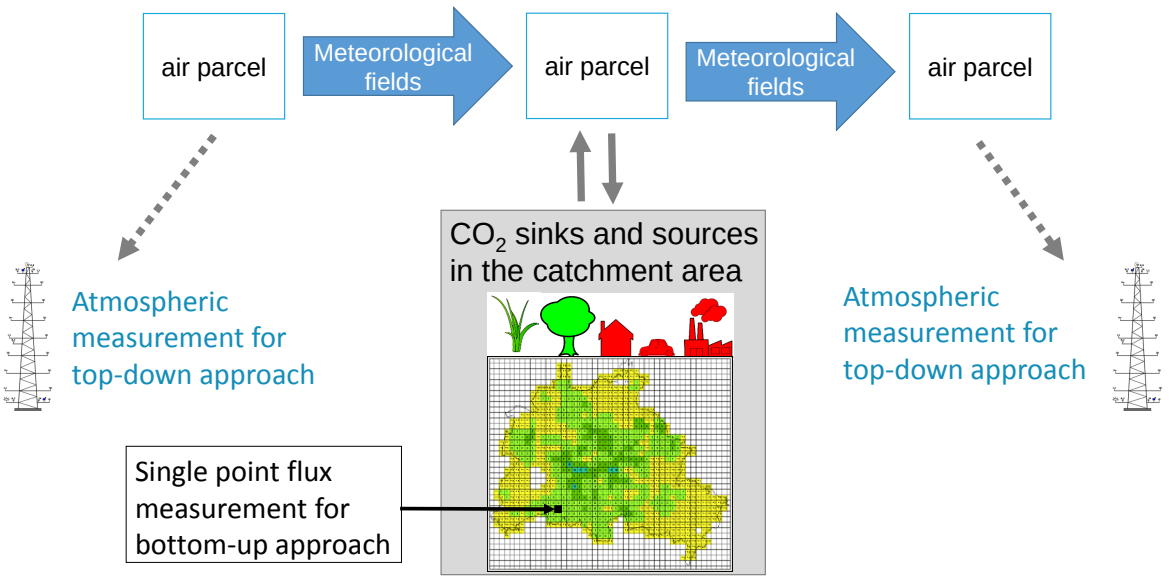

Fig. 1.3: Sketch of top-down and bottom-up approach using CO_2 as an example. Bottom-up approach: A single point measurement of e.g. a biospheric flux (black square) can be performed accurately at one location, but may not be representative of the entire biosphere in the region of interest. Top-down approach: Atmospheric CO_2 is influenced by all sources and sinks in the catchment area and is thus, more representative of a large region, but requires accurate meteorological trajectories in order to correctly trace the path of the air parcel.

1.4.2 Top-down approach

In top-down approaches greenhouse gas measurements in the "integrator" atmosphere are used to constrain greenhouse gas fluxes using an atmospheric inversion framework over a specified region. Emission estimates are optimized by relating the measured concentration to emissions in the catchment area of the measurement site using time-inverted meteorological fields (wind speed, wind direction, height of the planetary boundary layer etc., see Fig. 1.3). The measurements are typically performed at high towers, so that the measurements are representative of large spatial areas.

If the individual measurement stations are part of a regional network, the greenhouse gas measurements can be jointly inverted and fluxes can be estimated over larger areas such as Europe as a whole (Lauvaux et al., 2008; Broquet et al., 2013). For example, the ICOS (Integrated Carbon Observation System) network was launched in September

2015 and, in its final configuration, should provide greenhouse gas measurements from about 80 European measurement stations, distributed over the continent.

However, the derived inversion fluxes for e.g. the European carbon balance typically have uncertainties of currently about 50% (Schulze et al., 2009). The top-down flux accuracy is limited by the uncertainty in the atmospheric transport and in particular by the planetary boundary layer height, in which the greenhouse gases accumulate (Bastos et al., 2016), but also by measurement accuracy and precision of the greenhouse gas measurements. Finally, the greenhouse gas measurements are sometimes influenced by local sinks and sources and are thus not representative of a larger area (Gerbig et al., 2009). An additional difficulty of the top-down approach is that often only total net fluxes are derived, which are the sum of biogenic, oceanic and anthropogenic sources and sinks, which accumulate in the atmosphere. They are difficult to disentangle correctly especially as biogenic and anthropogenic emissions are often co-located (e.g. for CO_2). This means that an increase of CO_2 in the atmosphere can be attributed to emissions in a spatial region via inverse models, but it cannot be uniquely attributed to anthropogenic emissions, enhanced ecosystem respiration or reduced photosynthesis. In order to separate between anthropogenic and biogenic sources, usually the anthropogenic emissions are taken as given from emission inventories (bottom-up) and are then subtracted from total top-down fluxes to obtain land ecosystem fluxes. This approach of using bottom-up information is then still called top-down approach, but actually contains a mixed information from emission inventories (bottom-up) and from the atmospheric inversion (top-down). In these cases, estimates of land ecosystem fluxes incorporate the additional uncertainty of the anthropogenic emissions. An improvement of anthropogenic emission inventories will therefore also lead to an improvement of the top-down ecosystem fluxes. If it were possible to separate biogenic and anthropogenic contributions correctly without using bottom-up emission inventories (see Sect. 1.5.5 for separation of CO_2 contributions), their fluxes could be derived and studied independently from bottom-up information.

1.4.3 Comparing top-down and bottom-up approaches

Fig. 1.4 gives an example from Schulze et al. (2009), which nicely illustrates the top-down approach. By time-inverting meteorological fields, the origin of the enhanced atmospheric concentration measured at different stations can be traced back to a specific region. These total inversion fluxes are plotted in Fig. 1.4a for CO_2 with their

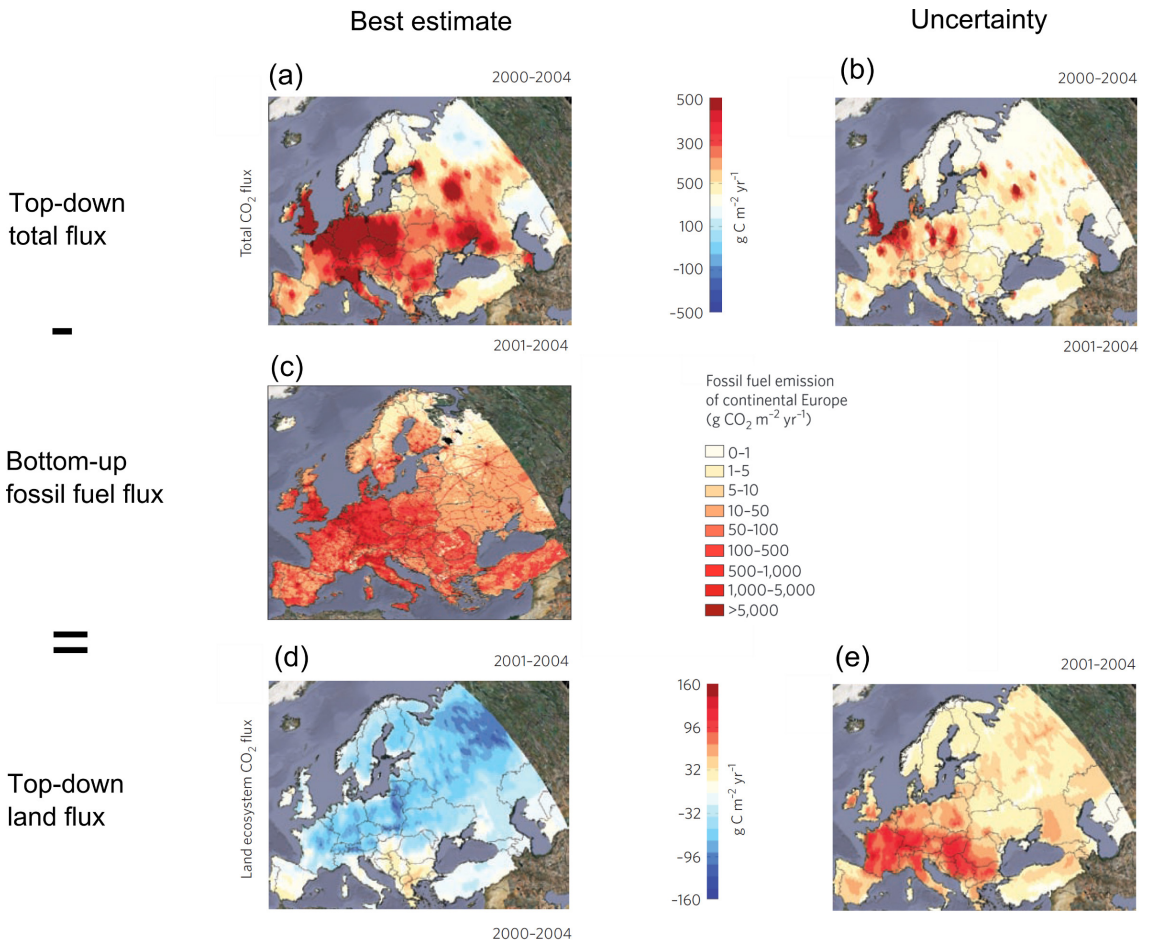

Fig. 1.4: Example of the principle scheme of top-down approach. The figure is adapted and modified from Schulze et al. (2009)

respective uncertainty (Fig. 1.4b). By subtracting the bottom-up emission inventory of anthropogenic fluxes (Fig. 1.4c) the ecosystem net flux can be obtained (Fig. 1.4d). Using this top-down approach, Schulze et al. (2009) found that, in total, the European ecosystem acts as carbon sink (ca. -0.31 $\pm$ 0.3 PgC yr^{-1}). However, the uncertainties (Fig. 1.4e) of the net land ecosystem fluxes (standard deviation of several model runs within a Monte-Carlo simulation) are of the same magnitude as the signal itself.

For comparison, Schulze et al. (2009) additionally followed the bottom-up approach for the estimation of biospheric fluxes in Europe and found a net carbon sink of -0.24 $\pm$ 0.5 PgC yr^{-1}, which is in good agreement to the top-down approach, but has an uncertainty of about 200 %. The uncertainty is mainly due to the uncertainty in up-scaling point flux measurements. Schulze et al. (2009) found similar results for N_2O and CH_4, where top-down and bottom-up approaches agreed only because of

large uncertainties of both approaches of more than 50 %. The large uncertainty of these approaches are unsatisfying, as they prevent a clear process understanding of the ecosystems. For a quantitative understanding of greenhouse gas cycles and prediction of future ecosystem responses, it is necessary to reduce the uncertainties of bottom-up, as well as of top-down approaches and reconcile these two approaches.

1.5 How to improve greenhouse gas flux estimates

Large uncertainties of flux estimates prevent a precise quantification of greenhouse gas cycles. The reason for the large uncertainties are manifold. Limiting factors of the top-down approach in estimating the ecosystem net fluxes are quality of the greenhouse gas measurements, difficulties in modeling the transport correctly and inaccuracies of anthropogenic emission inventories. Furthermore, the approach is limited by the sparse density of the measurement network and the low temporal resolution of measurements. These points are elaborated in more detail in the following.

1.5.1 Best practice for high-quality greenhouse gas measurements

In the past, model studies using *in-situ* data sets have provided estimates of regional, continental or global sinks and sources of greenhouse gases. Some studies have been supported by remote-sensing estimates of greenhouse gases (e.g. satellite measurements), which offer a dense global measurement of greenhouse gases. But, these remote-sensing techniques need still to be validated and corrected using accurate and precise *in-situ* measurements on e.g. air crafts (GGMT, 2013). Therefore precise *in-situ* measurements form the basis of top-down flux estimates. A high precision is vital since it maximizes the signal to noise ratio of an atmospheric measurement and thus supports unambiguous interpretation of greenhouse gas variations. Accuracy of the measurements is essential for bias-free flux estimates. Finally, different data records need to be compatible to each other. Various greenhouse gas measurements are performed using different instruments, measurement techniques and sometimes different calibration scales. Later, these measurements are used together in a top-down inversion to obtain a map of relevant net fluxes (see Fig. 1.4). However, biases between different instruments, stations and scales are directly propagated into derived surface fluxes (Masarie et al., 2011). In order to prevent large biases in surface fluxes from top-down approaches, the World Meteorological Organization (WMO) discussed and specified uniquely for all greenhouse

gases so-called "Inter-Laboratory Compatibility" (ILC) goals (GGMT, 2013). ILC goals state the degree of compatibility of concentration measurements, which needs to be met for instructive derivation of greenhouse gas fluxes from top-down approaches. For example, the European N_2O gradient caused by continental N_2O emissions is smaller than 0.5 ppb. Therefore, for N_2O measurements, the WMO has suggested that the laboratories and networks should agree within 0.1 ppb, so that quantitative information of N_2O fluxes can at all be achieved from joint N_2O measurements.

To optimize the quality of the top-down approaches, the quality of the data needs to be carefully and routinely monitored in terms of precision, accuracy and compatibility. The intermediate measurement precision is often monitored by replicate daily measurements of a constant cylinder gas under the same measurement conditions over time periods of years (see appendix A for intermediate measurement precision of the Fourier Transform Infrared (FTIR) analyzer). The accuracy of a measurement can only be assessed by comparing the measurement result to a known reference value (see appendix B for a list of vocabulary of metrology). For this purpose, cylinder gases are calibrated by the WMO Central Calibration Laboratory in Boulder, USA. The cylinder gas measurement results from a specific instrument can then be compared to the calibration reference value to obtain a measure for the accuracy of the instrument. Finally, comparisons between greenhouse gas measurements of different instruments are necessary to check and quantify the compatibility between instruments in different laboratories. This is important as biases between different laboratories and the uncertainty of the biases should be taken into account in top-down approaches (Thompson et al., 2014).

A rather straight-forward way of comparing different instruments is taking co-located flask (glass container) samples, analyzing these flasks in different laboratories and comparing their results. However, the intake line of an instrument including drying unit and pumps for a flask measurement is different from that of ambient air measurements. Therefore, problems during ambient air measurements due to the intake line will not be observed during flask measurements. Furthermore, the reasons of discrepancies cannot be followed up by a single flask measurement. This is however necessary to eliminate the biases. Finally, only one concentration can be compared with one flask. The flask comparison therefore does not span the entire range of ambient air concentrations. Another more comprehensive way of comparing instruments is to transport one instrument, which is well characterized with respect to accuracy and precision, to a station, install an independent ambient air intake line and perform co-located continuous mea-

surements of ambient air over a time period of weeks to months. The main advantage of this "travelling instrument approach" is that ambient air greenhouse gas measurements are compared under regular sampling conditions over a long period (Hammer et al., 2013a). Combined with tests of the sample intake line and with cylinder cross comparison, it is usually possible to attribute a reason to any discrepancy between measurements. It is therefore the most comprehensive way of comparing greenhouse gas measurements to each other, but it is the most labor-intensive approach as well. The WMO has recognized that for a comprehensive comparison of atmospheric measurements, a "travelling instrument approach" is the most appropriate approach and encourages its conduction (GGMT, 2013).

1.5.2 Model transport

When calculating surface fluxes from greenhouse gas measurements using the top-down approach, model advection and vertical mixing significantly influence the estimated inversion fluxes. Only if changes in model transport (such as mixing layer height, vertical winds etc.) can be determined accurately, the variability in concentration ratios can correctly be translated into a change in surface fluxes (Gerbig et al., 2009). At present, errors in model transport are often still the largest source of error in top-down approaches (Lin and Gerbig, 2005). Lin and Gerbig (2005) pointed out that horizontal transport accounts for up to 5 ppm error of the modelled CO_2 in summer, which largely exceeds measurement uncertainties. Gerbig et al. (2008) showed that also vertical transport uncertainties introduce large errors into the CO_2 fluxes, which may be on the order of 40-100 %, suggesting that the model transport is not accurate enough for reliable inversions of concentration. Improving model transport is thus necessary for the scientific community to advance with flux estimates based on the top-down approach. For example, Gerbig et al. (2009) suggested using Lidar (Light detection and ranging) instruments to routinely measure the atmospheric mixing height at a station, but they speculate that these measurements will not be routinely implemented within the next decade.

However, one should keep in mind that the atmospheric measurements of greenhouse gases can only be captured and measured now, whereas the model transport can be improved retrospectively. Therefore, a high accuracy, precision and compatibility of greenhouse gas measurements is vital, even though model transport errors often dom-

inate the flux uncertainties. Future improvement of model transport can lead to improved results of contemporary flux estimates.

1.5.3 "Smart" network design

In regions with a poor coverage of measurement sites large biases can be introduced into the inversion fluxes (Feng et al., 2016). A "smart" allocation of measurement stations within a measurement network is vital to determine the greenhouse gas budget over a specified region (Gerbig et al., 2009). The stations should be distributed such that they represent the entire region of interest. Therefore, the stations should be distributed over the entire specified region and each individual station should be representative of a large spatial region. In the ICOS network, it is recommended that stations are apart by about 300 km (ICOS, 2015). Also, as the atmospheric advection needs to be captured correctly in the model, the terrain of the measurement site should be homogenous and non-complex. Finally, the signal at the station must be large enough that the signal to noise ratio of the instruments is sufficient to detect fluxes.

1.5.4 Continuous measurements

In order to improve the understanding of greenhouse gas fluxes, a high temporal resolution of measurements is advantageous. The additional benefit of continuous measurements (in contrary to sporadic measurements) is two-fold. Firstly, the observation is always required at the same temporal resolution as the variation of the emission patterns, which is to be monitored and studied. Therefore, if one is e.g. interested in the diurnal pattern of greenhouse gas emissions in the catchment area of a measurement station, one also needs to measure the concentration on a sub-diurnal (e.g. hourly) basis. Another example is the observation of ecosystem responses. The ecosystem responds to changes in e.g. temperature, precipitation, solar irradiation etc., which vary on typical time scales of minutes to hours. To study the response of ecosystems to changes in these parameters, a high temporal resolution of greenhouse gas measurements is vital. Secondly, a continuous measurement of greenhouse gases, allows monitoring emissions coming from different wind directions if the wind direction changes quickly. This allows capturing the emissions from different catchment areas and therefore provides additional information on the spatial distribution of fluxes when used

in top-down approaches. So far, the temporal resolution of the greenhouse gas measurements was typically higher than that of inventories and meteorology and with that sufficient for top-down approaches, but in the future the temporal resolution of top-down approaches may further increase.

Gas chromatographs (GCs) have been used since the mid of the last century to measure gases such as CO_2, CO, CH_4, N_2O, SF_6 and H_2 and have provided unique data sets of atmospheric concentrations. GCs are able to measure the (dried) ambient air directly as well as flask samples of captured air. However, in the past, isotope measurements have not been measured routinely on high temporal resolution, but could provide additional information on the composition of the e.g. CO_2 signal (as will be discussed in Sect. 1.7.5). Isotope measurements on flasks or cylinders have been performed using isotope ratio mass spectrometry (IRMS), but only a limited number of flasks can be measured per day. The maintenance of GC and IRMS systems is very labor-intensive. Within the last decade, new optical instruments have been developed, which measure the same trace gases (and often also the trace gases' isotopes) as GCs or IRMSs with similar precision, but higher temporal resolution (Esler et al., 2000; Tuzson et al., 2011; Hammer et al., 2013a; Vogel et al., 2013). Maintaining these optical instruments is generally less labor-intensive, but nevertheless requires diligent and careful assessment and quality control. The emerge of many new instruments will contribute also to a denser network of continuous measurements, which will facilitate the study of ecosystem processes and improve top-down model approaches, if the quality of data is sufficient (Lauvaux et al., 2008; Broquet et al., 2013).

1.5.5 Separation between different CO_2 contributions

As explained in Sect. 1.3, it is not sufficient to estimate net fluxes of CO_2, but it is further necessary to separate individual CO_2 flux components to understand ecosystems behavior in response to climatic conditions (Ciais et al., 2005; Bastos et al., 2016). Within the top-down approach, this is a complicated task as natural and anthropogenic CO_2 fluxes are often heterogeneous, co-located and vary on time scales of hours. For Central Europe, oceanic fluxes are negligible, but a separation of ecosystem respiration, photosynthesis and anthropogenic emissions is desirable. Emission inventories summarize anthropogenic fluxes, but the fluxes often exhibit large uncertainties and biases (e.g. Wang et al., 2013). An independent measurement-based separation between anthropogenic and biogenic CO_2 contributions is therefore desirable. Differ-

ent tracers can be used to separate between contributions from different CO_2 sources and are introduced here briefly. The tracers are explained in more detail in the third publication (Sect. 2.3).

$^{14}C(CO_2)$

At present, measurements of $^{14}C(CO_2)$ are often used to distinguish between (fossil) anthropogenic and biogenic CO_2. ^{14}C is produced mainly in the upper troposphere and lower stratosphere via interaction of cosmic rays with nitrogen. It is then oxidized to $^{14}C(CO_2)$ and enters the living biosphere via photosynthesis. As $^{14}C(CO_2)$ is radioactive, it decays with a life time of about 5700 years (Roberts and Southon, 2007). In old materials, such as fossil fuels, all $^{14}C(CO_2)$ has decayed as the life-time of ^{14}C is much smaller than the age of the materials. Fossil fuel emissions therefore deplete the atmosphere in its $^{14}C/^{12}C$ ratio. By measuring the degree of depletion, the fossil fuel CO_2 contribution in the atmosphere can be estimated (Levin et al., 2003; Miller et al., 2012; Turnbull et al., 2015).

Besides its radioactive isotopologue $^{14}C(CO_2)$, CO_2 has various stable isotopologues, e.g. $^{12}C(CO_2)$ ($=^{12}C^{16}O^{16}O$) , $^{13}C(CO_2)$ ($=^{13}C^{16}O^{16}O$) and $^{18}O(CO_2)$ ($=^{12}C^{18}O^{16}O$). Isotopologues are molecules that differ only in their isotopic composition. In the clean atmosphere, about 98.4 % of all CO_2 isotopolgues are $^{12}C(CO_2)$, ca. 1.1 % are $^{13}C(CO_2)$, ca. 0.4 % are $^{18}O(CO_2)$ and only about 10^{-10} % are $^{14}C(CO_2)$ (Daansgard, 1953; Keeling, 1960). Due to similar chemical structures, but different masses, fractionation processes occur and shift the ratio of the isotopologues dependent on the chemical and physical processes, which the molecules underwent. The relative proportion of the isotopes in a sample (e.g. $^{13}R_S = {}^{13}C/{}^{12}C$ in the sample) is normally given relative to the proportion of isotopes in a standard material ($^{13}R_{Std} = {}^{13}C/{}^{12}C$ of the standard), following the δ-notation:

$$\delta^{13}\mathsf{C} = (^{13}\mathsf{R_S}/^{13}\mathsf{R_{Std}} - 1) \cdot 1000 \tag{1.1}$$

The values are then given in permil. It can be written analogously for e.g. $\delta^{18}O$. For $^{14}C(CO_2)$, fractionation as well as the radioactive decay influence the isotopologue ratio. This needs to be taken into account and therefore the depletion in ^{14}C is normally reported in the Δ-notation. The Δ-notation is a fractionation corrected measure for the activity of a sample relative to a standard activity, which is 95% of the reference

oxalic acid. It is assumed that the fractionation of ^{14}C is approximately twice as large as that of ^{13}C. Details can be found in Stuiver and Polach (1977).

$$\Delta^{14}C = \left(\frac{^{14}A_{Sample}}{^{14}A_{Standard}} \cdot (1 - 2 \cdot (25 + \delta^{13}C)) - 1 \right) \cdot 1000 \tag{1.2}$$

Again, the values are then given in permil. Nowadays, the radiocarbon content can be measured by measuring its radioactivity (conventional counting) or by directly counting the radiocarbon atoms in the sample (accelerator mass spectrometry). Both measurements are labor-intensive and presently still prohibit a high temporal resolution due to the duration of sample preparation and/or sample measurement.

The stable isotopologues of CO_2

Also the stable isotopic composition of CO_2 could potentially be used to disentangle biospheric and anthropogenic CO_2 contributions continuously at continental stations, as different CO_2 reservoirs exhibit different isotopic compositions. Many optical instruments are able to measure $\delta^{13}C(CO_2)$ (and sometimes even $\delta^{18}O(CO_2)$) continuously (Esler et al., 2000; Tuzson et al., 2011; Hammer et al., 2013a; Vogel et al., 2013, Vardag et al., 2015a).

$\delta^{13}C(CO_2)$

During photosynthesis, plants take up CO_2, but strongly discriminate against ^{13}C. This leads to a strong depletion of the $^{13}C/^{12}C$ ratio in plant tissue relative to the atmospheric $^{13}C/^{12}C$ ratio. Only weak discrimination is observed during respiration and therefore the respiratory fluxes carry a depleted $^{13}C/^{12}C$ signal similar to that of the plants (Ghashghaie and Badeck, 2014). The degree of depletion relative to atmospheric CO_2 ($\delta^{13}CO_2 \approx$ -8 ‰ at about 400 ppm) varies from plant to plant and from physiological parameters, but is typically about -18‰ for C4 plants and about -6 ‰ for C3 plants (Mook, 2000). C3 and C4 denote two different photosynthetic pathways of plants associated with different isotopic fractionation. The ocean shows typical $\delta^{13}C$ values of about 1 ‰ (Mook, 2000). Isotopic values of fossil fuel CO_2 depend on the fuel type and on the origin, formation and deposition conditions of the fuel. However, values for coal are typically about -25 ‰ (Mook, 2000), oil has a typical signature of about -29 ‰ (Mook, 2000) and natural gas of about -45 ‰ (Andres et al.,

1994). CO_2 sources increase and CO_2 sinks decrease the atmospheric concentrations. But, depending on what CO_2 source or sink has been emitting into the atmosphere, the $\delta^{13}C(CO_2)$ value will be altered more or less. Therefore, the relative proportion of the isotopes in an air mass carries information, from which sources or sinks the air mass originated. For example, the fact that CO_2 from the terrestrial biosphere and the ocean exhibit different $\delta^{13}C$ values has been used to distinguish between global carbon fluxes from these two reservoirs (Mook et al., 1983; Ciais et al., 1995 ; Miller and Tans, 2003; Alden et al., 2010). Fossil fuel emissions and their signatures were assumed to be known in these cases. In other case studies, the different ^{13}C signatures of fuel types have been used to determine the fraction of different fuel types and/or biospheric respiration to total CO_2 offset (Pataki, 2003; Newman et al., 2015).

In these studies, usually "Keeling plots" (Keeling, 1958; Keeling, 1961) were used to determine the mean isotopic source signature δ_S. The mean source signature is the contribution-weighted mean of the isotopic source signatures of all sources and therefore can potentially provide information on the shares of different CO_2 contributions. The principle idea behind the "Keeling plot" is to solve the balance equations of CO_2 and $\delta^{13}C(CO_2)$:

$$\mathsf{CO_{2,tot}} = \mathsf{CO_{2,bg}} + \mathsf{CO_{2,S}} \tag{1.3}$$

$$\mathsf{CO_{2,tot}} \cdot \delta^{13}\mathsf{C(CO_2)_{tot}} = \mathsf{CO_{2,bg}} \cdot \delta^{13}\mathsf{C(CO_2)_{bg}} + \mathsf{CO_{2,S}} \cdot \delta^{13}\mathsf{C(CO_2)_S} \tag{1.4}$$

The total measured signal (tot) is the sum of the background value (bg) and the source mix (S).

$$\begin{aligned} \delta^{13}\mathsf{C(CO_2)_{tot}} &= 1/\mathsf{CO_{2,tot}} \cdot (\mathsf{CO_{2,bg}} \cdot (\delta^{13}\mathsf{C(CO_2)_{bg}} - \delta^{13}\mathsf{C(CO_2)_S})) + \delta^{13}\mathsf{C(CO_2)_S} \\ &= 1/\mathsf{CO_{2,tot}} \cdot \mathsf{const} + \delta^{13}\mathsf{C(CO_2)_S} \end{aligned} \tag{1.5}$$

Since this Eq. 1.5 describes a linear function in $1/CO_{2,tot}$ and a y-intercept at the mean source signature δ_S, δ_S can be computed using CO_2 and $\delta^{13}C(CO_2)$ observations (see Fig. 1.5). Such an analysis is only valid if the mean source mix and the background concentration are constant and if no sources and sinks occur simultaneously (Miller and Tans, 2003). This "Keeling" analysis is principally also possible with continuous data to obtain the source signature on higher temporal resolution. However, this requires a careful routine check that all requirements are met. During the day, photosynthetic fluxes occur simultaneously to respiration fluxes and therefore hamper the Keeling

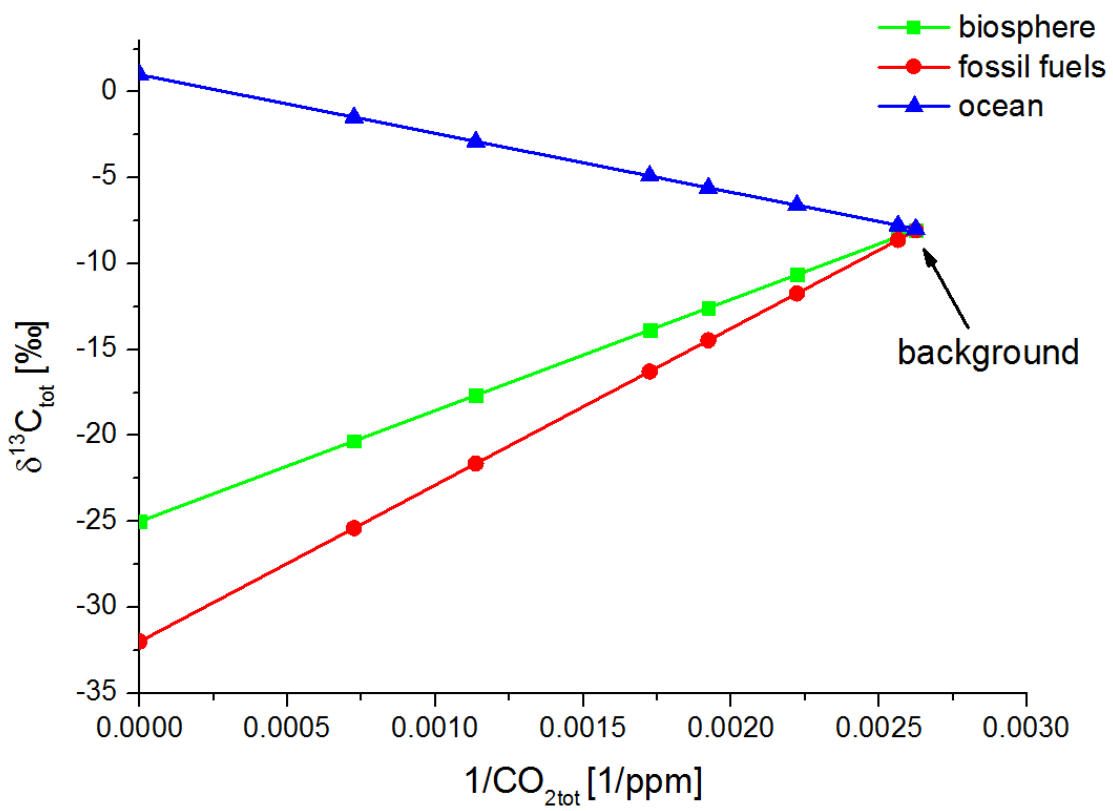

Fig. 1.5: Illustrative sketch of a "Keeling plot ". The intercept (mean source signature) depends on the source signature of the reservoirs (blue= ocean, green= biosphere, red= fossil fuels), which is responsible for the increase of CO_2.

analysis (Miller and Tans, 2003). This will be elaborated in the fourth manuscript (Sect. 2.4) in more detail.

In principle, one could use continuous $\delta^{13}C(CO_2)$ measurements to disentangle biogenic and anthropogenic CO_2 on a continuous and routine basis, without using a Keeling analysis, but also based on Eqs. 1.3 and 1.4. This will be discussed in more detail in the third publication where different tracers for anthropogenic fuel CO_2 are compared.

$\delta^{18}O(CO_2)$

Up to now, tracers, which distinguish between anthropogenic and biogenic net CO_2 fluxes have been presented. As described in Sect. 1.3, it is further desirable to separate between biospheric gross fluxes (respiration and photosynthesis) as both gross fluxes may respond differently to changes in climatic parameters such as heat or drought

(Ciais et al., 2005). $\delta^{18}O(CO_2)$ measurements can provide information on the gross carbon fluxes as ^{18}O in CO_2 depends not only on the fractionation of CO_2 (as does $\delta^{13}C(CO_2)$), but also on the isotopic signature of the water with which it is in contact. The exchange of ^{18}O between CO_2 and H_2O is responsible for this dependency (Francey and Tans, 1997; Farquhar et al., 1993). It is facilitated by carbonic anhydrase, which prominently occurs in plant tissue (Hesterberg and Siegenthaler, 1991). The isotopic signature of precipitation determines the isotopic signature of soil water, which nourishes plant tissue and leaf water. Leaf water, however, is consecutively enriched by evapotranspiration. During photosynthesis, atmospheric $\delta^{18}O(CO_2)$ is tagged by the isotopic signature of leaf water, whereas during respiration it is influenced by leaf and soil water with different isotopic signatures (Cuntz et al., 2003a; Cuntz et al., 2003b). The photosynthetic flux is therefore more enriched than the respiration flux, which could, in principle, be used to estimate gross carbon fluxes of the terrestrial biosphere. $\delta^{18}O(CO_2)$ therefore opens the door to a comprehensive process understanding of the biosphere and its feedback processes, but is often not routinely measured continuously alongside CO_2 and $^{13}C(CO_2)$.

CO

CO can be measured continuously as well. Since CO is usually co-emitted during incomplete combustion, CO measurements are often used as a continuous proxy for anthropogenic CO_2 contributions (Gamnitzer et al., 2006; Levin and Karstens, 2007; Lopez et al., 2013; Vogel et al., 2010; Turnbull et al., 2011). In this case, the mean ratio of CO to CO_2 during combustion processes is required together with the continuous CO measurement to obtain the continuous CO_2 concentration from incomplete combustion. However, non-fossil CO emissions as well as heterogeneity and changes of the CO/CO_2 ratio of various CO_2 emitters hamper the establishment of this tracer (Vogel, 2010).

1.6 Methodical and technical approach to study the greenhouse gas cycles

So far, the scientific problem was introduced and the principle requirements to study the greenhouse gas cycles and improve flux estimates have been motivated. Now, the methodical and technical approaches to address these problems will be explained.

1.6.1 Pseudo-data experiment

Measured data sets of CO_2, $\delta^{13}C(CO_2)$, $^{14}C(CO_2)$ or CO can be used to estimate fuel CO_2, all of which bear their own advantages and disadvantages (see Sect. 1.5.5). It is not clear, which of these fuel CO_2 tracers actually performs best and is closest to the real fuel CO_2 content. However, this needs to be evaluated for different measurement stations and under different circumstances (e.g. emission scenarios). To evaluate the different tracer approaches, it is helpful to use a model. In a model, in which the fuel contribution as well as the model tracer concentrations (CO_2, $\delta^{13}C(CO_2)$, $^{14}C(CO_2)$, CO) are known, the model tracers can be used as "pseudo data" to estimate fuel CO_2, which can then be compared with the actual model fuel CO_2. It is therefore possible to evaluate the performance of different tracers for a given measurement station and emission scenario using the model.

Another application where it is beneficial to use a model for evaluation of an approach, is the determination of the source signature. In a model, the source signature can be calculated from simulated "pseudo data" of $\delta^{13}C$ and CO_2 (via a Keeling plot) and can then compared to the known modeled source signature. In general, every approach, which needs to be checked before applied to real data, can be validated using modeled "pseudo data".

An additional advantage of the "pseudo data" approach is that the underlying emission fluxes, isotopic signatures of different sources and other parameters can be varied in the model, such that different situations and emission scenarios can be simulated and that a sensitivity analysis of all parameters is possible (Sect. 2.3). This analysis can then also provide an uncertainty estimate of the respective approaches when using real data. As the optimization of a measurement network requires thorough evaluation of all tracers and approaches under different circumstances and at different locations, the "pseudo data" approach is appropriate.

In the third and fourth publication (Sect. 2.3 and 2.4), the Stochastic Time Inverted Lagrangian Transport (STILT) model (Lin et al., 2003) is used to make a "pseudo data" experiment. The concentration at a measurement site is calculated with the STILT model by releasing particles at the measurement station, following them back in time using time-inverted meteorological fields and retracing them to the spatial region where they "hit" the surface. By multiplying this spatial region with the biogenic and fuel CO_2 emissions (fuel emissions from emission inventories and biogenic emissions

from biospheric models) at this region, the biogenic and fuel CO_2 concentration at the measurement location can be derived. More details on the STILT model are given in the third publication (Sect. 2.3).

1.6.2 The Fourier Transform Infrared (FTIR) instrument

It is challenging to find an instrument, which is able to measure all species required to study the greenhouse gas cycles and at the same time meets all requirements of accuracy, precision and time resolution for these species. In this work, a Fourier Transform Infrared (FTIR) spectrometer is used as this instrument is able to measure CO_2, CH_4, CO, N_2O and $^{13}C(CO_2)$ continuously with high precision and compatibly to other instruments. Here, the underlying measurement principle of the FTIR is explained only briefly. More details on the instrument can be found in Griffith et al. (2012) and Hammer et al. (2013a). In the appendix A, the general set-up and performance of the FTIR is discussed and summarized.

The FTIR spectrometer measures the broadband infrared spectrum in an optical cell with and without air sample and from that, calculates a transmittance spectrum of the air sample. To obtain the concentration, a theoretical spectrum is then fitted to this transmittance spectrum by a non-linear least square fitting algorithm. Since the different molecules (and isotopologues) absorb at different wavelengths (see Fig. 1.6), a simultaneous analysis of the different greenhouse gas concentrations of CO_2, CH_4, CO, N_2O and $^{13}C(CO_2)$ is possible. Since optical approaches do not have any memory effects (as do chemical measurement approaches) the temporal resolution of the measurements is only limited by the residence time of the gaseous sample in the cell. For the FTIR, the final resolution is three minutely. Moreover, the FTIR instrument is robust and compact (dimension: 1.5m x 0.8m x 0.8m) and can be carried by two people. It is therefore also suitable as "travelling campaign instrument" (TCI) (see Sect. 2.1) and enables its use in comparison campaigns where the TCI can detect instrumental or calibration biases independent of the station instrumentation. Its compactness also permits operation in field campaigns. Finally, the precision of the instrument is very good compared to other state of the art instruments and allows it to meet the WMO recommendations for all gases (Hammer et al., 2013a; see appendix A).

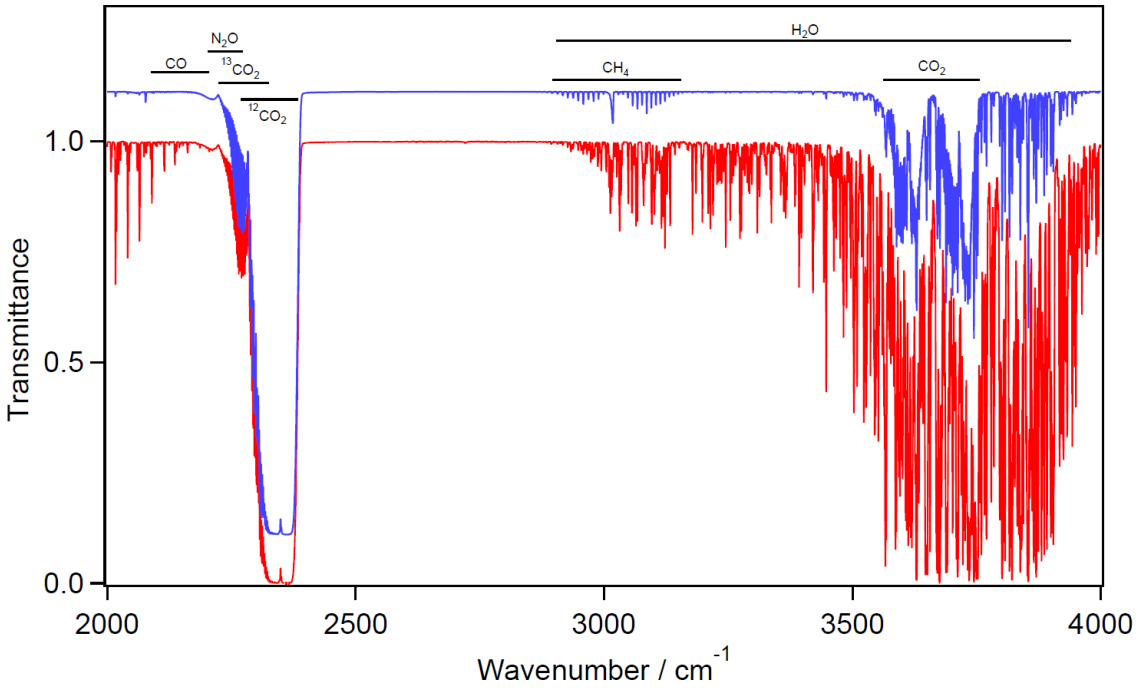

Fig. 1.6: Transmittance spectrum of an air sample. Red: undried air, blue: dried air. Figure adapted from Griffith et al. (2012). The dried spectrum was shifted up by 0.1 so that both spectra are distinguishable.

1.7 Overview over the individual publications

The aim of the present thesis is to assess possible approaches for improving estimates of natural greenhouse gas fluxes as well as of anthropogenic emissions in order to contribute to a profound understanding of biogenic processes, to support the development of emission mitigation policies and to improve projections of future changes of the climate system. Specific questions are addressed to achieve this aim.

- What is the current accuracy, precision and compatibility of greenhouse gas measurements?
- What are limiting factors of studying the greenhouse gas balance in more detail?
- Are $\delta^{18}O(CO_2)$ measurements feasible with the FTIR? If yes, what is the accuracy and precision?
- What benefits can continuous greenhouse gas and isotopologue measurements provide for understanding the greenhouse gas cycles?

- Which greenhouse gases should be measured at which measurement station to best separate between anthropogenic and biogenic CO_2?
- What are limiting factors of separating anthropogenic and biogenic CO_2?
- How can the mean source signature be determined correctly using continuous CO_2 and $\delta^{13}C(CO_2)$ data and what can be learned from the source signature?

Next, an overview over which questions will be addressed in which publication is given.

Publication 1 - Comparisons of continuous atmospheric CH_4, CO_2 and N_2O measurements - results from a travelling instrument campaign at Mace Head.

In the first publication, the quality of the FTIR data is assessed. A travelling instrument campaign is performed at the Advances Global Atmospheric Gases Experiment (AGAGE) and WMO station at Mace Head, Ireland to assess the compatibility between different instruments and different monitoring networks. Differences between the travelling campaign instrument (TCI) and the station instrumentation are investigated, discussed and interpreted. This provides the basis for assigning uncertainties to the data and eventually to the inverse model results when utilizing the data from these stations. Within the first publication, it is also assessed if, at present, temporal (diurnal and synoptic) patterns of greenhouse gas fluxes (CH_4 and CO_2) can be detected by the new optical instrumentation due to their high temporal resolution and which factors limit the study of greenhouse gas fluxes in more detail.

Publication 2 - First continuous measurements of $\delta^{18}C(CO_2)$ in air with a Fourier transform infrared spectrometer.

The FTIR instrument measures CO_2, CH_4, CO, N_2O and $^{13}C(CO_2)$ by measuring the molecular absorption at different wavelengths. As the spectral bands of CO_2, $^{13}C(CO_2)$ and $^{18}O(CO_2)$ overlap strongly and because the $^{18}O(CO_2)$ absorption band is rather weak (Esler et al., 2000), the detection and spectral separation of $^{18}O(CO_2)$ is very challenging. Therefore, in 2011, it was assumed, that the FTIR cannot resolve $^{18}O(CO_2)$. These measurements, however, could potentially provide a better process understanding of the biospheric processes in the carbon cycle (see Sect. 1.5.5). Given the fact

that the databases of spectral absorption bands and fitting algorithms have improved within the last years, the analysis of $^{18}O(CO_2)$ with the FTIR was revisited in this work and for the first time, the $^{18}O(CO_2)$ signal was extracted from the spectra. In the second publication, precision, accuracy and compatibility of the $\delta^{18}O(CO_2)$ measurements are assessed and the present and future benefit of these measurements is critically discussed.

Publication 3 - Estimation of continuous anthropogenic CO_2: model-based evaluation of CO_2, CO, $\delta^{13}C(CO_2)$ and $\Delta^{14}C(CO_2)$ tracer methods.

In the third publication, a new tracer method to determine fuel CO_2 continuously using $\delta^{13}C(CO_2)$ is formulated. In a model simulation study, different continuous tracers for anthropogenic CO_2 determination are compared, an uncertainty analysis of the different tracer methods is performed and a suited calibration strategy of fuel CO_2 is designed. Simulated "pseudo" data is used instead of real measured data, so that the results of the tracer-based estimates of fuel CO_2 can be compared to the simulated fuel CO_2 record. The simulation study is performed at three hypothetical very different European measurement stations, in order to declare station-type dependent recommendations on the use of anthropogenic CO_2 tracers. This publication seeks to evaluate the present and future potential of different tracers at different measurement locations for the estimation of continuous anthropogenic and biogenic CO_2. The outcome may function as a scientific guideline for the design of future measurement networks as well as the improvement of existing measurement networks.

Publication 4 - Evaluation of four years continuous $\delta^{13}C(CO_2)$ data using a running Keeling approach.

$^{13}C(CO_2)$ and CO_2 measurements can be processed into a mean isotopic source signature record by performing Keeling plots (see Sect. 1.5.5). The mean isotopic source signature can be used to separate between different CO_2 contributions, if the isotopic signatures from all sources are known. However, Miller and Tans (2003) pointed out that the determination of source signature only gives reasonable results if the mean source mix and the background concentration are constant and if sources and sinks do not occur simultaneously. Regardless of their findings, in many recent publications (e.g. Krevor et al., 2010; Guha and Ghosh, 2010; Gavrichkova et al., 2011; Kodama

et al., 2011; Rizzo et al., 2015) mean source signatures are frequently computed without checking the underlying assumptions and thus, introducing biases in the resulting mean source signature. This is especially tempting for continuous data as checking the prerequisites at high temporal resolution is tedious. Therefore, a routine way of determining the mean isotopic source signature from $\delta^{13}C(CO_2)$ and CO_2 is proposed in the fourth manuscript. It is based on the graphical method from Keeling (1961) (see Fig. 1.5). The results of the Keeling-based mean isotopic source signature are checked by comparing them with the "real" model isotopic source signature before applying this method to real data. This pseudo data experiment allows a validation of the new approach. Next, the approach is applied to measured data and its course is interpreted. Finally, it is critically discussed and elaborated what can be learned from Keeling plots, but also the limitations of Keeling plots are stated in all explicitness.

Part 2

Publications

General information on publications

This thesis is written in cumulative form. Following the requirements of the Faculty for Physics and Astronomy of the Heidelberg University, I have written four manuscripts, of which three have been published in internationally recognized, peer-reviewed journals during the course of my PhD. The fourth manuscript has been published in Biogeosciences Discussions and is under review for the journal Biogeosciences. In all four publications, I am first and main author. The publications have not been used in other dissertations. All publications have a Creative Commons Attribution 3.0 License. For information about the copyright of these publications please see: http://www.atmospheric-chemistry-and-physics.net/about/licence_and_copyright.html (also holds for publication in Atmospheric Measurement Technique, Biogeosciences discussion forum and Biogeosciences).

Publication 1

Vardag, S. N., Hammer, S., O'Doherty, S., Spain, T. G., Wastine, B., Jordan, A., and Levin, I.: Comparisons of continuous atmospheric CH_4, CO_2 and N_2O measurements – results from a travelling instrument campaign at Mace Head, Atmos. Chem. Phys., 14, 8403-8418, doi:10.5194/acp-14-8403-2014, 2014. http://www.atmos-chem-phys.net/14/8403/2014/

Publication 2

Vardag, S. N., Hammer, S., Sabasch, M., Griffith, D. W. T., and Levin, I.: First continuous measurements of δ^{18}O-CO_2 in air with a Fourier transform infrared spectrometer, Atmos. Meas. Tech., 8, 579-592, doi:10.5194/amt-8-579-2015, 2015. http://www.atmos-meas-tech.net/8/579/2015/

Publication 3

Vardag, S. N., Gerbig, C., Janssens-Maenhout, G., and Levin, I.: Estimation of continuous anthropogenic CO_2: model-based evaluation of CO_2, CO, δ^{13}C(CO_2) and

$\Delta^{14}C(CO_2)$ tracer methods, Atmos. Chem. Phys., 15, 12705-12729, doi:10.5194/acp-15-12705-2015, 2015. http://www.atmos-chem-phys.net/15/12705/2015/

Publication 4

Vardag, S. N., Hammer, S., and Levin, I.: Evaluation of four years continuous $\delta^{13}C(CO_2)$ data using a running Keeling approach, Biogeosciences Discuss., doi:10.5194/bg-2016-93, in review, 2016. http://www.biogeosciences-discuss.net/bg-2016-93/

Author contributions to the respective publications

Publication 1

The original idea behind performing a comprehensive quality control measurement campaign at Mace Head originated in discussions with Ingeborg Levin, Samuel Hammer and myself. I was responsible for maintaining the FTIR, improving its performance, as well as correcting and calibrating the FTIR data. I also calibrated the Heidelberg GC data based on scripts written by Samuel Hammer. I planned the measurement campaign and carried it out. Gerry Spain maintained the GC system at Mace Head. Simon O'Doherty analyzed the GC data at Mace Head. Benoit Wastine provided the calibrated cavity ring-down spectroscopy (CRDS) data. The analysis of the comparison campaign was led and initiated by myself and profited from discussion with Samuel Hammer and Ingeborg Levin. Armin Jordan provided us with our calibration cylinders and information on the calibration scales. Finally I wrote the paper with support from Ingeborg Levin and replied to referees' comments.

Publication 2

The initial assumption that the FTIR could be used to measure $\delta^{18}O(CO_2)$ was actually brought-up by David Griffith, who implemented the spectral window into the optical analysis routine. However, he withdrew the idea when he found that $^{12}C(CO_2)$, $^{13}C(CO_2)$ and $^{18}O(CO_2)$ strongly overlap. Nonetheless, I was hopeful to extract the $^{18}O(CO_2)$ signal from the spectra and therefore performed some additional tests. These tests were planned and discussed together with Samuel Hammer and Ingeborg Levin. Michael Sabasch provided the independent mass-spectrometric measurements of the stable carbon isotopologues. I, with support from Ingeborg Levin, wrote the paper and replied to the referees' comments in close communication with David Griffith.

Publication 3

My intention to write the third paper was to optimize the present ICOS measurement network, in particular with respect to which tracers should be measured at which station to gain most information on CO_2 fluxes. Therefore, I formulated a novel $\delta^{13}C(CO_2)$

tracer method, which can be used, alternatively to e.g. the CO-method, to continuously determine the anthropogenic CO_2 offset. I established this method in continuous exchange with Ingeborg Levin. To test which method is best to estimate anthropogenic CO_2 and to give explicit advices for different stations, I decided to launch a transport model. Christoph Gerbig helped me set-up the transport model and repeatedly helped me adjust the model code for my purposes. Greet Jaenssens-Maenhout provided the anthropogenic emission inventory data. Again, I wrote the paper with help of Ingeborg Levin and replied to all referees' comments.

Publication 4

The original idea to write a paper about how to determine the source signature correctly from Keeling plots came to me after reading various papers, which used a Keeling plot without checking the necessary assumptions. The idea was reinforced by the emerge of new optical instruments, which are able to measure CO_2 and $\delta^{13}C(CO_2)$ continuously. I developed the routine approach in exchange with Ingeborg Levin. I verified this approach using pseudo data (as in Publication 3) from the STILT model. In the last part, I applied the approach to real data. The real data was partly taken by Samuel Hammer (until Sept. 2011) and partly by myself. The discussion on the benefit of continuous $\delta^{13}C(CO_2)$ measurements profited from discussions with Samuel Hammer and Ingeborg Levin. I finally wrote the paper with support from Ingeborg Levin.

Publication 1

2.1 Comparisons of continuous atmospheric CH_4, CO_2 and N_2O measurements – results from a travelling instrument campaign at Mace Head

Vardag, S. N., Hammer, S., O'Doherty, S., Spain, T. G., Wastine, B., Jordan, A., and Levin, I.

Atmos. Chem. Phys., 14, 8403–8418, 2014
www.atmos-chem-phys.net/14/8403/2014/
doi:10.5194/acp-14-8403-2014

Atmospheric Chemistry and Physics
Open Access

Comparisons of continuous atmospheric CH_4, CO_2 and N_2O measurements – results from a travelling instrument campaign at Mace Head

S. N. Vardag[1], S. Hammer[1], S. O'Doherty[2], T. G. Spain[3], B. Wastine[4], A. Jordan[5], and I. Levin[1]

[1]Institut für Umweltphysik, Heidelberg University, Germany
[2]School of Chemistry, University of Bristol, Bristol, UK
[3]National University of Ireland, Galway, Ireland
[4]Laboratoire des Sciences du Climat et de l'Environnement (LSCE), CEA/CNRS/UVSQ, Gif sur Yvette, France
[5]Max Planck Institute for Biogeochemistry, Jena, Germany

Correspondence to: S. N. Vardag (svardag@iup.uni-heidelberg.de)

Received: 18 February 2014 – Published in Atmos. Chem. Phys. Discuss.: 25 April 2014
Revised: 8 July 2014 – Accepted: 12 July 2014 – Published: 21 August 2014

Abstract. A 2-month measurement campaign with a Fourier transform infrared analyser as a travelling comparison instrument (TCI) was performed at the Advanced Global Atmospheric Gases Experiment (AGAGE) and World Meteorological Organization (WMO) Global Atmosphere Watch (GAW) station at Mace Head, Ireland. The aim was to evaluate the compatibility of atmospheric methane (CH_4), carbon dioxide (CO_2) and nitrous oxide (N_2O) measurements of the routine station instrumentation, consisting of a gas chromatograph (GC) for CH_4 and N_2O as well as a cavity ring-down spectroscopy (CRDS) system for CH_4 and CO_2. The advantage of a TCI approach for quality control is that the comparison covers the entire ambient air measurement system, including the sample intake system and the data evaluation process. For initial quality and performance control, the TCI was run in parallel with the Heidelberg GC before and after the measurement campaign at Mace Head. Median differences between the Heidelberg GC and the TCI were well within the WMO inter-laboratory compatibility target for all three greenhouse gases. At Mace Head, the median difference between the station GC and the TCI were $-0.04\,\mathrm{nmol\,mol^{-1}}$ for CH_4 and $-0.37\,\mathrm{nmol\,mol^{-1}}$ for N_2O (GC-TCI). For N_2O, a similar difference ($-0.40\,\mathrm{nmol\,mol^{-1}}$) was found when measuring surveillance or working gas cylinders with both instruments. This suggests that the difference observed in ambient air originates from a calibration offset that could partly be due to a difference between the WMO N_2O X2006a reference scale used for the TCI and the Scripps Institution of Oceanography (SIO-1998) scale used at Mace Head and in the whole AGAGE network. Median differences between the CRDS G1301 and the TCI at Mace Head were $0.12\,\mathrm{nmol\,mol^{-1}}$ for CH_4 and $0.14\,\mu\mathrm{mol\,mol^{-1}}$ for CO_2 (CRDS G1301 – TCI). The difference between both instruments for CO_2 could not be explained, as direct measurements of calibration gases show no such difference. The CH_4 differences between the TCI, the GC and the CRDS G1301 at Mace Head are much smaller than the WMO inter-laboratory compatibility target, while this is not the case for CO_2 and N_2O.

1 Introduction

Since the industrial revolution, the global abundances of the long-lived greenhouse gases carbon dioxide (CO_2), methane (CH_4) and nitrous oxide (N_2O) have been rising in the atmosphere, causing an anthropogenic greenhouse effect. However, estimates of their global and regional sources and sinks are still associated with large uncertainties (Schulze et al., 2009). In order to monitor the temporal and spatial changes of the greenhouse gases and gain from this quantitative information about the fluxes and their variability using inverse modelling approaches, precise and compatible measurements in the atmosphere are required. Based on the size of atmospheric gradients and variability of the different

greenhouse gases, the World Meteorological Organization (WMO) experts have set inter-laboratory compatibility (ILC) targets for each individual greenhouse gas species (WMO, 2009), which need to be reached in order to allow merging data from different stations and networks for global and regional budget estimates.

In order to assure the quality and consistency of previous and future measurements, it is therefore important to compare different measurement techniques and their results and check whether the ILC targets have indeed been reached. This has been done through a number of different international comparison exercises, such as analysis of round-robin cylinders (Zhou et al., 2011), co-located flask sampling (Masarie et al., 2001) and recently also via in situ comparison of co-located instruments (Zellweger et al., 2012; Hammer et al., 2013a; Rella et al., 2013). For a fully comprehensive quality control of continuous atmospheric measurements, a travelling comparison instrument (TCI) approach has proven to be most appropriate (Hammer et al., 2013a); this was also recognized at the 16th WMO/IAEA Meeting on Carbon Dioxide, Other Greenhouse Gases, and Related Measurement Techniques (GGMT-2011).

Here we present the results of a measurement campaign at the World Meteorological Organization – Global Atmosphere Watch (GAW) and Advanced Global Atmospheric Gases Experiment (AGAGE) station Mace Head in the Republic of Ireland. A Fourier transform infrared spectrometer (FTIR) was used as the travelling instrument, which was manufactured by the University of Wollongong, Australia, (Griffith et al., 2012) and is normally run at the Institut für Umweltphysik at Heidelberg University for routine ambient air measurements (Hammer et al., 2013b). At Mace Head, it performed independent continuous ambient air measurements from March to May 2013 in parallel with the station gas chromatograph (GC-MD). N_2O and CH_4 mole fractions measured with the locally installed GC-MD system as well as CH_4 and CO_2 measurements performed by a cavity ring-down spectroscopy (CRDS) were compared with those made with the travelling FTIR instrument. Before and after the campaign the TCI was run in parallel with the Heidelberg GC (GC-HEI) (Hammer, 2008) in order to check its performance and stability.

As most of the time the TCI was sampling air from the 10 m level to obtain sufficient data for the GC-MD comparison, while the CRDS systems have their air intake at the 25 m level, we used the opportunity of this comparison campaign to investigate the corresponding vertical gradients of CO_2 and CH_4 at Mace Head from March to April 2013. Co-located measurements of the TCI and the CRDS at the same height performed in May 2013 allowed us to correct the earlier data for any systematic offsets between both instruments. Very small but still significant vertical gradients could indeed be resolved; these data these data are presented here as an Appendix. These results nicely illustrate how capable current optical instrumentation is in terms of precision. As our comparison study shows, the biggest challenge in fully exploiting this precision capability is now making sure that these instruments also measure highly accurate and compatible.

2 Methods, site descriptions and instrumentation

2.1 The TCI and its calibration

For the comparison campaign at Mace Head, we used the same in situ multi-species FTIR analyser as Hammer et al. (2013a), however we extended it beyond CO_2 and CH_4 to include N_2O. We used the FTIR since it turned out to be robust and compact and since it measures CO_2, CH_4 and N_2O continuously and simultaneously with a precision that allows it to meet all ILC targets for these species (Hammer et al., 2013b). The reproducibility of the 3-minute data recorded by the FTIR is generally better than $\pm 0.05\,\mu mol\,mol^{-1}$ for CO_2, $\pm 0.25\,nmol\,mol^{-1}$ for CH_4 and $\pm 0.05\,nmol\,mol^{-1}$ for N_2O. Within the Integrated non-CO_2 Greenhouse gas Observation System (InGOS) project, the three working standards of the FTIR system were calibrated relative to WMO Central Calibration Laboratory (CCL) tertiary standards by the Max-Planck-Institute for Biogeochemistry (MPI-BGC GasLab) in Jena, Germany, using CRDS for CH_4 and CO_2 and gas chromatography with electron-capture detection (GC-ECD) for N_2O. The scales in use were the WMO CO_2 X2007 scale (Tans et al., 2011), the WMO CH_4 X2004 scale (Dlugokencky et al., 2005) and the WMO N_2O X2006a scale (Hall et al., 2007).

2.2 Site description and routine instrumentation in Heidelberg

Heidelberg is a medium-sized city (ca. 150 000 inhabitants) located in the densely populated Rhine-Neckar region (49°25′ N, 8°43′ E) in Germany. Routine ambient air measurements are made on the university campus at the Institut für Umweltphysik, located to the north-west of the Heidelberg city centre. On the roof of the institute's building (at ca. 30 m a.g.l.), air is drawn through a permanently flushed intake line (1 / 2″ stainless steel) with a bypass to the GC-HEI system, which measures CO_2, CH_4, N_2O, SF_6, CO and H_2 simultaneously at a maximum temporal resolution of 5 min. The GC-HEI and the TCI have independent drying systems (GC-HEI: cryogenic cooler at $-45\,°C$, TCI: Nafion dryer in counterflow mode followed by $Mg(ClO_4)_2$) and sample pumps. The working gases for the GC-HEI system are calibrated on the WMO X2007 scale for CO_2, the WMO X2004 scale for CH_4 and the WMO X2006a scale for N_2O, based on Heidelberg tertiary standards calibrated at the WMO GAW CCL at National Oceanic and Atmospheric Administration (NOAA) in Boulder, USA. These standards, with a N_2O range of 306 to 343 $nmol\,mol^{-1}$, are also used to check the non-linearity of the electron-capture detector (ECD) regularly. The reproducibility of the GC-HEI measurements is

$\pm 0.05\,\mu mol\,mol^{-1}$ for CO_2, $\pm 2.4\,nmol\,mol^{-1}$ for CH_4 and $\pm 0.1\,nmol\,mol^{-1}$ for N_2O. A detailed description of the entire GC-HEI system can be found in Hammer (2008). To allow for better comparability between the continuous TCI measurements and the discrete GC-HEI measurements, a buffer volume was installed in the GC-HEI sample intake line. The buffer volume allows capturing and integrating the short-term mole fraction variations between the discontinuous GC-HEI measurements. Details of the integration scheme of the buffer can be found in Hammer et al. (2013a) while the standard operating conditions of the TCI are described in Hammer et al. (2013b).

Normally the FTIR uses the same main air intake line as the GC-HEI (with a separate bypass, pump and drying system, Hammer et al., 2013b), but for the performance test before the intercomparison campaign at Mace Head, a separate intake line was installed in Heidelberg for the TCI.

2.3 Site description and routine instrumentation at Mace Head

The Mace Head station is located on the west coast of Ireland (53°20′ N, 9°45′ W) about 100 m from the Atlantic shore. The station is operated by the National University of Ireland, Galway, and is classed as a global background station within the WMO-GAW network. At the station, trace gas measurements are carried out by the University of Bristol (UK) and by the Laboratoire des Sciences du Climat et de l'Environnement (LSCE) Gif sur Yvette (France) as part of the AGAGE (CH_4 and N_2O) (Prinn et al., 2000) and Integrated Carbon Observation System (ICOS) demonstration (CO_2 and CH_4) (http://www.icos-infrastructure.eu/) networks. A description of the station can be found in Jennings et al. (2003). A gas chromatography system with multiple detectors (GC-MD), including an ECD and a flame-ionization detector (FID) is used to measure N_2O and CH_4, while a reduction gas analyser (RGA) measures CO and H_2 within the AGAGE network. One working standard, which is measured alternately with ambient air or other samples, is used for on-site calibration. These whole air standards last for approximately 8 months and are analysed at Scripps Institute of Oceanography (SIO) before and after use at Mace Head, for details see Prinn et al. (2000). New working standards are always compared on-site with the old working standards and agree well with the values assigned at the SIO on a different instrument but applying the same non-linearity correction. For more than 15 years, weekly pressure-programmed injections of the standard were used to determine the non-linearity of the ECD response. It was also compared to non-linearities measured using primary gases spanning a range of concentrations. From May 2009 onwards, the non-linearity tests were discontinued, as it was found that the non-linearity between AGAGE instruments was remarkably consistent and stable, and because the pressure-programmed non-linearity tests also introduced occasional artifacts due to the variable amount of air being injected. The precision of the measurements is approximately $0.1\,nmol\,mol^{-1}$ for N_2O and $1.5\,nmol\,mol^{-1}$ for CH_4. The working gases for the GC-MD system are calibrated on the Tohoku University scale for CH_4 (Cunnold et al., 2002) and the SIO-1998 scale for N_2O (Prinn et al., 2000). The GC-MD intake line allows sampling of ambient air from a height of 10 m a.g.l. The ambient air is dried using a Nafion drier. A separate intake line ($1/2''$ O.D. Synflex) was installed at the same height for ambient air intake of the TCI. This 10 m intake line of the TCI was used from March until the end of April 2013.

Further, two CRDS instruments are running at the Mace Head station which draw air from a height of 25 m a.g.l. One instrument is a Picarro G1301, which belongs to the Irish Environmental Protection Agency (EPA) and measures CO_2 and CH_4 in un-dried ambient air since May 2009. The second instrument, a Picarro G2301, belongs to the LSCE and dries the ambient air with a cryogenic water trap to a dew point of about $-45\,°C$ before measuring CO_2 and CH_4. Each of the two instruments is equipped with a designated ambient air intake line ($1/2''$ O.D. Synflex). Both instruments share the same calibration and target cylinders, connected via a multi-position valve, as well as the same measurement sequence (i.e. ambient measurements and calibration are performed at the same time interval). A water vapour correction according to Chen et al. (2010) is applied to both instruments. Even though the water vapour correction of the (wet) G1301 instrument was tested at LSCE before installation at Mace Head, we found a weak correlation of the difference of both CRDS instruments (G1301–G2301) and the absolute humidity, of $0.13\,\mu mol\,mol^{-1}\ CO_2\,\%^{-1}\ H_2O$ for the period from March 2013 until July 2013. The H_2O-dependency is most likely due to an incomplete water vapour correction of the G1301 instrument. During the comparison period, the absolute humidity varied between 0.55 and 0.8 %, which could result in slightly increased CO_2 values of the G1301 instrument of 0.01–0.04 $\mu mol\,mol^{-1}$ compared to the dry G2301 instrument. The calibration suite of the CRDS systems consists of four cylinders filled with synthetic gas mixture by Deuste Steininger (Mühlhausen, Germany). They were calibrated by the MPI-BGC GasLab in Jena using CRDS. The two CRDS instruments are routinely calibrated once per month, according to a calibration sequence where each standard is measured four times for 20 min (the first 10 minutes are not used to calculate the response function since they still incorporate a settling-in effect). The measurement interval is 5 s. The sample flow rate is about 0.3 slpm at about 1 bar absolute pressure. In this study we will use hourly aggregates for the intercomparison, since the data is computed and stored like this in the common database.

The CRDS analysers measure CO_2 and CH_4 with a precision of about $0.02\,\mu mol\,mol^{-1}$ for CO_2 and $0.1\,nmol\,mol^{-1}$ for CH_4 (Crosson, 2008). A common target cylinder is used for quality control purposes and is measured on both instruments every 11 h. The (1σ) reproducibility of the target

cylinder measurement is about 0.02 µmol mol^{-1} for CO_2 and 0.21 nmol mol^{-1} for CH_4 for the G1301 from March to June 2013 and 0.03 µmol mol^{-1} for CO_2 and 0.33 nmol mol^{-1} for CH_4 for the G2301. For the last week of the measurement campaign, the TCI intake was moved to a height of 25 m a.g.l. in order to compare TCI measurements directly with the measurements performed with the CRDS instruments. Due to a malfunctioning pump, the G2301 was not measuring during this period. Therefore, we present here only ambient air comparisons between the non-dried CRDS G1301 and the TCI. The ambient air measurements of both CRDS instruments agreed within 0.02 ± 0.10 µmol mol^{-1} for CO_2 and -0.20 ± 0.70 nmol mol^{-1} for CH_4 during the comparison campaign (from 1 March 2013 to 31 May 2013 with two interruptions).

3 Experimental results

3.1 Quality check of the travelling instrument in Heidelberg

To assure that the TCI meets the WMO compatibility requirements, we studied precision, accuracy and compatibility (as defined in http://gaw.empa.ch/glossary/glossary.html) relative to the GC-HEI in Heidelberg before and after the measurement campaign. The reproducibility can be estimated by measuring a so-called target or surveillance gas every day under reproducible conditions, and the standard deviations of the target gas measurements are a good measure of the precision. It was 0.03 µmol mol^{-1} for CO_2, 0.16 nmol mol^{-1} for CH_4 and 0.05 nmol mol^{-1} for N_2O (see also Sects. 3.4.1 and 3.4.2) before as well as after the Mace Head campaign for the TCI. The accuracy of the measurements is determined by the closeness of agreement between the measured value and the accepted reference value (WMO, 2009). In order to determine the accuracy of the TCI, we measured the Heidelberg WMO CCL tertiary standards, which were calibrated by the WMO CCL at NOAA, Boulder (http://www.esrl.noaa.gov/gmd/ccl/). The differences between the TCI-measured value (working standards calibrated in the framework of InGOS project by the MPI-BGC GasLab Jena) and the nominal WMO CCL values of these cylinders are smaller than the WMO ILC targets for all CH_4, CO_2 and N_2O measurements (see Fig. 1). For CH_4, the mean difference (measured TCI value – WMO CCL value and standard error) of 0.04 ± 0.01 nmol mol^{-1} is negligible. For CO_2 in the ambient mole fraction range (380–480 µmol mol^{-1}), a difference of -0.03 ± 0.04 µmol mol^{-1} was observed, while the N_2O difference in the ambient range (325–338 nmol mol^{-1}) was -0.00 ± 0.03 nmol mol^{-1}. It can thus be confirmed that the accuracy of the TCI measurements meets the WMO ILC targets.

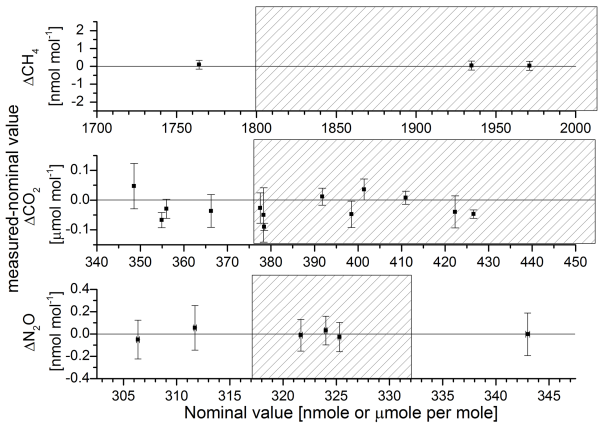

Figure 1. Difference between TCI-measured Heidelberg WMO CCL tertiary standards and their respective nominal value given by WMO CCL (TCI-measured – WMO CCL nominal value). The measurements were performed on 30 May 2013, 24 June 2013, 3 July 2013, 2 September 2013 and 3 September 2013. The standard deviation plotted combines the standard error of the repeated cylinder measurements and the error of the nominal WMO CCL tertiary cylinder value. Shaded areas indicate the calibrated TCI mole fraction ranges.

3.2 Comparison of direct target/standard gas measurements on different instruments

In order to check the calibration compatibility between different instruments in Heidelberg and at Mace Head, target and working standards were measured on all instruments directly. In Fig. 2, the differences between the cylinder measurements with the local instrumentation and with the TCI are plotted. For the TCI working standards, we plot the difference between the cylinder measurements with the local instrumentation and the assigned value (open symbols). For CH_4 and CO_2, all instruments compare well within the WMO ILC target. The GC-HEI and the TCI instruments agree very well with each other (-0.02 ± 0.04 µmol mol^{-1}, mean ± standard error) for CO_2. The G1301 CRDS instrument shows very good agreement with the TCI in CO_2 results (-0.01 ± 0.02 µmol mol^{-1}), while the G2301 results are consistently higher (0.05 ± 0.03 µmol mol^{-1}) than the CO_2 mole fraction determined using the TCI. Since both CRDS instruments are calibrated with the same cylinders, the difference between the CRDS instruments is remarkable. It is questionable if both CRDS instruments were functioning correctly during the direct measurements since the difference between the CRDS instruments was 0.06 µmol mol^{-1}, while it is was 0.02 µmol mol^{-1} during target and ambient air measurements (from 1 March 2013 until 31 May 2013). Nevertheless, all differences of direct analyses lie within the WMO ILC target for the Northern Hemisphere.

For N_2O, the values obtained with the GC-HEI were higher than those obtained with the TCI

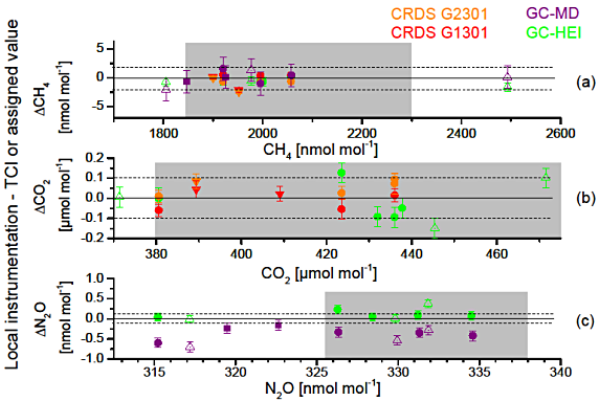

Figure 2. Differences (local instrument – TCI or assigned value in the case of the TCI standards shown as open symbols) of the measured mole fractions of **(a)** CH_4, **(b)** CO_2 and **(c)** N_2O of different cylinders: Mace Head AGAGE target cylinders (squares), Heidelberg target cylinders (circles), TCI working standards calibrated by MPI-BGC GasLab (upward open triangles) and Mace Head CRDS target cylinders (downward triangles). The grey shaded area shows the ambient mole fraction range during the measurement campaign at Mace Head. The direct cylinder measurements at Mace Head were performed partly at the beginning of the campaign (24–26 February 2013) and partly at the end of the campaign (21 May 2013).

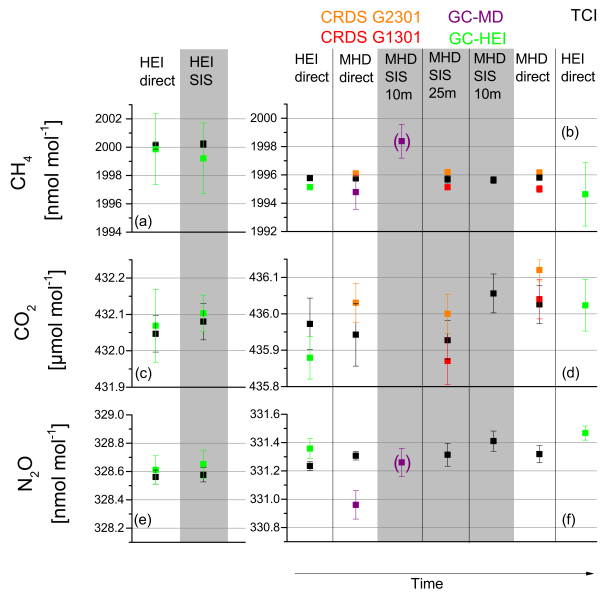

Figure 3. Direct cylinder gas measurement (direct) and SIS test on the 12 January 2013 for **(a)** CH_4, **(c)** CO_2 and **(e)** N_2O in Heidelberg (HEI) and on the 26/27 February 2013 for **(b)** CH_4, **(d)** CO_2 and **(f)** N_2O at Mace Head (MHD). Different cylinders were used for the SIS test in Heidelberg and Mace Head. Grey shaded areas show results when the cylinder was measured via the SIS. The SIS measurement of the GC-MD did not reach a stable value. The error bars given here are the reproducibility of direct measurements or the standard deviation during the SIS test, respectively.

(0.11 ± 0.05 nmol mol^{-1}). The reason for the difference between the GC-HEI and the TCI is not clear. The N_2O cylinder measurements with the GC-MD show significantly lower values than the TCI, by -0.40 ± 0.06 nmol mol^{-1}. This is a rather large and unexpected offset between the two instruments, since current known scale differences between SIO-1998 and WMO X2006a are of the order of 0.03 to 0.05 nmol mol^{-1} (Hall et al., 2007; B. Hall, personal communication, 2013) and thus cannot explain the difference in the cylinder measurements found here. We will discuss this point in Sect. 4 after having presented ambient air measurements of both instruments.

3.3 Sample intake system (SIS) tests

Since the ambient air sample intake systems of the different instruments can possibly introduce a bias into ambient air mole fraction measurements (Hammer et al., 2013a), a sample intake system (SIS) test was performed in Heidelberg as well as at Mace Head. For this purpose, a gas cylinder was connected via the respective intake line to the individual instruments. The pressure on the low pressure side of the regulator was chosen such that the pressure in the intake line was always very close to (but slightly higher than) ambient air pressure. Then the cylinder gas was flushed through the entire intake system and the measured results were compared to the direct measurements of the same cylinder. Figure 3 shows all results of these tests in Heidelberg and at Mace Head.

3.3.1 Sample intake system test in Heidelberg

A SIS test was performed in Heidelberg (Fig. 3a, c, e) on the independent intake lines of the GC-HEI (green symbols) and the TCI (black symbols). The measurements of the SIS cylinder on the TCI and the GC-HEI show similar differences as the direct cylinder measurements (see Fig. 2). For both instruments the measurements via the SIS agree with the direct cylinder measurements within their measurement uncertainties. The differences between the direct measurement and the measurement via the SIS of the TCI in Heidelberg ($\pm$ combined errors of their reproducibility and their standard deviations during the SIS tests) was SIS – direct $= 0.1 \pm 0.35$ nmol mol^{-1} for CH_4, 0.03 ± 0.07 µmol mol^{-1} for CO_2 and 0.02 ± 0.07 nmol mol^{-1} for N_2O; for the GC-HEI it was SIS – direct $= -0.65 \pm 3.5$ nmol mol^{-1} for CH_4, 0.03 ± 0.11 µmol mol^{-1} for CO_2 and 0.04 ± 0.11 nmol mol^{-1} for N_2O. These differences are not significant.

3.3.2 Sample intake system test at Mace Head

For Mace Head, one dedicated cylinder for the different SIS tests was available. This cylinder was different than the one used for the Heidelberg SIS test, but was first measured directly on the GC-HEI and the TCI in Heidelberg. At Mace

Head, a SIS test via the GC-MD 10 m sample intake line was performed first. Next, the cylinder was measured in parallel by the CRDS G1301, the CRDS G2301 and the TCI via their 25 m height intake lines followed by a TCI measurement through the 10 m height intake system. Prior to the SIS tests at 25 m and prior to the SIS test of the TCI at 10 m, the intake line was evacuated to a pressure of about 80 mbar. The cylinder was also measured directly on the TCI, the GC-MD, the CRDS G1301 and the CRDS G2301 at Mace Head and after return to Heidelberg (in March 2013) it was measured again on the GC-HEI system. All results are displayed in Fig. 3b, d, f. The comparison between the direct measurements before and after the campaign indicate a mole fraction change in the cylinder for CO_2 in the order of 0.1 µmol mol^{-1}. This change is observed by all instruments which measured the gas before and after the test. A significant mole fraction jump is seen between the SIS tests at 25 and 10 m. Significant increases of CO_2 mole fraction in cylinders have often been observed in the laboratory, in particular when cylinders are emptied at high flow rates and below a pressure of 35 bar (Chen et al., 2013). Since the SIS cylinder was emptied to a pressure of 20 bar, a mole fraction change in the SIS cylinder was not unexpected.

No significant mole fraction change was observed for CH_4, but for N_2O also a slight but not significant change of 0.1 nmol mol^{-1} was indicated by the GC-HEI (see Fig. 3f). For CH_4, we found that the TCI and the CRDS systems showed no significant difference between direct measurements and measurements via the SIS. The GC-MD showed a large difference of the order of 3.7 ± 1.7 nmol mol^{-1} (difference $\pm$ combined error of the standard deviation during the SIS test and the reproducibility during the direct measurement), but no stable value could be reached during the SIS test for the GC-MD and the data points for the GC-MD SIS test for CH_4 and N_2O must be discarded (bracketed symbols in Fig. 3). This is surprising since the residence time of the sample air in the intake line is less than a minute and an equilibrium should have been reached within the SIS test (duration of the 10 m SIS test was 2 h). Therefore, no SIS effect could be verified nor proven false for the GC-MD intake system during the SIS test. The TCI SIS test at 10 m showed a small, yet insignificant, SIS effect for N_2O (0.07 ± 0.10 nmol mol^{-1}), which could, however, be also due to a small N_2O drift in the cylinder mole fraction. For CO_2, the TCI and CRDS measurements show only small SIS influence within their measurement uncertainties: TCI at 25 m: -0.01 ± 0.08 µmol mol^{-1}, TCI at 10 m: 0.03 ± 0.08 µmol mol^{-1}, CRDS G1301: -0.07 ± 0.12 µmol mol^{-1} (SIS effect was determined relative to the TCI measurements at 25 m and after the SIS test), CRDS G2301: -0.02 ± 0.03 µmol mol^{-1} when taking into account the mole fraction jump after the SIS test at the 25 m intake of about 0.1 µmol mol^{-1}.

3.4 Comparison of ambient air measurements

3.4.1 Comparison of ambient air measurements in Heidelberg

Ambient air comparisons were performed in Heidelberg before and after the measurement campaign. For this purpose, the TCI data was smoothed exponentially ($\tau = 20$ min) to make them comparable to the GC-HEI measurements where an integration volume is installed. Details of this so-called buffer system can be found in Hammer et al. (2013a).

The CH_4 measurements of the TCI and the GC-HEI (Fig. 4a, b) show a difference of -0.25 ± 3.61 nmol mol^{-1} (median and interquartile range, see Fig. 5) before the campaign and a difference of -0.24 ± 2.43 nmol mol^{-1} after the campaign. In each intercomparison period this difference was constant over time (see Fig. 4b). The TCI target measurements were stable during both comparison periods and showed a reproducibility of 0.16 nmol mol^{-1} (see Fig. 4c).

All CO_2 measurements of the TCI in Heidelberg and the GC-HEI agree very well (see Fig. 4d, e). The difference (GC-HEI – TCI) between the instruments was nearly the same in both intercomparison phases (0.04 ± 0.22 µmol mol^{-1} before the camapign and 0.03 ± 0.31 µmol mol^{-1} after the campaign).

The N_2O measurements show a median difference of 0.03 ± 0.15 nmol mol^{-1} (GC-HEI – TCI) during the first comparison period in February and a median difference of -0.02 ± 0.14 nmol mol^{-1} in the second period in June 2013. The particular structure of the difference in ambient air measurements between the TCI and the GC-HEI (decrease after 15 June, see Fig. 4h) is partly due to a respective structure of the TCI and GC-HEI measurements, which can be detected in the N_2O target gas measurement of both instruments (see Fig. 4i). The reproducibility of the TCI in this last period was not worse than usual, showing that unexplained drifts and long term variability occur and can be detected by the target cylinder measurement. In addition, this example highlights that systematic variations, which are observed in the target gas measurements, are present at the same time in the ambient air measurement. Thus regular target gas measurements are essential as quality control measures and for a comprehensive uncertainty estimate of ambient air measurements.

Altogether, the measurement results of the FTIR in Heidelberg (TCI) and the GC-HEI have shown very good agreement, meeting the WMO ILC targets. Due to its high precision, the FTIR instrument is able to detect even small drifts in all components and is thus very well-suited as a travelling comparison instrument. This has been shown earlier for CO_2 and CH_4 by Hammer et al. (2013a) and it is confirmed here. Further we show this for the first time for N_2O.

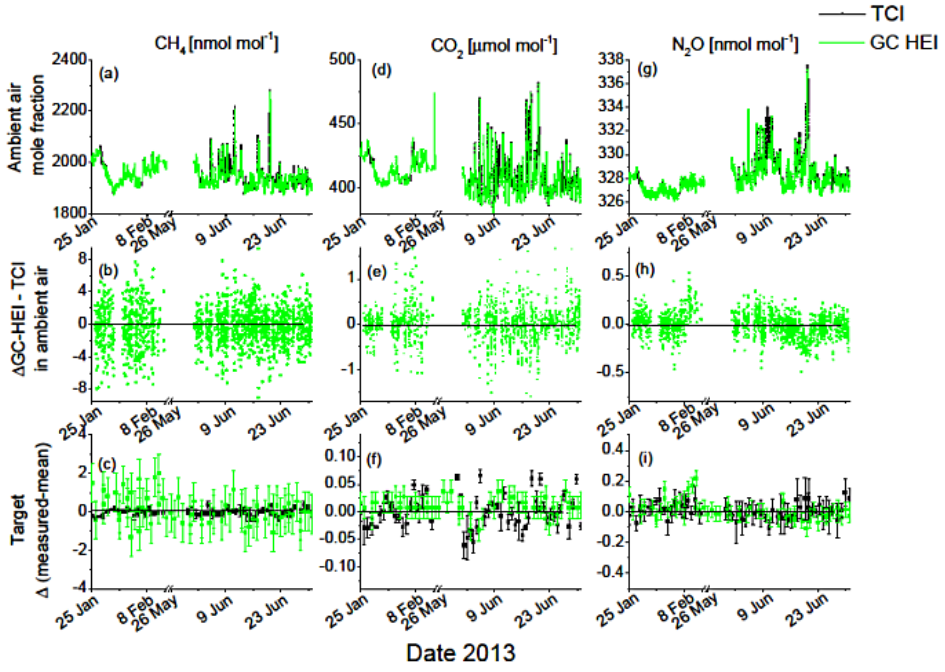

Figure 4. Upper panels: mole fraction of ambient air **(a)** CH_4, **(d)** CO_2 and **(g)** N_2O during the preparing and finalizing comparison periods in Heidelberg. From 25 January 2013 until 13 February 2013, both instruments were run in parallel, but with independent intake lines. From 1 June 2013 until 1 July 2013, both instruments used the same intake line. Middle panels: differences between the GC-HEI and the TCI for **(b)** CH_4, **(e)** CO_2 and **(h)** N_2O. Lower panels: TCI and GC-HEI daily target deviation from mean for **(c)** CH_4, **(f)** CO_2 and **(i)** N_2O. Notice the interruption in the x axis from February to May 2013 where the Mace Head measurement campaign took place.

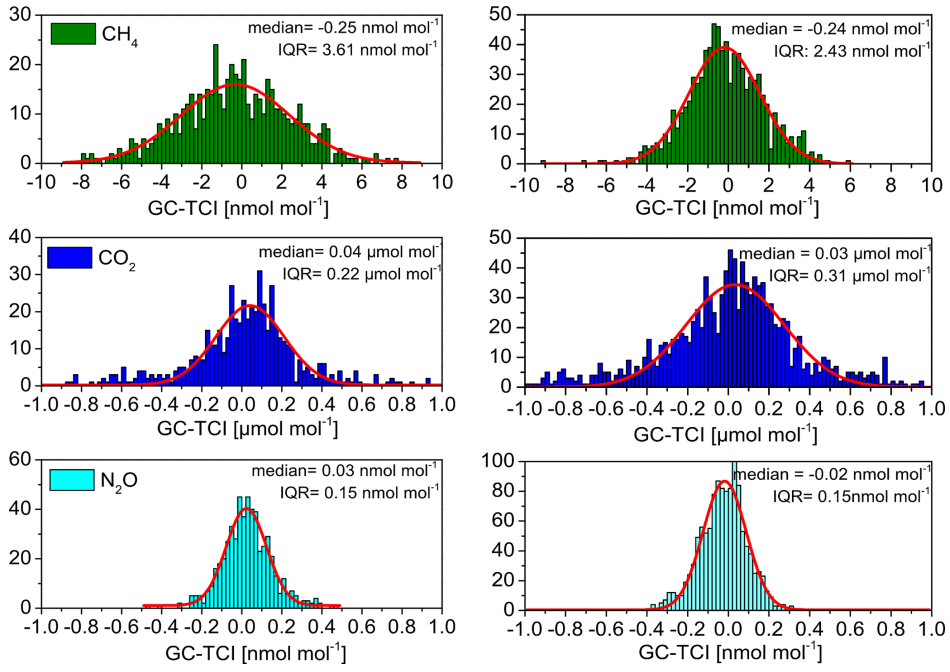

Figure 5. Distributions of the mole fraction differences measured with the GC-HEI and the TCI in Heidelberg (both with separate intake lines) from 25 January 2013 until 13 February 2013 (left panels) and from the 1 June 2013 to the 1 July 2013 with the same intake line (right panels). The red lines are Gauss fits to the distributions, IQR stands for interquartile range.

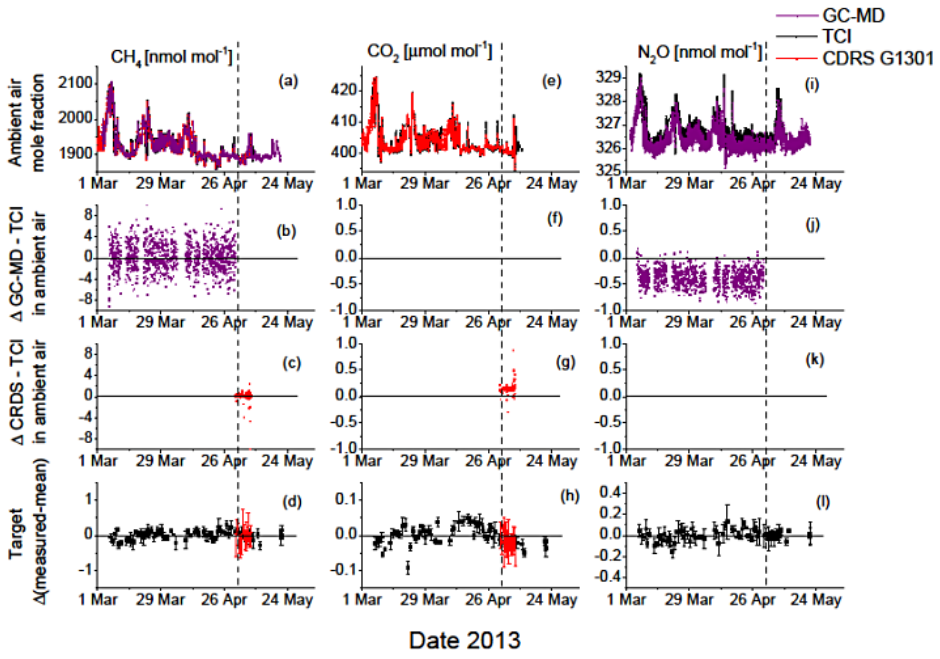

Figure 6. Upper panels: mole fraction of **(a)** CH_4, **(e)** CO_2 and **(i)** N_2O during the measurement campaign at Mace Head. All instruments were running in parallel with the TCI with independent intake lines to the same height. The GC-MD measured at a height of 10 m and the CRDS at a height of 25 m. On 1 May 2013, the TCI intake was switched on for 10 to 25 m (dashed vertical line). Here only comparisons of measurements made at the same height are shown and will be evaluated. Second row panels: difference between the GC-MD and the TCI for **(b)** CH_4 and **(j)** N_2O from 6 March 2013 until 1 May 2013. Third row panels: difference between the CRDS G1301 and the TCI for **(c)** CH_4 and **(g)** CO_2 from 1 May 2013 until 7 May 2013. Lowest panels: TCI and CRDS daily target measurement deviation from mean for **(d)** CH_4, **(h)** CO_2 and **(i)** N_2O. No GC-MD target measurements are available.

3.4.2 Comparison of ambient air measurements at Mace Head

At Mace Head, the TCI was connected to the intake line mounted at 10 m height from 6 March 2013 until 1 May 2013. Differences between the TCI and the GC-MD are shown in Fig. 6b and j and in Fig. 7 (left panels). From 1 May 2013 until 6 May 2013, the intake line of the TCI was mounted at a height of 25 m. During the measurements in May at 25 m height, the CRDS G2301 was not working and therefore only CRDS G1301 data are shown and compared here to the TCI (see Fig. 6c and g and Fig. 7 right panels). The flushing flow of the TCI intake line was adjusted to the flow of the GC-MD (ca. 5.5 slpm) so that the same ambient air was analysed simultaneously in both instruments. But ambient air measurements of the GC-MD are always discrete with a temporal resolution of about 20 min and without a buffer volume, whereas the TCI measurements are continuous and smoothed due to the TCI cell volume of 3 L flushed at 1 slpm. This should not introduce a bias into the averaged difference between both instruments, but the standard deviation of the distribution will be augmented slightly. The flushing flow of the TCI intake line was not adjusted to the flow of the CRDS G1301 (3.3 slpm) during the comparison period with the CRDS G1301. Further, the cavity volume of the CRDS is much smaller than that of the TCI. Therefore, essentially a slight temporal asynchrony can be introduced influencing the standard deviation of the differences. But comparison of the 1 min CRDS data with the 3 min TCI data (not shown here) revealed that both instruments measured temporally synchronously throughout the comparison.

The CH_4 measurements of the TCI, the GC-MD and the CRDS G1301 compare very well with each other. All differences lie within the WMO ILC targets. It is obvious that the scattering of the GC-MD is much larger than that of the CRDS (see Fig. 7) which is due to the higher reproducibility uncertainty of the GC-MD. The TCI target measurements were stable during the entire measurement period and showed a reproducibility of ± 0.12 nmol mol^{-1}. No target gas was measured with the GC-MD.

The CO_2 measurements of the CRDS G1301 and the TCI show an offset (CRDS G1301 – TCI) of 0.14 ± 0.04 µmol mol^{-1} (median and interquartile range (IQR), see Fig. 7 right panel). No CO_2 mole fraction dependence in the difference of both instruments was observed. The results of the ambient air measurements and the direct cylinder measurements do not agree with each other. This finding will be further discussed in Sect. 4.

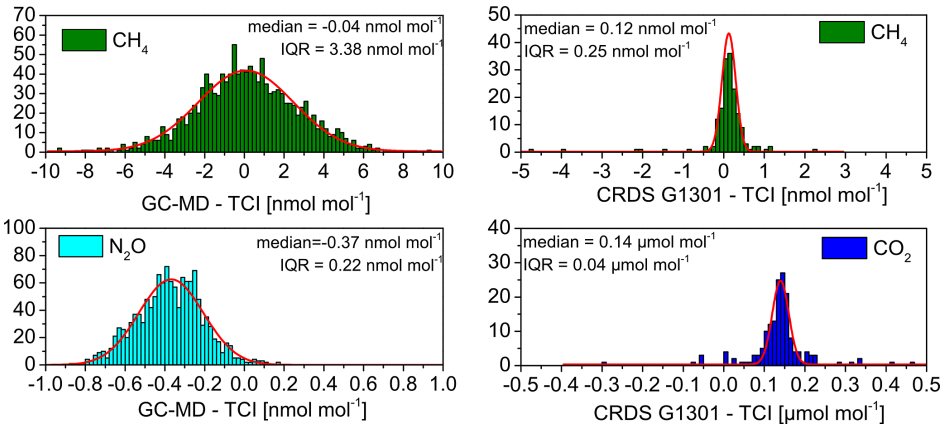

Figure 7. Left panels: distribution of the differences in CH_4 and N_2O between the discrete GC-MD measurements and the corresponding 3-minute averaged values of the TCI at Mace Head from 6 March 2013 until 1 May 2013 (both instruments with separate intake lines at a height of 10 m). Right panels: distribution of the differences between the hourly averaged CH_4 and CO_2 differences between the CRDS G1301 and the TCI from 1 May 2013 until 6 May 2013 (both instruments with separate intake lines at a height of 25 m). The red curves are Gauss fits to the distributions.

For N_2O, the ambient air measurements of the GC-MD and the TCI show a difference (GC-MD – TCI) of -0.37 ± 0.22 nmol mol^{-1} (median and IQR). A difference of -0.40 ± 0.06 nmol mol^{-1} (mean and standard error) was found for the direct cylinder gas comparison which is in very good agreement with the ambient air difference. The possible origin of the difference will also be discussed in Sect. 4.

4 Discussion of differences in ambient air measurements

The differences of the ambient air and calibration gas measurements as well as the sample intake effects of all instruments are summarized in Table 1.

4.1 Comparisons in Heidelberg

For CH_4, CO_2 and N_2O, the TCI and the GC-HEI ambient air measurements agreed within the WMO ILC targets before and after the measurement campaign. The compatibility between the GC-HEI and the TCI before and after the campaign at Mace Head, together with the stable TCI target gas record of CH_4, CO_2 and N_2O confirms the excellent performance of the TCI during the entire measurement campaign. Differences in CH_4, CO_2 and N_2O in direct cylinder measurements agreed within their uncertainties to differences in ambient air measurements. For N_2O, measurements with the GC-HEI were higher than with the TCI for direct cylinder analysis. This indicates that a TCI approach may potentially give more insight into differences between laboratories than direct cylinder measurement comparisons.

4.2 CH_4 comparison at Mace Head

At Mace Head, we found that the CH_4 measurements of the three different instruments, the FTIR (TCI), CRDS and GC-MD agree very well with each other better than the WMO ILC target value of ± 2 nmol mol^{-1} (WMO, 2009). The GC-MD obtained nearly the same values in the ambient air comparisons as the TCI (Table 1). The CRDS showed slightly higher CH_4 mole fractions, whereas the GC-HEI showed slightly lower CH_4 mole fractions. The good agreement between the CH_4 measurements of the two different networks NOAA and AGAGE also confirms that the measurements on the WMO CH_4 X2004 scale and the Tohoku University scale are very compatible (see also Dlugokencky et al., 2005).

4.3 CO_2 comparison at Mace Head

For CO_2, the difference in ambient air measurements at Mace Head between the TCI and the CRDS G1301 was 0.14 ± 0.04 µmol mol^{-1}. The working standards of the TCI as well as those of the CRDS G1301 have both been calibrated at the MPI-BGC GasLab in Jena (on the WMO X2007 scale). Therefore, possible scale propagation errors from WMO CCL primary standards to tertiary standards are not relevant for the ambient CO_2 mole fraction differences. Only scale propagation errors from tertiary to working standards at the MPI-BGC GasLab may principally contribute to this difference. However, large-scale transfer errors in the calibration of the TCI working standards seem unlikely since the difference between the assigned values of the Heidelberg WMO CCL tertiary cylinder gases and the TCI-measured values were only -0.03 ± 0.04 µmol mol^{-1} (see Fig. 1). Reference scale transfer errors in the calibration of the CRDS G1301 working standards have not been examined

Table 1. Median differences and interquartile ranges between the ambient air measurements (local instrumentation – TCI), mean difference and standard deviation of direct cylinder gas measurements and SIS effects (SIS – direct measurement) of the GC-HEI and the TCI in Heidelberg (before and after the measurement campaign) and of the GC-MD, the CRDS systems and the TCI at Mace Head.

Component		GC-HEI difference[1] before campaign	GC-MD difference[1]	CRDS G1301 [1] difference	CRDS G2301 difference	GC-HEI difference[2] after campaign
ΔCH_4	Ambient air	-0.25 ± 3.61	-0.04 ± 3.38	0.12 ± 0.25	–	-0.24 ± 2.43
(nmol mol^{-1})	Cylinder gases	-0.76 ± 0.22	-0.01 ± 1.58	-0.92 ± 0.46	-0.05 ± 0.42	–
	SIS effect of TCI	0.10 ± 0.35	-0.19 ± 0.15	-0.11 ± 0.13	-0.11 ± 0.13	–
	SIS effect of local instrument	-0.65 ± 3.50	–	0.13 ± 0.13	0.09 ± 0.10	–
ΔCO_2	Ambient air	0.04 ± 0.22	–	0.14 ± 0.04	–	0.03 ± 0.31
(µmol mol^{-1})	Cylinder gases	-0.02 ± 0.04	–	-0.00 ± 0.02	0.05 ± 0.03	–
	SIS effect of TCI	0.03 ± 0.07	0.03 ± 0.08	0.01 ± 0.08	0.01 ± 0.08	–
	SIS effect of local instrument	0.03 ± 0.11	–	-0.07 ± 0.12	-0.02 ± 0.03	–
ΔN_2O	Ambient air	0.03 ± 0.15	-0.37 ± 0.22	–	–	-0.02 ± 0.15
(nmol mol^{-1})	Cylinder gases	0.11 ± 0.05	-0.40 ± 0.06	–	–	–
	SIS effect of TCI	0.02 ± 0.07	0.08 ± 0.10	–	–	–
	SIS effect of local instrument	-0.04 ± 0.11	–	–	–	–

[1] Same sampling height, independent intake lines. [2] Same sampling height, same intake line as TCI.

so far, but direct analysis of cylinder gases by the CRDS G1301 yielded almost the same value as with the TCI (see Table 1), indicating excellent agreement of calibration. The discrepancy between the ambient air comparison and the direct cylinder gas comparison could possibly be due to a SIS effect of the CRDS G1301 or the TCI. However, the small and insignificant biases found (-0.07 ± 0.12 µmol mol^{-1} for the CRDS G1301 and 0.01 ± 0.08 µmol mol^{-1} for the TCI) would only explain slightly smaller CRDS G1301 values. The insignificant bias found during the SIS test can therefore not explain the CO_2 differences in ambient air measurements. Another reason for the difference between ambient air and cylinder measurements could be an incorrect water correction of the (not dried) G1301 instrument, which influences the wet ambient air measurement differently than the measurement of dry cylinder gas. However, it was found that an incomplete water correction could explain only 0.01–0.04 µmol mol^{-1} CO_2 of the difference. On the other hand, it seems worth noting that the difference between the two CRDS instruments was rather large during the direct cylinder measurements (0.06 ± 0.13 µmol mol^{-1}, see Fig. 2 and Table 1). This is surprising, since the same working standards were used for calibration of both instruments and since the CRDS instruments normally agree very well (target and ambient air differences usually agree within ca. 0.02 µmol mol^{-1}). Still, the differences between the CRDS G1301 and the TCI during ambient air measurements remain unexplained. Note that principally the calibration of the CRDS systems using synthetic working standards may introduce a bias into the CO_2 measurements (Nara et al., 2012), but should effect ambient air measurements to the same degree as direct real air cylinder measurements.

4.4 N_2O comparisons at Mace Head

For N_2O, the difference of ambient air measurements at Mace Head between the TCI and the GC-MD was found to be -0.37 ± 0.22 nmol mol^{-1} (GC-MD – TCI). Since a similar difference of -0.40 ± 0.06 nmol mol^{-1} was found for the direct cylinder gas measurements between both instruments, it is unlikely that the difference originates from the sample intake system. The difference in N_2O is significantly larger than the WMO ILC targets. Note, however, that the TCI is calibrated on the WMO N_2O X2006a scale whereas the GC-MD measured on the SIO-1998 scale. Hall et al. (2007) found a difference between the SIO-1998 and the WMO X2006 scale of 0.01 %, which corresponds to a difference of only $+0.03$ nmol mol^{-1} (SIO-1998 – WMO X2006). Scale update from WMO X2006 to WMO X2006a shows a mean difference for all calibrations in the ambient range of zero. But calibrations performed between 2007 and 2010 were still affected with the mean difference in the ambient range over this period being WMO2006A – WMO2006 $= -0.05$ nmol mol^{-1} (B. Hall, personal communication, 2013). Altogether, currently reported scale differences between WMO X2006a and SIO-1998 are all smaller than 0.1 nmol mol^{-1} and thus would not explain the observed differences in ambient air and direct cylinder gas measurements found during the Mace Head campaign.

Possibly, scale transfer errors from primary standards to working standards could partly explain this difference. For the WMO CCL tertiary standards, the reproducibility of N_2O assignments is about 0.08 nmol mol^{-1} (for the ambient range: 310–330 nmol mol^{-1}) (Hall et al., 2007). The scale transfer error of a set of tertiary cylinders will decrease with the number of tertiary cylinders; however the calibration errors are not always independent from each other, especially when tertiary standards were calibrated shortly after

each other. The calibration of working standards from WMO CCL tertiary standards introduces a further uncertainty. In our case, TCI working standards have been calibrated relative to a set of WMO CCL tertiary cylinder gases at the MPI-BGC GasLab in Jena. When analysing the Heidelberg WMO CCL tertiary cylinders by the TCI, no systematic difference in the ambient range was found (see Fig. 1). Therefore, we estimate the total scale transfer uncertainty from WMO CCL primary standards to working standards to be less than 0.1 nmol mol^{-1}.

Reference scale transfer uncertainties from SIO primary standards to tertiary standards used in the AGAGE network are generally small as well, as all working gases are calibrated at Scripps Institution of Oceanography (Prinn et al., 2000). Differences between high pressure tertiary SIO standards going to the stations and standards at low pressure when they are returned for recalibration at the Scripps laboratory are usually of the order of $\pm 0.03\,\%$ (1σ of the difference), which corresponds to about 0.1 nmol mol^{-1} in the ambient mole fraction range (R. Weiss, personal communication, 2013). This difference is thus a good upper estimate of scale transfer error in the AGAGE network. Merging the different scale propagation uncertainties, the observed difference of N_2O in ambient air between the GC-MD and the TCI includes a total uncertainty due to scale transfer which is of the order of 0.15 nmol mol^{-1}. Since the scale transfer uncertainty is smaller than the difference observed during the TCI campaign, this may point towards instrumental errors or to a potential difference between the two absolute scales. The absolute accuracy of the N_2O scales is due to uncertainties in the preparation of N_2O primary standards and is typically of the order of 0.3 nmol mol^{-1} (1σ standard deviation, Prinn et al., 2000; Hall et al., 2007). A scale difference of this order may therefore be possible, although it is not consistent with previous comparisons of the WMO X2006a and the SIO-1998 scales by Hall et al. (2007).

Intercomparison activities between the AGAGE network (on the SIO-1998 scale) and the NOAA flask network (WMO N_2O X2006a scale) are performed regularly and should capture a possible scale difference between both networks as well. The comparisons between AGAGE GC-MD in situ measurements and NOAA CCGG (carbon cycle greenhouse gases) flasks at five globally distributed observatories (Cape Grim, American Samoa, Trinidad Head, Mace Head and Ragged Point (Barbados)) show a mean difference between the two networks from August 2011 to August 2013 of -0.11 ± 0.14 nmol mol^{-1} (SIO-1998 – WMO N_2O X2006a). The comparison between AGAGE GC-MD in situ measurements and NOAA HATS (Halocarbons and other Atmospheric Trace Species) flasks at four common sites (Cape Grim, American Samoa, Trinidad Head and Mace Head) show a difference during the same time period of -0.14 ± 0.23 nmol mol^{-1} (both from P. Krummel, personal communication, 2013). Within their uncertainties, the difference between AGAGE and NOAA networks has been steadily increasing since the beginning of the intercomparison activity in 1994. The differences between the two networks found for the last two years during flask comparisons are within their uncertainties consistent with, however only about one third of, the differences found during the TCI comparison campaign at Mace Head (March–May 2013). This may reinforce the possibility of a current small-scale difference between the WMO X2006a scale and the SIO-1998 scale, which could be of the order of -0.1 to -0.4 nmol mol^{-1} (SIO-1998 – WMO X2006a). Note, however, that Thompson et al. (2014) estimated scale differences between SIO-1998 and WMO X2006a as having the opposite sign in the years from 1999 to 2009. This finding, along with our results during the TCI campaign, is in accordance with the intercomparison results at AGAGE sites showing a long-term trend of the flask–in situ difference. For the NOAA CCGG flasks the trend is about 0.04 nmol mol^{-1} per year and for NOAA HATS flasks the trend is about 0.08 nmol mol^{-1} per year (P. Krummel, personal communication, 2013).

5 Conclusions

New optical instrumentation allows measuring CH_4, CO_2 and also N_2O with very high precision, which essentially opens the door for merging data from different observation networks and estimating fluxes with great confidence. But even though a high compatibility between different instruments can be achieved (as shown for CH_4 and for the comparison period in Heidelberg), the compatibility between different networks still suffers from insufficient comparability of calibration scales, potential errors in scale transfer and also potential instrumental problems. It is thus of utmost importance to check, control and update the scale propagation for these greenhouse gases and assess in situ instrumentation and its calibration in order to be able to use the globally distributed data sets from different measurement programs for source, sink and flux estimation.

The comparison between the GC-MD and the TCI at Mace Head showed that the mole fraction measurements differ by ca. 0.4 nmol mol^{-1} in N_2O. This difference could partly be due to a general small reference scale difference between the WMO X2006a and the SIO-1998 scales and partly due to reference scale transfer and instrumental errors, such as remaining non-linearity effects.

The TCI campaign also showed differences between CO_2 measurements of the CRDS G1301 and the TCI as large as 0.14 µmol mol^{-1}, which were not seen when comparing the direct cylinder measurements. This difference between the direct measurement of target/standard gases and the ambient air measurements emphasizes the importance of the travelling instrument approach, which is a comprehensive comparison and quality control, and should include a sample intake system test and the entire evaluation process. But even though the origin of the discrepancy we found at Mace Head

could not be fully resolved so far, the TCI campaign revealed that there are possible problems with the CO_2 measurements and the water correction of the CRDS G1301, which need to be investigated in more detail. Earlier TCI campaigns at Cabauw, Netherlands, and Houdelaincourt (Observatoire Pérenne de l'Environnement, OPE), France, revealed differences in CO_2 between the TCI and the local instrumentation of $0.21 \pm 0.09\,\mu mol\,mol^{-1}$ and $0.13 \pm 0.10\,\mu mol\,mol^{-1}$ (TCI larger than local instrumentation contrary to the results from the TCI campaign at Mace Head) (Hammer et al., 2013a). Only between the GC-HEI and the TCI in Heidelberg were differences between both systems within the WMO ILC targets. This clearly shows the difficulty of performing compatible CO_2 measurements in the field and reaching the WMO ILC targets. Although in all three experiments working standards for the instruments had been calibrated in the same laboratory (MPI-BGC GasLab), CO_2 differences larger than $0.10\,\mu mol\,mol^{-1}$ remained between ambient air measurements that did not show up in direct calibration gas comparisons.

We can thus conclude that the TCI approach is well-suited as a comprehensive comparison measure. Due to the high precision of the TCI measurements in all three components, it was possible to detect even small differences and offsets between the greenhouse gas measurements of the local instruments and the TCI. Basically, the higher the precision and stability of the local instrument, the shorter the time period for parallel measurement of ambient air, but a comparison period of about 1 week still seems necessary to obtain satisfactory statistics and cover the typical range of ambient mole fractions. The preparation and follow-up processing of the campaign included a preparatory line test in Heidelberg and a preparatory and subsequent parallel measurement with the GC-HEI as well as direct measurements of working standards and/or target gases on every instrument.

As a proposal for improvement, calibrated data should be available within 24 h. This had already been pointed out by Hammer et al. (2013a), but has not yet transpired. Since the data evaluation is often time consuming, it was not performed in near-real-time, but only a month later for the CRDS and the GC-MD. Therefore, some problems were encountered only after the measurement campaign ended when additional tests could no longer be performed.

Finally, we were also able to demonstrate during the campaign at Mace Head that small gradients of CO_2 and CH_4 can be resolved. This starts a new era of highly precise atmospheric greenhouse gas observations and gradients, provided that calibration and systematic instrumental biases can be overcome.

Appendix A: Vertical mole fraction gradients of CH_4 and CO_2 at Mace Head

From 6 March 2013 to 1 May 2013 the TCI was measuring at 10 m height and the CRDS G1301 at 25 m height. Comparing the measurements at different heights along with measurements at the same height principally allows us to detect the vertical mole fraction gradients between 10 and 25 m. These may principally be used to estimate net greenhouse gases fluxes in the catchment area of the site. Since Mace Head station is located at the Atlantic coast, it samples two principally different regimes of air masses: a marine sector and a continental sector. As a criterion to distinguish between continental and marine air masses we use the ^{222}Rn daughter activity concentrations measured with a Heidelberg Radon monitor (Levin et al., 2002) at Mace Head station, that was installed there during the intercomparison campaign at about 5 m height. When the prevailing wind direction is from the west, the air masses have a marine footprint and the ^{214}Po concentration is low (< 0.5 Bq m^{-3}), whereas wind from other directions brings air masses with higher ^{214}Po concentrations (0.5–5 Bq m^{-3}) (see Fig. 8d). During the measurement campaign at Mace Head from the 6 March 2013 until 11 March 2013 and from the 18 March 2013 until 13 April 2013 the prevailing wind direction was from the east while from the 12 March 2013 until 18 March 2013 and from the 14 April 2013 until 30 April 2013 the main wind direction was from the west.

For the continental regime the median ^{214}Po activity concentration was 0.8 Bq m^{-3} and showed a diurnal cycle (green line in Fig. 8c). This variation is mainly caused by diurnal changes in the planetary boundary layer height because the ^{222}Rn flux from continental soils does not show a diurnal cycle. The data from the marine regime showed no significant diurnal cycle and a mean activity concentration of 0.2 Bq m^{-3}.

As a first step to determine vertical gradients, the differences between CRDS G1301 and TCI when measuring at the same height (i.e. from 1 May 2013–7 May 2013) must be compared. This comparison serves as a reference for determining the instrumental mole fraction differences. As described in Sect. 3, we found a difference between the CRDS G1301 and TCI measurements of 0.12 nmol mol^{-1} for CH_4 and 0.14 µmol mol^{-1} for CO_2. The difference when measuring at the same height (black curves in Fig. 8a, b) has no diurnal cycle, but shows this systematic offset. Other than the unresolved discrepancy between both instruments we therefore see no diurnal variation of mole fraction difference.

In a next step we compare the difference between instruments when measuring at different heights (25–10 m). For continental air masses we then see a weak diurnal cycle in CH_4. The mole fraction gradient decreases from ca. -1 nmol mol^{-1} during night time to -0.5 nmol mol^{-1} during day time (the TCI measurement at 10 m height being always higher than the CRDS measurement at 25 m height).

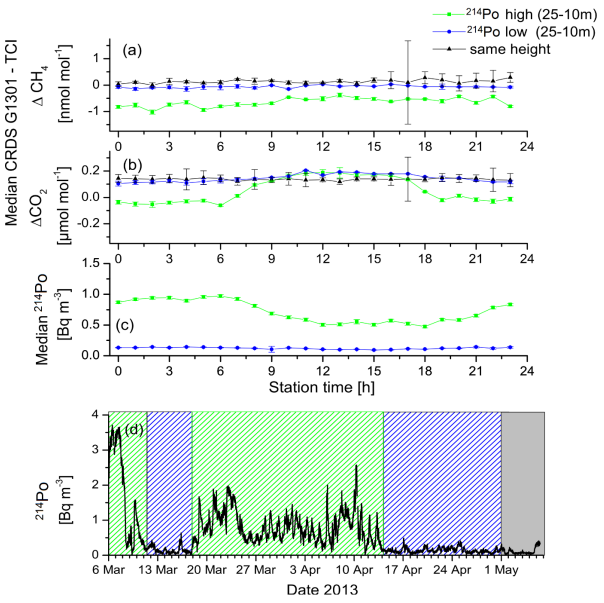

Figure A1. (a) Median diurnal CH_4 differences (CRDS G1301 – TCI) and **(b)** median diurnal CO_2 differences (CRDS G1301-TCI) between the CRDS G1301 at 25 m and the TCI at 10 m during periods of high (green) and low (blue) ^{222}Radon daughter (i.e. ^{214}Po) activity concentration and **(c)** median diurnal ^{214}Po activity concentration at about 5 m height a.g.l. during periods of high (green) and low (blue) ^{214}Po activity concentration (see Fig. 8d). Black symbols in **(a)** and **(b)** show the difference between instruments when measuring at the same height (25 m). Phases of continental (green) and marine (blue) air mass regimes during measurement at different heights are shown in **(d)**. The grey background at the end of the period denotes the time period when both instruments measured at the same height.

This finding suggests that there is a positive CH_4 flux from the ground throughout the whole day (24 h). For the marine air masses (low ^{214}Po activity concentration) there are only marginal differences in measured CH_4 compared to the measurements at the same height, which suggests only a very small or negligible CH_4 flux from the ocean. Supersaturation of CH_4 in the ocean mixed layer potentially leading to a CH_4 flux from the ocean to the atmosphere, has often been reported, but direct fluxes to the atmosphere due to this supersaturation are difficult to observe (Bakker et al., 2014).

For continental air masses we find a rather strong diurnal cycle in the CO_2 gradient. The difference between both levels (25–10 m) decreases during night from -0.16 to 0.06 µmol mol^{-1} relative to the offset between both instruments when measuring at the same height. The CO_2 level at 10 m height is thus higher than at 25 m height during the night time, but it is lower during the day time. This behavior is expected since ecosystem respiration during the night time leads to a positive CO_2 flux and plant photosynthesis during the day time leads to a CO_2 uptake. During marine air mass

regimes the diurnal cycle is decreased, but still a slight positive CO_2 flux from below is found during night time and a negative flux during the day time. This may either be due to surface ocean CO_2 respiration or uptake by phytoplankton or it might be due to some continental air mass influence also in the periods which we marked as marine situations. The latter would also explain the small CH_4 gradient. All in all, such small gradients of CO_2 (and CH_4) have, to our knowledge, not been resolved before. This shows that the modern instrumentation used here opens a new dimension in precision and evaluation of greenhouse gas measurements.

Acknowledgements. We are very grateful for the feedback, suggestions and input from B. Hall, P. Krummel, M. Ramonet, R. Weiss and C. Zellweger. We further thank D. Dodd and the Environmental Protection Agency, Ireland for providing the CRDS G1301 instrument data. We wish to thank M. Sabasch and D. Schmithuesen (both Institut für Umweltphysik) for their support during the campaign. This work has been funded by the InGOS EU project (284274). Further, we acknowledge the financial support given by Deutsche Forschungsgemeinschaft and Ruprecht-Karls-Universität Heidelberg within the funding program Open Access Publishing.

Edited by: J. B. Burkholder

References

Bakker, D. C. E., Bange, H. W., Gruber, N., Johannessen, T., Upstill-Goddard, R. C., Borges, A. V., Delille, B., Löscher, C. R., Naqvi, S. W. A., Omar, A. M., and Santana-Casiano, J. M.: Air-Sea Interactions of Natural Long-Lived Greenhouse Gases (CO_2, N_2O, CH_4) in a Changing Climate, in: Ocean-atmospheric interactions of gases and particles, edited by: Liss, P. S. and Johnson, M. T., Springer Verlag, 315 pp., doi:10.1007/978-3-642-25643-1, 2014.

Chen, H., Winderlich, J., Gerbig, C., Hoefer, A., Rella, C. W., Crosson, E. R., Van Pelt, A. D., Steinbach, J., Kolle, O., Beck, V., Daube, B. C., Gottlieb, E. W., Chow, V. Y., Santoni, G. W., and Wofsy, S. C.: High-accuracy continuous airborne measurements of greenhouse gases (CO_2 and CH_4) using the cavity ring-down spectroscopy (CRDS) technique, Atmos. Meas. Tech., 3, 375–386, doi:10.5194/amt-3-375-2010, 2010.

Chen, H., Dlugokencky, E., Hall, B., Kitzsis D., Novelli, P. C., and Tans, P. P: presentation at the 17th WMO/IAEA Meeting on Carbon Dioxide, Other Greenhouse Gases, and Related Measurement Techniques (GGMT-2013), Long-term stability of calibration gases in cylinders for CO_2, CH_4, CO, N_2O and SF_6, available at: http://ggmt-2013.cma.gov.cn/dct/page/70029 (last access: 17 February 2014), Beijing, China, 2013.

Crosson, E. R.: A cavity ring-down analyzer for measuring atmospheric levels of methane, carbon dioxide, and water vapor, Appl. Phys. B-Lasers O., 92, 403–408, 2008.

Cunnold, D. M., Steele, L. P., Fraser, P. J., Simmonds, P. G., Prinn, R. G., Weiss, R. F., Porter, L. W., Langenfelds, R. L., Wang, H. J., Emmons, L., Tie, X. X., and Dlugokencky, E. J.: In situ measurements of atmospheric methane at GAGE/AGAGE sites during 1985–2000 and resulting source inferences, J. Geophys. Res., 107, 4225, doi:10.1029/2001JD001226, 2002.

Dlugokencky, E. J., Myers, R. C., Lang, P. M., Masarie, K. A., Crotwell, A. M., Thoning, K. W., Hall, B. D., Elkins, J. W., and Steele, L. P.: Conversion of NOAA atmospheric dry air CH_4 mole fractions to a gravimetrically prepared standard scale, J. Geophys. Res., 110, D18306, doi:10.1029/2005JD006035, 2005.

Griffith, D. W. T., Deutscher, N. M., Caldow, C., Kettlewell, G., Riggenbach, M., and Hammer, S.: A Fourier transform infrared trace gas and isotope analyser for atmospheric applications, Atmos. Meas. Tech., 5, 2481–2498, doi:10.5194/amt-5-2481-2012, 2012.

Hall, B. D., Dutton, G. S., and Elkins, J. W.: The NOAA nitrous oxide standard scale for atmospheric observations, J. Geophys. Res., 112, D09305, doi:10.1029/2006JD007954, 2007.

Hammer, S.: Quantification of the regional H_2 sources and sinks inferred from atmospheric trace gas variability, Doctoral thesis, Heidelberg University, 2008.

Hammer, S., Konrad, G., Vermeulen, A. T., Laurent, O., Delmotte, M., Jordan, A., Hazan, L., Conil, S., and Levin, I.: Feasibility study of using a "travelling" CO_2 and CH_4 instrument to validate continuous in situ measurement stations, Atmos. Meas. Tech., 6, 1201–1216, doi:10.5194/amt-6-1201-2013, 2013a.

Hammer, S., Griffith, D. W. T., Konrad, G., Vardag, S., Caldow, C., and Levin, I.: Assessment of a multi-species in situ FTIR for precise atmospheric greenhouse gas observations, Atmos. Meas. Tech., 6, 1153–1170, doi:10.5194/amt-6-1153-2013, 2013b.

Jennings, S. G., Kleefeld, C., O'Dowd, C. D., Junker, C., Spain, T. G., O'Brien, P., Roddy, A. F., and O' Connor, T. C.: Mace Head Atmospheric Research Station – characterization of aerosol radiative parameters, Boreal Environ. Res., 8, 303-314, 2003.

Levin, I., Born, M., Cuntz, M., Langendörfer, U., Mantsch, S., Naegler, T., Schmidt, M., Varlagin, A., Verclas, S., and Wagenbach, D.: Observations of atmospheric variability and soil exhalation rate of radon-222 at a Russian forest site, Tellus B, 54, 462–475, doi:10.1034/j.1600-0889.2002.01346.x, 2002.

Masarie, K. A., Langenfelds, R. L., Allison, C. E., Conway, T. J., Dlugokencky, E. J., Francey, R. J., Novelli, P. C., Steele, L. P., Tans, P. P., Vaughn, B., and White, J. W. C.: NOAA/CSIRO Flask-Air Intercomparison Program: A strategy for directly assessing consistency among atmospheric measurements made by independent laboratories, J. Geophys. Res., 106, 20445–20464, doi:10.1029/2000JD000023, 2001.

Nara, H., Tanimoto, H., Tohjima, Y., Mukai, H., Nojiri, Y., Katsumata, K., and Rella, C. W.: Effect of air composition (N_2, O_2, Ar, and H_2O) on CO_2 and CH_4 measurement by wavelength-scanned cavity ring-down spectroscopy: calibration and measurement strategy, Atmos. Meas. Tech., 5, 2689–2701, doi:10.5194/amt-5-2689-2012, 2012.

Prinn, R. G., Weiss, R. F., Fraser, P. J., Simmonds, P. G., Cunnold, D. M., Alyea, F. N., O'Doherty, S., Salameh, P., Miller, B. R., Huang, J., Wang, R. H. J., Hartley, C., Steele, L. P., Sturrock, G., Midgley, P. M., and McCulloch, A.: A history of chemically and radiatively important gases in air deduced from ALE/GAGE/AGAGE, J. Geophys. Res., 105, 17751–17792, 2000.

Rella, C. W., Chen, H., Andrews, A. E., Filges, A., Gerbig, C., Hatakka, J., Karion, A., Miles, N. L., Richardson, S. J., Steinbacher, M., Sweeney, C., Wastine, B., and Zellweger, C.: High accuracy measurements of dry mole fractions of carbon dioxide and methane in humid air, Atmos. Meas. Tech., 6, 837–860, doi:10.5194/amt-6-837-2013, 2013.

Schulze, E. D., Luyssaert, S., Ciais, P., Freibauer, A., Janssens, I. A., Soussana, J. F., Smith, P., Grace, J., Levin, I., Thiruchittampalam, B., Heimann, M., Dolman, A. J., Valentini, R., Bousquet, P., Peylin, P., Peters, W., Rödenbeck, C., Etiope, G., Vuichard, N., Wattenbach, M., Nabuurs, G. J., Poussi, Z., Nieschulze, J., Gash, J. H., and the CarboEurope Team: Importance of methane and nitrous oxide for Europe's terrestrial greenhouse-gas balance, Nat. Geosci., 2842–2850, 2009.

Tans, P., Zhao, C., and Kitzis, D.: The WMO Mole Fraction Scales for CO_2 and other greenhouse gases, and uncertainty of the atmospheric measurements, Report of the 15th WMO/IAEA Meeting of Experts on Carbon Dioxide, Other Greenhouse Gases, and

Related Measurement Techniques, 7–10 September 2009, GAW Report No. 194, WMO TD No. 1553, 152–159, 2011.

Thompson, R. L., Chevallier, F., Crotwell, A. M., Dutton, G., Langenfelds, R. L., Prinn, R. G., Weiss, R. F., Tohjima, Y., Nakazawa, T., Krummel, P. B., Steele, L. P., Fraser, P., O'Doherty, S., Ishijima, K., and Aoki, S.: Nitrous oxide emissions 1999 to 2009 from a global atmospheric inversion, Atmos. Chem. Phys., 14, 1801–1817, doi:10.5194/acp-14-1801-2014, 2014.

WMO: Report of the 15th WMO/IAEA Meeting of Experts on Carbon Dioxide, Other Greenhouse Gases and Related Tracers Measurement Techniques (GGMT-2009), Jena, Germany, 7–10 September 2009, GAW Report No. 194, available at: http://www.wmo.int/pages/prog/arep/gaw/gaw-reports.html (last access: 17 February 2014), Jena, Germany, 2009.

Zellweger, C., Steinbacher, M., and Buchmann, B.: Evaluation of new laser spectrometer techniques for in-situ carbon monoxide measurements, Atmos. Meas. Tech., 5, 2555–2567, doi:10.5194/amt-5-2555-2012, 2012.

Zhou, L. X., Kitzis, D. R., Tans, P. P., Masarie, K., and Chao, D.: WMO round-robin inter-comparison: progress and a new website, Report of the 15th WMO/IAEA Meeting of Experts on Carbon Dioxide, Other Greenhouse Gases, and Related Tracers Measurement Techniques, 7–10 September 2009, GAW Report No. 194, WMO TD No. 1553, 212–217, 2011.

Publication 2

2.2 First continuous measurements of δ^{18}O-CO_2 in air with a Fourier transform infrared spectrometer

Vardag, S. N., Hammer, S., Sabasch, M., Griffith, D. W. T., and Levin, I.

Atmos. Meas. Tech., 8, 579–592, 2015
www.atmos-meas-tech.net/8/579/2015/
doi:10.5194/amt-8-579-2015

Atmospheric Measurement Techniques
Open Access

First continuous measurements of δ^{18}O-CO_2 in air with a Fourier transform infrared spectrometer

S. N. Vardag[1], S. Hammer[1], M. Sabasch[1], D. W. T. Griffith[2], and I. Levin[1]

[1]Institut für Umweltphysik, Heidelberg University, Heidelberg, Germany
[2]Department of Chemistry, University of Wollongong, Wollongong, Australia

Correspondence to: S. N. Vardag (svardag@iup.uni-heidelberg.de)

Received: 15 May 2014 – Published in Atmos. Meas. Tech. Discuss.: 3 July 2014
Revised: 27 October 2014 – Accepted: 7 January 2015 – Published: 4 February 2015

Abstract. The continuous in situ measurement of δ^{18}O in atmospheric CO_2 opens a new door to differentiating between CO_2 source and sink components with high temporal resolution. Continuous ^{13}C–CO_2 measurement systems have already been commercially available for some time, but until now, only few instruments have been able to provide a continuous measurement of the oxygen isotope ratio in CO_2. Besides precise $^{13}C/^{12}C$ observations, the Fourier transform infrared (FTIR) spectrometer is also able to measure the $^{18}O\,/\,^{16}O$ ratio in CO_2, but the precision and accuracy of the measurements have not yet been evaluated. Here we present a first analysis of δ^{18}O-CO_2 (and δ^{13}C-CO_2) measurements with the FTIR analyser in Heidelberg. We used Allan deviation to determine the repeatability of δ^{18}O-CO_2 measurements and found that it decreases from 0.25 ‰ for 10 min averages to about 0.1 ‰ after 2 h and remains at that value up to 24 h. We evaluated the measurement precision over a 10-month period (intermediate measurement precision) using daily working gas measurements and found that our spectrometer measured δ^{18}O-CO_2 to better than 0.3 ‰ at a temporal resolution of less than 10 min. The compatibility of our FTIR-spectrometric measurements to isotope-ratio mass-spectrometric (IRMS) measurements was determined by comparing FTIR measurements of cylinder gases and ambient air with IRMS measurements of flask samples, filled with gases of the same cylinders or collected from the same ambient air intake. Two-sample t tests revealed that, at the 0.01 significance level, the FTIR and the IRMS measurements do not differ significantly from each other and are thus compatible. We describe two weekly episodes of ambient air measurements, one in winter and one in summer, and discuss what potential insights and new challenges combined highly resolved CO_2, δ^{13}C-CO_2 and δ^{18}O-CO_2 records may provide in terms of better understanding regional scale continental carbon exchange processes.

1 Introduction

Quantitative understanding of the processes governing the carbon cycle is vital in order to assess the impact and fate of increasing anthropogenic CO_2 emissions to the atmosphere. The stable isotopes in CO_2 can provide information about the fluxes between the different carbon reservoirs, such as the atmosphere, the biosphere and the oceans. $^{13}CO_2$ measurements can be used to distinguish between terrestrial biosphere and marine fluxes (Keeling et al., 1989; Ciais et al., 1995), and are also used as a tracer for anthropogenic emissions, as most fossil fuel CO_2 emissions are depleted in ^{13}C relative to those of the biosphere (Tans, 1981). The interpretation of atmospheric δ^{18}O-CO_2 is more complex, since ^{18}O in CO_2 is strongly coupled to the water cycle (e.g. Francey and Tans, 1987; Farquhar et al., 1993; Cuntz et al., 2003a; 2003b, Buenning et al., 2014). During CO_2 exchange with soil and leaves, the ^{18}O isotopes of CO_2 are exchanged with those of H_2O (Hesterberg and Siegenthaler, 1991). Carbonic anhydrase facilitates the equilibration with leaf water (Gillon and Yakir, 2001; Farquhar et al., 1993). The isotopic composition of soil water is determined by the isotopic composition of precipitation, which itself has strong spatial variations (IAEA/WMO GNIP database available at http://isohis.iaea.org). Since precipitation at higher latitudes is depleted in ^{18}O (Dansgaard, 1964), the soil water and consequently

the CO_2 from root respiration and heterotrophic respiration is also depleted in ^{18}O at higher latitudes (Farquhar et al., 1993). The soil invasion flux will further influence the apparent soil respiration signature as the CO_2 diffuses into the soil, partially equilibrates with soil water and retro-diffuses out of the soil with a new isotopic composition (Tans, 1998; Miller et al., 1999). Isotopic exchange during soil invasion might even be enhanced due to carbonic anhydrase in soils (Wingate et al., 2009). Miller et al. (1999) reported that in most settings and especially in dry ground and for short residence times of air close to the soil surface (corresponding to high boundary layer mixing heights), the effect will be smaller than 5 ‰. Due to ^{18}O enrichment during evapotranspiration, the plant leaf water is enriched in ^{18}O relative to the soil water (Farquhar et al., 1993). During photosynthesis, CO_2 equilibrates with leaf water and about two-thirds of the CO_2 retro-diffuses into the atmosphere without being assimilated (Tans, 1998). The retro-diffused CO_2 changes the atmospheric δ^{18}O-CO_2 value, depending on the isotopic signature of the leaf water. In central Europe, we expect the discrimination against ^{18}O during net CO_2 assimilation to be positive (Farquhar et al., 1993; Cuntz et al. 2003b; Wingate et al., 2009). Still et al. (2009), Welp et al. (2011) and Buenning et al. (2014) have studied the susceptibility of atmospheric δ^{18}O-CO_2 to environmental parameters, such as precipitation, relative humidity, temperature, solar radiation and cloud cover, and estimated the influences of these parameters on the atmospheric δ^{18}O-CO_2 using regional and global scale models. They also assessed the effect of the isotopic composition of precipitation and water vapour. They found that many of these parameters should not be neglected when quantifying biospheric gross ^{18}O-CO_2 fluxes. They also highlight the complexity and the large uncertainties of the processes and sensitivities influencing atmospheric δ^{18}O-CO_2. Thus, in order to understand atmospheric δ^{18}O-CO_2 measurements in all their complexity, information about the regional isotopic composition of precipitation, environmental parameters such as temperature and water vapour deficit and a comprehensive land-surface model are necessary (Yakir and Wang, 1996; Ciais et al., 1997; Langendörfer et al., 2002; Cuntz et al., 2003a; Buenning et al., 2014).

The first step to understanding the ^{18}O-CO_2 fluxes to and from the terrestrial biosphere is to make reliable and comparable measurements at high temporal resolution. However, measurements via isotope-ratio mass-spectrometry (IRMS) are elaborate and time-consuming, limiting the number of continuous records of ^{18}O in CO_2 that exist to date (Flanagan et al., 1997; Langendörfer et al., 2002; Bowling et al., 2003; Pataki et al., 2003). A quantum cascade laser-based absorption spectrometer measuring $^{12}C^{16}O^{16}O$,$^{13}C^{16}O^{16}O$ and $^{12}C^{16}O^{18}O$ with a high temporal resolution provided first continuous records (Tuzson et al., 2011; Sturm et al., 2013). $^{12}C^{16}O^{16}O$ and $^{13}C^{16}O^{16}O$ have also been determined by Fourier transform infrared (FTIR) spectroscopy in several previous studies (e.g. Esler et al., 2000; Mohn et al., 2008; Cambaliza, 2010; Griffith et al., 2012). In principle, FTIR spectroscopy can also provide continuous measurements of $^{12}C^{16}O^{18}O$. However, in their original study, Esler et al. (2000) remarked that the degree of precision is too poor for a useful determination in natural abundances using a 1 cm^{-1} resolution spectrometer. Given improvements in the instrumentation and spectral analysis methods since that time, we have revisited the practicality of continuous measurements of $\delta^{18}O$ in CO_2 using FTIR spectroscopy.

The scope of this manuscript is to answer two important questions: first, is it possible to measure δ^{18}O-CO_2 using FTIR spectroscopy, and if yes, how well can we measure it in terms of precision, accuracy and compatibility to conventional IRMS observations? Second, what insight into regional scale carbon exchange processes can one gain from a highly resolved δ^{18}O-CO_2 record (along with the continuous CO_2, CO and δ^{13}C-CO_2 records) in the catchment area of our measurement site?

2 FTIR measurement principle and calibration procedure

The in situ FTIR analyser used in Heidelberg was developed and built at the University in Wollongong, Australia and is described in detail by Griffith et al. (2012) and Hammer et al. (2013a). It was used during two travelling instrument campaigns by Hammer et al. (2013b) and Vardag et al. (2014) for CO_2, CH_4 and N_2O measurements. Briefly, the FTIR spectrometer obtains a broadband transmittance spectrum of the sample air as the ratio of the infrared spectra measured with and without a sample in the optical cell. The measured transmittance spectrum is fitted by non-linear least squares using the program MALT (Multi-Layer Absorption Transmittance) to model the spectrum (Griffith, 1996; Griffith et al., 2012). The model adjusts sample composition and instrument parameters to obtain the best fit to the measured spectrum, and the best-fit sample concentrations are taken as the retrieved values.

The analyser is a prototype of the now commercially available Spectronus FTIR trace gas analyser (Ecotech, Knoxfield, Australia). While functionally equivalent, there are some component differences. The FTIR spectrometer is an IRcube (Bruker Optics, Ettlingen, Germany) coupled to a glass multipass White cell (model 24 PA, IRanalysis Inc., Anaheim, CA) with 3.5 L volume and 24 m optical path. Spectra were recorded at 1 cm^{-1} resolution and typically co-added to 3 min averages (approximately one cell exchange time at the typical flow rate). The sample handling system comprises four selectable inlets, an optional dryer (Nafion, Permapure PD-100T-24SS), followed by a granulated magnesium perchlorate trap), two mass flow controllers (model D-5111, Bronkhorst, Germany) and a four-head diaphragm vacuum pump (model MV2, Vacuubrand, Germany). One mass flow controller upstream of the cell controls sample air-

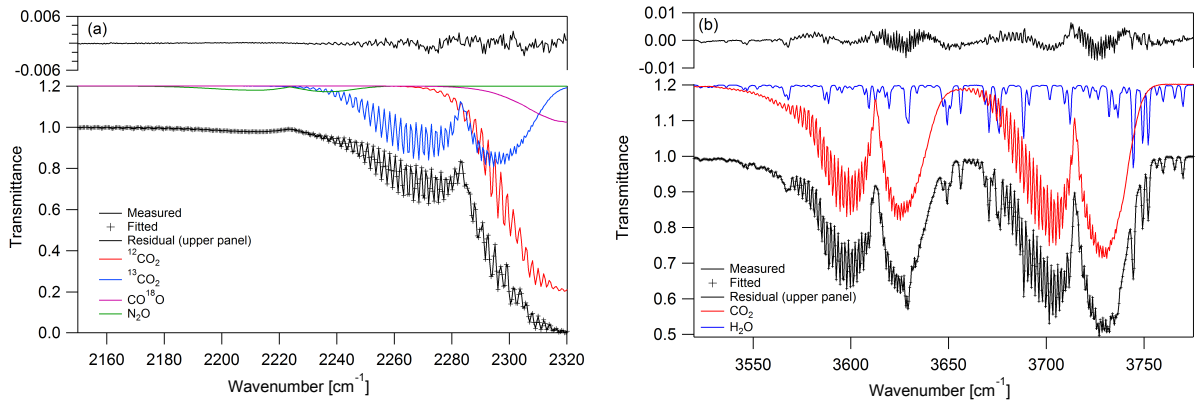

Figure 1. (a) Spectra of CO_2 isotopologues and N_2O in the 2150–2320 cm^{-1} region. The coloured traces show the individual isotopologues, the black spectra are a measured air spectrum (black line), calculated best-fit spectrum (+ symbols) and the fitting residual (black, upper panel). **(b)** Spectrum including CO_2 and H_2O near 3600 cm^{-1}. The individual trace gas and isotopologue spectra are shifted by 0.2 upwards for clarity.

flow, while the other downstream of the cell actively controls pressure via a proportional–integral software control loop to better than ±0.1 hPa. The FTIR housing and the cell are both thermostated and stable within 0.01 °C (1σ). A Windows PC controls sample flow, spectrum collection and online analysis. Sample air is delivered to the analyser at 1500–1800 hPa pressure through a clean diaphragm pump (model N86K.18, KNF Neuberger, Freiburg, Germany). In this work all measurements of both air samples and tank gases were dried (< 10 µmol mol^{-1} water vapour) and made at 1100 hPa pressure, 30 °C and a flow of 1 SLPM (standard litre per minute). The measurements were performed in the laboratory under stable temperature conditions (±1 °C).

Figure 1a shows the CO_2 isotopologue components (coloured traces) of the infrared absorption spectrum of air in the 2150–2320 cm^{-1} spectral region routinely used for CO_2 FTIR analysis by the analyser (Griffith et al., 2012). The black traces show a measured spectrum and typical fit to the composite air spectrum including $^{12}C^{16}O_2$, $^{13}C^{16}O_2$ and $^{12}C^{18}O^{16}O$. Although the $^{12}C^{18}O^{16}O$ isotopologue is heavily overlapped by the parent and $^{13}C^{16}O_2$ isotopologues, its contribution to the total absorption is significant and repeatable and provides the basis for quantification of this isotopologue. The upper panel of Fig. 1a shows a typical spectral residual which is well above the detector noise level above 2240 cm^{-1}. This residual is systematic and constant in shape from spectral fit to fit. The MALT spectrum calculation model is not able to improve this fit, which may be due to either (or both) an imperfect instrument line shape (ILS) or actual line shapes, which are not Voigt shaped as assumed in the model. To investigate the ILS contribution further, we have recorded spectra of air under the same conditions (temperature, pressure, resolution, cell path length) in a Bruker IFS 125/HR spectrometer at the University of Wollongong. This high resolution spectrometer is maintained in a well-aligned condition as part of the Total Carbon Column Observing Network (TCCON, Wunch et al., 2011) and its ILS is well characterised through high resolution test cell measurements (Hase et al., 2013) to be very close to the theoretically ideal shape calculated in the MALT model (modulation efficiency > 0.99, phase error $< 0.5°$). Fitting these IFS 125/HR spectra resulted in residuals very similar in shape and magnitude to that in Fig. 1a (upper panel), which indicates that imperfect ILS is not the primary cause of the lack of fit. To investigate the possible effects of non-Voigt molecular line shapes, typical FTIR analyser spectra were fitted with two independent spectrum fitting models, GFIT (Geoff Toon, Jet Propulsion Laboratory) and PROFITT (Frank Hase, Karlsruhe Institute of Technology). These spectrum models optionally extend to non-Voigt line shapes including effects of speed dependent cross sections, line narrowing and line mixing (e.g. Ngo et al., 2013). Using several different line shape models did not remove the spectral residuals – in some cases they were slightly reduced or of different shape, but total residuals were reduced by at most 25 %.

Thus, from these two tests we conclude that the residuals are not primarily due to an imperfect instrument line shape, but rather due to the inadequacy of currently available line shape models for the calculation. The imperfect fit is exacerbated by the fact that the residuals are dominated by absorption in the line wings of strongly absorbed lines, which are the least accurately modelled. We must therefore accept the imperfect fits as unavoidable until further advances in line shape models become available. If $^{12}C^{18}O^{16}O$ is removed from the fit, the residuals are two to three times larger; in this case, the least squares fit routine adjusts the amounts of $^{12}C^{16}O_2$ and $^{13}C^{16}O_2$ in the fit by unrealistic amounts to attempt to minimise the residual. The results in this paper show that the $^{12}C^{18}O^{16}O$ amount retrieved from fitting these

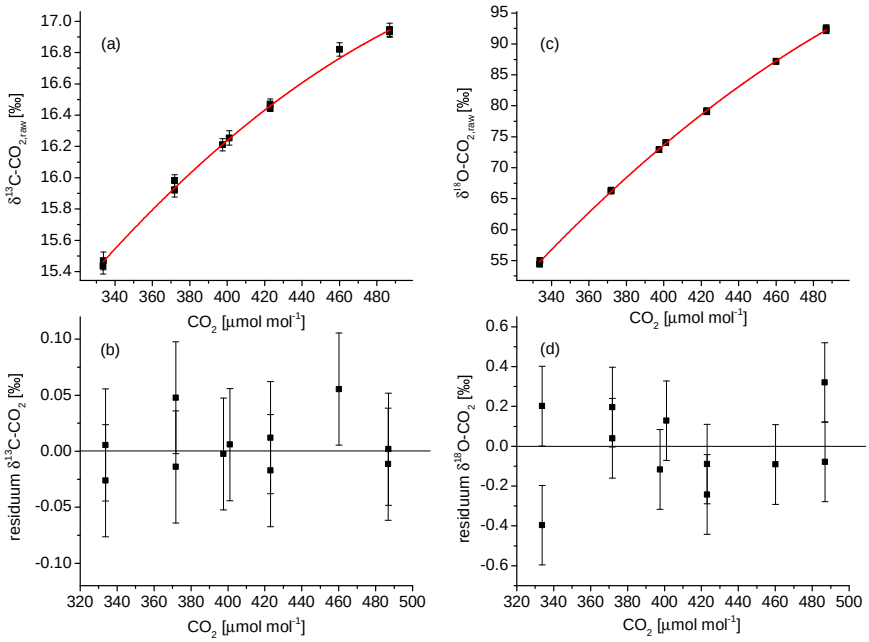

Figure 2. CO_2 dependence of raw δ^{13}C-CO_2 and δ^{18}O-CO_2 (**a** and **b**) and their residuals from the cubic fit (**b** and **d**). The experimental results shown here were obtained in August 2012; the same experiment was repeated in March 2014 and showed no significant difference to the earlier measurements.

spectra, despite the residuals, provides a consistent basis for quantification of this isotopologue.

Total CO_2 can also be retrieved from the region around 3600 cm^{-1} without isotopic discrimination. The fit to this region is shown in Fig. 1b, from Griffith et al. (2012). Retrieval of CO_2 from this region is more precise (i.e. lower noise, better repeatability) than that of $^{12}C^{16}O_2$ near 2300 cm^{-1}, firstly because the bands are not saturated and are of near optimum absorption (50 %), and secondly, because the whole bands have lower temperature sensitivity due to the inclusion of both high and low-J lines with both positive and negative temperature sensitivity. As detailed below, the total CO_2 retrieval, scaled if required, can be used as a proxy for $^{12}C^{16}O_2$ in isotopic calculations with acceptable accuracy.

2.1 Data evaluation and calibration

In the following, we describe the data evaluation and calibration procedure for the isotopologue ratio δ^{18}O-CO_2, but the procedure is analogous for δ^{13}C-CO_2.

Step 1: Calculate the raw δ^{18}O-CO_2 value from FTIR measurements

The FTIR computes the raw δ^{18}O-CO_2 value using the ratio of the raw value of the rare isotopologue and the raw value of the common isotopologue:

$$\delta^{18}\text{O-CO}_{2\text{HITRAN}} = \left[\frac{\left(\frac{^{12}C^{18}O^{16}O_{raw}}{^{12}C^{16}O^{16}O_{raw}}\right)_{sample}}{R_{HITRAN}} - 1 \right] \cdot 1000\ ‰ \qquad (1)$$

with $R_{HITRAN} = 0.0040104$ (Rothman et al., 2005). For ^{13}C, the equivalent value of R_{HITRAN} is 0.0112372.

Following Coplen (2011) and common usage, we use the terminology δ^{18}O-CO_2, even though the δ-notation is originally defined with the isotope ratio (in contrast to isotopologue ratio). The FTIR analysis implicitly uses the HITRAN scale (Rothman et al., 2005), which is referred to Vienna Pee Dee Belemnite (VPDB) for δ^{13}C and to Vienna Standard Mean Ocean Water (VSMOW) for δ^{18}O; during the calibration (step 3) the final reference scale of the calibrated data can be changed to any other scale. We chose the VPDB scale for δ^{13}C-CO_2 ($(^{13}C^{16}O_2/^{12}C^{16}O_2)_{VPDB} = 0.0112372$) and VPDB-$CO_2$ scale for δ^{18}O-CO_2 ($(^{12}C^{18}O^{16}O/^{12}C^{16}O_2)_{VPDB-CO_2} = 0.0041767$) following Allison et al. (1995). We abbreviate δ^{13}C-CO_2 and δ^{18}O-CO_2 on the VPDB-CO_2 scale with δ^{13}C-$CO_{2,VPDB}$ and δ^{18}O-$CO_{2,VPDB}$ respectively.

Step 2: Cross-sensitivity and interspecies interference corrections

To first order, the fitting software MALT takes into account pressure, temperature and interspecies overlapping absorp-

Table 1. Interspecies interference and cross-sensitivity correction factors for δ^{13}C-CO_2 and δ^{18}O-CO_2 used in Eqs. (2) and (3). Reference values were $T_{ref} = 31.8\,°C$, $F_{ref} = 1.0$ SLPM, $P_{ref} = 1100$ hPa and $H_2O_{ref} = 0$ µmole mole^{-1}, for temperature, flow, pressure and water vapour content, respectively.

	δ^{13}C-CO_2	δ^{18}O-CO_2
dC_{raw}/dT [‰ °C^{-1}]	0.127	4.256
dC_{raw}/dF [‰ SLPM^{-1}]	−0.91424	−2.92166
dC_{raw}/dP [‰ hPa^{-1}]	0.00249	−0.18694
dC_{raw}/dH_2O [‰ (µmole mole^{-1})$^{-1}$]	0	0
a [‰]	−10.344	−252.786
b [‰ (µmole mole^{-1})$^{-1}$]	0.0461902	1.162269
c [‰ (µmole mole^{-1})$^{-2}$]	−0.0000658108	−0.00179787
d [‰ (µmole mole^{-1})$^{-3}$]	0.000000034299	0.000001093919

tion bands in the fit. However, small second order effects remain due to real imperfections in temperature and pressure measurements, spectrometer instrumental line shape and the assumption of the MALT models (such as Voigt line shapes, see above), necessitating small empirical corrections to the raw measured mole fraction (C_{raw}) (Griffith et al., 2012; Hammer et al., 2013a). A cross-sensitivity correction for sample temperature (T) and pressure (P), H_2O amount and flow rate (F), as well as an interspecies-sensitivity correction for CO_2 mole fraction (corr(CO_2)) is applied for every measurement following Eq. (2):

$$C_{corr} = \frac{dC_{raw}}{dT} \cdot (T - T_{ref}) - \frac{dC_{raw}}{dF} \cdot (F - F_{ref}) - \frac{dC_{raw}}{dP} \cdot (P - P_{ref}) - \frac{dC_{raw}}{dH_2O} \cdot (H_2O - H_2O_{ref}) - \mathrm{corr}(CO_2) \quad (2)$$

Where P_{ref}, T_{ref}, etc. are the reference values to which pressure, temperature etc. are corrected, and the CO_2 correction follows:

$$\mathrm{corr}(CO_2) = a + b \cdot C_{raw} + c \cdot {C_{raw}}^2 + d \cdot {C_{raw}}^3 \quad (3)$$

Table 1 lists all cross-sensitivity parameters and CO_2-interspecies interference corrections.

Hammer et al. (2013a) describe in detail the set-up of the experiment to determine the CO_2 sensitivity. We use a cubic fit to describe the CO_2 interspecies correction (Fig. 2a and b; coefficient of determination $R^2 = 0.99$ for δ^{13}C-CO_2 and for δ^{18}O-CO_2), with residuals showing no further concentration dependence (Fig. 2b and d).

Step 3: Calibration

The cross-sensitivity corrected data are calibrated on the VPDB gas scale using a linear instrument response function (typically linear to the degree of $R^2 = 0.9998$). We derive the calibration response function weekly from three reference tanks with known values for CO_2, δ^{13}C-CO_2 and δ^{18}O-CO_2. Our reference standards span ranges from about 370 to 470 µmol mol^{-1} for CO_2 mole fraction, a δ^{13}C-$CO_{2,VPDB}$ range from −8.7 to −12.8 ‰ and a δ^{18}O-$CO_{2,VPDB}$ range from −1.9 to −5.0 ‰ as determined by the Heidelberg IRMS (Neubert, 1998).

Step 4: Smoothed working standard correction

We have found that regular measurements of different cylinder gases on the FTIR analyser show small but correlated sub-weekly variations of δ^{18}O-CO_2. One can thus use a smoothed working standard correction in order to account for these small instrumental variations on a sub-weekly time scale. For this purpose, we smooth daily working gas measurements using a 10-point moving average and interpolate the residual variation to the date of sample measurement using a cubic spline interpolation. We then subtract the smoothed residual variations from the long-term mean value of this gas vs. the reference standards from all sample measurements. By performing this correction, typically less than 0.2 ‰, the standard deviation of a weekly measured target or surveillance gas reaches about 0.2 ‰ for δ^{18}O-CO_2. Step 4 is not obligatory, but further increases the precision of the measurement. In the data presented in Sect. 4, we have applied this smoothed working standard correction.

Figure 3 illustrates the application for the entire calibration procedure. For δ^{13}C-CO_2, Fig. 3 shows raw (a), corrected (b) and calibrated (c) FTIR measurements against IRMS reference values of δ^{13}C-CO_2, and Fig. 3d shows the difference between calibrated FTIR measurements and IRMS values (FTIR-IRMS) against CO_2 mole fractions. Figure 3e–h show corresponding data for δ^{18}O-CO_2. The cross-sensitivity correction forces δ^{13}C-CO_2 and δ^{18}O-CO_2 onto a linear regression line (Fig. 3b and f), so that we can then apply a linear calibration. The large correction for δ^{18}O-CO_2 is most likely related to the systematic residual in the fitting of the spectra (Fig. 1a).

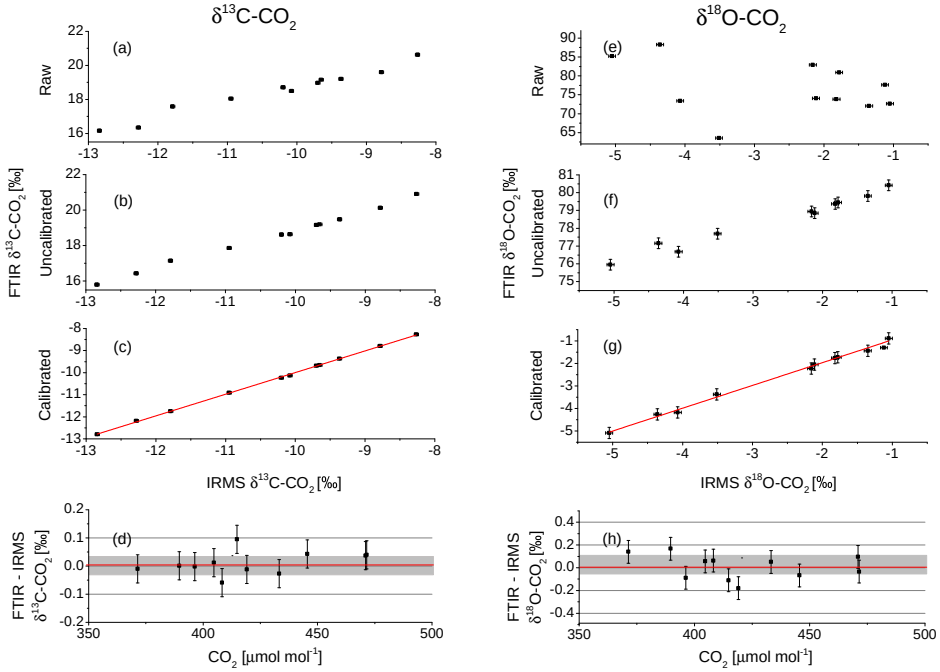

Figure 3. (a) Raw, **(b)** cross- and interspecies corrected (but still un-calibrated) and **(c)** calibrated δ^{13}C-CO_2 measurements and **(e)** raw, **(f)** cross- and interspecies corrected (but still un-calibrated); **(g)** calibrated δ^{18}O-CO_2 measurements of different target cylinders against the IRMS measurement of the same cylinders. Lowest panels: **(d)** calibrated FTIR δ^{13}C-CO_2 value minus reference value measured by the Heidelberg IRMS, **(h)** same as **(d)** for δ^{18}O-CO_2, both plotted versus the CO_2 mole fraction of the samples. The red lines in the lowest panels give the mean difference between the FTIR and the IRMS measurements. Grey areas illustrate the standard deviation of the differences.

2.2 Remarks on the calibration procedure

2.2.1 Using total CO_2 instead of $^{12}C^{16}O_2$ to calculate δ^{13}C-CO_2 and δ^{18}O-CO_2

As pointed out above, the precision of total CO_2 measurement in the 3600 cm^{-1} range is significantly higher ($\sim$ 50 %) than that of $^{12}C^{16}O_2$ in the region of 2300 cm^{-1}, due to an optimum absorption strength and a lower temperature sensitivity. $^{12}C^{16}O_2$, $^{13}C^{16}O_2$ as well as $^{12}C^{16}O^{18}O$ absorb in this region, but the minor isotopologue absorptions are weak and are barely distinguishable. Thus, we calculate the raw δ^{13}C-CO_2 and δ^{18}O-CO_2 values using total CO_2 from the 3600 cm^{-1} region instead of $^{12}C^{16}O_2$. There is a small bias between measurements of CO_2 and$^{12}C^{16}O_2$, but as long as the isotopic composition of the sample is close to the isotopic composition of the reference standards, the bias in δ^{13}C-CO_2 and δ^{18}O-CO_2 is negligible (< 0.03 ‰ for δ^{13}C-CO_2 and < 0.05 ‰ for δ^{18}O-CO_2) after calibration (step 3). However, for strongly depleted cylinder gases, as may be the case for synthetic gas mixtures, the biases may become as large as 0.2 ‰. If necessary, the bias introduced by total CO_2 can be corrected iteratively using Eqs. (8) and (9) of Griffith et al. (2012):

$$^{12}C^{16}O_2 = \frac{CO_2}{X} \quad (4)$$

where X is an isotopic partition sum with a value very close to unity.

2.2.2 Direct isotopologue calibration

Griffith et al. (2012) described two methods for calibration of isotopic fractionations, either

a. the isotopologue amounts are calibrated independently and the isotopologue δ values calculated directly from the calibrated isotopologue amounts, or

b. the isotopologue δ values are calculated from raw measurements of the isotopologues and the calibration is carried through on the δ-values.

These methods were referred to as “absolute” and “empirical” calibration respectively by Griffith et al. (2012), but to avoid ambiguity we will refer to them here as (a) isotopologue calibration and (b) ratio or δ-calibration. The correction and calibration method described above and used in this work is the ratio calibration, (b). In principle, it is equally valid to use (direct) isotopologue calibration. In this case, we

correct the isotopologue amounts $^{16}O^{12}C^{16}O$, $^{16}O^{13}C^{16}O$ and $^{16}O^{12}C^{18}O$ (step 2), calibrate them individually (step 3) and finally compute δ^{18}O-CO_2 and δ^{13}C-CO_2 from the calibrated amounts, i.e.

$$\delta^{18}O - CO_{2,VPDB} = \left[\frac{\left(\frac{^{12}C^{18}O^{16}O}{^{12}C^{16}O^{16}O}\right)_{sample}}{\left(\frac{^{12}C^{18}O^{16}O}{^{12}C^{16}O^{16}O}\right)_{VPDB-CO_2}} - 1 \right] \cdot 1000\,‰ \quad (5)$$

with $(^{12}C^{18}O^{16}O/^{12}C^{16}O_2)_{VPDB-CO_2} = 0.0041767$ (Allison et al., 1995), which takes into account that CO_2 contains two oxygen atoms.

In principle, both methods should lead to the same results, but they are sensitive to errors in different ways (Griffith et al., 2012). In practice, we find they differ by about 0.11 ± 0.03 ‰ for δ^{13}C-CO_2 and by 0.08 ± 0.15 ‰ for δ^{18}O-CO_2 (mean $\pm$ standard deviation for a 2-month period in 2014). The discrepancy between both calibration methods is most likely due to small inaccuracies in interspecies interference corrections. The ratio calibration requires a large CO_2-interspecies interference correction over a large CO_2 range (see Fig. 2c). Only if the CO_2 interspecies interference correction is well determined can we obtain a reliable δ^{18}O-CO_2 value from the ratio method. For the independent isotopologue calibration, no explicit interspecies CO_2 correction is required, but a very accurate determination of all CO_2 isotopologue calibration equations is vital. The decision on which method to use should thus be based on which correction can be performed with higher accuracy. In this work, we have found for the Heidelberg spectrometer that the empirical calibration method better fits the Heidelberg IRMS values.

2.3 Direct cylinder comparison to mass spectrometric values

In order to check the FTIR calibration as well as the compatibility of the FTIR and the Heidelberg IRMS Finnigan MAT 252, we analysed measurements of different test cylinders in March and April 2014 on both instruments. The IRMS values are linked to the VPDB scale via three pure CO_2 reference gases (RM8562, RM8563 and RM8564). The FTIR reference cylinders were calibrated by the IRMS and thus the FTIR and the IRMS are on the same scale. For all cylinder measurements with the IRMS, we filled cylinder air into evacuated flasks from an intermediate transfer volume; we then analysed these flasks by both techniques like regular flask samples, since pressure regulator effects have often disturbed the IRMS analyses. The precision of the IRMS is about 0.02–0.03 ‰ for δ^{13}C-CO_2 and 0.05–0.1 ‰ for δ^{18}O-CO_2 (standard deviation of repeated flask measurements). Further, Wendeberg et al. (2013) have shown that the Heidelberg IRMS scale does not exhibit any significant scale contraction errors or errors through cross contamination between sample and standard measurements in the IRMS. For more details on the IRMS, see Neubert (1998). A two-sample t test reveals that, at the 0.01 significance level, the means of the FTIR and the IRMS measurements (Fig. 3d and h) for δ^{13}C-CO_2 and for δ^{18}O-CO_2 do not differ significantly and thus, are compatible.

3 Characterisation of δ^{18}O-CO_2 and δ^{13}C-CO_2 measurements with the Heidelberg FTIR

3.1 Allan deviation

We performed an Allan deviation repeatability test (Werle et al., 1993; Werle et al., 2011) on the FTIR system over 6 days from 17 September 2011 to 23 September 2011, with flowing sample supplied from a reference gas cylinder with a δ^{13}C-CO_2 value of about -10.1 ‰ and a δ^{18}O-CO_2 value of about -3.7 ‰. We used the Allan deviation as a measure for the repeatability (following JCGM, 2008) as shown in Fig. 4. Allan deviation is the standard deviation of the pairwise differences between adjacent measurements averaged over different averaging periods. In the absence of drift and with only white (random) noise, the Allan deviation will decrease with the square root of the averaging time. We found that the Allan deviations after 10 min were δ^{13}C-$CO_2 = \pm 0.03$ ‰ and δ^{18}O-$CO_2 = \pm 0.25$ ‰ (Fig. 4a and b). After 30 min, the Allan deviations decrease to δ^{13}C-$CO_2 = \pm 0.02$ ‰ and δ^{18}O-$CO_2 = \pm 0.15$ ‰. From 2 hours to up to 1 day, the Allan deviations stayed below about δ^{13}C-$CO_2 = \pm 0.02$ ‰ and δ^{18}O-$CO_2 = \pm 0.10$ ‰. No significant increase in Allan deviation could be observed within 1 day, since drifts on this time scale are small compared to the noise. Further, we can confirm that the frequency of smoothed working standard correction is adequate, since between daily working standard gas measurements the system remains stable within 0.02 ‰ for δ^{13}C-CO_2 and 0.10 ‰ for δ^{18}O-CO_2. In Heidelberg, a typical diurnal variation of δ^{18}O-CO_2 is of the order of 1 ‰ (see Sect. 4). Thus, the system is stable enough to resolve diurnal ambient δ^{18}O-CO_2 variations (see Sect. 4).

3.2 Intermediate measurement precision

We monitored the intermediate measurement precision (following JCGM, 2008) by measuring standard gases every day or week under reproducible conditions. The averaging time for each cylinder measurement was 9 min. We used the standard deviation of the 9 min cylinder gas averages to estimate the intermediate measurement precision of our instrumental set-up. For δ^{13}C-CO_2 and δ^{18}O-CO_2, we found that the intermediate measurement precision was 0.04 ‰ and 0.27 ‰, respectively for the period from December 2012 to October 2013 (see Fig. 5a and b). The Allan deviation at 9 min is very close to the standard deviation of the daily working cylinder measurements, which shows that for our system and laboratory conditions the repeatability dominates the intermediate measurement precision.

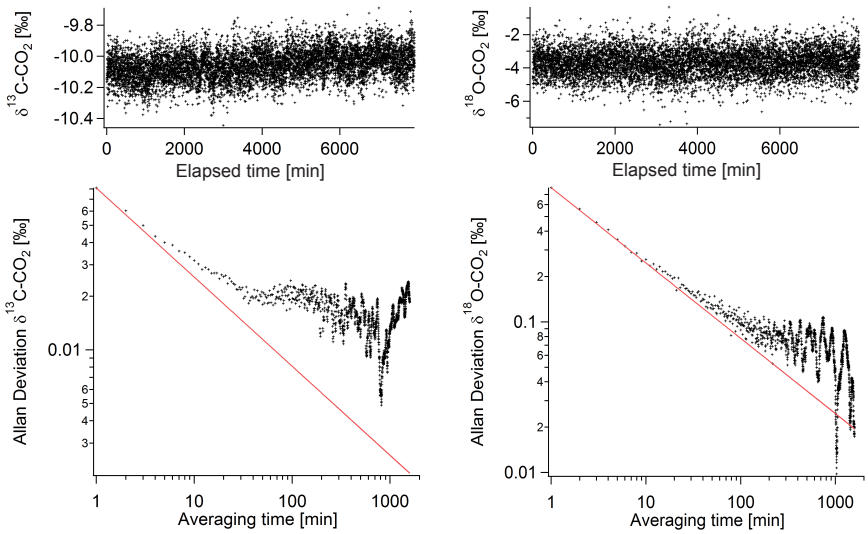

Figure 4. Allan deviation of δ^{13}C-CO_2 (left) and δ^{18}O-CO_2 (right) measured over the course of 6 days in September 2011 with the FTIR.

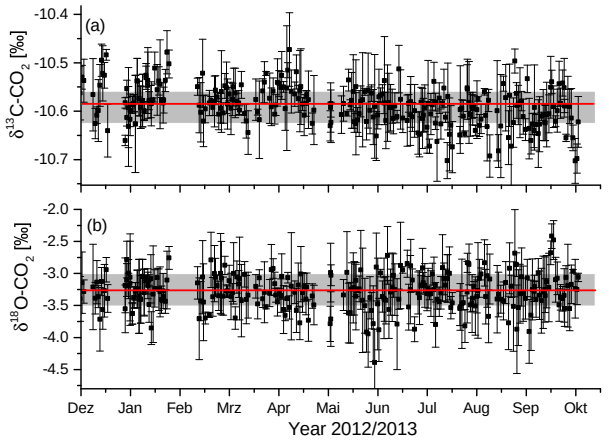

Figure 5. Repeated daily working gas measurements (9 min averages) depict an intermediate measurement precision of **(a)** ±0.04 ‰ for δ^{13}C-CO_2 and of **(b)** ±0.27 ‰ for δ^{18}O-CO_2 **(b)** for the period from December 2012 to October 2013. Red lines: mean values, grey areas: standard deviation.

Note that in our calibration procedure we now use the daily measured cylinder (working standard gas) in a final correction step (step 4) to account for sub-weekly variations of the instrument response. Since we only recognised the need to correct for this variability well after commencement of the measurements, we do not yet have a long-term record for a real surveillance cylinder. Therefore, Fig. 5 displays the working standard measurements without any sub-weekly smoothing applied, and thus gives an upper estimate of the intermediate measurement precision of real measurements where we apply step 4 of our calibration procedure in addition.

3.3 Compatibility of ambient air measurements

In the previous sections, we have evaluated the repeatability, as well as the intermediate measurement precision of the FTIR measurements. The results make us confident that the FTIR spectrometer is of sufficient precision and stability to resolve atmospheric signals, such as the diurnal variation of δ^{13}C-CO_2 and δ^{18}O-CO_2. Further, we have shown in Sect. 2.3 that the FTIR cylinder gas measurements are compatible to those of the Heidelberg IRMS. In order to show that not only the direct cylinder measurements, but also the ambient air measurements are compatible with the IRMS analyses, we compared in situ ambient air samples, which we measured with both instruments.

For this purpose, an automated flask sampler (Neubert et al., 2004) collected dried (dew point −40 °C) ambient air from the same intake line as the FTIR into 2.5 litre glass flasks. Every flask was flushed with a flow rate of about 1.1 SLPM for 2 h and then pressurised to 2000 hPa absolute pressure and closed. Then the automated flask sampler opened, flushed and filled the next flask to 2000 hPa. Pressurising the flasks took about 5 min. With this procedure, we were able to capture a diurnal isotopic profile with a 2-hourly resolution in the flasks, which could be analysed by mass spectrometry. We then compared these values to the continuous values measured by the FTIR spectrometer; the results are shown in Fig. 6. We used 9 min averaged values from the FTIR spectrometer to compare them to the flask results to account for atmospheric variability and to minimise differences due to lack of temporal synchronisation between the event sampler and the FTIR, and to reduce the noise on the FTIR measurement. We found that the mean residual and standard error is 0.01 ± 0.02 ‰ for δ^{13}C-CO_2 and 0.08 ± 0.14 ‰ for δ^{18}O-

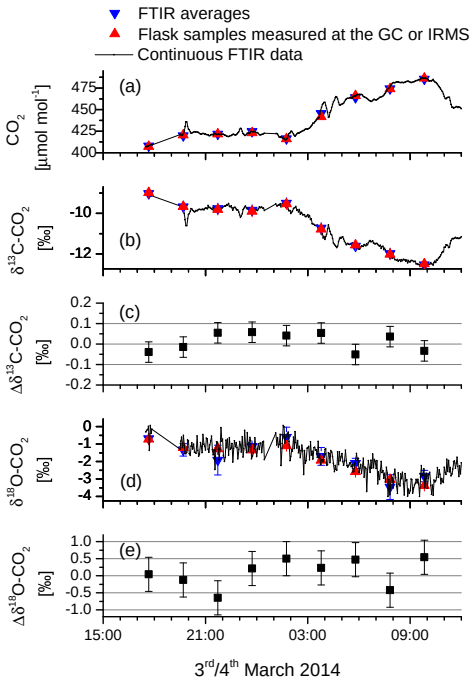

Figure 6. Diurnal cycle event sampled on the 3–4 March 2014 at the Institut für Umweltphysik in Heidelberg. Red: GC concentration (in case of CO_2) or IRMS isotopologue value (in case of isotopologues) of flasks samples; blue: 9 min averaged values from FTIR; black: continuous 3 min values from the FTIR. **(a)** CO_2 mole fraction; **(b)** δ^{13}C-CO_2 value; **(c)** residual of 9 min average δ^{13}C-CO_2 FTIR and IRMS measurement (FTIR - IRMS); **(d)** δ^{18}O-CO_2 value; **(e)** residual of 9 min averaged δ^{18}O-CO_2 FTIR and IRMS measurement (FTIR – IRMS). All error bars on the (blue) averaged FTIR data are the standard deviation during the 9 min of averaging time. The error bars on the (red) IRMS values show the typical intermediate measurement precision of our IRMS measurements. The residual (FTIR-IRMS) has an error bar, which combines the IRMS uncertainty and the FTIR uncertainty and the variability of atmospheric signal during the flask filling time.

CO_2 (FTIR – IRMS). We tested the compatibility between the FTIR and the IRMS ambient air measurements with a two-sample t test and found that at the 0.01 significance level, the means of the FTIR and the IRMS measurements in ambient air do not differ from each other for δ^{13}C-CO_2 or for δ^{18}O-CO_2. Note, that the standard deviation of the differences between the FTIR and the IRMS is 0.05 ‰ for δ^{13}C-CO_2 and 0.42 ‰ for δ^{18}O-CO_2 and with that the standard deviation for δ^{18}O-CO_2 differences is higher than expected from the combined Allan deviation (0.25 ‰ for 9 min averages) and the uncertainty of the IRMS measurement (ca. 0.05–0.1 ‰).

The slightly larger variability in δ^{18}O-CO_2 ambient air comparison than in cylinder gas comparisons (Sect. 2.3) reflects the fact that there are more contributions to the difference between the FTIR and the IRMS flask measurement. There are the storage effect of the flasks themselves, which could be slightly wet and thus alter the δ^{18}O value of the CO_2 in the flask, or some other possible interference of the automated flask sampler (i.e. varying integration time due to flow and pressure variations).

4 Example period of continuous trace gas and stable isotopologue measurements in Heidelberg

In this section, we illustrate how we might potentially use a highly resolved δ^{18}O-CO_2 record at a typical European monitoring station, such as Heidelberg, in order to disentangle regional scale carbon exchange processes. Note, however, that for a quantitative evaluation, we would require explicit information on local CO_2 source signatures and on the exchanging water reservoirs. We look here at two very different periods in which the FTIR measured δ^{18}O-CO_2 along with δ^{13}C-CO_2, total CO_2 and CO in Heidelberg (see Fig. 7).

In order to interpret the atmospheric δ^{18}O-CO_2 variation, we must estimate the isotopic signature or discrimination of the processes influencing the isotopic content. The Heidelberg catchment area is typical of many European urban areas with the most important CO_2 fluxes associated with plant photosynthesis, leaf and soil respiration, as well as fossil fuel burning. In the greater catchment area, discrimination during photosynthesis tends to enrich atmospheric CO_2 with respect to ^{13}C and ^{18}O (Cuntz et al., 2003b). Typical mean δ^{13}C fractionation relative to the atmosphere during photosynthesis is about – (2–8) ‰ for C4 plants and about – (12–20) ‰ for C3 plants (Mook, 1994). As a first approximation, the $^{13}CO_2$ / $^{12}CO_2$ ratio captured during photosynthesis is released during respiration, which leads to an overall depletion of the atmospheric $^{13}CO_2$ / $^{12}CO_2$ ratio. In addition, ^{18}O discrimination during respiration tends to deplete the atmosphere in its δ^{18}O-CO_2 value. Neubert (1998) measured the isotopic composition of soil-respired CO_2 in the surroundings of Heidelberg and found values of $\delta^{18}O\text{-}CO_{2,VPDB} \approx -10$ ‰ with a tendency of slightly more depleted values in winter (−15 ‰) than in summer (−5 ‰) and $\delta^{13}C\text{-}CO_{2,VPDB} \approx -25$ ‰. For the discrimination during photosynthesis, typical mean values for the central European continent are between 0 and +20 ‰ for ^{18}O (Farquhar et al., 1993; Cuntz et al., 2003b). Further, the invasion flux will influence the apparent soil respiration signature (Tans, 1998; Miller et al., 1999), but we cannot quantify the magnitude of this effect for our catchment area without intensive sampling and isotopic soil flux modelling. Therefore, we only consider the invasion flux in a sense that a larger range must be attributed to the signature of the apparent soil respiration flux when qualitatively discussing our atmospheric δ^{18}O-CO_2 records here.

For the isotopic signature of fossil fuels, most studies assume a common δ^{18}O fossil fuel signature of $\delta^{18}O\text{-}CO_{2,VPDB} \approx -17$ ‰, corresponding to the ambient oxy-

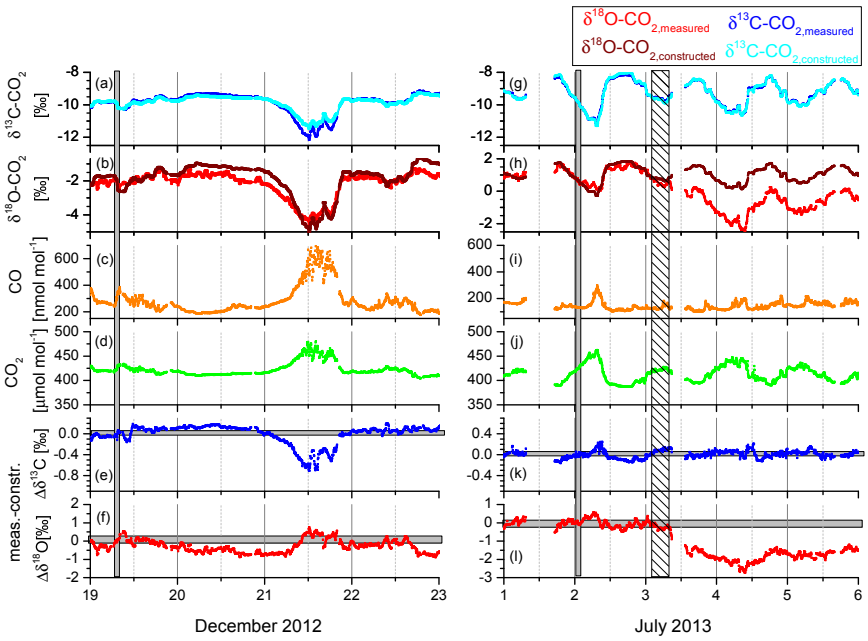

Figure 7. Trace gas records in winter (left panel) and summer (right panel) in Heidelberg. **(a)** and **(g)** show the measured (dark blue) and artificially constructed (light blue) δ^{13}C-CO_2 value, **(b)** and **(h)** the measured (red) and artificially constructed (burgundy) δ^{18}O-CO_2 value, **(c)** and **(i)** the measured CO value, **(d)** and **(j)** the measured CO_2 value. Panels **(e)** and **(k)** give the difference between the measured and constructed δ^{13}C-CO_2 value with a mean isotopic source signature of δ^{13}C-$CO_{2,\mathrm{VPDB}} \approx -25$ ‰ in the wintertime and δ^{13}C-$CO_{2,\mathrm{VPDB}} \approx -27$ ‰ in the summertime. Panels **(f)** and **(l)** give the difference between the measured and constructed δ^{18}O-CO_2 value with a mean isotopic signature of δ^{18}O-$CO_{2,\mathrm{VPDB}} \approx -28$ ‰ in the wintertime and δ^{18}O-$CO_{2,\mathrm{VPDB}} \approx -12$ ‰ in the summertime. Grey vertical bars indicate the "reference periods", in which the isotopic source signature for artificially constructed δ^{13}C-CO_2 and δ^{18}O-CO_2 was determined from Keeling plots of about 20 individual atmospheric 3 min average measurements. The dashed vertical bar in the right panel shows a period of high precipitation. Grey horizontal bars in **(f)** and **(l)** mark the 1σ-uncertainty of the isotope measurements.

gen isotopic signature, but incomplete combustion can lead to a range of different isotopic signatures. The ^{18}O signature of fossil fuel emissions varies from about δ^{18}O-$CO_{2,\mathrm{VPDB}} \approx -11$ to -40 ‰ (Schumacher et al., 2011). Traffic exhausts tend to be less depleted in ^{18}O relative to other fossil fuel CO_2 emissions (δ^{18}O-$CO_{2,\mathrm{VPDB}} \approx -15$ ‰), followed by natural gas burning (δ^{18}O-$CO_{2,\mathrm{VPDB}} \approx -28$ ‰). Combustion of coal, on the other hand, leads to a δ^{18}O-CO_2 value of about -38 ‰ (Schumacher et al., 2011). To our knowledge, the potential range of these values is not well known. For δ^{13}C, typical signatures are δ^{13}C-$CO_{2,\mathrm{VPDB}} \approx -29$ ‰ for traffic exhausts, -25 ‰ for coal combustion and -39 ‰ for natural gas emissions (Widory and Javoy, 2003; Kaul, 2007). With these examples of isotopic signatures, we can now look at our atmospheric CO_2 records that show values of δ^{13}C-CO_2 between δ^{13}C-$CO_{2,\mathrm{VPDB}} \approx -8$ and -12 ‰, while δ^{18}O-CO_2 varies between δ^{18}O-$CO_{2,\mathrm{VPDB}} \approx -2$ to -4 ‰ in winter and 0 to -2 ‰ in summer (Fig. 7).

Since all CO_2 sources with a negative isotopic signature relative to atmospheric CO_2 lead to δ^{13}C-CO_2 or δ^{18}O-CO_2 depletion, a differentiation between different depleting sources is difficult. Therefore we used the following approach: We first constructed an artificial δ^{13}C-CO_2 and δ^{18}O-CO_2 record using the slope (a_{ref}) and offset (b_{ref}) of so-called "Keeling plots" (Keeling, 1958), determined from measured atmospheric δ- and CO_2 concentration values in an exemplary and short nighttime reference period (grey bars in Fig. 7) according to:

$$\delta_{\mathrm{meas}} = a_{\mathrm{ref}} \cdot \frac{1}{\mathrm{CO_2}} + b_{\mathrm{ref}} \quad (6)$$

Note that in the nighttime reference periods, for which the reference slope and offsets were calculated, we can neglect photosynthetic sinks. Therefore, we can interpret the δ^{13}C source signature of the reference period as the flux-weighted average of all sources (Miller and Tans, 2003). We then applied the parameters (a_{ref} and b_{ref}) from the reference period to the entire CO_2 record to calculate artificially constructed $\delta^{13}C_{\mathrm{constr}}$ and $\delta^{18}O_{\mathrm{constr}}$ values:

$$\delta_{\mathrm{constr(t)}} = a_{\mathrm{ref}} \cdot \frac{1}{\mathrm{CO_2(t)}} + b_{\mathrm{ref}}, \quad (7)$$

Fig. 7a, b, g and h show the constructed δ^{13}C-CO_2 and δ^{18}O-CO_2 records in burgundy and light blue. During the ref-

erence period in which the Keeling plot slopes and offsets were derived, the Keeling plot had a high correlation coefficient ($r^2 > 0.85$) and showed an isotopic ^{13}C and ^{18}O source signature that was typical for the respective season (source δ^{13}C-$CO_2 \approx -25$ ‰ in the winter and -27 ‰ in the summer period, δ^{18}O-$CO_2 \approx -28$ ‰ in the winter and -12 ‰ in the summer period). To identify influences from enriching or depleting sources and sinks relative to those in the reference period, we then calculated the difference between the measured and the artificially constructed (Eq. 6) δ^{13}C-CO_2 and δ^{18}O-CO_2 record (Fig. 7e, k, f and l):

$$\Delta\delta(\mathrm{t}) = \delta_{\mathrm{meas}}(\mathrm{t}) - \delta_{\mathrm{constr}}(\mathrm{t}). \quad (8)$$

Negative $\Delta\delta$ values occur in periods when the apparent sources are more depleted than in the reference period and positive values occur when apparent sources are more enriched than in the reference period. During photosynthetic CO_2 uptake, the equilibration of back-diffusing CO_2 with enriched leaf water leads to an enrichment of atmospheric δ^{18}O-CO_2 and thus to positive $\Delta\delta^{18}$O values. We now have a tool that allows differentiation between more and less depleted fluxes relative to the reference period.

In the wintertime, relative fossil fuel contributions in the Heidelberg catchment area are higher than in the summertime (Levin et al., 2003). Fossil fuel CO_2 emissions lead to high concentration of CO_2 (Fig. 7d) and deplete atmospheric CO_2 in its heavy isotopes ^{13}C and ^{18}O (original measurements: dark blue and red in Fig. 7a, b). During incomplete combustion of fossil fuels, CO (Fig. 7c) is often emitted as well. A typical example of a pollution event is shown in Fig. 7 (left panel) on 21 December 2012. The difference between the measured and artificially constructed δ^{13}C-CO_2 (Fig. 7e) decreases rapidly on 21 December. Environmental parameters such as relative humidity, global radiation and temperature (not shown here) remain constant during the event, but low wind speed leads to an atmospheric inversion and, accompanied with a slight change of wind direction, to a more local source (mix), which is more depleted in ^{13}C than during the reference period ($\delta^{13}C_{\mathrm{ref}} = -25$ ‰). The strong influence of a more ^{13}C depleted source mix points towards a high contribution from fossil fuel sources, including domestic heating (natural gas). At the same time, the isotopic signature of δ^{18}O-CO_2 is very close to the isotopic signature during the reference period (-28 ‰) and increases during the pollution event. The different behaviour of δ^{13}C and δ^{18}O in CO_2 points towards a larger influence from traffic or natural gas combustion, as both sources are slightly more enriched in ^{18}O, but less enriched in ^{13}C with respect to coal-fired combustion (Schumacher et al., 2011). One can see that the fact that different fossil fuel types influence both stable isotopes ^{13}C and ^{18}O in CO_2 in a different way can potentially be used to differentiate between different emission groups in situations when biogenic fluxes are low (i.e. in winter). However, for a quantitative analysis we must know the exact isotopic signatures of all fluxes in the area of influences.

In the summertime, we expect biosphere fluxes to be much larger than during winter and at the same time fossil fuel (especially residential heating) emissions to be smaller than in winter. In fact, we do not find large deviations in $\delta^{13}CO_2$ from those determined in the reference period (-27 ‰), pointing towards a relatively constant mixture of biogenic and fossil fuel emissions. On the other hand, the measured δ^{18}O-CO_2 decreased rapidly on 3 July, compared to the reference period with a source isotopic signature of ≈ -12 ‰. This decrease is not accompanied by changes of any other tracer, such as CO, $\delta^{13}CO_2$ or CO_2, and also not by drastic changes of environmental parameters such as relative humidity, temperature or wind speed (not shown here). A possible explanation for the decrease is a change in the hydrological conditions. After 4 dry days, a sudden heavy rain occurred in Heidelberg on 3 July (see dashed bar in Fig. 7, right panel). The rainfall replenished the water reservoirs with an ^{18}O-depleted signature (Daansgard et al., 1964) and equilibration between the soil and leaf water reservoirs and CO_2 most probably caused the atmospheric δ^{18}O-CO_2 to become depleted relative to the reference period. This example illustrates the close coupling between δ^{18}O in the water and carbon cycle. It is thus crucial to study also the hydrological conditions, such as precipitation and its isotopic signature, in order to quantitatively use the δ^{18}O-CO_2 records for carbon cycle research.

5 Discussion

5.1 Instrumental performance

The main scope of this work was to ascertain whether the FTIR analyser is capable of measuring δ^{18}O-CO_2 in the atmosphere and if so, to assess how well it performs. We have seen that the FTIR succeeds in measuring atmospheric δ^{18}O-CO_2 with a high repeatability (Allan deviation after 1 day: 0.1 ‰) and good intermediate measurement precision (δ^{18}O-$CO_2 = 0.27$ ‰ for daily repeated working standard gas measurements on 9 min averages over 10 months). We were also able to confirm a good compatibility to the IRMS. Some optimisation, concerning the calibration, the fitted spectral windows and the theoretical spectrum modelling could lead to improved results. However, the current performance of the spectrometer suffices to quantify typical diurnal and synoptic variations at an urban site, which is an important step towards quantification of gross biospheric fluxes using FTIR-based δ^{18}O-CO_2 measurements.

5.2 Quantitative interpretation of continuous δ^{13}C-CO_2 and δ^{18}O-CO_2 record

We further investigated which insight may be gained from continuous isotopologue records at an urban site. For δ^{13}C, the different carbon sources and sinks are relatively well understood, but for δ^{18}O, high temporal variability of the res-

piratory and photosynthetic fluxes (due to a strong variation of environmental parameters such as precipitation, temperature and humidity) makes it difficult to separate the different CO_2 fluxes. For our qualitative study, we could use observations from Neubert (1998) in the catchment area of Heidelberg, as well as globally resolved model data for assimilation isofluxes from Cuntz et al. (2003b). However, for a quantitative apportionment of the CO_2 fluxes at a high temporal resolution, sampling of the isotopic content of precipitation, soil respiration and foliage gas exchange in the catchment area will be necessary with similarly high temporal resolution (Stern et al., 1999; Langendörfer et al., 2002). Further, isotope soil-atmosphere flux models are required to quantify the effect of this process at the measurement site. All of these unknowns largely limit current applicability of our new continuous isotope measurements. Future sophisticated regional models of the water and the carbon cycle may, however, be able to fully exploit the wealth of new information now available.

6 Summary and conclusion

The analysis of δ^{18}O in CO_2 using FTIR spectroscopy is novel. We evaluated the measurements of ^{18}O in CO_2 using the FTIR with respect to repeatability, intermediate measurement precision and compatibility. The Allan deviation test showed that the instrument measures δ^{18}O-CO_2 with good stability over the course of a day (the frequency of the working standard measurement) to within 0.1 ‰. Averages of 9 min show a standard deviation of about 0.25 ‰, which is in agreement with the intermediate measurement precision based on daily working standard gas measurements.

Evaluation of diurnal ambient air variations is therefore possible using, for example, 30 min averages. The high temporal resolution of the FTIR measurement is a major advantage over the IRMS analyses. Even though the FTIR precision does not reach the WMO inter-laboratory compatibility targets (WMO, 2012), a number of interesting scientific applications seem possible using FTIR spectroscopy. In particular, investigation of the processes that govern the δ^{18}O-CO_2 variability of atmospheric CO_2 on the regional scale seem very promising if comprehensive knowledge on the isotopic signature of different CO_2 sources and sinks, as well as of the influencing water reservoirs, is available.

Acknowledgements. We thank Geoff Toon, Frank Hase and Joseph Mendonca for valuable discussions on molecular line shapes spectra and for fitting our spectra with different line shape models. Four anonymous reviewers are gratefully acknowledged for their valuable comments, which helped to improve our manuscript. This work has been funded by the InGOS EU project (284274). We further acknowledge the financial support given by Deutsche Forschungsgemeinschaft and Ruprecht-Karls-Universität Heidelberg within the funding program Open Access Publishing.

Edited by: G. Phillips

References

Allison, C., Francey, R., and Meijer, H.: Recommendations for the reporting of stable isotope measurements for carbon and oxygen in CO_2 gas, Reference and intercomparison materials for stable isotopes of light element, IAEA-TECDO, 155–162, 1995.

Bowling, D. R., McDowell, N. G., Welker, J. M., Bind, B. J., Law, B.E., and Ehleringer, J. R.: Oxygen isotope content of CO_2 in nocturnal ecosystem respiration: 1. Observations in forests along a precipitation transect in Oregon, USA, Global Biogeochem. Cy., 17, 1120, doi:10.1029/2003GB002081, 2003.

Buenning, N., Noone, D., Randerson, J., Riley, W. J., and Still, C.: The response of the $^{18}O/^{16}O$ composition of atmospheric CO_2 to changes in environmental conditions, J. Geophys. Res.-Biogeosci., 119, 55–79, doi:10.1002/2013JG002312, 2014.

Cambaliza, M. O. L.: Measurement of forest ecosystem-atmosphere exchange of δ^{13}C-CO_2 using Fourier Transform Infrared spectroscopy and disjunct eddy covariance, Dissertation, Washington State University, Department of Civil and Environmental Engineering, USA, 2010.

Ciais, P., Tans, P. P., White, J. W. C., Trolier, M., Francey, R. J., Berry, J. A., Randall, D. R., Sellers, P. J., Collatz, J. G., and Schimel, D. S.: Partitioning of ocean and land uptake of CO_2 as inferred by δ^{13}C measurements from the NOAA Climate Monitoring and Diagnostics Laboratory Global Air Sampling Network, J. Geophys. Res., 100, 5051–5070, doi:10.1029/94JD02847, 1995.

Ciais, P., Denning, A. S., Tans, P. P., and Berry, J. A.: A three-dimensional synthesis study of δ^{18}O in atmospheric CO_2 1.surface fluxes, J. Geophys. Res., 102, 5857–5872, doi:10.1029/96JD02360, 1997.

Coplen, T. B.: Guidelines and recommended terms for expression of stable-isotope-ratio and gas-ratio measurement results. Rapid Commun. Mass Spectrom., 25, 2538–2560, doi:10.1002/rcm.5129, 2011.

Cuntz, M., Ciais, P., Hoffmann, G., and Knorr, W.: A comprehensive global three-dimensional model of δ^{18}O in atmospheric CO_2: 1. Validation of surface processes, J. Geophys. Res., 108, 4527, doi:10.1029/2002jd003153, 2003a.

Cuntz, M., Ciais, P., Hoffmann, G., Allison, C. E., Francey, R. J., Knorr, W., Tans, P. P., White, J. W. C., and Levin, I.: A comprehensive global three-dimensional model of δ^{18}O in atmospheric CO_2: 2. Mapping the atmospheric signal, J. Geophys. Res., 108, 4528, doi:10.1029/2002JD003154, 2003b.

Daansgard, W.: Stable isotopes in precipitation, Tellus, 16, 436–468, doi:10.1111/j.2153-3490.1964.tb00181.x, 1964.

Esler, M. B., Griffith, D. W. T, Wilson, S. R., and Steele, L. P.: Precision trace gas analysis by FT-IR Spectroscopy. 2. The $^{13}C/^{12}C$ Isotope Ratio of CO_2, Anal. Chem, 72, 216–221, 2000.

Farquhar, G. D., Lloyd, J., Taylor, J. A., Flanagan, L. B., Syvertsen, J. P., Hubick, K. T., Wong, S. C., and Ehleringer, J. R.: Vegetation effects on the isotope composition of oxygen in atmospheric CO_2, Nature, 363, 439–443, doi:10.1038/363439a0, 1993.

Flanagan, L. B., Brooks, J. R., Varney, G. T., and Ehleringer, J. R.: Discrimination against $C^{18}O^{16}O$ during photosynthesis and the

oxygen isotope ratio respired CO_2 in boreal forest ecosystems, Global Biogeochem. Cy., 11, 83–98, 1997.

Francey, R. J. and Tans, P. P.: Latitudinal variation in oxygen-18 of atmospheric CO_2, Nature, 327, 495–497, doi:10.1038/327495a0, 1987.

Gillon, J. and Yakir, D.: Influence of carbonic anhydrase activity in terrestrial vegetation on the ^{18}O content of atmospheric CO_2, Science, 291, 2584–2587, doi:10.1126/science.1056374, 2001.

Griffith, D. W. T.: Synthetic calibration and quantitative analysis of gas phase infrared spectra, Appl. Spectrosc., 50, 59–70, 1996.

Griffith, D. W. T., Jamie, I. M., and Meyers, R. A. (Eds.): Fourier Transform Infrared Spectrometry in Atmospheric and Trace Gas Analysis, Encyclopedia of Analytical Chemistry, Wiley, Chichester, 2000.

Griffith, D. W. T., Deutscher, N. M., Caldow, C., Kettlewell, G., Riggenbach, M., and Hammer, S.: A Fourier transform infrared trace gas and isotope analyser for atmospheric applications, Atmos. Meas. Tech., 5, 2481–2498, doi:10.5194/amt-5-2481-2012, 2012.

Hammer, S., Griffith, D. W. T., Konrad, G., Vardag, S., Caldow, C., and Levin, I.: Assessment of a multi-species in situ FTIR for precise atmospheric greenhouse gas observations, Atmos. Meas. Tech., 6, 1153-1170, doi:10.5194/amt-6-1153-2013, 2013a.

Hammer, S., Konrad, G., Vermeulen, A. T., Laurent, O., Delmotte, M., Jordan, A., Hazan, L., Conil, S., and Levin, I.: Feasibility study of using a "travelling" CO_2 and CH_4 instrument to validate continuous in situ measurement stations, Atmos. Meas. Tech., 6, 1201–1216, doi:10.5194/amt-6-1201-2013, 2013b.

Hase, F., Drouin, B. J., Roehl, C. M., Toon, G. C., Wennberg, P. O., Wunch, D., Blumenstock, T., Desmet, F., Feist, D. G., Heikkinen, P., De Mazière, M., Rettinger, M., Robinson, J., Schneider, M., Sherlock, V., Sussmann, R., Té, Y., Warneke, T., and Weinzierl, C.: Calibration of sealed HCl cells used for TCCON instrumental line shape monitoring, Atmos. Meas. Tech., 6, 3527–3537, doi:10.5194/amt-6-3527-2013, 2013.

Hesterberg, R. and Siegenthaler, U.: Production and stable isotopic composition of CO_2 in a soil near Bern, Switzerland. Tellus B, 43, 197–205, doi:10.1034/j.1600-0889.1991.00013.x, 1991.

JCGM: Joint Committee for Guides in Metrology: International vocabulary of metrology – basic and general concepts and associated terms (VIM), 3rd Edn., 2008.

Kaul, M.: Isotopenverhältnisse im atmosphärischem Kohlendioxid und seine Quellen im Raum Heidelberg, Staatsexamen thesis, Universität Heidelberg, Heidelberg, Germany, 2007.

Keeling, C. D.: The concentration and isotopic abundance of atmospheric carbon dioxide in rural areas, Geochim. Cosmochim. Ac. 13, 322–334, 1958.

Keeling, C. D., Bacastow, R. B., Carter, A. F., Piper, S. C., Whorf, T. P., Heimann, M., Mook, W. G. and Roeloffzen, H.: A three-dimensional model of atmospheric CO_2 transport based on observed winds: 1. Analysis of observational data, Aspects of Climate Variability in the Pacific and the Western Americas, edited by: Peterson, D. H., Vol. 55, American Geophysical Union, Washington, D. C., 165–236, 1989.

Langendörfer, U., Cuntz, M., Ciais, P., Peylin, P., Bariac, T., Milyukova, I., Kolle, O., Naegler, T., and Levin, I.: Modelling of biospheric CO_2 gross fluxes via oxygen isotopes in a spruce forest canopy: a ^{222}Rn calibrated box model approach. Tellus B, 54, 476–496, doi:10.1034/j.1600-0889.2002.01345.x, 2002.

Levin, I., Kromer, B., Schmidt, M., and Sartorius, H.: A novel approach for independent budgeting of fossil fuel CO_2 over Europe by $^{14}CO_2$ observations, Geophys. Res. Lett., 30, 2194, doi:10.1029/2003GL018477, 2003.

Miller, J. B. and Tans, P. P.: Calculating isotopic fractionation from atmospheric measurements at various scales, Tellus B, 55, 207–214. doi:10.1034/j.1600-0889.2003.00020.x, 2003.

Miller, J. B., Yakir, D., White, J. W. C., and Tans, P. P.: Measurement of $^{18}O/^{16}O$ in the soil-atmosphere CO_2 flux, Global Biogeochem. Cy., 13, 761–774, doi:10.1029/1999GB900028, 1999.

Mohn, J., Zeeman, M. J., Werner, R. A., Eugster, and W., Emmenegger, L.: Continuous field measurements of $\delta^{13}C - CO_2$ and trace gases by FTIR spectroscopy, Isotopes Environ. Health Stud., 44, 241–251, 2008.

Mook, W.: Environmental isotopes in the hydrological cycle – Principles and applications, Introductory course on Isotope Hydrology, Department of Hydrogeology and Geographical Hyrdology, 1994.

Neubert, R.: Measurement of stable isotopomers of atmospheric carbon dioxide, PhD thesis, University of Heidelberg, Heidelberg, Germany, 1998.

Neubert, R. E. M., Spijkervet, L. L., Schut, J. K., Been, H. A., and Meijer, H. A. J.: A computer-controlled continuous air drying and flask sampling system, J. Atmos. Ocean. Technol., 21, 651–659, 2004.

Ngo, N. H., Lisak, D., Tran, H., and Hartmann, J.-M.: An isolated lineshape model to go beyond the Voigt profile in spectroscopic databases and radiative transfer codes. J. Quant. Spectrosc. Ra., 129, 89–100, 2013.

Pataki, D. E., Bowling, D. R., and Ehleringer, J. R.: Seasonal cycle of carbon dioxide and its isotopic composition in an urban atmosphere: Anthropogenic and biogenic effects, J. Geophys. Res., 108, 4735, doi:10.1029/2003JD003865, 2003.

Rothman, L. S., Jacquemart, D., Barbe, A., Benner, D. C., Birk, M., Brown, L. R., Carleer, M. R., C. Chaucerian, J., Chance, K., Dana, V., Devi, V. M., Flaud, J.-M., Gamache, R. R., Goldman, A., Hartmann, J.-M., Jucks, K. W., Maki, A. G., Mandin, J.-Y., Massie, S. T., Orphali, J., Perrin, A., Rinsland, C. P., Smith, M. A. H., Tennyson, J., Tolchenov, R. N., Toth, R. A., Auwera, J. V., Varanasi, P., and Wagner, G.: The HITRAN 2004 molecular spectroscopic database, J. Quant. Spectrosc. Ra., 96, 139–204, doi:10.1016/j.jqsrt.2004.10.008, 2005.

Schumacher, M., Werner, R. A., Meijer, H. A. J., Jansen, H. G., Brand, W. A., Geilmann, H., and Neubert, R. E. M.: Oxygen isotopic signature of CO_2 from combustion processes, Atmos. Chem. Phys., 11, 1473–1490, doi:10.5194/acp-11-1473-2011, 2011.

Seibt, U., Wingate, L., Lloyd, J., and Berry, J. A.: Diurnally variable $\delta^{18}O$ signatures of soil CO_2 fluxes indicate carbonic anhydrase activity in a forest soil, J. Geophys. Res., 111, G04005, doi:10.1029/2006JG000177, 2006.

Stern, L., Baisden, W. T., and Amundson, R.: Processes controlling the oxygen isotopic ratio of soil CO_2: analytical and numerical modelling, Geochim Cosmochim. Ac. 63, 799–814, 1999.

Still, C. J., Riley, W. J., Biraud, S. C., Noone, D. C., Buenning, N. H., Randerson, J. T., Tom, M. S., Welker, J., White, J .W. C., Vachon, R., Farquhar, G. D., and Berry, J. A.: Influence of clouds and diffuse radiation on ecosystem-atmosphere

CO_2 and $CO^{18}O$ exchanges, J. Geophys. Res., 114, G01018, doi:10.1029/2007JG000675, 2009.

Sturm, P., Tuzson, B., Henne, S., and Emmenegger, L.: Tracking isotopic signatures of CO_2 at the high altitude site Jungfraujoch with laser spectroscopy: analytical improvements and representative results, Atmos. Meas. Tech., 6, 1659–1671, doi:10.5194/amt-6-1659-2013, 2013.

Tans, P. P.: Oxygen isotopic equilibrium between carbon dioxide and water in soils. Tellus B, 50, 163–178, doi:10.1034/j.1600-0889.1998.t01-1-00004.x, 1998.

Tans, P. P. and Bolin, B. (Eds.): $^{13}C/^{12}C$ of industrial CO_2, Carbon Cycle Modelling, Scope Ser., 16, 127–129, 1981.

Tuzson, B., Henne, S., Brunner, D., Steinbacher, M., Mohn, J., Buchmann, B., and Emmenegger, L.: Continuous isotopic composition measurements of tropospheric CO_2 at Jungfraujoch (3580 m a.s.l.), Switzerland: real-time observation of regional pollution events, Atmos. Chem. Phys., 11, 1685–1696, doi:10.5194/acp-11-1685-2011, 2011.

Vardag, S. N., Hammer, S., O'Doherty, S., Spain, T. G., Wastine, B., Jordan, A., and Levin, I.: Comparisons of continuous atmospheric CH_4, CO_2 and N_2O measurements – results from a travelling instrument campaign at Mace Head, Atmos. Chem. Phys., 14, 8403–8418, doi:10.5194/acp-14-8403-2014, 2014.

Welp, L. R., Keeling, R. F., Meijer, H. A., Bollenbacher, A. F., Piper, S. C., Yoshimura, K., Francey, R. J., Allison, C. E., and Wahlen, M.: Interannual variability in the oxygen isotopes of atmospheric CO_2 driven by El Niño, Nature, 477, 579–582, 2011.

Wendeberg, M., Richter, J. M., Rothe, M., and Brand, W. A.: Jena Reference Air Set (JRAS): a multi-point scale anchor for isotope measurements of CO_2 in air, Atmos. Meas. Tech., 6, 817–822, doi:10.5194/amt-6-817-2013, 2013.

Werle, P. O., Mücke, R., and Slemr, F.: The limits of signal averaging in atmospheric trace-gas monitoring by tunable diode-laser absorption spectroscopy (TDLAS), Appl. Phys. B, 57.2, 131–139, 1993.

Werle, P.: Accuracy and precision of laser spectrometers for trace gas sensing in the presence of optical fringes and atmospheric turbulence, Appl. Phys. B, 10, 251–253, 2011.

Widory, D. and Javoy, M.: The carbon isotope composition of atmospheric CO_2 in Paris, Earth Planet. Sci. Lett., 215, 289–298, 2003.

Wingate, L., Seibt, U., Maseyk, K., Ogée, J., Almeida, P., Yakir, D., Pereira, J. S., and Menunccini, M.: Evaporation and carbonic anhydrase activity recorded in oxygen isotope signatures of net CO_2 fluxes from a Mediterranean soil, Global Change Biol., 14, 2178–2193, doi:10.1111/j.1365-2486.2008.01635.x, 2008.

Wingate, L., Ogée, J., Cuntz, M., Genty, B., Reiter, I., Seibt, U., Yakir,D., Maesyk, K., Pendall, E. G., Barbour, M. M., Mortazavi, B., Burlett, R., Peylin, P., Miller, J., Mencuccini, M., Shim, J. H., Hunt, J. Grace, J.: The impact of soil microorganisms on the global budget of δ^{18}O in atmospheric CO_2 Proc. Natl. Acad. Sci., 106, 22411–22415, doi:10.1073/pnas.0905210106, 2009.

WMO: Report of the 16th WMO/IAEA Meeting of Experts on Carbon Dioxide, Other Greenhouse Gases and Related Tracers Measurement Techniques (GGMT-2011): Wellington, New Zealand, 25–28 October 2011, GAW Report No. 206, available at: http://www.wmo.int/pages/prog/arep/gaw/gaw-reports.html (last access: 23 October 2014), Welligton, New Zealand, 2012.

Wunch, D., Toon, G. C., Blavier, J.-F., Washenfelder, R., Notholt, J., Connor, B., Griffith, D. W. T.. and Wennberg, P. O.: The Total Carbon Column Observing Network (TCCON). Phil. Trans. Roy. Soc. A, 369, 2087–2112, 2011.

Yakir, D. and Wang, X.-F.: Fluxes of CO_2 and water between terrestrial vegetation and the atmosphere estimated from isotope measurements, Nature, 380, 515–517, doi:10.1038/380515a0, 1996.

Publication 3

2.3 Estimation of continuous anthropogenic CO_2: model-based evaluation of CO_2, CO, $\delta^{13}C(CO_2)$ and $\Delta^{14}C(CO_2)$ tracer methods

Vardag, S. N., Gerbig, C., Janssens-Maenhout, G., and Levin, I.

Atmos. Chem. Phys., 15, 12705–12729, 2015
www.atmos-chem-phys.net/15/12705/2015/
doi:10.5194/acp-15-12705-2015

Atmospheric Chemistry and Physics Open Access

Estimation of continuous anthropogenic CO_2: model-based evaluation of CO_2, CO, $\delta^{13}C(CO_2)$ and $\Delta^{14}C(CO_2)$ tracer methods

S. N. Vardag[1], C. Gerbig[2], G. Janssens-Maenhout[3], and I. Levin[1]

[1]Institut für Umweltphysik, Heidelberg University, Germany
[2]Max Planck Institute for Biogeochemistry, Hans-Knöll-Str. 10, 07745 Jena, Germany
[3]European Commission, Joint Research Centre, Ispra, Via Fermi 2749, 21027 Ispra, Italy

Correspondence to: S. N. Vardag (svardag@iup.uni-heidelberg.de)

Received: 3 July 2015 – Published in Atmos. Chem. Phys. Discuss.: 24 July 2015
Revised: 27 October 2015 – Accepted: 30 October 2015 – Published: 16 November 2015

Abstract. We investigate different methods for estimating anthropogenic CO_2 using modeled continuous atmospheric concentrations of CO_2 alone, as well as CO_2 in combination with the surrogate tracers CO, $\delta^{13}C(CO_2)$ and $\Delta^{14}C(CO_2)$. These methods are applied at three hypothetical stations representing rural, urban and polluted conditions. We find that, independent of the tracer used, an observation-based estimate of continuous anthropogenic CO_2 is not yet feasible at rural measurement sites due to the low signal-to-noise ratio of anthropogenic CO_2 estimates at such settings. The tracers $\delta^{13}C(CO_2)$ and CO provide an accurate possibility to determine anthropogenic CO_2 continuously, only if all CO_2 sources in the catchment area are well characterized or calibrated with respect to their isotopic signature and CO to anthropogenic CO_2 ratio. We test different calibration strategies for the mean isotopic signature and CO to CO_2 ratio using precise $\Delta^{14}C(CO_2)$ measurements on monthly integrated as well as on grab samples. For $\delta^{13}C(CO_2)$, a calibration with annually averaged $^{14}C(CO_2)$ grab samples is most promising, since integrated sampling introduces large biases into anthropogenic CO_2 estimates. For CO, these biases are smaller. The precision of continuous anthropogenic CO_2 determination using $\delta^{13}C(CO_2)$ depends on measurement precision of $\delta^{13}C(CO_2)$ and CO_2, while the CO method is mainly limited by the variation in natural CO sources and sinks. At present, continuous anthropogenic CO_2 could be determined using the tracers $\delta^{13}C(CO_2)$ and/or CO with a precision of about 30 %, a mean bias of about 10 % and without significant diurnal discrepancies. Hypothetical future measurements of continuous $\Delta^{14}C(CO_2)$ with a precision of 5 ‰ are promising for anthropogenic CO_2 determination (precision ca. 10–20 %) but are not yet available. The investigated tracer-based approaches open the door to improving, validating and reducing biases of highly resolved emission inventories using atmospheric observation and regional modeling.

1 Introduction

Earth's carbon budget is strongly influenced by anthropogenic CO_2 emissions into the atmosphere (Keeling et al., 1996; Le Quéré et al., 2015). In order to support studies of the carbon cycle and to determine net and gross carbon fluxes quantitatively, various measurement sites monitor the atmospheric CO_2 mole fraction worldwide. In top-down approaches and in conjunction with atmospheric transport models, these CO_2 measurements are used to infer total CO_2 emissions (Bousquet et al., 2000; Gurney et al., 2002; Peylin et al., 2013), but a differentiation into biogenic, oceanic and anthropogenic CO_2 sources and sinks is not feasible with CO_2 concentration measurements alone. Inverse model studies commonly utilize anthropogenic CO_2 emission inventories to estimate anthropogenic CO_2 and are then able to separate anthropogenic from biogenic or oceanic carbon sink and source influences. However, currently available emission inventories exhibit large discrepancies between each other of about 10–40 % at the country level (Peylin et al., 2011), and increase further with decreasing spatial scale (Gurney et al., 2005). These discrepancies suggest that biases may be on the order of about 70–100 % for highly resolved ($0.1° \times 0.1°$) data sets and uncertainties (1σ) of emission inventories may be between 30 and 150 % (Wang et al., 2013). In order to

better study and quantify the biospheric carbon fluxes, their underlying processes and potential feedbacks, it is desirable to reduce the current uncertainties as well as biases of emission inventories. Validation and improvement of emission inventories requires accurate and precise anthropogenic CO_2 estimates (as well as accurate and precise transport models) on all relevant timescales ranging from hours to years. We hereafter refer to anthropogenic CO_2 as fuel CO_2 and include non-combustion emissions such as emissions from cement industry or non-energy use of fuels as well as agricultural waste burning. Fossil fuel CO_2 excludes all contributions from biofuel emissions or from agricultural waste burning. We define biofuel CO_2 as non-fossil fuel CO_2 released during combustion, including solid (e.g., wood, waste, charcoal, municipal renewable waste, bagasse, vegetal waste and dung), liquid (e.g., biodiesel, bio gasoline and black liquor) and gaseous (from compost or cattle farm) biomaterial. It does not include large-scale biomass burning. For some purposes, e.g., when validating fossil fuel emission reductions, it may actually be advantageous to estimate only the fossil fuel CO_2 contribution, which is the fuel CO_2 contribution without biofuel CO_2. However, when solving for biospheric fluxes, the biofuel CO_2 is important as well, since it equally contributes to the instantaneously measured CO_2 concentration and needs to be separated from the biospheric flux. In the following, we seek to constrain the fuel CO_2 (fossil fuel CO_2 plus biofuel CO_2).

^{14}C measurements are commonly used as surrogate to differentiate between biogenic and fossil fuel CO_2 contributions in the atmosphere, since fossil fuels do not contain any ^{14}C, in contrast to biogenic sources (Levin et al., 2003). The ^{14}C / C isotope ratio in CO_2 is expressed on the $\Delta^{14}C(CO_2)$ scale, which denotes the deviation of the ^{14}C / C ratio in CO_2 from a standard material in per mill (Stuiver and Polach, 1977). We use the depletion of $\Delta^{14}C(CO_2)$ at a polluted measurement site relative to $\Delta^{14}C(CO_2)$ in clean background air to derive quantitative information on the contribution of fossil fuel CO_2 to total measured CO_2 mole fraction at the polluted site. Radiocarbon (^{14}C) is thus used as quantitative tracer for fossil fuel contributions (e.g., Levin et al., 2003; Levin and Karstens, 2007; Turnbull et al., 2006, 2015; Newman et al., 2015). However, there are a number of problems when using $^{14}C(CO_2)$ as a tracer for anthropogenic emissions. First, precise $\Delta^{14}C(CO_2)$ measurements from conventional counting or accelerator mass spectrometry (AMS; see list of all abbreviations in Appendix D) (better than 2 ‰) are time and cost intensive, thus currently prohibiting the coverage of large periods and large area of such measurements. Attempts have been made to sample $^{14}C(CO_2)$ with a higher measurement frequency using gas chromatography (GC) coupled to continuous-flow AMS (McIntyre et al., 2013), but the technique is not applicable to atmospheric ^{14}C samples so far and the precision in $\Delta^{14}C(CO_2)$ is lower than for AMS or conventional counting. This results in less precise fossil fuel CO_2 estimates. These studies indicate, however, that the measurement precision using GC and continuous-flow AMS may reach 5 ‰ in future. The benefit of such hypothetical quasi-continuous but reduced precision fossil fuel CO_2 estimates is assessed for the first time in this work in order to check whether these measurements would provide beneficial constraints for determining CO_2 continuously.

Second, a complication of applying $\Delta^{14}C(CO_2)$ measurements for fossil fuel CO_2 estimation is that nuclear power plants as well as nuclear fuel reprocessing plants emit $^{14}C(CO_2)$ and can bias regional $\Delta^{14}C(CO_2)$-based estimates of fossil fuel contributions if not taken into account (Levin et al., 2003; Graven and Gruber, 2011; Vogel et al., 2013b). Moreover, biofuel CO_2 contributions cannot be monitored with $\Delta^{14}C(CO_2)$ measurements, since they have a similar $\Delta^{14}C(CO_2)$ signature as the biosphere or may even be elevated in ^{14}C due to the bomb radiocarbon $^{14}C(CO_2)$ stored in wood material. This could become especially problematic, since the use of biofuels is expected to play an increasingly important role for the energy supply in the near future (Coyle, 2007). With these shortcomings of $\Delta^{14}C(CO_2)$ as a tracer for anthropogenic CO_2 recognized, it is worth considering other tracers for the estimation of fuel CO_2 contributions.

Turnbull et al. (2015) showed that for an urban study area in the middle of the North American continent, the local CO_2 offset relative to clean air, ΔCO_2, can be used as a tracer for fuel CO_2 contributions if all other CO_2 sources and sinks, such as from the living biosphere, are negligible. This may be the case for wintertime periods in urban areas when using a background station upwind and close to the urban area. However, we do not expect ΔCO_2 to be a quantitative tracer when biospheric fluxes occur within the study area. This is normally the case in spring, summer and autumn.

Since CO is often co-emitted during (incomplete) combustion and since CO can be measured continuously, the CO offset relative to clean air, ΔCO, is frequently used as a tracer for fuel CO_2 (Meijer et al., 1996; Gamnitzer et al., 2006; Rivier et al., 2006; Turnbull et al., 2006, 2011; Levin and Karstens, 2007; Vogel et al., 2010; Newman et al., 2013). If the mean ratio of the CO offset (Δx) relative to the fuel CO_2 offset (Δy_F), i.e., $\Delta x / \Delta y_F \equiv \overline{R_F}$, is known and relatively constant within 1 month, it is principally possible to derive a continuous Δy_F estimate from Δx measurements by dividing Δx by monthly mean $\overline{R_F}$. The overbar is used to emphasize that we use one averaged value for R_F, even though it actually varies with the relative fraction of the different emission groups in a varying catchment area of the measurement site. CO is also produced during oxidation of methane and hydrocarbons, particularly during summer (Granier et al., 2000). The main sinks of CO are photooxidation and reaction with OH (Parrish et al., 1993) as well as soil uptake (Inman et al., 1971), leading to a rather short atmospheric lifetime of CO of several weeks in summer (Prather et al., 2001). Natural CO sinks and sources vary on timescales of hours to seasons. Further, relative contributions of different fuel

CO_2 sectors (e.g., energy production, road traffic, residential heating, industrial emissions) with different emission ratios (ΔCO / ΔCO_2) may vary on short timescales of hours to longer timescales of years if, for example, combustion technologies, processes and procedures change in the long term. Therefore, the mean $\overline{R_F}$ ($= \Delta x/\Delta y_F$) is a function of space and time and might need to be calibrated using, for example, $\Delta^{14}C(CO_2)$ measurements (Levin and Karstens, 2007). If $\overline{R_F}$ does not vary significantly within the timescale of the calibration, continuous Δy_F can be estimated. However, if $\overline{R_F}$ varies strongly on timescales of smaller than the calibration interval, further corrections (e.g., diurnal or seasonal) may be necessary (Vogel et al., 2010). These corrections are only reliable if $\overline{R_F}$ variations are systematic. Since this is not always the case, additional or other continuous tracers may need to be considered to improve fuel CO_2 estimates.

One of these tracers may be $\delta^{13}C(CO_2)$, since fuel emissions tend to be more depleted in $^{13}CO_2$ than fluxes from the biosphere. Zondervan and Meijer (1996), Pataki et al. (2006) and Djuricin et al. (2010) attempted to estimate fuel CO_2 emissions in specific case studies using mass spectrometric measurements of $\delta^{13}C(CO_2)$, in addition to $\Delta^{14}C(CO_2)$ measurements. Recently, new optical instrumentation allows for $\delta^{13}C(CO_2)$ to be measured continuously (e.g., Esler et al., 2000; Tuzson et al., 2011; Hammer et al., 2013; Vogel et al., 2013a), thus opening the door for $\delta^{13}C(CO_2)$ as a continuous tracer for fuel CO_2 contributions. In order to use $\delta^{13}C(CO_2)$ measurements at an urban site, the mean isotopic signature of the sources (and sinks) in the catchment area of the site, $\overline{\delta_F}$, must be known (Newman et al., 2015) and relatively constant and potentially require calibration (as discussed for CO). Further, the signature of fuel CO_2 emissions must be significantly different from biospheric CO_2 emissions in order to differentiate properly between them.

In many settings, we will exhibit neither a constant ratio $\overline{R_F}$ nor a constant fuel source signature $\overline{\delta_F}$. This will especially be the case if multiple sources (i) with different emission ratios $R_{F,i}$ and from different fuel $\delta^{13}C(CO_2)$ source signatures $\delta_{F,i}$ are located in the catchment area of the measurement site. In these cases, it may be advantageous to divide the fuel emissions into (two) different groups. CO will only be an adequate tracer for a certain emission group if this group has a significantly different ratio $\overline{R_F}$ ($= \Delta x/\Delta y_F$) than any other emission group. By analogy, $\delta^{13}C(CO_2)$ will only be a good tracer for a certain emission group if the group's emissions are significantly more depleted or enriched with respect to the other groups. If we divide all fuel CO_2 contributions into two emission groups, of which one is well constrained by CO and the other by $\delta^{13}C(CO_2)$, we may then join both tracers to determine the total fuel CO_2 contributions. In several published studies, the CO mole fraction has been used as a tracer for traffic emissions only (e.g., Schmidt et al., 2014), since these often exhibit high ΔCO / ΔCO_2 ratios. However, in some regions, emission inventories (e.g., Landesamt für Umwelt, Messungen und Naturschutz Baden-Württemberg, available at http://www.ekat.baden-wuerttemberg.de/) show that the emission ratio $\overline{R_{tr}}$ ($= (\Delta x/\Delta y)_{tr}$) has been decreasing during the last decade, degrading CO as a tracer for traffic contributions. At the same time, diesel/gasoline for vehicles is blended with an increasing amount of biodiesel/biogasoline (on the order of 5 % for OECD countries; IEA, 2014). More in general, emission inventories show that (the sum of solid, liquid and gaseous) biofuel CO_2 emissions in OECD countries have increased (IEA, 2014) and that the mean emission ratio of biofuel emissions $\overline{R_{bf}}$ ($= (\Delta x/\Delta y)_{bf}$) is very high (EDGARv4.3 emission inventory; EC-JRC/PBL, 2015), qualifying CO as a tracer for biofuel contributions. However, the emission ratio varies depending on the combustion type. Later we examine separately whether these two emission groups, traffic and biofuel emissions, could possibly be traced with CO.

In the present study, we investigate how continuous CO_2, CO, $\delta^{13}C(CO_2)$ and $\Delta^{14}C(CO_2)$ measurements as well as the combination of these tracers could be used to estimate continuous fuel CO_2. In order to validate how precisely and accurately we may be able to determine fuel CO_2 using continuous (hourly) CO_2, CO, $\delta^{13}C(CO_2)$ and $\Delta^{14}C(CO_2)$ as tracers, we use a modeled data set, in which, contrary to measured data sets, CO_2 contributions from all source categories, i.e., the biosphere, from fossil fuel and from biofuel burning are traced separately. Using the modeled mole fractions and isotope records of CO_2, CO, $\delta^{13}C(CO_2)$ and $\Delta^{14}C(CO_2)$, we estimate the total fuel CO_2 offset using these tracers. We then discuss advantages and disadvantages of the different tracers. Using a modeled data set has the additional advantage that isotopic signatures, emission ratios of different emission sectors etc. can be varied in order to also investigate the sensitivity of these source characteristics on the fuel CO_2 estimate. This enables us to judge how accurately the sources in the catchment of the measurement site need to be characterized for a certain required accuracy of fuel CO_2, and if a calibration, using, for example, precise $\Delta^{14}C(CO_2)$ measurements, is advantageous. In the course of this, we also compare different possible sampling strategies for calibration. We further assess which measurement precision is needed to achieve continuous fuel CO_2 estimates with sufficient precision. Additionally, we investigate the diurnal cycle of the tracer-based continuous fuel CO_2 estimates and compare them to the modeled reference fuel CO_2 in order to determine whether we can reproduce the diurnal cycle correctly and hence whether we would introduce significant biases when using, for example, only afternoon values of fuel CO_2 in inverse models.

We discuss the model results for three typical European sites, which differ in their annual mean fuel CO_2 offset. We define three pollution regimes, which we call "rural", "urban" and "polluted". Rural sites have mean fuel CO_2 offsets of 0–5 µmol mol^{-1}. We here use the (hypothetical) station Gartow (53°0′ N, 11°3′ E) as an example with an annual

mean fuel CO_2 offset of 3 µmol mol^{-1}. Gartow is located in northern Germany about 160 km northwest of Berlin. Urban sites span a range from 5 to 20 µmol mol^{-1}. We use Heidelberg (49°3′ N, 8°4′ E) as an example, which is a typical urban measurement site with large fuel CO_2 emissions but also similarly high biogenic sources and sinks in the catchment, which are also active during relatively mild winters. The mean modeled fuel CO_2 offset in Heidelberg is about 16 µmol mol^{-1} (24 h). Polluted sites exhibit annual mean fuel CO_2 offsets larger than 20 µmol mol^{-1}. A station in the outskirts of Berlin (52°5′ N, 13°6′ E) is used as an example site with modeled mean fuel CO_2 offset of 25 µmol mol^{-1}. For all sites, we looked at the same height above ground level (30 m a.g.l). Note that this classification relates only to the mean annual offset and not to single pollution events. We assess whether an estimation of continuous fuel CO_2 is possible at all sites and what may be the best tracer. Finally, we give an outlook on how to apply this model study to a real measured data set. Our investigation aims at providing the basis for the decision of whether it is worthwhile conducting continuous measurements of CO_2, CO, $\delta^{13}C(CO_2)$ and $\Delta^{14}C(CO_2)$ at a particular measurement station in order to quantitatively and precisely estimate continuous fuel CO_2 within a measurement network.

2 The modeling framework

For the study's purpose of theoretically assessing precision and accuracy of different tracer configurations for fuel CO_2 estimation, it is only of secondary importance that modeled time series be correct, but it is mainly important that the model provides a reasonably realistic data set. In this study, we simulate mole fractions and isotopic records for the Heidelberg site (urban; see Levin et al., 2003) and for two hypothetical stations Gartow (rural) and Berlin (polluted) for the year 2012. All three stations may potentially be part of the German ICOS atmospheric network (see http://www.icos-infrastructure.eu/).

We used the Stochastic Time-Inverted Lagrangian Transport (STILT) model (Lin et al., 2003) as well as preset source and sink distributions (see below). To simulate the atmospheric transport we used meteorological fields from the European Centre for Medium-Range Weather Forecast with 3-hourly temporal resolution and 25 km × 25 km spatial resolution (Trusilova et al., 2010). Details of the STILT model are given in Lin et al. (2003) and in Gerbig et al. (2003); here we only provide a few relevant details. By emitting 100 particles (representing the observed air parcel) at the measurement location and inverting the meteorological fields in time, it is possible to follow the particles' trajectories backward in time using mean wind and a parameterization for the turbulent motion. For each of the trajectories, the sensitivity to emission fluxes is derived based on the residence time within the lower half of the mixed layer during each advection time step (typically 0.25 to 1 h). The sensitivity of the observed tracer mole fraction to upstream emissions was derived by combining the sensitivities of each trajectory on a common horizontal grid (here $1/12°$ latitude × $1/8°$ longitude, corresponding to about 10 km × 10 km). To reduce impact from undersampling of upstream areas at times when particles are distributed over extensive areas with large gaps between neighboring particles, the effective horizontal size of the grid cells is increased dynamically with increasing separation of the particles (Gerbig et al., 2003). This allows efficient simulations with a relatively small ensemble size. The sensitivity of the mole fraction at the measurement site to emissions located upstream is typically called the footprint. The particles are traced back in time until they leave the model domain, which extends from 16° W to 36° E and from 32 to 74° N. Initial/lateral CO_2 tracer boundary conditions for CO_2 tracer far-field mole fractions are taken from analyzed CO_2 fields, generated by the global atmospheric tracer transport model, TM3 (Heimann and Körner, 2003), based on optimized fluxes (Rödenbeck, 2005) transported at a spatial resolution of 4° × 5° with 19 vertical levels and a temporal resolution of 6 h (s96 v3.6, http://www.bgc-jena.mpg.de/~christian.roedenbeck/download-CO2-3D/). The footprint is multiplied by the biospheric and anthropogenic surface emissions to estimate the mole fraction change at the measurement site.

For the biospheric CO_2 fluxes, we use the vegetation photosynthesis and respiration model (VPRM; Mahadevan et al., 2008). The Net Ecosystem Exchange is calculated for different biome types based on SYNMAP (Jung et al., 2006) using land surface water index and enhanced vegetation index from MODIS (http://modis.gsfc.nasa.gov/) satellite data, as well as air temperature and shortwave radiation from ECMWF. VPRM results are computed at $1/12° \times 1/8°$ resolution with hourly resolution. We neglect biospheric CO and CH_4 fluxes in the model. CO destruction by OH and CO production via CH_4 oxidation is taken into account (Gerbig et al., 2003). However, CO production via non-methane hydrocarbon (NMHC) oxidation and CO uptake by soils (Conrad, 1996) are not included in the model. When using CO as a tracer for fuel CO_2, neglecting natural CO sources and sinks may be problematic since natural sources would lead to an overestimation and natural sinks to an underestimation of fuel CO_2. We will discuss this in more detail in Sects. 3.3.2 and 3.4.

Anthropogenic emissions of CO_2, CO and CH_4 are from a preliminary version of the EDGARv4.3 emission inventory (EC-JRC/PBL, 2015) which was also used for the UNEP Emissions Gap Report (Rogelj et al., 2014) for the base year 2010 and has a spatial resolution of $0.1° \times 0.1°$. The emissions are further separated following IPCC emission categories, which are again separated into fuel types (i.e., hard coal, brown coal, oil, natural gas, derived gas, biofuels etc.). To extrapolate the emissions to the year 2012 specifically we follow the approach taken

in the COFFEE data set (CO_2 release and Oxygen uptake from Fossil Fuel Emission Estimate) (Steinbach et al., 2011) and use specific temporal factors (seasonal, weekly and daily cycles) (Denier van der Gon et al., 2011) for different emission categories, and apply country and fuel type specific year-to-year changes at national level taken from the BP statistical review of World Energy 2014 (available at http://www.bp.com/en/global/corporate/about-bp/energy-economics/statistical-review-of-world-energy.html).

The STILT model calculates the total trace gas mole fraction of CO_2 (y_{tot}) at the measurement site as the sum of a background mole fraction y_{bg}, contributions from the biosphere y_{bio}, from different fossil fuel types $y_{ff,i}$ and different biofuel types $y_{bf,j}$:

$$y_{tot} = y_{bg} + y_{bio} + \sum_i y_{ff,i} + \sum_j y_{bf,j}. \quad (1)$$

The last two terms of Eq. (1) form the total fuel CO_2 (y_F). We can associate a total isotopic $\delta^{13}C(CO_2)$ (δ_{tot}) record to the total CO_2 record following Mook (2001):

$$\delta_{tot} y_{tot} \approx \delta_{bg} y_{bg} + \delta_{bio} y_{bio} + \sum_i \delta_{ff,i} y_{ff,i} + \sum_j \delta_{bf,j} y_{bf,j}. \quad (2)$$

The isotopic signatures attributed to the different emission types, e.g., $\delta_{ff,i}$ and δ_{bio}, are listed in Table 1. Note that we do not implement a diurnal cycle into the biospheric signature.

The total CO mole fraction (x_{tot}) can be balanced in analogy to CO_2, but we neglect biospheric CO contributions as they are expected to be small:

$$x_{tot} = x'_{bg} + \sum_i x_{ff,i} + \sum_j x_{bf,j} = x'_{bg} + \sum_i \frac{y_{ff,i}}{\overline{R_{ff,i}}} + \sum_j \frac{y_{bf,j}}{\overline{R_{bf,i}}}. \quad (3)$$

The emission ratios $\overline{R_{ff,i}}$ ($= (\Delta x/\Delta y)_{ff,i}$) depend on the emission category as well as fuel type and are determined by the emission characteristics (implied emission factors) given in EDGARv4.3. The footprint-weighted mean ratios, e.g., $\overline{R_F}$, are listed in Table A1 for Heidelberg. For the background values $\Delta^{14}C_{bg}$, y_{bg}, δ_{bg} and x'_{bg}, we use those mole fractions where CH_4 mole fraction reaches a minimum value within 2 days. This is mainly the case in the afternoon, when vertical mixing is strongest (for more details on the choice of background, see Appendix A2). Note that the CO background x'_{bg} is denoted with a prime, since it has been corrected for chemical reactions with OH (sink) and for production from oxidation of CH_4 by applying a first-order chemical reaction on hourly OH and CH_4 fields. The contributions of fossil fuel and biofuel CO are, however, not corrected for these chemical reactions in the model, since the CO which is released in the footprint area of the measurement site typically travels only a fraction of its actual lifetime until arriving at the measurement site.

Table 1. $\delta^{13}C(CO_2)$ source signature of fuel types and biosphere as used in the model. The isotopic signature of the biosphere follows the findings of Ballantyne et al. (2011) for Europe. The assigned isotopic fuel values were chosen from mean measured isotopic signatures in Heidelberg (Kaul, 2007, and unpublished data) or, if not available, are similar to isotopic $\delta^{13}C(CO_2)$ values reported in Andres et al. (1994) or (for biogas) Widory et al. (2012).

Emission source	$\delta_{ff,i}\,\delta_{bf,j}$ or δ_{bio} [‰]
Hard coal	−27
Brown coal	−29
Peat	−30
Solid waste	−30
Heavy oil	−31
Light oil	−31
Natural gas	−48
Derived gas	−30
Solid biomass	−29
Bioliquid	−31
Biosphere	
Jan	−27
Feb	−26
Mar	−25
Apr	−24
May	−23
Jun	−22
Jul	−22
Aug	−23
Sep	−24
Oct	−25
Nov	−26
Dec	−27

The $\Delta^{14}C(CO_2)$ ($\Delta^{14}C_{tot}$) balance is also simulated and follows

$$y_{tot}\left(\Delta^{14}C_{tot}+1\right) \approx y_{bg}\left(\Delta^{14}C_{bg}+1\right) + y_{bio}\left(\Delta^{14}C_{bio}+1\right) + \sum_i y_{ff,i}\left(\Delta^{14}C_{ff,i}+1\right) + \sum_j y_{bf,j}(\Delta^{14}C_{bf,j}+1), \quad (4)$$

with $\Delta^{14}C_{bio}$, $\Delta^{14}C_{bf,j}$ and $\Delta^{14}C_{ff,i}$ listed in Table A1 and CO_2 mole fractions taken from model results. As all fossil fuel CO_2 sources are devoid of $^{14}C(CO_2)$, fuel CO_2 contributions are separated into fossil fuel and biofuel contributions.

In the following, we use six different tracers or tracer combinations to derive continuous fuel CO_2: (a) CO_2-only, (b) CO, (c) CO as a tracer for traffic and $\delta^{13}C$ as a tracer for all fuel CO_2 except that of traffic, (d) CO as a tracer for biofuel CO_2 and $\delta^{13}C(CO_2)$ as a tracer for fossil fuel CO_2, (e) $\delta^{13}C(CO_2)$ and (f) $\Delta^{14}C(CO_2)$. The six tracer combinations were qualitatively motivated and described in the Introduction and the equations are derived in Appendix A1 and are summarized in Table 2. They are briefly specified here with

Table 2. Tracer or tracer combinations, required parameters and formula for estimation of targeted fuel CO_2 concentration. In cases (c) and (d) we further divide fuel CO_2 into traffic CO_2 and non-traffic CO_2, or fossil fuel CO_2 and biofuel CO_2, respectively. In case (f) we can only estimate fossil fuel CO_2 with $\Delta^{14}C(CO_2)$and therefore lack biofuel CO_2 for a comprehensive fuel CO_2 estimate.

Case	Required parameters	Formula (for derivation see Appendix A1)
(a) CO_2		$y_F = \Delta y$
(b) CO	$\overline{R_F}$	$y_F = \frac{\Delta x}{\overline{R_F}}$
(c) CO (tr) $+\delta^{13}$C-CO_2	$\overline{R_{tr}}, \overline{m_{tr}}, \overline{\delta_{tr}}, \overline{\delta_{F\text{-}tr}}$	$y_F = \frac{\Delta x(t)\cdot\overline{m_{tr}}}{\overline{R_{tr}}} + \frac{y_{tot}\delta_{tot} - y_{bg}\delta_{bg} - (y_{tot} - y_{bg} - y_{bf})\delta_{bio} - y_{tr}\overline{\delta_{tr}}}{\overline{\delta_{F\text{-}tr}} - \delta_{bio}} y_{tot}$
(d) CO (bf) $+\delta^{13}$C-CO_2	$\overline{R_{bf}}, \overline{m_{bf}}, \overline{\delta_{bf}}, \overline{\delta_{ff}}$	$y_F = \frac{\Delta x(t)\cdot\overline{m_{bf}}}{\overline{R_{bf}}} + \frac{y_{tot}\delta_{tot} - y_{bg}\delta_{bg} - (y_{tot} - y_{bg} - y_{tr})\delta_{bio} - y_{bf}\overline{\delta_{bf}}}{\overline{\delta_{ff}} - \delta_{bio}} y_{tot}$
(e) δ^{13}C-CO_2	$\overline{\delta_F}$	$y_F = \frac{y_{tot}\delta_{tot} - y_{bg}\delta_{bg} - (y_{tot} - y_{bg})\delta_{bio}}{\overline{\delta_F} - \delta_{bio}} y_{tot}$
(f) Δ^{14}C-CO_2	$\Delta^{14}C_{bf}$, $\Delta^{14}C_{bio}$	$y_F \approx y_{ff} = \frac{y_{bg}(\Delta^{14}C_{bg} - \Delta^{14}C_{bio}) - y_{tot}(\Delta^{14}C_{tot} - \Delta^{14}C_{bio}) - y_{bf}(\Delta^{14}C_{bio} - \Delta^{14}C_{bf})}{\Delta^{14}C_{bio} + 1}$

their underlying assumptions. When using CO_2 as a tracer for anthropogenic CO_2 (case a in Table 2), we assume that all CO_2 stems from anthropogenic sources and no biospheric sources or sinks exist in the catchment area. In the CO-based method (case b in Table 2), we use CO as a tracer for anthropogenic CO_2 as CO is co-emitted during incomplete combustion. We assume to know the monthly mean ratio of fuel CO_2 to CO. In the $\delta^{13}C(CO_2)$ approach (case e in Table 2), we use the isotopic depletion of fuel CO_2 relative to biospheric CO_2 and assume to know the mean isotopic signature of fuel and biospheric CO_2. The $\Delta^{14}C(CO_2)$-based approach (case f in Table 2) makes use of the fact that fossil fuel CO_2 contains no $^{14}C(CO_2)$, in contrast to biospheric (and biofuel) $\Delta^{14}C(CO_2)$. Both need to be known for calculation. We also investigate the combination of CO and $\delta^{13}C(CO_2)$, with CO as a tracer for (1) traffic CO_2 (case c in Table 2) and (2) biofuel CO_2 and $\delta^{13}C(CO_2)$ for the respective remaining fuel CO_2 (case d in Table 2). This separation was made since in Europe traffic and biofuel emissions both show a rather large ratio of CO / CO_2 compared to emissions from other sectors, which makes CO a suitable tracer for these sectors. When separating between traffic and non-traffic fuel CO_2, we need to know the monthly mean values for $\overline{R_{tr}}$, $\overline{m_{tr}}$, $\overline{\delta_{tr}}$ and $\overline{\delta_{F\text{-}tr}}$. This holds equally true for separation between fossil fuel and biofuel CO_2. The different targeted emission groups (fuel CO_2, fossil fuel CO_2, fuel CO_2 without traffic, traffic CO_2, biofuel CO_2 and biospheric CO_2) are also listed and characterized in Table A1.

3 Results

We investigated how well the different tracer combinations perform at a typical urban, rural and polluted measurement site. First, we will discuss the upper limit of precision and accuracy of fuel CO_2 estimation using these tracers when assuming all parameters (e.g., $\overline{\delta_F}$) are known at every time step. Here, the smallest possible time step is hours. We then investigate how the use of averaged accurate parameters and variables affects the fuel CO_2 estimate. Next, we also perform a sensitivity analysis to identify which parameters and variables need to be known at which precision and accuracy for fuel CO_2 estimation with satisfying accuracy (of, for example, better than 10 %). Finally, we discuss the diurnal variation in fuel CO_2 and include a realistic measurement uncertainty into our considerations.

3.1 High (hourly) resolution of parameters and variables

The integrated footprint-weighted parameters (e.g., $\overline{R_F}$, $\overline{R_{tr}}$, $\overline{R_{bf}}$, $\overline{\delta_F}$, $\overline{\delta_{ff}}$, $\overline{\delta_{bf}}$, $\overline{\delta_{tr}}$, $\overline{\delta_{F\text{-}tr}}$, $\overline{m_{bf}}$ and $\overline{m_{tr}}$) are needed for the estimation of fuel CO_2 using the tracers CO and $\delta^{13}C(CO_2)$ (see Appendix A1 for derivation and Table 2 for summary of all equations). These parameters are dependent on the emission characteristics of the sources in the catchment area of the measurement site. If, for example, the mean isotopic signature of fuel CO_2 sources in the catchment area varies or if the catchment area itself varies, the integrated footprint-weighted parameter $\overline{\delta_F}$ will change. Typically, the integrated footprint-weighted parameters vary on timescales of hours, weeks, months and years. If, for a given measurement site, we could determine these parameters on the timescale of hours (which is the temporal resolution of our model), we would be able to estimate fuel CO_2 entirely correctly (difference of estimated and modeled fuel CO_2 would be zero) using CO and $\delta^{13}C(CO_2)$ or any combination of these tracers.

In contrast to methods using CO and/or $\delta^{13}C(CO_2)$, CO_2-only will overestimate fuel CO_2 when biospheric CO_2 contributions are positive (which will often be the case during nighttime and in winter) and underestimate fuel CO_2 when the biospheric CO_2 is negative (which may be the case during daytime in summer). This leads to time-dependent biases depending on the proportion of biospheric CO_2 to total CO_2 at the location, which is in general not negligible compared to the fuel CO_2 signal.

As $\Delta^{14}C(CO_2)$ is not sensitive to biofuel contributions, $\Delta^{14}C(CO_2)$-based fuel CO_2 estimates will underestimate the fuel CO_2 contributions approximately by the amount of biofuel CO_2 to the regional CO_2 concentration offset. Additionally, any $^{14}C(CO_2)$ emissions from nearby nuclear power plants or nuclear fuel reprocessing plants could potentially mask the depletion of fuel CO_2 contributions. Nuclear power plant emissions were not implemented in this model, but we will shortly discuss their possible effects in Sect. 5.

3.2 Low (monthly) resolution of parameters and variables

Normally it is not be possible to determine parameters such as $\overline{R_F}$, $\overline{R_{tr}}$, $\overline{R_{bf}}$, $\overline{\delta_F}$, $\overline{\delta_{ff}}$, $\overline{\delta_{bf}}$, $\overline{\delta_{tr}}$, $\overline{\delta_{F\text{-}tr}}$, $\overline{m_{bf}}$ and $\overline{m_{tr}}$ with hourly resolution. Thus we investigate how using monthly median values of these parameters may influence the fuel CO_2 estimates. We will discuss later how we can obtain their monthly mean values and for now we assume their monthly median value is known. Note that we use the median instead of the mean value for the footprint-weighted parameters, since the median is less sensitive to outliers. Using only monthly median values will introduce sub-monthly inaccuracies into the fuel CO_2 estimate since the footprint-weighted parameters vary on sub-monthly timescales. The variability in the discrepancy between estimated and reference (directly modeled) fuel CO_2 estimates will depend on the magnitude of sub-monthly variations of $\overline{R_F}$, $\overline{R_{tr}}$, $\overline{R_{bf}}$, $\overline{\delta_F}$, $\overline{\delta_{ff}}$, $\overline{\delta_{bf}}$, $\overline{\delta_{tr}}$, $\overline{\delta_{F\text{-}tr}}$, $\overline{m_{bf}}$ and $\overline{m_{tr}}$, as well as on their absolute values. For example, the more depleted the fuel CO_2 emissions are, the larger the isotopic difference between emissions from the biosphere and from fuel burning and the better the tracer $\delta^{13}C(CO_2)$ will be for fuel CO_2 emissions as both emission groups can be isotopically distinguished clearly (see Appendix C). For our model setting, the sub-monthly variations (standard deviation) are about ± 3 $(\text{nmol mol}^{-1})/(\mu\text{mol mol}^{-1})$ for $\overline{R_F}$, $\overline{R_{tr}}$ and $\overline{R_{bf}}$; ± 0.2 $(\text{nmol mol}^{-1})/(\text{nmol mol}^{-1})$ for $\overline{m_{bf}}$ and $\overline{m_{tr}}$; and ± 2 ‰ for $\overline{\delta_F}$, $\overline{\delta_{ff}}$, $\overline{\delta_{bf}}$, $\overline{\delta_{tr}}$ and $\overline{\delta_{F\text{-}tr}}$ (variations due to varying footprints in the STILT model and temporal emission patterns of the different emission sectors). This variation is propagated into the fuel CO_2 estimate. The corresponding distribution of the difference between the estimated and modeled fuel CO_2 can be seen in Fig. 1 for the station Heidelberg and in Figs. 2 and 3 for Gartow and Berlin.

The mean difference between the modeled and tracer-based fuel CO_2 estimate provides a measure for the accuracy of the fuel CO_2 determination with the different tracer methods. In principle, one cannot assume that, when using the correct median values for $\overline{R_F}$, $\overline{R_{tr}}$, $\overline{R_{bf}}$, $\overline{\delta_F}$, $\overline{\delta_{ff}}$, $\overline{\delta_{bf}}$, $\overline{\delta_{tr}}$ and $\overline{\delta_{F\text{-}tr}}$, no median bias will be introduced into the CO_2 estimate. The reason is that the values for $\overline{R_F}$, $\overline{R_{tr}}$, $\overline{R_{bf}}$, $\overline{\delta_F}$, $\overline{\delta_{ff}}$, $\overline{\delta_{bf}}$, $\overline{\delta_{tr}}$ and $\overline{\delta_{F\text{-}tr}}$ are calculated on an hourly basis independent of the total fuel CO_2 value (y_F) at that time and are then averaged monthly. However, if y_F and $\overline{R_F}$, $\overline{R_{tr}}$, $\overline{R_{bf}}$, $\overline{\delta_F}$, $\overline{\delta_{ff}}$, $\overline{\delta_{bf}}$, $\overline{\delta_{tr}}$ and $\overline{\delta_{F\text{-}tr}}$ are correlated, sub-monthly over- and underestimation of y_F due to sub-monthly variation in $\overline{R_F}$, $\overline{R_{tr}}$, $\overline{R_{bf}}$, $\overline{\delta_F}$, $\overline{\delta_{ff}}$, $\overline{\delta_{bf}}$, $\overline{\delta_{tr}}$ and $\overline{\delta_{F\text{-}tr}}$ will not necessarily average out. An analysis of the bias (difference between modeled and tracer-based fuel CO_2 estimate; x axis in Figs. 1–3) introduced when using monthly median footprint-weighted parameters is therefore vital. The standard deviations of the Gaussian fits to the difference distributions (Figs. 1–3) provide a measure for the precision of fuel CO_2 determination.

All methods using $\delta^{13}C(CO_2)$ and/or CO (Figs. 1b–e, 2b–e and 3b–e) are able to estimate fuel CO_2 without significant systematic biases if the annual median parameters $\overline{\delta_{ff}}$, $\overline{\delta_{bf}}$, $\overline{\delta_{tr}}$, $\overline{\delta_{F\text{-}tr}}$ and $\overline{R_F}$ are known (see Sect. 3.3. for the case that they are not accurately known). Mean and median differences of modeled and estimated fuel CO_2 are within 10 % of the annual mean fuel CO_2 signal. The benefit when using CO additionally to $\delta^{13}C(CO_2)$ is very small, which is due to the fact that traffic or biofuel CO_2 contributions are not very distinct with respect to their isotopic signature or their $CO\,/\,CO_2$ emission ratio from the other fuel CO_2 contributions for our model settings. When using CO as a tracer for fuel CO_2 (Figs. 1b, 2b and 3b) the standard deviation of the difference between the estimated and the true fuel CO_2 value is larger than when using $\delta^{13}C(CO_2)$. The reason is the large sub-monthly variation in footprint-weighted $\overline{R_F}$ in our modeled data.

Generally, the absolute standard deviation of the different tracer distributions is larger at the polluted station than at urban and rural stations. At the same time, we found that the variation in the footprint-weighted parameters such as $\overline{R_F}$, $\overline{R_{tr}}$, $\overline{R_{bf}}$, $\overline{\delta_F}$, $\overline{\delta_{ff}}$, $\overline{\delta_{bf}}$, $\overline{\delta_{tr}}$, $\overline{\delta_{F\text{-}tr}}$, $\overline{m_{bf}}$ and $\overline{m_{tr}}$ is largest in rural areas and smallest in polluted areas, which is probably due to the fact that the many polluters homogenize partly in polluted catchment areas, whereas the emissions of the few different polluters are temporally and spatially distinct at cleaner sites. Hence, the larger spread of the fuel CO_2 estimate at polluted stations is not the result of larger source heterogeneity but is rather due to the larger absolute signals (and with that larger absolute variations) of fuel CO_2 in the catchment area of these sites. Only CO_2 as a tracer for fuel CO_2 shows less variability at the polluted site Berlin, which is due to smaller contribution from the biosphere in its catchment area. However, the relative variability (i.e., $1\sigma\,/\,\text{mean}(y_F)$) is significantly higher in Gartow (e.g., the $\delta^{13}C$ method: 20 %) than it is in Heidelberg or Berlin (both ca. 5 %). Differences and spreads of the CO_2-only and $^{14}C(CO_2)$ method have already been described in Sect. 3.1.

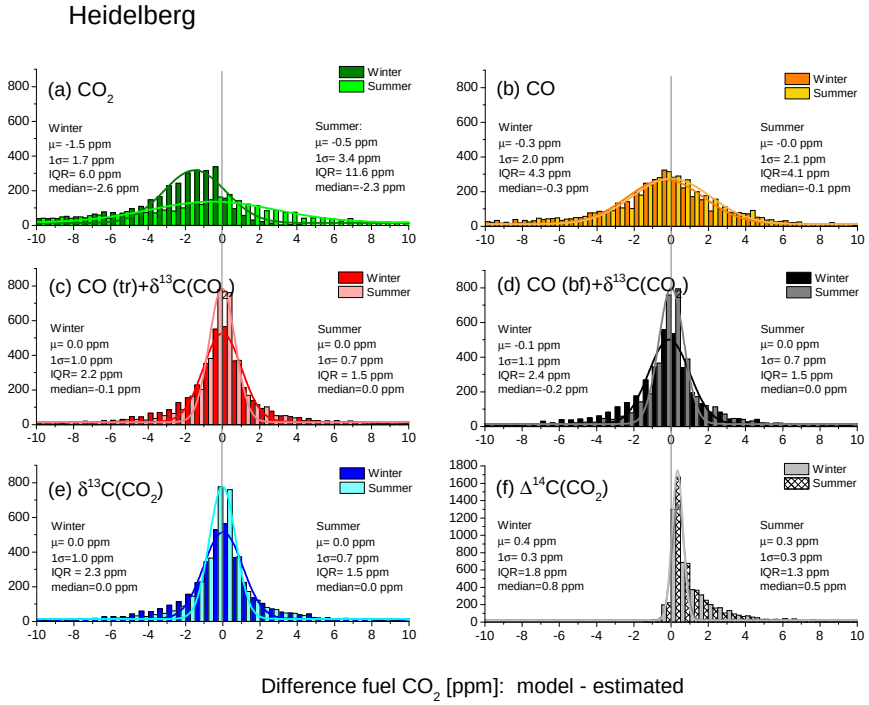

Figure 1. Histograms showing the differences between the modeled fuel CO_2 (assumed as correct) and the tracer-based estimated fuel CO_2 for the year 2012 for Heidelberg using the different tracers and tracer configurations listed in Table 2. Differences result from sub-monthly variations of parameters. Note the different y axis scale. Darker colors denote the winter periods and lighter colors the summer periods (see legend). The distributions were fitted with a Gaussian fit and the shift (μ) and the standard deviation (σ) for the Gaussian fits are given in the figure. Since the histograms do not follow Gaussian distributions (especially for $^{14}C(CO_2)$ due to non-normally distributed biofuel CO_2 contributions within 1 year) we also give the interquartile range (IQR) in the figure to remind the reader that the uncertainty may be underestimated when using the Gaussian standard deviation for uncertainty analysis. The CO_2 mole fractions are given in parts per million (ppm), which is equivalent to $\mu mol\,mol^{-1}$. Note that, in Heidelberg, mean fuel CO_2 for summer is 15 $\mu mol\,mol^{-1}$ and that for winter is 16 $\mu mol\,mol^{-1}$.

We have found that only small median differences occur when using $\delta^{13}C(CO_2)$ or CO as a tracer for fuel CO_2. This finding is only valid under the premise that the median values of all input and footprint-weighted parameters are known. If one or more of the parameters or variables are assigned incorrectly, this will lead to a systematic error of the fuel CO_2 estimate. The sensitivity of this misassignment for the different parameters and variables will be assessed in the next chapter.

3.3 Sensitivity of fuel CO_2 estimates on misassigned parameters and variables

We have investigated how well we are able to estimate fuel CO_2 in a setting in which, for example, the monthly averages of all parameters are perfectly well known but temporally varying on a shorter timescale. However, since, in reality, parameters such as $\overline{\delta_F}$ or $\overline{R_F}$ are only approximately known, we need to investigate how a misassignment of one of these parameters will influence fuel CO_2 estimates. This will provide information on how well certain parameters and variables need to be assigned for a fuel CO_2 estimate with targeted accuracy. For this purpose, we misassign one parameter and, at the same time, keep the other parameters at their correct value. We then determine how the fuel CO_2 estimate changes (y axis in Fig. 4) when the misassignment of the parameter (x axis) varies. The sensitivities of all methods to the most important parameters and variables are shown in Fig. 4 for example of the urban site Heidelberg. We have done this analysis for the parameters CO_{2tot} (Fig. 4a), $\delta^{13}C_{tot}$ (Fig. 4b), CO_{2bg} (Fig. 4c), $\delta^{13}C_{bg}$ (Fig. 4d), $\overline{\delta_F}$ (Fig. 4e), $\overline{\delta_{bio}}$ (Fig. 4f), $\overline{\delta_{bf}}$ (Fig. 4g), $\overline{\delta_{tr}}$ (Fig. 4h), CO offset (Fig. 4i), $\overline{m_{bf}}$ and $\overline{m_{tr}}$ (Fig. 4j), $\overline{R_{tr}}$ and $\overline{R_{bf}}$ (Fig. 4k), $\overline{R_F}$ (Fig. 4l), $\Delta^{14}C_{tot}$ (Fig. 4m), $\Delta^{14}C_{bg}$ (Fig. 4n), $\Delta^{14}C_{bio}$ (Fig. 4o), and $\Delta^{14}C_{bf}$ (Fig. 4p). The variation in these values was chosen in a way that the range includes the typical measurement precision for CO_{2meas}, CO_{2bg}, δ_{bg}, δ_{meas}, $\Delta^{14}C_{bg}$ and $\Delta^{14}C_{meas}$. The variation in the CO offset was chosen in a way that it displays the measurement precision of total CO and of the background CO but also includes realistic contributions from natural CO sources and sinks. For the parameters $\overline{R_F}$, $\overline{R_{tr}}$, $\overline{R_{bf}}$, $\overline{\delta_F}$, $\overline{\delta_{ff}}$, $\overline{\delta_{bf}}$,

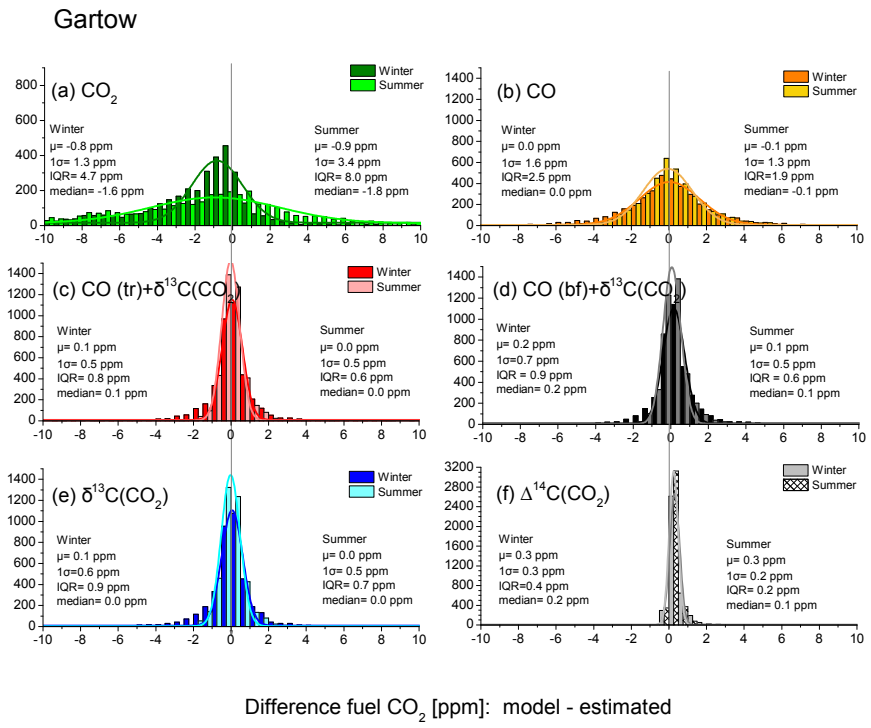

Figure 2. Same as Fig. 1 but for Gartow. In Gartow, mean fuel CO_2 for summer is 2 µmol mol^{-1} and that for winter is 4 µmol mol^{-1}.

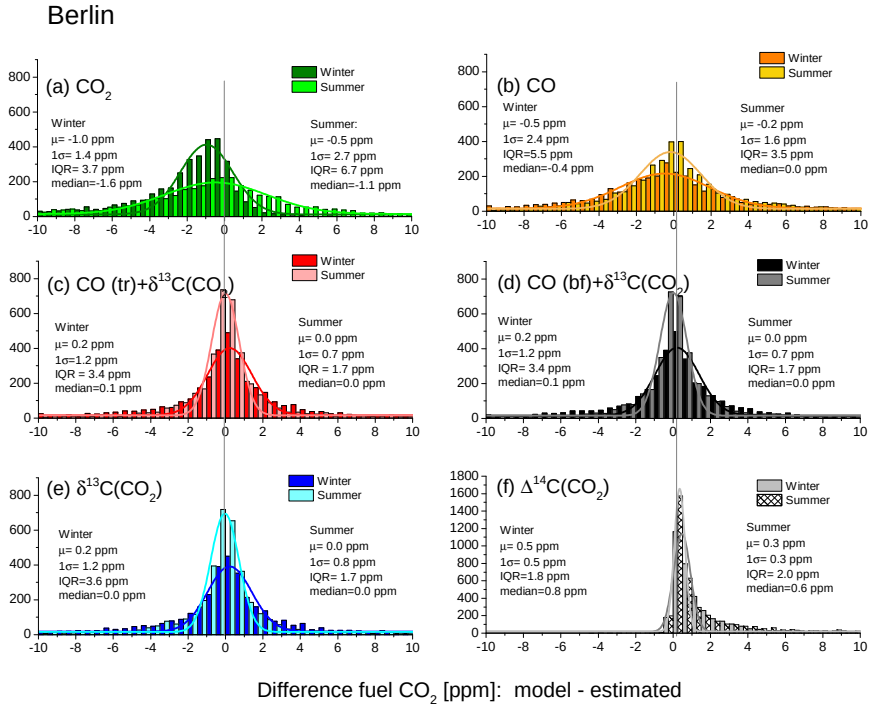

Figure 3. Same as Fig. 1 but for Berlin. In Berlin, mean fuel CO_2 for summer is 23 µmol mol^{-1} and that for winter is 27 µmol mol^{-1}.

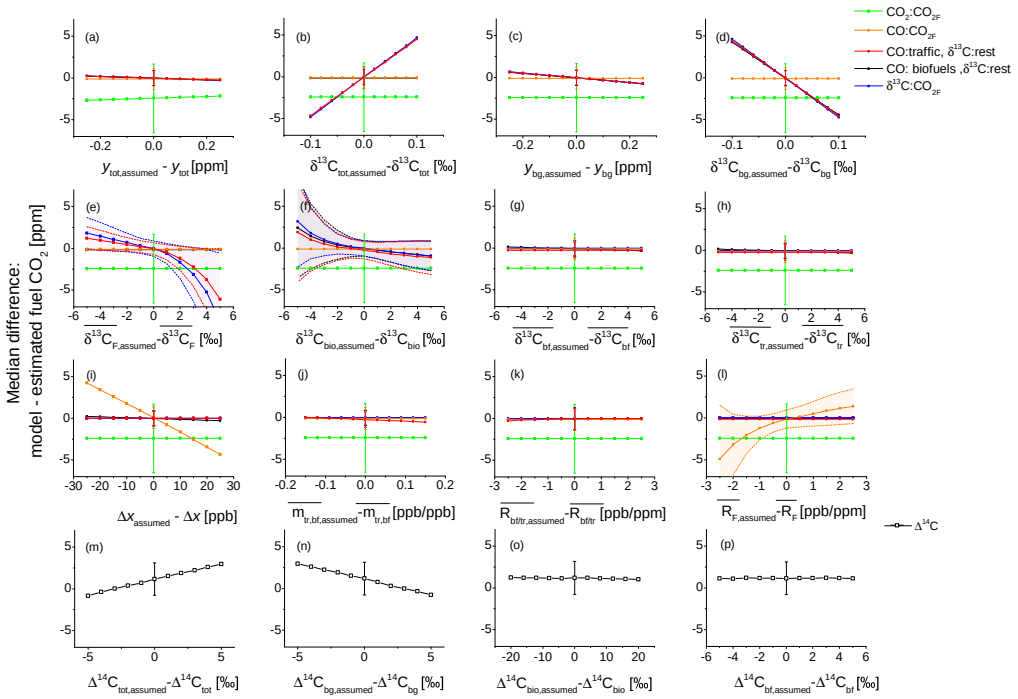

Figure 4. Sensitivity analysis: median difference between the modeled fuel CO_2 and the tracer-based estimated fuel CO_2 value (y axis) at a typical urban site (Heidelberg) when using parameters/variables for fuel CO_2 estimation ("assumed") deviating from the correct parameters/variables used in STILT. The error bars given at $x = 0$ (assumed value = model value) denote the interquartile ranges (IQR) for all x positions. If the IQRs vary depending on the assumed value, the errors (IQRs) are drawn as shaded areas.

$\overline{\delta_{tr}}$, $\overline{\delta_{F\text{-}tr}}$, $\overline{m_{bf}}$, and $\overline{m_{tr}}$ as well as for $\Delta^{14}C_{bio}$ and $\Delta^{14}C_{bf}$, we selected realistic ranges of sub-monthly parameter variation.

The error bars given at $x = 0$ of Fig. 4 show the interquartile ranges (IQR) and stem from the sub-monthly variability in $\overline{\delta_F}$, $\overline{R_F}$, $\overline{m_{bf}}$ and $\overline{m_{tr}}$, which was discussed in Sect. 3.2. One can directly identify critical parameters and variables for which the difference between the modeled and estimated fuel CO_2 (y axis) changes significantly with increasing misassignment of parameters/variables (x axis).

3.3.1 Sensitivity of CO_2-only method

We confirm that the CO_2-only method (green in Fig. 4) is insensitive to the variation in the displayed parameters/variables.

3.3.2 Sensitivity of CO method

Critical parameters/variables of the CO method (orange in Fig. 4) are the CO offset ΔCO (Fig. 4i), as well as the ratio $\overline{R_F}$ ($= \Delta x / y_F$) (Fig. 4l). In practice, the CO offset is derived by subtracting the CO background as well as natural CO source and sink contributions from the total measured CO mole fraction. Typical fuel CO offsets are on the order of 40 nmol mol^{-1}. In our model we have not included natural CO sources and sinks, but in practice the uncertainty of the CO mole fraction measurement and of the natural CO contributions will add to the uncertainty of the fuel CO_2 estimate. Assuming, for example, a CO background which is 15 nmol mol^{-1} too large, or assuming an additional sink resulting in a 15 nmol mol^{-1} lower CO background, which may be a realistic diurnal variation in natural CO variation (Gros et al., 2002; Vogel, 2010), would lead to a significant overestimation of fuel CO_2 of about 2.5 µmol mol^{-1} (median). Therefore, for a real data set, it is vital to determine the natural CO contributions and sinks (also soil sinks) using chemistry models or calibration with, for example, $\Delta^{14}C(CO_2)$ (see Sect. 4). In Heidelberg, the median modeled ratio $\overline{R_F}$ is about 5 (µmol mol^{-1})/(nmol mol^{-1}) and shows a rather large variation of 3 (nmol mol^{-1})/(µmol mol^{-1}). Figure 4l shows that such a variation in $\overline{R_F}$ contributes significantly to the imprecision of fuel CO_2 in the CO method. Also, the correct determination of $\overline{R_F}$ is vital for accurate fuel CO_2 estimates using CO.

3.3.3 Sensitivity of methods using $\delta^{13}C(CO_2)$

The sensitivities of fuel CO_2 estimates using $\delta^{13}C(CO_2)$ only (blue in Fig. 4) and combinations of $\delta^{13}C(CO_2)$ and CO are rather similar (red and black in Fig. 4). Note that the sensitivity on δ_{bg} or δ_{tot} is plotted when keeping y_{bg} and y_{tot} constant. Changing the y_{bg} or y_{tot} values at the same time

when changing δ_{bg} or δ_{tot} (following a Keeling curve (Keeling, 1958, 1960) with typical mean $\delta^{13}C$ source of -25 ‰) results in sensitivity about a factor of 10 smaller and is therefore not critical. However, small $\delta^{13}C(CO_2)$ variations (e.g., due to finite measurement precision or small inaccuracies) which are uncorrelated with CO_{2tot} lead to large biases in fuel CO_2, e.g., a measurement bias of $\delta_{tot} = 0.1$ ‰, leads to a fuel CO_2 misassignment of 5 ($\mu mol\,mol^{-1}$) (see Fig. 4b). Therefore, a high measurement precision as well as accuracy of $\delta^{13}C(CO_2)$ is required for precise and accurate fuel CO_2 estimation. Further critical parameters of the methods using $\delta^{13}C(CO_2)$ are the isotopic signature of fuel CO_2 and the isotopic signature of biospheric CO_2 in the footprint (see Fig. 4e, f). The isotopic signatures of fuel and biospheric CO_2 must therefore be well known (or potentially calibrated; see Sect. 4) if we want to use $\delta^{13}C(CO_2)$ as a tracer for fuel CO_2. In particular, assuming more enriched fuel isotopic signatures or too depleted biospheric signatures biases the fuel CO_2 estimates strongly, because in these cases, biospheric and fuel CO_2 sources are difficult to distinguish using $\delta^{13}C(CO_2)$.

3.3.4 Sensitivity of $\Delta^{14}C(CO_2)$ method

Figure 4m–p display the sensitivity of the $\Delta^{14}C(CO_2)$-based estimate of fuel CO_2 on the variables $\Delta^{14}C_{tot}$, $\Delta^{14}C_{bg}$ and $\Delta^{14}C_{bio}$. While fuel CO_2 is rather insensitive to misassignment of $\Delta^{14}C(CO_2)_{bio}$ (Fig. 4o) and $\Delta^{14}C(CO_2)_{bf}$ (Fig. 4p), it is very sensitive to $\Delta^{14}C(CO_2)_{tot}$ (Fig. 4m) and $\Delta^{14}C(CO_2)_{bg}$ (Fig. 4n) as has already been described in Turnbull et al. (2007). Thus, precise and accurate $\Delta^{14}C(CO_2)$ measurements are important for fuel CO_2 determination. Note that the best currently achieved measurement precision of conventional counting or AMS measurements is ±2 ‰ (equivalent to about $\pm 1.0\,\mu mol\,mol^{-1}$ fuel CO_2), but the hypothetical future continuous GC-AMS measurements may be on the order of ±5 ‰ (equivalent to about $\pm 3\,\mu mol\,mol^{-1}$ fuel CO_2). The reason why the fuel (biofuel + fossil fuel) CO_2 estimate based on ^{14}C is biased by about $1.1\,\mu mol\,mol^{-1}$ is due to the fact that biofuel CO_2, in contrast to fossil fuel CO_2, contains $^{14}C(CO_2)$ and is therefore not detectable through a lack of $^{14}C(CO_2)$.

3.4 Measurement precision and sub-monthly variation in parameters/variables

In Sects. 3.3.1–3.3.4, we have seen how sensitive the fuel CO_2 estimates are to the total mole fractions and δ/Δ values. Since they have a large impact on the fuel CO_2 estimate, we now include their uncertainty in our analysis of precision of fuel CO_2 estimation. In order to display the effect of a limited measurement precision of CO_2, CO, $\delta^{13}C(CO_2)$ and $\Delta^{14}C(CO_2)$ we construct random realizations with mean value zero and a specific standard deviation. Additionally, we add a random variation to the CO offset and the biospheric/biofuel isotopic (δ/Δ) signature in order to simulate the effect of variability in CO to CO_2 ratio and of isotopic end members. These random uncertainties were not included in Sects. 3.1 and 3.2 and in Figs. 1–3. Note that in reality these variations may not be randomly distributed but have a distinct sub-monthly pattern. For example, we may introduce a systematic bias in one direction if we have unaccounted production of CO from VOCs or if we have unaccounted CO (e.g., soil) sinks. These sources and sinks will not occur randomly, but have a distinct sub-monthly pattern. Depending on the sign of the net natural CO flux, the bias may be positive or negative. However, for simplicity, we also include the natural CO variation here as a random vector as no natural CO sinks or sources are included in the modeled CO offset but we want to show the possible effect of their variation.

The random vectors which were used in this study in this study are summarized and explained in Table 3. The distributions of the difference between estimated (including measurement and parameter uncertainties and sub-monthly variations) and modeled fuel CO_2 can be seen in Figs. 5–7. Note that a possible misassignment of parameters or variables as investigated in Fig. 4 is not accounted for in either Figs. 1–3 or Figs. 5–7.

When including the measurement uncertainties and (input and footprint-weighted) parameter variability in the considerations, the mean bias remains unaltered, since the included uncertainty is random. However, the distributions of the CO and $\delta^{13}C(CO_2)$-based approaches for rural sites (such as Gartow), medium polluted sites (such as Heidelberg) and polluted sites (such as Berlin) widen significantly by about the same amount for all three sites. This is due to identical assumed measurement precisions and parameter variations. Since the absolute fuel CO_2 offset is larger in Berlin (annual modeled average ca. $25\,\mu mol\,mol^{-1}$) than in Heidelberg ($16\,\mu mol\,mol^{-1}$) and in Gartow ($3\,\mu mol\,mol^{-1}$), the relative variability ($=1\sigma/\,\mathrm{mean}(y_F)$) is smallest for the measurement site in Berlin (e.g., ca. 15 % for the $\delta^{13}C(CO_2)$ method) and largest for Gartow (110 % for the $\delta^{13}C(CO_2)$ method). At present, it is therefore questionable whether the estimation of continuous fuel CO_2 is possible at rural measurement sites. Even $\Delta^{14}C(CO_2)$ measurements with a precision of 5 ‰ result in a variability in fuel CO_2 of 60 %, but a $\Delta^{14}C(CO_2)$ precision of 2 ‰ would lead to a variability in fuel CO_2 of only 35 % at rural sites (not shown here). The reduced precision of fuel CO_2 estimates which we observe when including limited measurement precision into our considerations highlights again the necessity of performing precise atmospheric measurements of $\delta^{13}C(CO_2)$ and CO_2 if we want to use $\delta^{13}C(CO_2)$ as a tracer for fuel CO_2.

For urban sites, CO and $\delta^{13}C(CO_2)$-based methods show a very similar precision of about $4\,\mu mol\,mol^{-1}$ (1σ). At urban sites, $\delta^{13}C(CO_2)$ is slightly more precise than CO. It is worth pointing out that CO_2-only may be an adequate tracer for fuel CO_2 in polluted areas in the wintertime as absolute biases are small (< 4 %) and the precision (ca. 12 %) is rather good.

Table 3. Magnitude, physical reason and reference of parameter variation (included in Figs. 5–7).

Component	Variation (random)	Physical reason for variation	Reference
y_{tot}, y_{bg}	0.05 µmol mol^{-1}	measurement uncertainty	Hammer et al. (2013)
δ_{meas}, δ_{bg}	0.05 ‰	measurement uncertainty	e.g., Tuzson et al. (2011); Vardag et al. (2015)
x_{tot}	15 nmol mol^{-1}	natural CO sources and sinks	Gros et al. (2002); Vogel (2010)
δ_{bio}	2 ‰	heterogeneity of biosphere	compare with Pataki et al. (2003)
$\Delta^{14}C_{meas}$, $\Delta^{14}C_{bg}$	5 ‰	measurement uncertainty	McIntyre et al. (2013)
$\Delta^{14}C_{bio}$	5 ‰	heterogeneity of biosphere and turnover times	compare with Taylor et al. (2015)
$\Delta^{14}C_{bf}$	10 ‰	source/age of biofuels	–
$\overline{R_F}$, $\overline{R_{tr}}$, $\overline{R_{bf}}$, $\overline{\delta_F}$ $\overline{\delta_{ff}}$, $\overline{\delta_{bf}}$, $\overline{\delta_{tr}}$, $\overline{\delta_{F\text{-}tr}}$, $\overline{m_{bf}}$ and $\overline{m_{tr}}$	– Sub-monthly variation already included as only monthly median values are used, but parameters vary at an hourly timescale	footprint or source mix change	

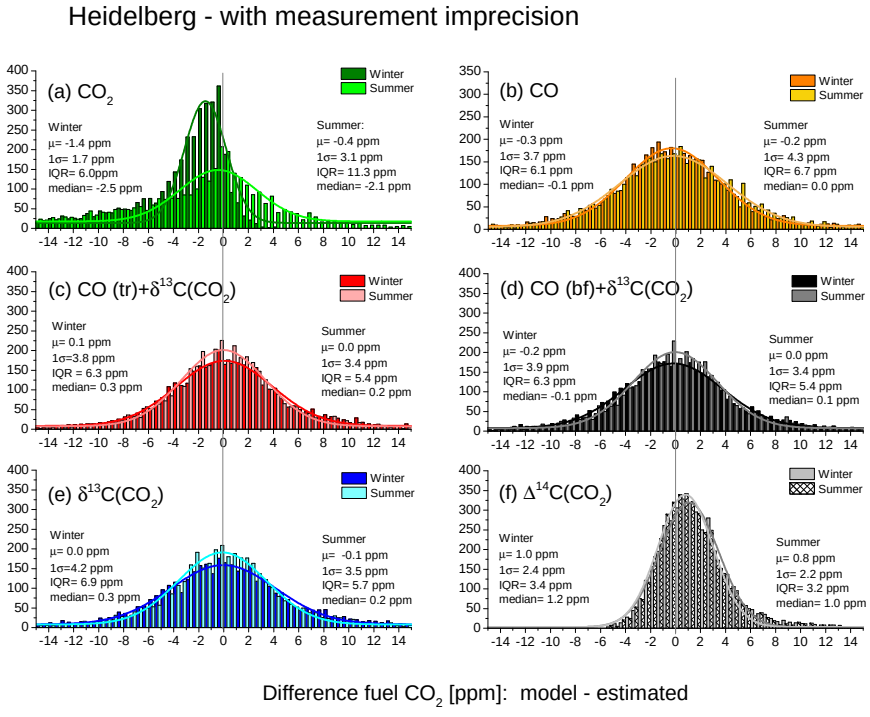

Figure 5. Same as Fig. 1 but now also including measurement imprecision.

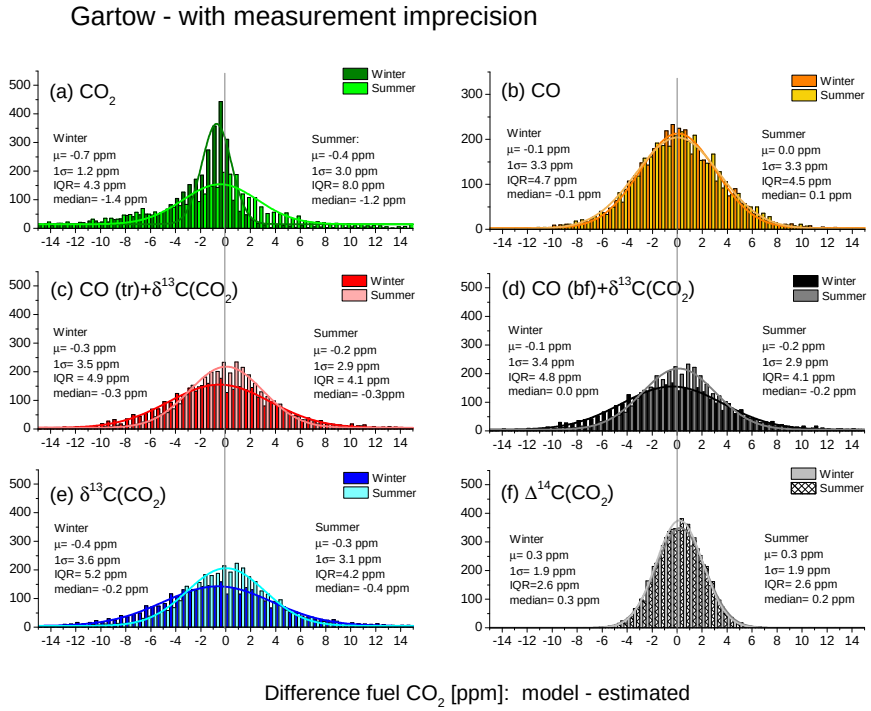

Figure 6. Same as Fig. 2 but now also including measurement imprecision.

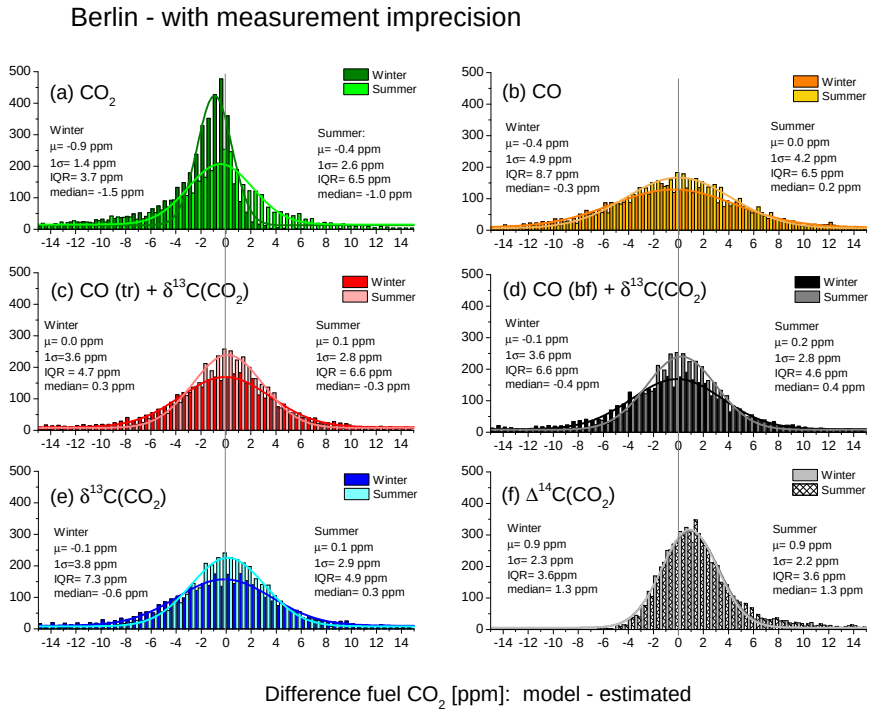

Figure 7. Same as Fig. 3 but now also including measurement imprecision.

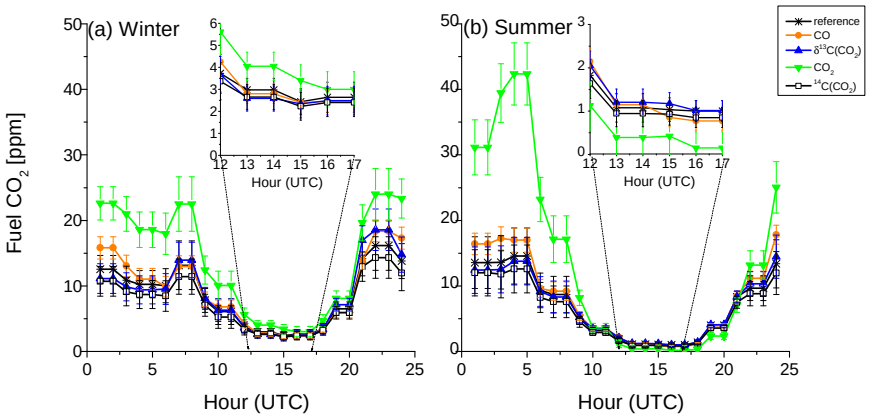

Figure 8. Comparison of median diurnal cycle of fuel CO_2 given in model reference or estimated with one of six different tracer methods at the measurement station Heidelberg. Error bars denote the standard error of the fuel CO_2 estimate at each hour for the respective half year. The diurnal cycle of the CO + $\delta^{13}C(CO_2)$ methods are not shown since they are very similar to the $\delta^{13}C(CO_2)$ method.

$\Delta^{14}C(CO_2)$ measurements with a precision of 5 ‰ would be the best tracer at all stations but are currently not available.

3.5 Comparison of the estimated fuel CO_2 diurnal cycle with different tracer configurations

As the diurnal cycle of CO_2 emissions is coupled to a diurnal change of the atmospheric mixing layer height, fuel CO_2 mole fraction varies during the day. In our calculations, we only use monthly median values of $\overline{R_F}$, $\overline{R_{tr}}$, $\overline{R_{bf}}$, $\overline{\delta_F}$, $\overline{\delta_{ff}}$, $\overline{\delta_{bf}}$, $\overline{\delta_{tr}}$, $\overline{\delta_{F\text{-}tr}}$, $\overline{m_{bf}}$ and $\overline{m_{tr}}$ for fuel CO_2 estimation. Discrepancies between the modeled reference diurnal cycle and the tracer-based diurnal cycle may be introduced due to a diurnal cycle of the parameters $\overline{R_F}$, $\overline{R_{tr}}$, $\overline{R_{bf}}$, $\overline{\delta_F}$, $\overline{\delta_{ff}}$, $\overline{\delta_{bf}}$, $\overline{\delta_{tr}}$, $\overline{\delta_{F\text{-}tr}}$, $\overline{m_{bf}}$ and $\overline{m_{tr}}$. We thus need to test whether we are able to reproduce the diurnal fuel CO_2 pattern in order to estimate fuel CO_2 from tracers at sub-diurnal resolution. Therefore, we calculate the median diurnal fuel CO_2 cycles with the different methods and compare them to the reference model diurnal cycle for summer and for winter (see Fig. 8 for the urban station Heidelberg).

One can see that the $\delta^{13}C(CO_2)$ method reproduces the reference diurnal cycle within its variability very well (standard errors of the respective hour in a half year are denoted as error bars in Fig. 8). Median hourly differences are about 0.1 ± 0.7 µmol mol^{-1} for methods using $\delta^{13}C(CO_2)$. The CO_2-only method largely overestimates fuel CO_2 contributions during the night by up to 10 µmol mol^{-1} in winter and by about 15–25 µmol mol^{-1} in summer. During the afternoon, the CO_2-only method overestimates fuel CO_2 in winter and underestimates it in summer. Even though the absolute difference is small during the afternoon, the relative difference is still large. The CO_2-only method is therefore not able to trace the diurnal fuel CO_2 variation at a site like Heidelberg correctly. Using $\Delta^{14}C(CO_2)$ for fuel CO_2 estimation leads to a slight median underestimation throughout the day (and season), which is due to the presence of $^{14}C(CO_2)$ in biofuel CO_2 masking all biofuel CO_2 contributions. The CO method slightly overestimates fuel CO_2 during nighttime by about 10 % in winter and 20 % in summer. The standard deviation of the hourly medians of the differences between model and CO-based fuel CO_2 is about 15 % of the total fuel CO_2.

One could consider implementing a diurnal correction into the fuel CO_2 estimate in a way that, in addition to monthly varying values for $\overline{R_F}$, $\overline{R_{tr}}$, $\overline{R_{bf}}$, $\overline{\delta_F}$, $\overline{\delta_{ff}}$, $\overline{\delta_{bf}}$, $\overline{\delta_{tr}}$, $\overline{\delta_{F\text{-}tr}}$, $\overline{m_{bf}}$ and $\overline{m_{tr}}$, hourly correction factors are implemented (see Vogel et al., 2010). This will be advantageous if the parameters exhibit a significant diurnal cycle themselves. However, for our setting, implementing a diurnal correction factor only slightly improves the agreement between the model and the estimated fuel CO_2 (not shown here). The reason is that the (hourly) median footprint-weighted parameters do not influence the (hourly) median fuel CO_2 estimates linearly, and that the synoptic variations of the footprint-weighted parameters are larger than the diurnal variations. Therefore, an hourly median correction factor does not necessarily improve the hourly fuel CO_2 estimate. We note that no diurnal systematic variability in the isotopic biospheric (respiration and photosynthesis) signature or in the non-fuel CO sinks and sources (which would be treated as an enhancement or reduction of the CO offset ΔCO) was implemented but rather only random uncertainties of ±2 ‰ for δ_{bio} and ±15 nmol mol^{-1} for ΔCO. This assumption of random variability will not be correct if systematic (e.g., diurnal) variation in $\delta^{13}C_{bio}$ and non-fossil ΔCO variation occur. For $\delta^{13}C_{bio}$ the diurnal changes are expected to be small (< 1 ‰ (Flanagan et al., 2005) corresponding to fuel CO_2 biases of < 0.5 µmol mol^{-1}), but for CO these may be larger (e.g., diurnal natural ΔCO variation of about 10 nmol mol^{-1} may occur from dry deposition of CO in forest soils during night and from photochemical production of CO by hydro-

carbons during the day (Gros et al., 2002) corresponding to ca. 2.5 µmol mol^{-1} fuel CO_2). Therefore, in a real setting, it might be necessary to model natural CO concentration in order to not introduce a bias into diurnal y_F structures.

In inverse model studies, often only afternoon hours are used to derive fluxes, as the atmospheric mixing can be better simulated by the models during conditions with a well-developed mixed layer (Gerbig et al., 2008). Therefore, it is especially important to check the afternoon values of fuel CO_2. Figure 8 shows an enlarged inlay of the diurnal cycle during the afternoon hours. Since in this model study we use the minimum of total CH_4 values within 2 days as a background value (Appendix A2), the afternoon offsets are very small, leading to a low signal-to-noise ratio. However, differences between the $\delta^{13}C(CO_2)$, CO, and $\Delta^{14}C(CO_2)$-based and reference fuel CO_2 are very small as well (mean differences < 10 % of afternoon fuel CO_2 value, standard deviation of differences about 30 %). Therefore, it seems justified to use an ensemble of afternoon values of continuous fuel CO_2 estimates (based on $\delta^{13}C(CO_2)$ or CO) for inverse model studies despite the small absolute fuel CO_2 values of about 1–2 µmol mol^{-1} in the afternoon hours at an urban site.

4 Calibration of $\overline{\delta_F}$, $\overline{\delta_{F\text{-}tr}}$, $\overline{\delta_{ff}}$ and $\overline{R_F}$ with $\Delta^{14}C(CO_2)$ measurements

In order to estimate fuel CO_2 accurately with methods using CO and/or $\delta^{13}C(CO_2)$, the parameters $\overline{\delta_F}$, $\overline{\delta_{F\text{-}tr}}$, $\overline{\delta_{ff}}$ (and δ_{bio}) and $\overline{R_F}$ need to be known with high accuracy, since biases are otherwise introduced into the fuel CO_2 estimate (see Fig. 4). However, for the evaluation of a measured data set, $\overline{\delta_F}$, $\overline{\delta_{F\text{-}tr}}$, $\overline{\delta_{ff}}$, δ_{bio} and $\overline{R_F}$ are not per se available but require either extensive source sampling campaigns or good bottom-up inventories. Alternatively, these parameters could also be "calibrated" using fossil fuel CO_2 estimates from $\Delta^{14}C(CO_2)$ measurements with high precision (in addition to biofuel contributions, which need to be added on top). For this purpose, Eqs. (1) and (2) can be rearranged and solved for calibration of $\overline{\delta_F}$, $\overline{\delta_{F\text{-}tr}}$, $\overline{\delta_{ff}}$ or $\overline{R_F}$ (for derivation see Appendix B).

Since $\Delta^{14}C(CO_2)$ measurements are time-consuming and costly, in practice only a limited number of $\Delta^{14}C(CO_2)$ measurements can be regularly performed. For example, in the Integrated Carbon Observation System (ICOS) atmospheric network, the radiocarbon measurement capacity was designed for about 50 radiocarbon measurements per station per year, of which about 26 will be used for integrated sampling for long-term monitoring of fossil fuel CO_2.

Previous radiocarbon calibration approaches have suggested integrated (e.g., monthly) sampling of $\Delta^{14}C(CO_2)$ for CO tracer calibration (cf. Levin and Karstens, 2007, and Vogel et al., 2010, for $\overline{R_F}$). Another possible approach for tracer calibration is to take grab samples rather than integrated samples (e.g., Turnbull et al., 2011). Grab samples could be taken throughout the year and the derived parameters $\overline{\delta_F}$, $\overline{\delta_{F\text{-}tr}}$, $\overline{\delta_{ff}}$, and $\overline{R_F}$ could then be averaged to one median value or separated into seasons and averaged to separate values, for instance, for summer and winter. The optimal sampling strategy depends on the structure, variation and noise of $\overline{\delta_F}$, $\overline{\delta_{F\text{-}tr}}$, $\overline{\delta_{ff}}$, and $\overline{R_F}$ within 1 year. Principally, it would also be possible to take all the samples consecutively at 2 h intervals during a so-called "event" and calculate the median value from the event. Therefore, we compare here four different sampling strategies for parameter calibration, all using a total of n samples per year (in ICOS: $n \approx 24$). Note that we include sub-monthly variation in the parameters and measurement uncertainties in the observations (as in Sect. 3.4).

1. Integrated sample calibration: take $n/24$ integrated samples each month and their associated background samples (for $n \approx 24$, consisting of 12 monthly integrated samples at the measurement station as well as 12 monthly integrated samples at the background station) and calibrate $\overline{\delta_F}$, $\overline{\delta_{F\text{-}tr}}$, $\overline{\delta_{ff}}$, and $\overline{R_F}$ on a monthly basis from the integrated samples (this corresponds to the approach suggested by Levin and Karstens, 2007, and Vogel et al., 2010, for $\overline{R_F}$). In this approach, the mean ΔCO and fuel ΔCO_2 (from integrated CO and $\Delta^{14}C(CO_2)$ sampling) over the course of 1 month are used to calculate monthly $\frac{\Delta x}{\Delta y_F}$. However, since the mean of ratio $< \overline{R_F} > = < \frac{\Delta x}{\Delta y_F} >$ is actually required, and not the ratio of means $\frac{<\Delta x>}{<\Delta y_F>}$ (Vogel et al., 2010), biases may be introduced into the fuel CO_2 estimate (the same holds for the factors in $\overline{\delta_F}$, $\overline{\delta_{F\text{-}tr}}$ and $\overline{\delta_{ff}}$).

2. Annual grab sample calibration: randomly select a number of samples $n/2$ (and their associated afternoon background ($n/2$)) each year and calibrate annual median $\overline{\delta_F}$, $\overline{\delta_{F\text{-}tr}}$, $\overline{\delta_{ff}}$, and $\overline{R_F}$. Biases introduced by this sampling strategy are twofold. First, the random choice of grab samples may not represent the median annual value. This potential bias decreases with increasing number of grab samples used. Second, the potential seasonal cycle of the parameters is not considered. Therefore, in the annual grab sample calibration, the wintertime and summertime fuel CO_2 estimates will always be shifted against each other if $\overline{\delta_F}$, $\overline{\delta_{F\text{-}tr}}$, $\overline{\delta_{ff}}$, and $\overline{R_F}$ exhibit a seasonal cycle, but only one annual median value for these parameters would be used.

3. Seasonal grab sample calibration: randomly select a number of samples $n/4$ (and their associated afternoon background ($n/4$)) in summer and in winter and calibrate a median $\overline{\delta_F}$, $\overline{\delta_{F\text{-}tr}}$, $\overline{\delta_{ff}}$, and $\overline{R_F}$ with half-yearly resolution. Here, again, the random choice of grab samples may not represent the median half annual value, and a potential bias may be even larger here than in the annual grab sample calibration, since only half the samples are available to obtain a robust value for $\overline{\delta_F}$, $\overline{\delta_{F\text{-}tr}}$, $\overline{\delta_{ff}}$, and

Table 4. Absolute mean difference of tracer-based estimate and modeled (assumed as correct) fuel CO_2 in µmol mol^{-1} for the tracers CO and $\delta^{13}C(CO_2)$ for different sampling strategies and respective standard deviation (both determined from a Gaussian fit to the difference histogram) for an urban setting (here: Heidelberg). Depending on the random selection of grab samples, the bias of the calibration with annually distributed grab samples is sometimes positive and sometimes negative. Therefore, the mean absolute difference between the modeled and calibrated value was determined in a Monte Carlo simulation and is shown with a "±" sign in front of the mean value to show that the bias does not have a unique sign. The standard deviation denotes the 1σ uncertainty of the difference, which is always bidirectional. Note that we only show the results for CO and $\delta^{13}C(CO_2)$, since the results when using a combination of these tracers are very similar to those of the $\delta^{13}C(CO_2)$ method. Measurement uncertainties are included in all calibration methods.

Method		CO mole fraction		δ^{13}C-CO_2	
		Summer	Winter	Summer	Winter
No uncertainties, monthly median values known (as shown in Fig. 1)		0.0 ± 2.1	-0.3 ± 2.0	0.0 ± 0.7	0.1 ± 1.0
Measurement uncertainties included, monthly median values known (as shown in Fig. 5)		-0.2 ± 4.3	-0.3 ± 3.7	-0.1 ± 3.5	0.0 ± 4.2
Calibration with integrated samples (method 1)	n=24	-0.8 ± 4.9	-0.7 ± 4.0	-2.4 ± 5.2	-1.8 ± 5.1
Calibration with annually distributed grab samples (method 2)	n=24	$\pm 1.2 \pm 5.3$	$\pm 1.5 \pm 4.7$	$\pm 0.8 \pm 4.0$	$\pm 1.6 \pm 4.9$
	n=96	$\pm 1.1 \pm 5.2$	$\pm 1.3 \pm 4.5$	$\pm 0.5 \pm 3.8$	$\pm 1.1 \pm 4.5$
Calibration with seasonal grab sample calibration (method 3)	n=24	$\pm 1.2 \pm 5.3$	$\pm 1.5 \pm 4.7$	$\pm 1.6 \pm 4.6$	$\pm 1.6 \pm 4.9$
	n=96	$\pm 0.8 \pm 4.8$	$\pm 1.1 \pm 4.3$	$\pm 0.9 \pm 4.3$	$\pm 0.8 \pm 4.3$
Seasonal event calibration (method 4)	n=24	$\pm 2.1 \pm 6.1$	$\pm 2.0 \pm 5.1$	$\pm 1.2 \pm 4.3$	$\pm 1.9 \pm 5.1$
	n=96	$\pm 1.5 \pm 5.6$	$\pm 1.9 \pm 4.9$	$\pm 1.1 \pm 4.2$	$\pm 1.3 \pm 4.6$

$\overline{R_F}$ for summer and winter. In return, it is in principal possible to detect the seasonal variation in $\overline{R_F}$ and $\overline{\delta_F}$, $\overline{\delta_{F\text{-tr}}}$, $\overline{\delta_{ff}}$.

4. Seasonal event calibration: Randomly select an "event day" each season. On this day, select $n/2-2$ consecutive grab samples (and one associated afternoon background) and calibrate a median $\overline{R_F}$ and $\overline{\delta_F}$, $\overline{\delta_{F\text{-tr}}}$, $\overline{\delta_{ff}}$ with half-yearly resolution. This approach is similar to approach 3 but entails a greater risk of choosing an event, which is not representative of the entire season, since subsequent samples are not independent of each other. On the other hand, it has the advantage of using more calibrations for the same number of radiocarbon measurements than approach 3 since only one background sample is needed for each event. However, if the background sample is biased, it will influence the entire event.

Comparing these sampling strategies to each other using one model run is difficult, since the result changes from random realization to random realization, depending on the selection of calibration samples in sampling strategy 2–4. We have therefore performed a Monte Carlo simulation (with 500 runs) and used the root median square difference between the obtained and originally modeled reference values $\overline{R_F}$ and $\overline{\delta_F}$, $\overline{\delta_{F\text{-tr}}}$, $\overline{\delta_{ff}}$ to calculate the difference between tracer-based estimate and modeled reference fuel CO_2.

Table 4 shows the absolute mean difference and standard deviation (as determined from a Gaussian fit to the difference histogram of modeled and tracer-based fuel CO_2, in analogy to Fig. 5) for an urban setting. One can see that the "integrated sample calibration" causes biases due to the covariance of the factors in Eqs. (B1)–(B4). The effect is much stronger for methods using $\delta^{13}C$ (ca. 15 % of mean fuel CO_2 offset in Heidelberg (16 µmol mol^{-1})) than it is for the CO method (ca. 5 %). This bias is directed meaning that it is not a random uncertainty but actually a systematic bias introduced by computation. This is different from the calibrations on grab samples, which have a bidirectional absolute difference. Bidirectional differences may be advantageous over unidirectional differences when analyzing long-term records as bidirectional differences contribute to long-term noise rather than biases. For CO, it seems that the integrated calibration approach works well, but a uni-directed bias remains. Note that the differences found here are not due to the insensitivity of biofuel CO_2 contributions of $\Delta^{14}C(CO_2)$, as we add the (assumed as known) biofuel CO_2 prior to "calibration" (see Eqs. B1–B3).

We further find that, since $\overline{\delta_F}$, $\overline{\delta_{F\text{-tr}}}$ $\overline{\delta_{ff}}$, and $\overline{R_F}$ do not exhibit a strong annual cycle but show rather large, high-frequent variations, the best sampling strategy for 24 available radiocarbon measurements per year (as would be the case for the ICOS network) is using all available samples to calibrate well-defined median annual values of $\overline{\delta_F}$, $\overline{\delta_{F\text{-tr}}}$

$\overline{\delta_{\mathrm{ff}}}$, and $\overline{R_{\mathrm{F}}}$ (sampling strategy 2). With 96 (or more) available radiocarbon measurements, it may only be advisable to group the calibrations into half-yearly intervals. Having such many radiocarbon grab samples available may be a realistic scenario if the parameters do not show any trend over the course of several years. Note that a monthly grab sample calibration (not shown here) results in large biases of about $\pm 3\,\mu\mathrm{mol\,mol}^{-1}$ for CO-based as well as $\delta^{13}\mathrm{C}(\mathrm{CO_2})$-based methods and is thus not advisable.

The accuracy of the seasonal event calibration is slightly worse than the accuracy of the seasonal calibration (see Table 4) due to non-representativeness of a single event for the entire season.

5 Discussion and conclusion

In this work, we analyzed the advantages and disadvantages of different tracers for estimating continuous fuel CO_2 at different types of measurement stations. The accuracy and precision of continuous fuel CO_2 estimates at three example stations – one rural, one urban and one polluted site – were calculated. This should serve as orientation for the development of an atmospheric measurement strategy, so that the best tracer configuration for a particular station can be chosen to resolve the different CO_2 source components over a country or region. The results can be used to plan and construct new measurement networks and sampling strategies with the goal of deriving fuel CO_2 concentrations at high temporal resolution.

The results of our model study suggest that, with our current measurement precision of continuous tracers such as CO or $\delta^{13}\mathrm{C}(\mathrm{CO_2})$ (or $\Delta^{14}\mathrm{C}(\mathrm{CO_2})$), in general it is not possible to estimate fuel CO_2 in rural areas ($5\,\mu\mathrm{mol\,mol}^{-1}$ or less of fuel CO_2) with a precision better than 100 % (due to the small signal-to-noise ratio). It could still be possible to monitor single pollution events since the signal-to-noise ratio is much higher during such events. At present, it does not thus seem helpful to equip measurement stations in rural areas with continuous $\delta^{13}\mathrm{C}(\mathrm{CO_2})$ and CO measurements with the objective of monitoring continuous fuel CO_2. However, it seems that tracer-based fuel CO_2 monitoring may be possible at urban or polluted sites (as planned, for example, within the Megacities Carbon Project) and may have the potential to improve the fuel CO_2 bottom-up inventories.

We find that CO_2-only cannot be used as a tracer for fuel CO_2, as a significant contribution of CO_2 is released or taken up by the biosphere even in wintertime. Only during winter in strongly polluted areas do biogenic CO_2 contributions lead to a relatively small bias of about 5 % with the CO_2-only approach and a small variation (σ / mean(y_{F}): 5 %; see Fig. 7).

In contrast to CO_2-only, CO and $\delta^{13}\mathrm{C}(\mathrm{CO_2})$ can be used as a tracer for fuel CO_2 in summer and in winter at urban and polluted sites. The accuracy of CO- and/or $\delta^{13}\mathrm{C}(\mathrm{CO_2})$-based fuel CO_2 estimates depends to a large degree on how well the different parameters such as $\overline{R_{\mathrm{F}}}$, $\overline{\delta_{\mathrm{F}}}$, and δ_{bio} are known. Misassignment leads to significant biases in the fuel CO_2 estimate (Fig. 4). Therefore, in practice, it is important to screen and monitor all sources and sinks in the catchment area of the measurement site and to determine the median isotopic source signature and the median ratios $\overline{R_{\mathrm{F}}}$, $\overline{R_{\mathrm{tr}}}$, $\overline{R_{\mathrm{bf}}}$ as well as the CO offset as accurately as possible, for example, by calibration with co-located $\Delta^{14}\mathrm{C}(\mathrm{CO_2})$ measurements. The accuracy of the fuel CO_2 estimate after $^{14}\mathrm{C}$ calibration depends strongly on the number of radiocarbon samples available for calibration and on the sampling strategy used. For example, in the ICOS project, approximately 24 radiocarbon samples will be available for calibration of $\overline{R_{\mathrm{F}}}$, $\overline{\delta_{\mathrm{F}}}$, $\overline{\delta_{\mathrm{ff}}}$, or $\overline{\delta_{\mathrm{F\text{-}tr}}}$. With that number of calibration samples available, due to the large noise of the calibrated footprint-weighted parameters $\overline{\delta_{\mathrm{F}}}$ $\overline{\delta_{\mathrm{ff}}}$, or $\overline{\delta_{\mathrm{F\text{-}tr}}}$, it may be advantageous to group all calibrations to obtain robust annual median values for $\overline{\delta_{\mathrm{F}}}$, $\overline{\delta_{\mathrm{ff}}}$, or $\overline{\delta_{\mathrm{F\text{-}tr}}}$. If a large number of precise radiocarbon measurements are available, or if the parameters do not change over the course of several years and thus several years of calibration samples can be accumulated, it is advantageous to apply radiocarbon calibrations at half-yearly resolution. Note that due to changes in technology and technical processes, as well as due to a year-to-year variation in extreme temperatures, the contribution from fuel CO_2 different sectors is likely to change within a period of four years. However, this could be checked, for example, using nighttime Keeling plot intercepts (Vardag et al., 2015). For calibration of $\overline{R_{\mathrm{F}}}$, integrated $\Delta^{14}\mathrm{C}(\mathrm{CO_2})$ calibration could be used with rather small but systematic biases or grab samples could be used for slightly larger but random uncertainty. The accuracy will then typically be better than 10 % for the CO method or the $\delta^{13}\mathrm{C}(\mathrm{CO_2})$ method.

The precision of CO- and $\delta^{13}\mathrm{C}(\mathrm{CO_2})$-based approaches is very similar for all site classes, but for polluted sites $\delta^{13}\mathrm{C}(\mathrm{CO_2})$ seems slightly more precise. For Heidelberg it is about 25 % (e.g., 1σ / mean(y_{F})). For CO, the uncertainty originates mainly from the large variation in $\overline{R_{\mathrm{F}}}$ in our model runs due to the inhomogeneity of fuel CO sources in the footprint area of urban or polluted measurement stations and due to natural CO sources. The uncertainty of the $\delta^{13}\mathrm{C}(\mathrm{CO_2})$ approach is mainly determined by the limited measurement precision of $\delta^{13}\mathrm{C}(\mathrm{CO_2})$. Thus in order to use $\delta^{13}\mathrm{C}(\mathrm{CO_2})$ as a tracer for fuel CO_2 it is vital to perform isotopic measurements with a precision of at least 0.05 ‰. The combination of $\delta^{13}\mathrm{C}(\mathrm{CO_2})$ and CO for fuel CO_2 estimation is favorable in cases where each of two emission groups is well distinguishable by one of the tracers. Since for our model setting this is only partly the case (EDGAR emission inventory; see Table A1), the combination of these tracers provides only little additional information.

We have found that hypothetical future $\Delta^{14}\mathrm{C}(\mathrm{CO_2})$ measurements with 5 ‰ absolute precision of background and measured $\Delta^{14}\mathrm{C}(\mathrm{CO_2})$ values (see Figs. 5f–7f) would generally be a very precise tracer for continuous fuel CO_2 es-

timation at rural (1σ / mean(y_F) $\approx 60\,\%$), urban (ca. 15 %) and polluted (ca. 10 %) stations. The precision of fuel CO_2 estimates is determined mainly by the limited measurement precision of background and total $\Delta^{14}C(CO_2)$ (± 5 ‰). Note, however, that $\Delta^{14}C(CO_2)$ measurements with 5 ‰ precision are not yet fully developed and commercially available. For comparison, a $\Delta^{14}C(CO_2)$ measurement precision of 1 % would be needed to achieve a fuel CO_2 precision similar to that of $\delta^{13}C(CO_2)$- and CO-based methods. An uncertainty of 2 %, which could be a realistic near-future precision of laser-based instruments (Galli et al., 2013), would lead to relative uncertainties of 260, 50 and 30 %, respectively. The downside of $\Delta^{14}C(CO_2)$ is its inability to determine biofuel CO_2. Therefore, the $\Delta^{14}C(CO_2)$ methods will underestimate the fuel CO_2 (biofuel plus fossil fuel) contributions approximately by the share of biofuel in CO_2 at the site. This may be only a small contribution, as was the case for the studied year 2012 (e.g., 5 % in Heidelberg), but may increase in the future. Note also that we have not investigated the effect of nuclear power plant $^{14}C(CO_2)$ contributions at the measurement site, which could additionally bias fuel CO_2 estimates derived from $\Delta^{14}C(CO_2)$ measurements. Dispersion model results for Heidelberg (M. Kuderer, personal communication, 2015) suggest that the nuclear power facilities (most importantly Philippsburg, located about 25 km southwest of Heidelberg) increase monthly mean $\Delta^{14}C(CO_2)$ by about (2 ± 2) ‰, corresponding to a misassignment in fuel CO_2 of about $0.8 \pm 0.8\,\mu mol\,mol^{-1}$ ($\approx 5\,\%$). If there are nuclear power plants or fuel reprocessing plants in the catchment area of the measurement site and if monthly mean emission data of pure $^{14}C(CO_2)$ from these nuclear facilities are available, it is advisable to correct for them at the highest possible temporal resolution using, for example, transport models (Vogel et al., 2013b). Note that for the calibration of $\overline{R_F}$, $\overline{\delta_F}$, $\overline{\delta_{ff}}$ or $\overline{\delta_{F\text{-}tr}}$ using $\Delta^{14}C(CO_2)$ grab samples, it should be possible to choose the calibration grab samples via trajectory forecast such that no nuclear power plant influences are encountered in the grab samples. However, this limits the footprint area that can be sampled and calibrated.

We have compared the diurnal cycle of the tracer-based fuel CO_2 estimates for Heidelberg and found that the tracer configurations using CO, $\delta^{13}C(CO_2)$ and $\Delta^{14}C(CO_2)$ were able to reproduce the diurnal cycle well and show a mean difference of better than $5 \pm 15\,\%$ and a root mean square difference of 15 % at the most. This seems surprising, since one might expect a diurnal pattern of $\overline{\delta_F}$ and $\overline{R_F}$ due to a varying share of emissions of different emission sectors in the footprint, leading to a systematic deviation of the estimated from the real modeled diurnal cycle. However, since the diurnal patterns are small (e.g., peak-to-peak difference of $\delta^{13}C(CO_2)$ ca. 2 ‰), the mean diurnal variations are not significantly improved when using a diurnal correction of the mean isotopic source signatures. One should keep in mind that natural CO contributions may also vary systematically on a diurnal basis. Such a natural systematic variation was not included in the model simulation but will potentially introduce a diurnal bias into the continuous fuel CO_2 estimate in a real setting. Therefore, it may be necessary to model or approximate natural CO in a real setting. It may be possible to approximate the (sub-monthly) natural CO component using formaldehyde (HCHO) measurements, since the production of CO from NMHC passes HCHO as an intermediate molecule (Atkinson, 2000). However, the high dry deposition rate of HCHO may complicate the interpretation further. Since afternoon values are often used in inverse model studies to derive fluxes, it is important that afternoon fuel CO_2 values can be estimated accurately. This could be confirmed for $\delta^{13}C(CO_2)$ and CO in this study (see Fig. 8).

In order to better study the biospheric carbon fluxes on all relevant scales, it is important to improve fuel CO_2 bottom-up inventories, so that fuel and biospheric CO_2 can be separated for independent use in inverse model approaches. At present, emission inventories typically have uncertainties of 30–150 % at regional resolution (Wang et al., 2013). We were able to show in our study that some tracer-based approaches such as CO and $\delta^{13}C(CO_2)$-based methods lead to uncertainties of fuel CO_2 of 30 % and accuracies of 10 % (after calibration). However, for retrieving improved emission estimates using inverse models, also the model transport errors need to be taken into account and convoluted with the accuracy of fuel CO_2 estimates. At the moment, the model transport errors are usually larger during nighttime (ca. 100 %) than in the afternoon (ca. 40 %) (excluding at mountain sites), which is why mainly afternoon values are used in model inversions (Gerbig et al., 2008). Obviously, but unfortunately during the afternoon hours, the fuel CO_2 signal is very small, complicating the unbiased estimation of fuel CO_2 emissions using continuous tracers in inverse transport models in these hours until better transport models and boundary layer height models exist.

Appendix A: Methods of continuous fuel CO_2 determination

A1 Tracer configurations and their emission groups

We formally introduce six different tracers or tracer combinations, which we use to estimate fuel CO_2 continuously: CO_2 is used as the sole tracer for fuel CO_2. CO, $\delta^{13}C(CO_2)$ and $\Delta^{14}C(CO_2)$ records are each used solely with CO_2 to estimate fuel CO_2. Further, CO is used as a tracer for traffic (and $\delta^{13}C(CO_2)$ as a tracer for fuel CO_2 minus traffic) and finally CO is used as a tracer for biofuels (and $\delta^{13}C(CO_2)$ as a tracer for fuel CO_2 minus biofuels). The different emission groups are also listed and characterized in Table A1.

A1.1 CO_2 as the sole tracer for fuel CO_2

When using CO_2 alone as "tracer" for fuel CO_2 ($y_F = y_{ff} + y_{bf}$), the total regional CO_2 offset is assumed to solely origi-

Table A1. Annual or half-yearly (summer: S; winter: W) averaged $\Delta^{14}C(CO_2)$, $\delta^{13}C(CO_2)$, $\Delta CO / \Delta CO_2$ ratios, and mean fraction of CO_2 and CO relative to total CO_2 and CO offsets as used in our model study for the measurement site Heidelberg for the year 2012. Biosphere $\Delta^{14}C(CO_2)$ values are based on Taylor et al. (2015). The $\Delta CO / \Delta CO_2$ ratio and the fractions of CO_2 and CO offset were taken from the STILT model runs, which were fed with anthropogenic emissions from the EDGAR emission inventory. Note that fractions of biofuels in traffic CO_2 emissions are not included. δ values were derived by assigning an isotopic value to each fuel type and weighting these depending on the respective share of the fuel type to total fuel CO_2 at the measurement site. The δ values of the biosphere are the half-yearly mean values from Table 1. Analogously, R_x (and $\Delta^{14}C_x$) values were derived by assigning an emission ratio CO / CO_2 (and $\Delta^{14}C(CO_2)$value) to each emission sector and weighting these depending on the respective share of the emission sector to total fuel CO_2 at the site.

Emission group	$\Delta^{14}C$-CO_2[‰]	$\delta^{13}C$ [‰]		$\overline{R}_x = (\Delta CO / \Delta CO_2)_x$	% of ΔCO_2		% of ΔCO	
		S	W	[ppb ppm^{-1}]	S	W	S	W
Fuel CO_2	−995	−31.5	−33.5	7	50	80	100	100
Fossil fuel CO_2 (excl. biofuels)	−1000	−32	−34	3	45	70	50	37
Biofuel CO_2	90	−27	−28	30	5	10	$\overline{m_{bf}} = 50$	$\overline{m_{bf}} = 63$
Fuel CO_2 excl. traffic CO_2 (but incl. biofuels)	−990	−31.5	−33.8	7	35	67	70	80
Traffic fuel CO_2	−1000	−31	−31	7	15	13	$\overline{m_{tr}} = 30$	$\overline{m_{tr}} = 20$
Biospheric CO_2	60	−23	−25.5	0	50	20	0	0

nate from fuel emissions:

$$y_F = \Delta y, \tag{A1}$$

with $\Delta y = y_{tot} - y_{bg}$.

This simple approach is valid if (nearly) all CO_2 emissions are from fuel burning, as might be the case in cold winters or in areas without biospheric activity (e.g., megacities).

A1.2 CO as a tracer for fuel CO_2

The CO offset ($\Delta x = x_{tot} - x'_{bg}$) can be used to estimate fuel CO_2 offset if it is divided by the mean ratio $\overline{R_F} = \Delta x / \Delta y_F$ of all fuel sources:

$$y_F = \frac{\Delta x}{\overline{R_F}}. \tag{A2}$$

Note that, in reality, the ratio $\overline{R_F}$ varies depending on the share of emissions of different emission sectors in the catchment area and their temporal emission patterns, as well as due to natural CO sources and sinks, at least in summer (Prather et al., 2001). We show $\overline{R_F}$ with an overbar to emphasize that this is a footprint-weighted average of the fuel emission ratio.

A1.3 CO as a tracer for traffic CO_2 and $\delta^{13}C(CO_2)$ as a tracer for all fuel CO_2, except for traffic CO_2

We now include $\delta^{13}C(CO_2)$ in fuel CO_2 estimation as a tracer for all fuel CO_2 except those of traffic ($y_{F\text{-}tr} = y_{ff} + y_{bf} - y_{tr}$).

$$y_{tot} = y_{bg} + y_{bio} + y_{tr} + y_{F-tr} \tag{A3}$$

$$y_{tot}\delta_{tot} = y_{bg}\delta_{bg} + y_{bio}\delta_{bio} + y_{tr}\overline{\delta_{tr}} + y_{F-tr}\overline{\delta_{F\text{-}tr}} \tag{A4}$$

In analogy to $\overline{R_F}$ we show $\overline{\delta_{tr}}$ and $\overline{\delta_{F\text{-}tr}}$ with an overbar to emphasize that these are footprint-weighted averages of the emission groups traffic CO_2 and fuel CO_2 excluding traffic, respectively. Solving Eq. (A3) for y_{bio}, we can substitute y_{bio} in Eq. (A4). In analogy to Eq. (A2), we use CO as a tracer for traffic CO_2:

$$y_{tr}(t) = \frac{x_{tr}(t)}{\overline{R_{tr}}}, \tag{A5}$$

with the mean $\Delta CO / \Delta CO_2$ ratio of traffic $\overline{R_{tr}} = (\Delta x / \Delta y)_{tr}$. CO_{tr} can be determined from

$$CO_{tr}(t) = \Delta CO(t) \cdot \overline{m_{tr}}, \tag{A6}$$

with $\overline{m_{tr}} = (\Delta x_{tr} / \Delta x)$ being the share of traffic CO to the total CO offset. $\overline{m_{tr}}$ needs to be estimated from bottom-up inventories and can be found in Table A1 (right column) and is also dependent on the footprint area of the measurement site and the sources and sinks lying in this area. Equations (A3)–(A6) can then be rearranged:

$$y_{F-tr} = \frac{y_{tot}\delta_{tot} - y_{bg}\delta_{bg} - \left(y_{tot} - y_{bg} - y_{tr}\right)\delta_{bio} - y_{tr}\overline{\delta_{tr}}}{\overline{\delta_{F\text{-}tr}} - \delta_{bio}}. \tag{A7}$$

Total fuel CO_2 (y_F) contribution can then be determined as the sum of y_{tr} (Eq. A5) and $y_{F\text{-}tr}$ (Eq. A7).

A1.4 CO as a tracer for biofuel CO_2 and $\delta^{13}C(CO_2)$ as a tracer for all fuel CO_2, except for biofuel CO_2

This method of fuel CO_2 estimation is in analogy to case A.1.3, but instead of separating fuel CO_2 into traffic contributions (y_{tr}) and others ($y_{F\text{-}tr}$), we separate it into biofuel contributions (y_{bf}) and others ($y_{F\text{-}bf} = y_{ff}$); this leads to

$$y_{F-bf} = \frac{y_{tot}\delta_{tot} - y_{bg}\delta_{bg} - (y_{tot} - y_{bg} - y_{bf})\delta_{bio} - y_{bf}\overline{\delta_{bf}}}{\overline{\delta_{ff}} - \delta_{bio}}. \quad \text{(A8)}$$

Analogously to Eq. (A10), we formulate for y_{bf}:

$$y_{bf}(t) = \frac{\Delta x(t) \cdot \overline{m_{bf}}}{\overline{R_{bf}}}, \quad \text{(A9)}$$

with $\overline{m_{bf}} = (\Delta x_{bf}/\Delta x)$ from bottom-up inventories (see Table A1). Total fuel CO_2 (y_F) is calculated as the sum of y_{bf} (Eq. A9) and $y_{F\text{-}bf}$ (Eq. A9).

A1.5 $\delta^{13}C(CO_2)$ as the sole tracer for fuel emission

When using δ_{tot} as a tracer for all fuel contributions, Eq. (A3) and Eq. (A4) simplify to

$$y_F = \frac{y_{tot}\delta_{tot} - y_{bg}\delta_{bg} - (y_{tot} - y_{bg})\delta_{bio}}{\overline{\delta_F} - \delta_{bio}} \quad \text{(A10)}$$

if all fuel CO_2 ($y_{F\text{-}tr}$ and y_{tr}) contributions are pooled to y_F.

A1.6 $\Delta^{14}C(CO_2)$ as a tracer for fossil fuel CO_2

Following Levin et al. (2008), we can derive fossil fuel CO_2 from $\Delta^{14}C(CO_2)$and total CO_2 measurements according to

$$y_{ff} = \quad \text{(A11)}$$
$$\frac{y_{bg}\left(\Delta^{14}C_{bg} - \Delta^{14}C_{bio}\right) - y_{tot}\left(\Delta^{14}C_{tot} - \Delta^{14}C_{bio}\right) - y_{bf}\left(\Delta^{14}C_{bio} - \Delta^{14}C_{bf}\right)}{1 + \Delta^{14}C_{bio}}.$$

However, since $\Delta^{14}C_{bio} \approx \Delta^{14}C_{bf}$, and because biofuel contributions are not known, we neglect the last term of the numerator in the following. Note that, since $\Delta^{14}C(CO_2)$ is not sensitive to biofuel contributions, it is only possible to estimate the fossil fuel CO_2 contributions without biofuel contributions.

A2 Determination of parameters and variables

The background values y_{bg}, x'_{bg}, δ_{bg} and $\Delta^{14}C_{bg}$ should represent the regional clean air to which the source contributions from the footprint area are added. Since there are often no nearby clean-air observations available for a polluted station, we use those mole fractions as a background where the air masses in the boundary layer are well mixed with the free troposphere. This is usually the case in the afternoon and is associated with low mole fractions. Since CO_2 and CO both have local sinks relevant on the timescale of days, we here use CH_4 as an indicator for a well-mixed boundary layer and assume that, when the CH_4 mole fraction reaches a minimum value (within 2 days), vertical mixing is strongest. In principal, if continuous radon measurements were available, these could also be used as an indicator for vertical mixing (Dörr et al., 1983), instead of CH_4. We checked that the CH_4 minimum values always represent a lower envelope of the simulated greenhouse gas record and does not vary at the synoptic timescale. We then use the total mole fractions and isotopic records y_{tot}, x_{tot}, δ_{tot}, and $\Delta^{14}C_{tot}$ observed during situations with minimal CH_4 mole fractions as background values.

Further, in order to solve Eqs. (A2)–(A11), we need the input parameters δ_{bio} and $\Delta^{14}C_{bio}$. These input parameters were assigned with the objective of creating a realistic modeled data set (see Tables 1 and A1). Additionally, the integrated footprint-weighted parameters $\overline{R_F}$, $\overline{R_{tr}}$, $\overline{R_{bf}}$, $\overline{\delta_F}$, $\overline{\delta_{ff}}$, $\overline{\delta_{bf}}$, $\overline{\delta_{tr}}$, $\overline{\delta_{bio}}$, $\overline{\delta_{F\text{-}tr}}$, $\overline{m_{bf}}$ and $\overline{m_{tr}}$ are required (see Table A1). We call these parameters footprint-weighted since the ratios and isotopic signatures depend on the relative contribution from the different emission sectors (with their sector specific emission ratios and isotopic signatures) within the footprint of the measurement site. We represent the integrated footprint-weighted parameters with an overbar to draw attention to the fact that the parameters are averaged over the (e.g., monthly) footprint area. Even though the emission factors of the source categories used here are fixed for every pixel, integrated footprint-weighted $\overline{R_F}$, $\overline{R_{tr}}$, $\overline{R_{bf}}$, $\overline{\delta_F}$ $\overline{\delta_{ff}}$, $\overline{\delta_{bf}}$, $\overline{\delta_{tr}}$, $\overline{\delta_{bio}}$, $\overline{\delta_{F\text{-}tr}}$, $\overline{m_{bf}}$ and $\overline{m_{tr}}$ are not constant in time, because the footprint of the measurement site and the emission patterns are temporally variable. Thus, the footprint-weighted parameters change when the emissions from the different sectors or the footprint of the measurement site vary. Note that for our model study we do not require the parameters to be absolutely correct, since we do not compare them to measured data. However, since we want to provide a realistic case study, we seek to use the most realistic parameters (see values in Tables 1 and A1).

Appendix B: "Calibration" with $\Delta^{14}C(CO_2)$

Solving Eqs. (A3), (A8), (A9) and (A11) for fuel CO_2 requires $\overline{R_F}$, $\overline{\delta_F}$, $\overline{\delta_{ff}}$ and $\overline{\delta_{F\text{-}tr}}$. If these values are not known, they may be derived from $\Delta^{14}C(CO_2)$observations (what we then call $\Delta^{14}C(CO_2)$-calibrated). For the calibration, y_{ff} must be known. The idea is to calibrate fossil fuel CO_2, e.g., with precise $\Delta^{14}C(CO_2)$measurements, on a lower time resolution (e.g., monthly) and assume that the footprint-weighted parameters $\overline{R_F}$, $\overline{\delta_F}$, $\overline{\delta_{ff}}$ and $\overline{\delta_{F\text{-}tr}}$ do not change significantly within this calibration interval.

Re-arranging Eqs. (1) and (2) for $\overline{\delta_{ff}}$ leads to

$$\overline{\delta_{ff}} = \quad \text{(B1)}$$
$$\frac{y_{tot}\delta_{tot} - y_{bg}\delta_{bg} - (y_{tot} - y_{bg} - y_{ff} - y_{bf})\delta_{bio} - y_{bf}\overline{\delta_{bf}}}{y_{ff}},$$

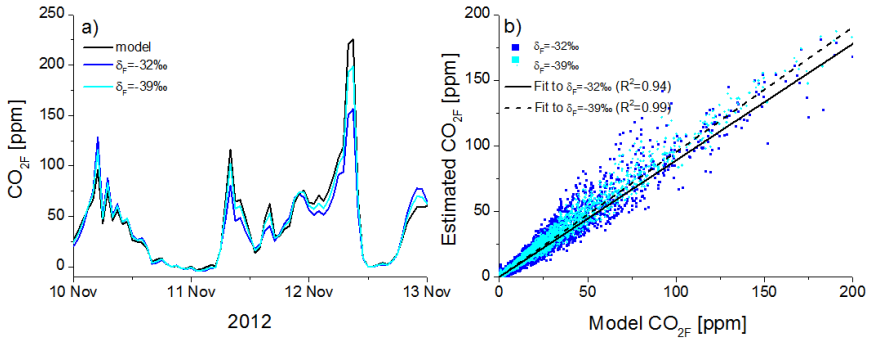

Figure B1. (a) Example period showing fuel CO_2 of different fuel CO_2 estimation methods and reference modeled fuel CO_2. Dark blue: mean δ_F is −32 ‰; cyan: mean δ_F is −39 ‰. **(b)** Correlation plot between estimated and modeled fuel CO_2 for mean $\delta_F = -32$ ‰ (dark blue and solid line) and mean $\delta_F = -39$ ‰ (cyan and dotted line) during the entire year of 2012. Fuel CO_2 can be estimated much better using $\delta^{13}C(CO_2)$ when the fuel $\delta^{13}C$ signature is strongly depleted with respect to the biosphere. Note that the slope slightly changes when using more depleted sources. This is because few high fuel CO_2 peaks span the linear regression and therefore determine the slope to a large degree, but as a general tendency for the Heidelberg data set, the high fuel CO_2 peaks exhibit an isotopic signature, which is more enriched as the isotopic signature of the mean fuel source mix.

which could then be used in Eq. (A9). Note that we require the biofuel CO_2 in addition to the fossil fuel CO_2 from $\Delta^{14}C(CO_2)$.

$\overline{\delta_F}$ can then be derived if the y_{bf} concentration is known.

$$\overline{\delta_F} = \frac{\overline{\delta_{ff}} y_{ff} + \overline{\delta_{bf}} y_{bf}}{y_{ff} + y_{bf}} \tag{B2}$$

If fossil fuel emissions are divided into fossil fuel contributions without traffic ($y_{F\text{-}tr}$) and traffic contributions (y_{tr}), we can derive $\overline{\delta_{F\text{-}tr}}$ required for solving Eq. (A8):

$$\overline{\delta_{F\text{-}tr}} = \frac{\overline{\delta_F} y_F - \overline{\delta_{tr}} y_{tr}}{y_F - y_{tr}}. \tag{B3}$$

Analogously, the ratio $\overline{R_F}$ could be calibrated following

$$\overline{R_F} = \frac{\Delta x}{\Delta y_F}. \tag{B4}$$

In order to calculate the monthly mean value of $\langle\overline{\delta_F}\rangle$ and $\langle\overline{R_F}\rangle$, the mean ratios $\langle\frac{\Delta x}{\Delta y_F}\rangle$ (Eqs. B1–B4) are needed. However, from integrated $\Delta^{14}C(CO_2)$ sampling, we only have the mean fossil fuel CO_2 and fuel CO_2 values and can thus only calculate $\langle\Delta x\rangle/\langle\Delta y_F\rangle$. Using the product (or ratio) of the means rather than the mean of the product (ratio) is only correct if the factors are uncorrelated. Since the factors in Eqs. (B1)–(B4) (and Δx and Δy_{ff}) are correlated, the integrated calibration cannot be applied without introducing a bias into monthly mean $\langle\overline{\delta_F}\rangle$, $\langle\overline{\delta_{ff}}\rangle$, $\langle\overline{\delta_{F\text{-}tr}}\rangle$ and $\langle\overline{R_F}\rangle$. Instead of using integrated $\Delta^{14}C(CO_2)$ samples in order to obtain the monthly fossil fuel CO_2 values, it is possible to take grab samples and analyze these for $\Delta^{14}C(CO_2)$ (and with that y_{ff}), total CO_2, $\delta^{13}C(CO_2)_{tot}$ and CO in order to calculate the individual (non-averaged) values for $\overline{\delta_F}$, $\overline{\delta_{F\text{-}tr}}$, $\overline{\delta_{ff}}$ and $\overline{R_F}$ (see Sect. 4).

Appendix C: Influence of more depleted fuel $\delta^{13}C(CO_2)$ signatures

We have argued that we only require a realistic set of input parameters, rather than an absolutely correct set of parameters to estimate uncertainties of the different tracer methods. However, the results presented so far are to some degree dependent on the emission characteristics used in our model (see Table A1). When using CO as a tracer for fuel CO_2, it would be advantageous if natural sources of CO were negligible and if the emission ratio $\overline{R_F}$ were the same for all sources. When using CO_2 as a tracer for fuel CO_2, biospheric CO_2 emissions should be negligible, and when using $\delta^{13}C(CO_2)$, it would be advantageous if fuel CO_2 emissions were strongly depleted compared to biospheric emissions. It is beyond the scope of this work to show explicitly, for all cases, how the "choice" of different emission characteristics influences the fuel CO_2 estimate in terms of precision and accuracy. However, in Fig. B1, we illustrate for this latter case how the presence of more depleted fuel sources in the footprint area of the measurement site could improve the tracer $\delta^{13}C(CO_2)$ for fuel CO_2 estimation. This should serve as an example showing how much the emission characteristics at a site may influence the precision of fuel CO_2 estimates using different tracer configurations.

Figure B1 shows that fuel CO_2 can be estimated much better when the mean source mix in the catchment area of the measurement site exhibits a strongly depleted isotopic source signature. The regression coefficient improves from 0.94 to 0.99 and the precision within 1 year decreases significantly by 40 % when choosing $\overline{\delta_F}$ that is 7 ‰ more depleted (−39 ‰ instead of −32 ‰). The precision of $\delta^{13}C(CO_2)$-based fuel CO_2 will increase with decreasing isotopic signature of fuel CO_2 sources. Analogously, the precision of CO-based fuel

CO_2 estimates will increase with decreasing inhomogeneity of CO / CO_2 ratio of fuel CO_2 sources. This effect should be taken into account when designing a measurement network and thus highlights the importance of a thorough source evaluation in the catchment area prior to instrumental installation.

Appendix D: List of abbreviations

AMS	Accelerator mass spectrometry
bf	Biofuel
bg	Background
bio	Biosphere
EDGAR	Emissions Database for Global Atmospheric Research
F	Fuel
F-bf	Fuel excluding biofuels (i.e., ff)
ff	Fossil fuel
F-tr	Fuel excluding traffic
GC	Gas chromatography
ICOS	Integrated Carbon Observation System
IQR	Interquartile range
m_x	CO share of emission group x to CO offset
NPP	Nuclear power plant
ppm	parts per million, equivalent to $\mu mol\,mol^{-1}$
R_x	Ratio of CO to CO_2 in the emission group x
SD	Standard deviation
STILT	Stochastic Time-Inverted Lagrangian Particle model
tot	Total
x	CO mole fraction
y	CO_2 mole fraction

Acknowledgements. We thank Ute Karstens and Thomas Koch for valuable modeling lessons and help with setting up the model. We are also grateful for valuable discussions on fossil fuel CO_2 in Heidelberg with Felix R. Vogel and Samuel Hammer. We would also like to thank Jocelyn Turnbull and the anonymous referee for their valuable feedback. This work has been funded by the InGOS EU project (284274) and ICOS BMBF project (01LK1225A). Further, we acknowledge the financial support given by Deutsche Forschungsgemeinschaft and Ruprecht-Karls-Universität Heidelberg within the funding program Open Access Publishing.

Edited by: J. Kaiser

References

Andres, R. J., Marland, G., Boden, T., and Bischof, S.: Carbon dioxide emissions from fossil fuel consumption and cement manufacture, 1751–1991; and an estimate of their isotopic composition and latitudinal distribution (No. CONF-9307181–4). Oak Ridge National Lab., TN (United States); Oak Ridge Inst. for Science and Education, TN (United States), 1994.

Atkinson, R.: Atmospheric chemistry of VOCs and NO_x, Atmos. Environ., 34, 2063–2101, 2000.

Ballantyne, A. P., Miller, J. B., Baker, I. T., Tans, P. P., and White, J. W. C.: Novel applications of carbon isotopes in atmospheric CO_2: what can atmospheric measurements teach us about processes in the biosphere?, Biogeosciences, 8, 3093–3106, doi:10.5194/bg-8-3093-2011, 2011.

Bousquet, P., Peylin, P., Ciais, P., Le Quéré, C., Friedlingstein, P., and Tans, P. P.: Regional changes in carbon dioxide fluxes of land and oceans since 1980, Science, 290, 1342–1346, 2000.

BP: The role of biofuels beyond 2020, Technical report issued September 2013, available at: http://www.bp.com/en/global/alternative-energy/our-businesses/biofuels.html, last access: February 2015.

Conrad, R.: Soil microorganisms as controllers of atmospheric trace gases (H_2, CO, CH_4, OCS, N_2O, and NO), Microbiol. Rev., 60, 609–640, 1996.

Coyle, W.: The future of biofuels, Economic Research Service, Washington, DC, 2007.

Denier van der Gon, H. D., Hendriks, C., Kuenen, J., Segers, A., and Visschedijk, A.: Description of current temporal emission patterns and sensitivity of predicted AQ for temporal emission patterns, TNP Report, EU FP7 MACC deliverable report D_D-EMIS_1.3, available at: https://gmes-atmosphere.eu/documents/deliverables/d-emis/MACC_TNO_del_1_3_v2.pdf, 2011.

Djuricin, S., Pataki, D. E., and Xu, X.: A comparison of tracer methods for quantifying CO_2 sources in an urban region, J. Geophys. Res., 115, D11303, doi:10.1029/2009JD012236, 2010.

Dörr, H., Kromer, B., Levin, I., Münnic, K. O., and Volpp, H.-J.: CO_2 and radon 222 as tracers for atmospheric transport, J. Geophys. Res., 88, 1309–1313, doi:10.1029/JC088iC02p01309, 1983.

Esler, M. B., Griffith, D. W. T., Wilson, S. R., and Steele, L. P.: Precision trace gas analysis by FT-IR spectroscopy. 2. The $^{13}C/^{12}C$ isotope ratio of CO_2, Anal. Chem, 72.1, 216–221, 2000.

EC-JRC/PBL European Commission – Joint Research Centre/PBL Netherlands Environmental Assessment Agency, The Emissions Database for Global Atmospheric Research (EDGAR) version 4.3, available at: http://edgar.jrc.ec.europa.eu/, 2015.

Flanagan, L. B., Ehleringer, J. R., and Pataki D. E. (Eds.): Stable isotopes and biosphere-atmosphere interactions, Elsevier Academic Press, San Diego, US, 318 pp., 2005.

Galli, I., Bartalini, S., Cancio, P., De Natale, P., Mazzotti, D., Giusfredi, G., Fedi, M. E., and Mando, P. A.: Optical detection of radiocarbon dioxide: first results and AMS intercomparison, Radiocarbon, 55, 213–223, 2013.

Gamnitzer, U., Karstens, U., Kromer, B., Neubert, R. E., Meijer, H. A., Schroeder, H., and Levin, I.: Carbon monoxide: A quantitative tracer for fossil fuel CO_2?, J. Geophys. Res.-Atmos., 111, 2156–2202, doi:10.1029/2005JD006966, 2006.

Gerbig, C., Lin, J. C., Wofsy, S. C., Daube, B. C., Andrews, A. E., Stephens, B. B., Bakwin, P. S., and Grainger, C. A.: Toward constraining regional-scale fluxes of CO_2 with atmospheric observations over a continent: 2. Analysis of COBRA data using a receptor-oriented framework, J. Geophys. Res.-Atmos., 108, 4756, doi:10.1029/2003JD003770, 2003.

Gerbig, C., Körner, S., and Lin, J. C.: Vertical mixing in atmospheric tracer transport models: error characterization and propagation, Atmos. Chem. Phys., 8, 591–602, doi:10.5194/acp-8-591-2008, 2008.

Granier, C., Pétron, G., Müller, J.-F., and Brasseur, G.: The impact of natural and anthropogenic hydrocarbons on the tropospheric budget of carbon monoxide, Atmos. Environ., 34, 5255–5270, 2000.

Graven, H. D. and Gruber, N.: Continental-scale enrichment of atmospheric $^{14}CO_2$ from the nuclear power industry: potential impact on the estimation of fossil fuel-derived CO_2, Atmos. Chem. Phys., 11, 12339–12349, doi:10.5194/acp-11-12339-2011, 2011.

Gros, V., Tsigaridis, K., Bonsang, B., Kanakidou, M., and Pio, C.: Factors controlling the diurnal variation of CO above a forested area in southeast Europe, Atmos. Environ., 36, 3127–3135, 2002.

Gurney, K. R., Law, R. M., Denning, A. S., Rayner, P. J., Baker, D., Bousquet, P., Bruhwiler, L., Chen, Y., Ciais, C., Fan, S., Fung, I. Y., Gloor, M., Heimann, M., Higuchi, John,J., Maki, T., Maksyutov, S., Masarie, K., Peylin, P., Prather, M., Pak, B. C., Randerson, J., Sarmiento, J., Taguc, S., Takahashi, T., and Yuen, C. W.: Towards robust regional estimates of CO_2 sources and sinks using atmospheric transport models, Nature, 415, 626–630, 2002.

Gurney, K. R., Chen, Y.-H., Maki, T., Kawa, S. R., Andrews, A., and Zhu, Z.: Sensitivity of atmospheric CO_2 inversions to seasonal and interannual variations in fossil fuel emissions, J. Geophys. Res., 110, D10308, doi:10.1029/2004JD005373, 2005.

Hammer, S., Griffith, D. W. T., Konrad, G., Vardag, S., Caldow, C., and Levin, I.: Assessment of a multi-species in situ FTIR for precise atmospheric greenhouse gas observations, Atmos. Meas. Tech., 6, 1153–1170, doi:10.5194/amt-6-1153-2013, 2013.

Heimann, M. and Koerner, S.: The global atmospheric tracer model TM3, Technical Reports, Max-Planck-Institute for Biogeochemie, 5, 131 pp., 2003.

IEA, International Energy Agency: Key World Energy Statistics 2014, available at: http://www.iea.org/publications/freepublications/publication/key-world-energy-statistics-2014.html (last access: 30 September 2015), 2014.

Inman, R. E., Ingersoll, R. B., and Levy, E. A.: Soil: A natural sink for carbon monoxide, Science, 172, 1229–1231, doi:10.1126/science.172.3989.1229, 1971.

Jung, M., Henkel, K., Herold, M., and Churkina, G.: Exploiting synergies of global land cover products for carbon cycle modeling, Remote Sens. Environ., 101, 534–553, 2006.

Kaul, M.: Isotopenverhältnisse im atmosphärischem Kohlendioxid und seine Quellen im Raum Heidelberg, Staatsexamensarbeit, 2007.

Keeling, C. D.: The concentration and isotopic abundances of atmospheric carbon dioxide in rural areas, Geochim. Cosmochim. Acta, 13, 322–334, 1958.

Keeling, C. D.: The concentration and isotopic abundances of carbon dioxide in the atmosphere, Tellus, 12.2, 200–203, 1960.

Keeling, C. D.: The concentration and isotopic abundance of carbon dioxide in rural and marine air, Geochim. Cosmochim. Acta, 24, 277–298, 1961.

Keeling, R. F., Piper, S. C., and Heimann, M.: Global and hemispheric CO_2 sinks deduced from changes in atmospheric O_2 concentration, Nature, 381, 218–221, 1996.

Le Quéré, C., Moriarty, R., Andrew, R. M., Peters, G. P., Ciais, P., Friedlingstein, P., Jones, S. D., Sitch, S., Tans, P., Arneth, A., Boden, T. A., Bopp, L., Bozec, Y., Canadell, J. G., Chini, L. P., Chevallier, F., Cosca, C. E., Harris, I., Hoppema, M., Houghton, R. A., House, J. I., Jain, A. K., Johannessen, T., Kato, E., Keeling, R. F., Kitidis, V., Klein Goldewijk, K., Koven, C., Landa, C. S., Landschützer, P., Lenton, A., Lima, I. D., Marland, G., Mathis, J. T., Metzl, N., Nojiri, Y., Olsen, A., Ono, T., Peng, S., Peters, W., Pfeil, B., Poulter, B., Raupach, M. R., Regnier, P., Rödenbeck, C., Saito, S., Salisbury, J. E., Schuster, U., Schwinger, J., Séférian, R., Segschneider, J., Steinhoff, T., Stocker, B. D., Sutton, A. J., Takahashi, T., Tilbrook, B., van der Werf, G. R., Viovy, N., Wang, Y.-P., Wanninkhof, R., Wiltshire, A., and Zeng, N.: Global carbon budget 2014, Earth Syst. Sci. Data, 7, 47–85, doi:10.5194/essd-7-47-2015, 2015.

Levin, I. and Karstens, U.: Inferring high-resolution fossil fuel CO_2 records at continental sites from combined (CO_2)-C-14 and CO observations, Tellus B, 59, 245–250, doi:10.1111/j.1600-0889.2006.00244.x, 2007.

Levin, I., Kromer, B., Schmidt, M., and Sartorius, H.: A novel approach for independent budgeting of fossil fuel CO_2 over Europe by $^{14}CO_2$ observations, Geophys. Res. Lett., 30, 2194, doi:10.1029/2003GL018477, 2003.

Levin, I., Hammer, S., Kromer, B., and Meinhardt, F.: Radiocarbon observations in atmospheric CO_2: Determining fossil fuel CO_2 over Europe using Jungfraujoch observations as background, Sci. Total Environ., 391, 211–216, 2008.

Lin, J. C., Gerbig, C., Wofsy, S. C., Andrews, A. E., Daube, B. C., Davis, K. J., and Grainger, C. A.: A near-field tool for simulating the upstream influence of atmospheric observations: The Stochastic Time-Inverted Lagrangian Transport (STILT) model, J. Geophys. Res., 108, 4493, doi:10.1029/2002JD003161, 2003.

Mahadevan, P., Wofsy, S. C., Matross, D. M., Xiao, X., Dunn, A. L., Lin, J. C., Gerbig, C., Munger, J. W., Chow, V. Y., and Gottlieb, E. W.: A satellite-based biosphere parameterization for net ecosystem CO_2 exchange: Vegetation Photosynthesis and Respiration Model (VPRM), Global Biogeochem. Cy., 22, GB2005, doi:10.1029/2006GB002735, 2008.

McIntyre, C. P., McNicholm, A. P., Roberts, M. L., Seewald, J. S., von Reden, K. F., and Jenkins, W. J.: Improved Precision of ^{14}C Measurements for CH_4 and CO_2 Using GC and Continuous-Flow AMS Achieved by Summation of Repeated Injections, Radiocarbon, 55, 677–685, 2013.

Meijer, H. A. J., Smid, H. M., Perez, E., and Keizer, M. G.: Isotopic characterization of anthropogenic CO_2 emissions using isotopic and radiocarbon analysis, Phys. Chem. Earth, 21, 483–487, 1996.

Mook, W. M. E.: Environmental Isotopes in the Hydrological Cycle. Principles and Applications, UNESCO/IAEA Series, http://www-naweb.iaea.org/napc/ih/documents/global_cycle/Environmental%20Isotopes%20in%20the%20Hydrological%20Cycle%20Vol%201.pdf, 2001.

Newman, S., Jeong, S., Fischer, M. L., Xu, X., Haman, C. L., Lefer, B., Alvarez, S., Rappenglueck, B., Kort, E. A., Andrews, A. E., Peischl, J., Gurney, K. R., Miller, C. E., and Yung, Y. L.: Diurnal tracking of anthropogenic CO_2 emissions in the Los Angeles basin megacity during spring 2010, Atmos. Chem. Phys., 13, 4359–4372, doi:10.5194/acp-13-4359-2013, 2013.

Newman, S., Xu, X., Gurney, K. R., Hsu, Y.-K., Li, K.-F., Jiang, X., Keeling, R., Feng, S., O'Keefe, D., Patarasuk, R., Wong, K. W., Rao, P., Fischer, M. L., and Yung, Y. L.: Toward consis-

tency between bottom-up CO2 emissions trends and top-down atmospheric measurements in the Los Angeles megacity, Atmos. Chem. Phys. Discuss., 15, 29591–29638, doi:10.5194/acpd-15-29591-2015, 2015.

Parrish, D. D., Trainer, M., Holloway, J. S., Yee, J., Warshawsky, S., Fehsenfeld, F., Forbes,G., and Moody, J.: Relationships between ozone and carbon monoxide at surface sites in the North Atlantic region, J. Geophys. Res., 103, 13357–13376, doi:10.1029/98JD00376, 1993.

Pataki, D. E., Ehleringer, J. R., Flanagan, L. B., Yakir, D., Bowling, D. R., Still, C. J., Buchmann, N., Kaplan, J. O., and Berry, J. A.: The application and interpretation of Keeling plots in terrestrial carbon cycle research, Global Biogeochem. Cy., 17, 1022, doi:10.1029/2001GB001850, 2003.

Pataki, D. E., Alig, R. J., Fung, A. S., Golubiewski, N. E., Kennedy, C. A., McPherson, E. G., Nowak, D. J., Pouyat, R. V., and Romero Lankao, P.: Urban ecosystems and the North American carbon cycle, Global Change Biol., 12, 2092–2102, doi:10.1111/j.1365-2486.2006.01242.x, 2006.

Peylin, P., Houweling, S., Krol, M. C., Karstens, U., Rödenbeck, C., Geels, C., Vermeulen, A., Badawy, B., Aulagnier, C., Pregger, T., Delage, F., Pieterse, G., Ciais, P., and Heimann, M.: Importance of fossil fuel emission uncertainties over Europe for CO_2 modeling: model intercomparison, Atmos. Chem. Phys., 11, 6607–6622, doi:10.5194/acp-11-6607-2011, 2011.

Peylin, P., Law, R. M., Gurney, K. R., Chevallier, F., Jacobson, A. R., Maki, T., Niwa, Y., Patra, P. K., Peters, W., Rayner, P. J., Rödenbeck, C., van der Laan-Luijkx, I. T., and Zhang, X.: Global atmospheric carbon budget: results from an ensemble of atmospheric CO_2 inversions, Biogeosciences, 10, 6699–6720, doi:10.5194/bg-10-6699-2013, 2013.

Prather, M., Ehhalt, D., Dentener, F., Derwent, R. G., Dlugokencky, E., Holland, E., Isaksen, I. S. A., Katima, J., Kirchhoff, V., Matson, P., Midgley, P. M., and Wang, M.: Atmospheric chemistry and greenhouse gases, in: Climate Change 2001, edited by: Houghton, J. T., 239–287, Cambridge Univ. Press, New York, 2001.

Rödenbeck, C.: Estimating CO_2 sources and sinksfrom atmospheric mixing ratio measurements using a global inversion of atmospheric transport, Max Planck Institute for Biogeochemistry, Jena, Germany, available at: http://www.bgc-jena.mpg.de/bgc-systems/pmwiki2/uploads/Publications/6.pdf, 2005.

Rogelj, J., McCollum, D., Smith, S., Calvin, K., Clarke, L., Garg, A., Jiang, K., Krey, V., Lowe, J., Riahi, K., Schaeffer, M., van Vuuren, D., Wenying, C., Crippa, M., and Janssens-Maenhout, G.: Chapter 2 of The emission gap report 2014: What emission levels will comply with temperature limit. In: The emission gap report 2014: a UNEP synthesis report, United Nations Environment Programme (UNEP), 2014.

Rivier, L., Ciais, P., Hauglustaine, D. A., Bakwin, P., Bousquet, P, Peylin, P., and Klonecki, A.: Evaluation of SF_6, C_2Cl_4 and CO to approximate fossil fuel CO_2 in the Northern Hemisphere using a chemistry transport model, J. Geophys. Res., 111, D16311, doi:10.1029/2005JD006725, 2006.

Schmidt, A., Rella, C. W., Göckede, M., Hanson, C., Yang, Z., and Law, B. E.: Removing traffic emissions from CO_2 time series measured at a tall tower using mobile measurements and transport modeling, Atmos. Environ., 97, 94–108, doi:10.1016/j.atmosenv.2014.08.006, 2014.

Steinbach, J., Gerbig, C., Rödenbeck, C., Karstens, U., Minejima, C., and Mukai, H.: The CO_2 release and Oxygen uptake from Fossil Fuel Emission Estimate (COFFEE) dataset: effects from varying oxidative ratios, Atmos. Chem. Phys., 11, 6855–6870, doi:10.5194/acp-11-6855-2011, 2011.

Stuiver, M. and Polach, H. A.: Reporting of C-14 data-Discussion, Radiocarbon, 19, 355–363, 1977.

Taylor, A. J., Lai, C. T., Hopkins, F. M., Wharton, S., Bible, K., Xu, X., Philipps, C., Bush, S., and Ehleringer, J. R.: Radiocarbon-Based Partitioning of Soil Respiration in an Old-Growth Coniferous Forest, Ecosystems, 18, 1–12, 2015.

Trusilova, K., Rödenbeck, C., Gerbig, C., and Heimann, M.: Technical Note: A new coupled system for global-to-regional downscaling of CO_2 concentration estimation, Atmos. Chem. Phys., 10, 3205–3213, doi:10.5194/acp-10-3205-2010, 2010.

Turnbull, J. C., Miller, J. B., Lehman, S. J., Tans, P. P., Sparks, R. J., and Southon, J.: Comparison of $^{14}CO_2$, CO, and SF_6 as tracers for recently added fossil fuel CO_2 in the atmosphere and implications for biological CO_2 exchange. Geophys. Res. Lett., 33, L01817, doi:10.1029/2005GL024213, 2006.

Turnbull, J. C., Lehman, S. J., Miller, J. B., Sparks, R. J., Southon, J. R., and Tans, P. P.: A new high precision $^{14}CO_2$ time series for North American continental air, J. Geophys. Res., 112, D11310, doi:10.1029/2006JD008184, 2007.

Turnbull, J. C., Karion, A., Fischer, M. L., Faloona, I., Guilderson, T., Lehman, S. J., Miller, B. R., Miller, J. B., Montzka, S., Sherwood, T., Saripalli, S., Sweeney, C., and Tans, P. P.: Assessment of fossil fuel carbon dioxide and other anthropogenic trace gas emissions from airborne measurements over Sacramento, California in spring 2009, Atmos. Chem. Phys., 11, 705–721, doi:10.5194/acp-11-705-2011, 2011.

Turnbull, J. C., Sweeney, C., Karion, A., Newberger, T., Lehman, S. J., Tans, P. P., Davis, K. J., Lauvaux, T., Miles, N. L., Richardson, S. J., Cambaliza, M. O., Shepson, P. B., Gurney, K., Patarasuk, R., and Razlivanov, I.: Toward quantification and source sector identification of fossil fuel CO_2 emissions from an urban area: Results from the INFLUX experiment, J. Geophys. Res.-Atmos., 120, 292–312, 2015.

Tuzson, B., Henne, S., Brunner, D., Steinbacher, M., Mohn, J., Buchmann, B., and Emmenegger, L.: Continuous isotopic composition measurements of tropospheric CO_2 at Jungfraujoch (3580 m a.s.l.), Switzerland: real-time observation of regional pollution events, Atmos. Chem. Phys., 11, 1685–1696, doi:10.5194/acp-11-1685-2011, 2011.

Vardag, S. N., Hammer, S., O'Doherty, S., Spain, T. G., Wastine, B., Jordan, A., and Levin, I.: Comparisons of continuous atmospheric CH_4, CO_2 and N_2O measurements – results from a travelling instrument campaign at Mace Head, Atmos. Chem. Phys., 14, 8403–8418, doi:10.5194/acp-14-8403-2014, 2014.

Vardag, S. N., Hammer, S., Sabasch, M., Griffith, D. W. T., and Levin, I.: First continuous measurements of δ^{18}O-CO_2 in air with a Fourier transform infrared spectrometer, Atmos. Meas. Tech., 8, 579–592, doi:10.5194/amt-8-579-2015, 2015.

Vogel, F. R.: $^{14}CO_2$-calibrated carbon monoxide as proxy to estimate the regional fossil fuel CO_2 component at hourly resolution, PhD thesis, Ruprecht-Karls University Heidelberg, Germany, 2010.

Vogel, F., Hammer, S., Steinhof, A., Kromer, B., and Levin, I.: Implication of weekly and diurnal ^{14}C calibration on

hourly estimates of CO-based fossil fuel CO_2 at a moderately polluted site in southwestern Germany, Tellus B, 62, doi:10.3402/tellusb.v62i5.16600, 2010.

Vogel, F. R., Huang, L., Ernst, D., Giroux, L., Racki, S., and Worthy, D. E. J.: Evaluation of a cavity ring-down spectrometer for in situ observations of $^{13}CO_2$, Atmos. Meas. Tech., 6, 301–308, doi:10.5194/amt-6-301-2013, 2013a.

Vogel, F., Levin, I., and Worthy, D.: Implications for Deriving Regional Fossil Fuel CO_2 Estimates from Atmospheric Observations in a Hot Spot of Nuclear Power Plant $^{14}CO_2$ Emissions, Radiocarbon, North America, 55, May 2013b.

Wang, R., Tao, S., Ciais, P., Shen, H. Z., Huang, Y., Chen, H., Shen, G. F., Wang, B., Li, W., Zhang, Y. Y., Lu, Y., Zhu, D., Chen, Y. C., Liu, X. P., Wang, W. T., Wang, X. L., Liu, W. X., Li, B. G., and Piao, S. L.: High-resolution mapping of combustion processes and implications for CO_2 emissions, Atmos. Chem. Phys., 13, 5189–5203, doi:10.5194/acp-13-5189-2013, 2013.

Widory, D., Proust, E., Bellenfant, G., and Bour, O.: Assessing methane oxidation under landfill covers and its contribution to the above atmospheric CO_2 levels: The added value of the isotope (δ^{13}C and δ^{18}O CO2; δ^{13}C and δD CH_4) approach, Waste Manage, 32, 1685–1692, 2012.

Zondervan, A. and Meijer, H. A. J.: Isotopic characterisation of CO_2 sources during regional pollution events using isotopic and radiocarbon analysis, Tellus B, 48, 601–612, doi:10.1034/j.1600-0889.1996.00013.x, 1996.

Publication 4

2.4 Evaluation of four years continuous $\delta^{13}C(CO_2)$ data using a running Keeling approach

Vardag, S. N., Hammer, S., and Levin, I.

Biogeosciences Discuss., doi:10.5194/bg-2016-93, 2016
Manuscript under review for journal Biogeosciences
Published: 16 March 2016

Biogeosciences Discussions
Open Access
EGU

Evaluation of four years continuous $\delta^{13}C(CO_2)$ data using a running Keeling approach

Sanam Noreen Vardag, Samuel Hammer, and Ingeborg Levin
Institut für Umweltphysik, Heidelberg University, Germany
Correspondence to: S. N. Vardag (svardag@iup.uni-heidelberg.de)

Abstract. As different carbon dioxide (CO_2) emitters have different carbon isotope ratios, measurements of atmospheric $\delta^{13}C(CO_2)$ and CO_2 concentration contain information on the CO_2 source mix in the catchment area of an atmospheric measurement site. Often, this information is illustratively presented as mean isotopic source signature. Recently an increasing number of continuous measurements of $\delta^{13}C(CO_2)$ and CO_2 have become available, opening the door to quantification of CO_2 shares from different sources at high temporal resolution. Here, we present a method to compute the CO_2 source signature (δ_S) continuously without introducing biases and evaluate our result using model data. We find that biases in δ_S are smaller than 0.2 ‰ with uncertainties of about 1.2 ‰ for hourly data. Applying the method to a four year data set of CO_2 and $\delta^{13}C(CO_2)$ measured in Heidelberg, Germany, yields a distinct seasonal cycle of δ_S. Disentangling this seasonal source signature into its source components is, however, only possible if the isotopic end members of these sources, i.e., the biosphere, δ_{bio}, and the fuel mix, δ_F, are known. From the mean source signature record in 2012, δ_{bio} could be reliably estimated only for summer to (-25 $\pm$ 1) ‰ and δ_F only for winter to (-32.5 $\pm$ 2.5) ‰. As the isotopic end members δ_{bio} and δ_F were shown to change over the season, no year-round estimation of the fossil fuel or biosphere share is possible from the measured mean source signature record without additional information from emission inventories or other tracer measurements, such as $\Delta^{14}C(CO_2)$.

1 Introduction

A profound understanding of the carbon cycle requires closing the atmospheric CO_2 budget at regional and global scale. For this purpose it is necessary to distinguish between CO_2 contributions from oceanic, biospheric and anthropogenic sources and sinks. Monitoring these CO_2 contributions separately is desirable for improving process understanding, investigating climatic feedbacks on the carbon cycle and also to verify emission reductions and designing CO_2 mitigation strategies (Marland et al., 2003; Gurney et al., 2009; Ballantyne et al., 2010). A possibility to distinguish between different CO_2 sources and sinks utilizes concurrent $^{12}CO_2$ and $^{13}CO_2$ observations in the atmosphere. The carbon isotope ratio can be used to identify and even quantify different CO_2 emitters if every emitter has its specific known $\delta^{13}CO_2$ signature. For example, the CO_2 fluxes from land and ocean can be distinguished using the ratio of stable carbon isotopologue $^{13}CO_2/^{12}CO_2$ in addition to CO_2 concentration measurements (Mook et al., 1983; Ciais et al., 1995; Alden et al., 2010). In other studies, measurements of $^{13}CO_2$ have been used to distinguish between different fuel types (Pataki, 2003; Lopez et al. 2013) or to detect ecosystem behavior (Torn et al., 2011), giving only a few examples of the many published in the literature.

Biogeosciences Discuss., doi:10.5194/bg-2016-93, 2016
Manuscript under review for journal Biogeosciences
Published: 16 March 2016

In the last decade, new optical instrumentation has been developed, simplifying continuous isotopologue measurements. This led to an increasing deployment of these instruments, therby increasing the temporal and spatial resolution of $^{13}C(CO_2)$ and CO_2 data (Bowling et al., 2003; Tuzson et al., 2008; McManus et al., 2010; Griffith et al., 2012; Vogel et al., 2013; Vardag et al., 2015a, Eyer et al., 2016). These data records may lead to an improved understanding of regional CO_2 fluxes allowing estimates of mean $\delta^{13}C$ source signatures at high temporal resolution. Estimating mean source signatures from concurrent $\delta^{13}C(CO_2)$ and CO_2 records over time provides e.g. insight into temporal changes in the signatures of two different CO_2 sources such as fossil fuels and the biosphere, if their relative share to the CO_2 offset is known. This may e.g. give insight into biospheric responses to climatic variations like drought, heat, floods, vapor pressure etc. (Ballantyne et al., 2010; Ballantyne et al., 2011; Bastos et al., 2016). Likewise, the mean source signature can be used to separate between different source CO_2 contributions, if the isotopic end members of these sources are known at all times (Pataki, 2003; Torn et al., 2011; Lopez et al. 2013; Newman et al., 2015).

Many studies have successfully used the Keeling- or Miller-Tans- approach (Keeling, 1958, 1961; Miller and Tans, 2003) to determine source signatures in specific settings (e.g. Pataki, 2003; Ogée et al., 2004; Lai et al., 2004; Knohl et al., 2005; Karlsson et al., 2007; Ballantyne et al., 2010). However, the situations in which Keeling and Miller-Tans plots yield correct results need to be selected carefully (Miller and Tans, 2003). Only if all possible pitfalls are precluded, the Keeling intercept (or the Miller-Tans slope) can be interpreted as gross flux-weighted mean isotopic signature of all CO_2 sources and sinks in the catchment area of the measurement site. Especially in polluted areas with variable source/sink distribution, estimation of isotopic signature using a Keeling- or Miller-Tans-plot requires a solid procedure, e.g. accounting for wind direction changes or simultaneously occurring CO_2 sinks and sources. In this study, we discuss the possible pitfalls of CO_2 source signature determination from a continuous data set using the Keeling approach and follow a specific modification of this method for automatic and bias-free mean source signature determination. We test this method with model-simulated CO_2 mole fraction and $\delta^{13}C(CO_2)$ data. Using a modeled data set where all source signatures are known, enables us to check if the calculated source signature is correct, which is vital when evaluating measured data with an automated routine. Having found a method to determine the isotopic signature of the mean source signature correctly from measured CO_2 and $\delta^{13}C(CO_2)$ data, we discuss, which information can be reliably extracted from these results.

2 Determination of source signature

2.1 Classical Keeling and Miller-Tans approach

Keeling (1958, 1961) showed that the mean isotopic signature of a source mix can be calculated by re-arranging the mass balance of total CO_2

$$CO_{2tot} = CO_{2bg} + CO_{2S} \quad (1)$$

and of $\delta^{13}C$ of total CO_2, i.e. δ_{tot}:

$$\delta_{tot} \cdot CO_{2tot} = \delta_{bg} \cdot CO_{2bg} + \delta_S \cdot CO_{2S} \quad (2)$$

Biogeosciences Discuss., doi:10.5194/bg-2016-93, 2016
Manuscript under review for journal Biogeosciences
Published: 16 March 2016

to:

$$\delta_{tot} \approx CO_{2bg}/CO_{2tot} \cdot (\delta_{bg} - \delta_S) + \delta_S \quad (3)$$

where CO_{2bg} and δ_{bg} are the concentration and $\delta^{13}C(CO_2)$ of the background component and CO_{2S} and δ_S are the concentration and $\delta^{13}C(CO_2)$ of the mean source, respectively. In a graphical evaluation when plotting δ_{tot} versus $1/CO_{2tot}$, this yields δ_S as the δ-intercept of the regression of all measurement points (cf. Fig.1a).

Miller and Tans (2003) have suggested an alternative approach to determine the mean isotopic signature by re-arranging Eqs. 1 and 2 such that δ_S is the regression slope when plotting $CO_{2tot} \cdot \delta_{tot}$ versus CO_{2tot}:

$$CO_{2tot} \cdot \delta_{tot} = \delta_S \cdot CO_{2tot} - CO_{2bg}(\delta_{bg} - \delta_S) \quad (4)$$

They argue that this approach might be advantageous since the isotopic signature does not need to be determined from extrapolation to $1/CO_2$=0, which could introduce large errors in the δ_S estimate. Zobitz et al. (2006) have compared the Keeling and the Miller-Tans approach (Eqs. 3 and 4) and found no significant differences between both approaches when applied to typical ambient CO_2 variations. We were able to reproduce this result with our model-simulated data set (cf. Sect. 3.2). Differences between both approaches were (0.00 ± 0.04) ‰ when applying certain criteria (standard deviation of intercept < 2 ‰, CO_2 range within 5 hours >5 ppm), which will be motivated in Sect. 2.3. In our study, we use a Keeling plot for calculation of the mean source signature, but using a Miller-Tans plot seems just as good. Note that the isotopic signature of the mean source δ_S can be determined from linear regression without requiring a background CO_2 and $\delta^{13}C(CO_2)$ value. However, the Keeling and Miller-Tans approaches are only valid if the background and the isotopic signature of the source mix δ_S are constant during the period investigated (Keeling, 1958, Miller and Tans, 2003). Further, the approaches are only valid when sources and sinks do not occur simultaneously. Miller and Tans (2003) gave an example, which showed that as soon as sources and sinks of different isotopic signature/fractionation occur simultaneously, the determination of isotopic signature of the source/sink mix is not *per se* possible. In these cases, the results cannot be interpreted as mean flux-weighted source signature anymore. This has very unfortunate consequences, since in principle we are interested in determining the isotopic signature of the source mix of a region during all times, i.e. also during the day when photosynthesis cannot be neglected. Pataki (2003), Miller and Tans (2003) and Zobitz et al. (2006) compared different fitting algorithms for the regression and came to different recommendations. Orthogonal distance regression (ODR) and weighted total least squares fits (WTLS) (model 2 fits) take into account errors on x and y, whereas ordinary least squares (OLS) minimization (model 1 fit) only takes into account y-errors. Zobitz et al. (2006) have found differences between both fitting algorithms especially at small CO_2 ranges. We have also applied a model 1 (OLS) and model 2 (WTLS) fit to our simulated data and have not found any significant differences ((0.00 ± 0.01) ‰) between them when applying certain criteria (error of intercept < 2 ‰, CO_2 range within 5 hours >5 ppm, see Sect. 2.2). In this study, however, we use a WTLS-fit for the determination of the intercept and its uncertainty.

2.2 Running Keeling approach

For a continuous long-term data set, we suggest an automatic routine to determine the mean isotopic signature of the source mix. We call this approach the "running" Keeling approach. It is similar to the moving Keeling plot for CH_4 currently suggested

Biogeosciences Discuss., doi:10.5194/bg-2016-93, 2016
Manuscript under review for journal Biogeosciences
Published: 16 March 2016

by Röckmann et al. (2016). In our case of CO_2 we also have to take into account the possibility of simultaneously occuring sinks and sources, which is not important in the case of CH_4. Our running Keeling approach is a specific case of the classical Keeling approach (Eq. 3) (Keeling, 1961) as it uses only five hourly-averaged measurement points of CO_2 and $\delta^{13}C(CO_2)$ fitting a regression line through these five data points (cf. Fig. 1a, illustrated only for three data points for clarity of inspection). We choose 5 hours as a compromise of maximum number of data points in a minimizing period, in which the source mix does not change significantly. No background value is included in the regression. The running Keeling approach works such that, e.g. for the determination of the mean source signature at 3 pm, we use the hourly CO_2 and $\delta^{13}C(CO_2)$ measurements from 1 pm to 5 pm and fit a regression line. Next, for the determination of the source signature at 4 pm, we use the CO_2 and $\delta^{13}C(CO_2)$ measurements from 2 pm to 6 pm and so on.

2.3 Filter criteria of the running Keeling approach

In order to prevent pitfalls in the regression-based determination of mean isotopic signature, we set a few criteria for the running Keeling plots to "filter" out situations, in which a Keeling plot cannot be performed. These filter criteria are also similar in type to the ones introduced by Röckmann et al. (2016). We here explain why these filter criteria are needed for CO_2 and how they are set. A prerequisite for the Keeling plot is that the source mix as well as the background need to stay constant during the investigated period (see Fig. 1a). Varying source mixes may occur when e.g. the wind direction and therewith the footprint of the measurement site change, or if the emission patterns themselves change over time. This may lead to strong biases of the regression-based mean isotopic source signature (illustrated in Fig. 1b). We eliminate these cases by inspecting the error of the determined intercept δ_S. If the source mix or the background significantly change within five hours, the data points will not fall on a straight line and the error of the intercept will increase. We here set an error of 2 ‰ (in a WTLS fit) as threshold between an acceptable and a "bad" fit, after having inspected many Keeling plots individually. Also, we demand a monotonous increase of CO_2 within 5 hours, as a decrease of would be due to either a sink of CO_2 or a breakdown of the boundary layer inversion associated with a change of catchment area of the measurement, both biasing the resulting mean source signature.

As mentioned before, the determination of a mean isotopic signature is not *per se* possible during the day when CO_2 sinks and sources are likely to occur simultaneously (Miller and Tans, 2003). This can be explained in the Keeling plot by the vector addition of CO_2 source and sink mixing lines with different isotopic signatures, resulting in a vector with an intercept different from the expected one, leading to an isotopic signature, which can even lie outside the expected range of the isotopic source end members (see Fig. 1c). This potential bias is stronger, the smaller the net CO_2 signal is. Therefore, e.g. for evaluation of the Heidelberg data, we demand an increase in CO_2 during the 5 hour period of at least 5 ppm to exclude periods where the photosynthetic sink is similarly strong as CO_2 sources. This normally leads to an exclusion of daytime periods, when the boundary layer inversion typically breaks up and the photosynthetic sink is most pronounced. During winter, it may happen that the inversion does not break up due to the cold surface temperatures, but in this season, photosynthetic activity is typically much smaller than fossil fuel emissions and therefore biases of the regression-based mean source signature are only small. In the next section, we show that with these filter criteria, which we chose empirically, we are able to successfully remove those

Biogeosciences Discuss., doi:10.5194/bg-2016-93, 2016
Manuscript under review for journal Biogeosciences
Published: 16 March 2016

source signatures, where the underlying assumptions for the Keeling approach are not met. In Sect. 3.2, we will also briefly discuss how sensitive the result is to the choice of filter criteria.

3 Test of the running Keeling approach with modeled data

We apply the running Keeling method to a modeled CO_2 and $\delta^{13}C(CO_2)$ data set. As also pointed out by Röckmann et al. (2016) in their CH_4 study, this has the advantage that we can test and evaluate our filter criteria as we know exactly the individual isotopic source signatures that created the modeled data set and thus, the contribution-weighted mean isotopic source signature at every point in time. Details on the STILT model and on the computation of the modelled CO_2 and $\delta^{13}C(CO_2)$ record as well as of the resulting mean source signature, δ_S^{STILT}, are given in Appendix A.

3.1 Filter criteria of modeled source signature

We apply the same filter criteria to the calculated mean source signature of the STILT modelled data set δ_S^{STILT}, as to the regression-based mean source signature (Sect. 2.3). The "unfiltered" source signatures (black in Fig. 2a) are 0-2‰ more enriched than the "filtered" source signatures (blue). This offset is mainly caused by the daytime source signatures, which are on average more enriched than nighttime source signatures (Fig. 2b), but more likely to be filtered out based on the criteria of Sect. 2.3.

3.2 Evaluation of running Keeling approach

We can now evaluate the running Keeling method and the filter criteria based on the model data and test if they allow a bias-free retrieval of the mean source signature. In Fig. 3a, we compare the regression-based source signatures to the filtered reference source signature of Fig 2a, which we have extracted from the model. We do not only compare the mean difference of the mean source signature, but the hourly differences of the mean source signature as well as the smoothed difference. This enables us to clearly state how well we are able to determine the hourly mean source signature and its long-term trend.

Fig. 3a displays the filtered seasonal changes of the source signature for the year 2012. The running Keeling approach is able to extract the seasonal variability of the mean isotopic signature correctly. The median difference (and inter-quartile range) between smoothed regression-based (red) and smoothed modeled (blue) approach (both smoothed with 50% percentile filter with window size of 100 hours, no smooting 50 points in front of large data gaps) is 0.0 ± 0.4 ‰. On a shorter diurnal time scale, we also compare individual hourly results for the source signature (stars in Fig. 3b,c). The inter-quartile range of the filtered hourly difference between both the reference δ_S^{STILT} and the running Keeling signature is ca. 1.2 ‰ throughout the year, but the median difference is small (0.2 ‰). The source signature of the model reference and running Keeling source signature show the same temporal pattern both, in summer and in winter. Further, we find that if we do not apply all of the criteria described in Sect. 2.2 (unfiltered data in Fig. 3b,c), we see larger differences between regression-based source signature (from the running Keeling plot) and the STILT reference values. Note, however, that with the criteria established in Sect. 2.3, we have rejected about 85% of all estimated source signatures. Depending on the application, it may be worthwhile to loosen

Biogeosciences Discuss., doi:10.5194/bg-2016-93, 2016
Manuscript under review for journal Biogeosciences
Published: 16 March 2016

the filter criteria to increase the data coverage. For example, if one sets no criteria for the minimal CO_2 range, but only for the error of the slope (< 2‰), about 60% of all data remain for the estimated source signature, but the median difference between model- and Keeling-based results increases to 0.3 ‰ and the interquartile range increases to 2.4‰ (hourly data), which is about twice of what we found before. Withdrawing all filter criteria, but using only night time values, leads to a coverage of about 35% (night time) and an interquartile range of 3.5 ‰. The filter criteria, which we use here (Sect. 2.3) are, thus, rather strict, but we are confident to precisely extract the correct source signature from the $\delta^{13}C(CO_2)$ and CO_2 record at highest temporal resolution.

4 Application of the running Keeling approach

4.1 The measured source signature record in Heidelberg

We now apply this approach to real measured data. We use the Heidelberg CO_2 and $\delta^{13}C(CO_2)$ record on hourly time resolution (Fig. B1) to compute the isotopic source signature via regression (Fig. 4). The quality of the Heidelberg CO_2 and $\delta^{13}C(CO_2)$ record is assessed in the Appendix B. We observe a distinct seasonal cycle of the mean isotopic source signature in Heidelberg. Smoothed minimum values of about -32 ‰ are reached in winter. Maximum values of about -26 ‰ occur in summer. This principal pattern is reproduced every year. Additionally, the first year shows a more enriched summer maximum source signature. A number of data points (less than 0.5%) lie outside the range of realistic end members between -20 and -45 ‰ of any source in the catchment area (see Table 1). These outliers can be explained statistically by the uncertainty of the running Keeling approach. From the model analysis, we expect the inter-quartile range of δ_S for the Heidelberg catchment area to be about 1.2 ‰, in accordance to Fig. 4 (1.8 ‰). Our record of the mean source signature in Heidelberg provides a first insight into the source characteristics at the measurement station. It reaches its minimum in winter when we expect residential heating (mainly isotopically depleted natural gas, see Tab. 1) to contribute significantly to the source mix. The source signature reaches its maximum in summer when more enriched biospheric fluxes are expected to dominate the CO_2 signal. This observed seasonal cycle in Heidelberg (Fig. 4) is very similar to the filtered modelled source signature (Fig. 3a) in amplitude as well as phase.

4.2 Extracting information on the isotopic end members δ_{bio} and δ_F from δ_S

We now want to elaborate what quantitative information can be drawn from the mean source signature record in Heidelberg about its components. Details on the Heidelberg measurement site and catchment area can be found in Vogel et al. (2010).

4.2.1 Formulation of question

For a continental measurement site such as Heidelberg, we have to assume that there are at least two main source types of CO_2 in the catchment area: Fuel CO_2 and CO_2 from the biosphere. In this simplest case, we essentially have one equation (δ_S, Eq.

Biogeosciences Discuss., doi:10.5194/bg-2016-93, 2016
Manuscript under review for journal Biogeosciences
Published: 16 March 2016

6) with three unknown variables (δ_{bio}, δ_F and the fuel (or biosphere) share f_F) and only if two of these variables are known, the third variable can be quantified from the measurements:

$$\delta_S = \frac{CO_{2F}}{\Delta CO_2} \cdot \delta_F + \frac{\Delta CO_2 - CO_{2F}}{\Delta CO_2} \cdot \delta_{bio} \tag{5}$$

$$= f_F \cdot \delta_F + (1 - f_F) \cdot \delta_{bio} \tag{6}$$

Which of the variables is the one to be estimated depends, of course, on the research question. If the fossil fuel share and end members are well known from inventories, one could be especially interested in determining the isotopic end member δ_{bio} in order to study biospheric processes and their feedback to climatic parameters (Ciais et al., 2005; Ballantyne et al., 2010; Salmon et al., 2011). Contrary, one may be interested in determining the relative share of fossil fuel CO_2 in the catchment area (with known δ_{bio} and δ_F) to monitor emission changes independently from emission inventories. In our discussion, we focus on the determination of the fossil fuel share, but the arguments for most parts are analog for other research questions.

As noted, a quantification of the relative shares of fossil fuel and the biospheric CO_2 at continental stations is only possible if information on the isotopic end members of both source categories are available. For example, Vardag et al. (2015b) used the isotopic signatures of δ_{bio} (assumed to be known within a fixed uncertainty) and δ_F (obtained by calibration with $\Delta^{14}C(CO_2)$) to calculate the fossil fuel CO_2 contribution from the (continuously) measured CO_2 and $\delta^{13}C(CO_2)$ signal. However, knowing the isotopic signatures δ_{bio} and δ_F over the entire course of the year, requires an extensive number of measurements at the relevant sources throughout the year and further assumptions how to extrapolate the source signature of the point measurements to a mean source signature of all relevant sources. Therefore, we ask here, if we can obtain information on these end members from our measured source signature record, despite the fact that we have three unknown variables and only one equation. In the following, we discuss this question exemplary for the year 2012, for which we have modeled data, inventory information and an almost complete measurement record.

4.2.2 One source approximation

In general, in order to obtain information on δ_{bio} (δ_F), we require information on the fuel CO_2 share and δ_F (on the fuel CO_2 share and δ_{bio}). However, in cases where the relative share of the biosphere (fossil fuels) is negligible, the isotopic signature of δ_F (δ_{bio}) would equal the mean isotopic signature. In these cases, the number of unknown variables would be reduced to one as the fossil fuel (biospheric) share is $\approx 100\%$ and δ_{bio} (δ_F) does not contribute significantly to the mean source signature. In a typical catchment area, the relative share of fossil fuels and of the biosphere will not be negligible throughout the year, but in winter, fossil fuel CO_2 will dominate while in summer the biospheric CO_2 will dominate the CO_2 offset compared to the background. E.g. from the STILT model results for Heidelberg (Sect. 3.2 and Appendix A), we perceive that on cold winter days in Heidelberg, the fossil fuel share can be about 90 to 95% of the total CO_2 offset. In summer, it reaches a minimum at about 20%. We may, thus, be able to obtain information about the isotopic end members of δ_F in winter (δ_{bio} in summer), when the mean source signature is dominated by the fossil fuel (biospheric) share.

Biogeosciences Discuss., doi:10.5194/bg-2016-93, 2016
Manuscript under review for journal Biogeosciences
Published: 16 March 2016

To calculate the resulting isotopic end members of δ_i from the measured source signature (and with that to solve Eq. 6), we require the fossil fuel CO_2 share from STILT and the bottom-up emission inventory EDGAR. However, as we only require the share and not the absolute concentration, we are largely independent from potentially large model transport errors. We assume an absolute uncertainty of 10 % of the fossil fuel share (and of the biospheric share respectively).

To determine δ_F in addition to the fuel CO_2 share, we require a value for δ_{bio}. Here we use a typical mean value of the isotopic end member of δ_{bio}= -25 ‰ and assume a seasonal cycle as determined for Europe by Ballantyne et al. (2011) (see Fig. 2 and 3 in Ballantyne et al. (2011)) displayed in Fig. 5a as solid green line. We show δ_{bio} with two possible uncertainties of 0.5 and 2 ‰. As expected, the uncertainty of the unknown δ_F is only acceptably small when the relative share of the biosphere becomes negligible, which is the case in winter (Fig. 5a). The isotopic end member of δ_F in winter is about (-31 $\pm$ 2.5) ‰ in January to March 2012 and decreases to (-32.5 $\pm$ 2.5) ‰ in November to December 2012. Further, Fig. 5a shows that the best estimate of the resulting isotopic signature δ_F is more depleted in summer than in winter. This curvature is opposite from what we would expect from EDGAR (2010) transported by STILT (see assumed δ_F in Fig. 5b). Only when assuming an uncertainty of the biospheric end member of $\pm$ 2 ‰ or more, the uncertainty range of the estimated δ_F allows more enriched δ_F signature in summer than in winter. This suggests that the isotopic source signature of the biosphere in summer is most probably more depleted (by about 2 ‰) than the previously assumed δ_{bio} value based on Ballantyne et al. (2011).

To estimate δ_{bio} (Fig. 5b), we require (besides the fossil fuel share) the isotopic source signature δ_F. Here we use δ_F calculated with the STILT model on the basis of EDGAR emissions and source signatures according to Tab. 1. Its annual mean value is -31 ‰ and it shows a seasonal cycle with more enriched signatures in summer than in winter. We show the results for δ_{bio} for two possible δ_F uncertainties of 1 and 3 ‰ (see Fig. 5b). The best-estimate of the isotopic end member of δ_{bio} in summer is about -25.0 ± 1 ‰ in June to August 2012. This reinforces the presumption that δ_{bio} is more depleted than the assumed δ_{bio} value based on Ballantyne et al. (2011) during summer.

4.2.3 Evaluation of the precision

The uncertainty of the isotopic end members in Fig. 5a and b has three components: 1) The uncertainty of the fossil fuel CO_2 share estimated from STILT, which we assume to be about 10% (absolute) in our case, 2) the uncertainty of the other known isotopic end member (0.5 and 2 ‰ for δ_{bio} or 1 and 3 ‰ for δ_F) and 3) the uncertainty of the measured mean source signature itself (ca. 0.5 ‰, see Sect. 3.2). Note, that an uncertainty of 10% of the fossil fuel share is at the low end of uncertainties. However, an uncertainty of 20% of the fossil fuel share would increase the uncertainty in the unknown isotopic end members by only 0.2 - 0.4 ‰ for δ_{bio} in summer and δ_F in winter, respectively.

The derived uncertainty of δ_F in winter is about 2.5 ‰ and that of δ_{bio} in summer is about 1.5 ‰. An uncertainty of ± 2.5 ‰ for δ_F is rather large if we want to use this observation-based top-down result for further quantitative source apportionment. Vardag et al. (2015b) showed that a misassignment of 2.5 ‰ in δ_F leads to a bias in the continuous fuel CO_2 estimate of about 15% for an urban measurement site like Heidelberg. The observation-based biospheric end member δ_{bio} has an uncertainty of only about 1 ‰ in June to August 2012, which is a very well constraint value for this period.

Biogeosciences Discuss., doi:10.5194/bg-2016-93, 2016
Manuscript under review for journal Biogeosciences
Published: 16 March 2016

4.2.4 Evaluation of accuracy

If both isotopic end members stayed constant over the course of one year, we would now be able to actually estimate the fossil fuel CO_2 share (and its uncertainty) continuously throughout the year without requiring any additional information, such as inventories or $\Delta^{14}C(CO_2)$ for calculation of δ_F from the mean source signature. However, from bottom-up information, we would neither expect the isotopic value of the biosphere nor that of the fossil fuel mix to remain constant throughout the year. In contrary, we would expect the biosphere to show a distinct seasonal pattern e.g. due to the change in fraction of respiration from C3/C4 plants over the course of the year or influences of climatic conditions on biospheric respiration (e.g. Still et al., 2003; Ciais et al., 2005). A seasonal cycle of δ_F is also expected with more enriched values in summer, when the contribution of residential heating (and therewith of depleted natural gas) is much smaller than in winter. Therefore, if we have varying isotopic end members of δ_F and δ_{bio}, we cannot estimate the fossil fuel share correctly for the entire year. But, if the amplitude of these changes is small, the biases in fossil fuel CO_2 will be small as well. Vardag et al. (2015b) have shown that from a limited number of $^{14}C(CO_2)$ grab samples distributed over the year, the true annual mean value of δ_F can be obtained. Here we show that from the mean $\delta^{13}C$ source signature only a reliable winter value is obtained, potentially introducing summer biases (as well as annual averaged biases) into the fuel CO_2.

4.2.5 Possible strategy to obtain δ_F and δ_{bio}

To determine δ_{bio}, one can take the summer value of δ_{bio} from the source signature record following Sect. 4.2.2. As no reliable determination of δ_{bio} is possible during the rest of the year based only on atmospheric observations, there must be either very good bottom-up literature values for the catchment area of interest or frequent measurement campaigns at the sources must be performed. However, the disadvantage of using a bottom-up approach is that usually only information from few specific sites are available, which need then to be upscaled correctly such that they are representative of the entire catchment area. For a determination of δ_F in the entire year, one can use $\Delta^{14}C(CO_2)$ measurements (following Vardag et al. (2015b)) or rely on the bottom-up inventory information. To obtain correct source signatures of the different fossil fuel categories, measurements close to these sources are required to support or refute the inventory-model based estimates. These measurements again need to be upscaled correctly.

5 Conclusions

Many measurement stations are currently being equipped with new optical instruments, which measure $\delta^{13}C(CO_2)$ aiming at a more quantitative understanding of the carbon fluxes in their catchment area. If this additional $\delta^{13}C(CO_2)$ data stream is not directly digested in regional model calculations, the mean isotopic source signature is often computed from the $\delta^{13}C(CO_2)$ and CO_2 records for the analysis of the source composition. Essentially, this source signature provides the same degree of information as the measured $\delta^{13}C$ and CO_2 records themselves, but is a more intuitive and therefore common form for further interpretations.

Biogeosciences Discuss., doi:10.5194/bg-2016-93, 2016
Manuscript under review for journal Biogeosciences
Published: 16 March 2016

We re-emphasize here that a bias-free determination of source signature requires carefully selecting the data for situations, in which determination of source signature with a Keeling plot can provide reliable results. This excludes periods, when sinks and sources occur simultaneously, when the source mix changes or when the signal-to-noise ratio is too low (Keeling, 1958; Keeling, 1961; Miller and Tans, 2003). We therefore developed filter criteria and show that the routine and accurate determination of $^{13}C(CO_2)$ source signature is possible, if the introduced filter criteria are applied. As suggested by Röckmann et al. (2016), we use a modeled data set for validation of the approach. We find that for a station like Heidelberg, the bias introduced by our analysis is only (0.2 ± 1.2) ‰ for hourly data. The uncertainty decreases in the long-term to (0.0 ± 0.4) ‰. We are therefore able to estimate the source signature correctly. However, as the filter criteria are such that the source signatures are more likely to be filtered out during the day than during the night, the long-term source signature is not representative of real daily averages, but only of periods, where the data was not filtered out (mainly nighttime). This problem does not occur for CH_4, which has only weak daytime sinks.

By applying the running Keeling plot procedure to a real measured data set in Heidelberg, we are able to determine the source signature over the course of four years. We find a distinct seasonal cycle of the mean source signature with values of about -26 ‰ in summer and about -32 ‰ in winter. This general behavior was expected due to the larger relative contribution of more depleted fossil fuel CO_2 in winter. For a unique interpretation of the mean source signature, possible sources in the catchment area need to be identified. As soon as there are more than one source, the source signature is a function of the isotopic end members of all sources, as well as of their relative shares. Therefore, to study the seasonal and diurnal changes of fossil fuel shares at a continental station, information on the isotopic end members of the fossil fuel mix as well as of the biosphere are required on the same time resolution. Unfortunately, the isotopic end members are often not known with high accuracy. The uncertainty of the isotopic end members often impedes or even prevents a unique straightforward determination of the source contribution in the catchment area (e.g. (Pataki, 2003; Torn et al., 2011, Lopez et al. 2013; Röckmann et al., 2016) and calls for elaborated statistical models based on Bayesian statistics . This important fact is sometimes mentioned, but the consequences for quantitative evaluations are rarely emphasized, preserving the high expectations associated with isotope measurements.

We showed that for the urban site Heidelberg, we can use the observation-based mean source signature record to estimate the isotopic end member δ_F in winter and the isotopic end member δ_{bio} in summer within the uncertainties of ± 2.5 ‰ and ± 1 ‰, respectively, when assuming an uncertainty of ± 10 % for the fossil fuel and biospheric CO_2 share and an uncertainty of the other isotopic end member δ_F of ± 3 ‰ and δ_{bio} of ± 2 ‰. However, in the winter season we cannot obtain any reliable information on δ_{bio} and in summer we cannot study δ_F. If the isotopic end members would not change within seasons, it would be possible to determine these constant isotopic signature from our obtained estimates. However, this is not a valid assumption.

Finally, we could show, that even though it is not possible to determine the isotopic end members throughout the year, it is possible to refute certain literature values. E.g. a respiration signature of -23 ‰ in August and September 2012 as reported by Ballantyne et al. (2011) is most likely too enriched as this would lead to more depleted δ_F values in summer than in winter, which is in contrast to what we would expect based on emission inventories.

Biogeosciences Discuss., doi:10.5194/bg-2016-93, 2016
Manuscript under review for journal Biogeosciences
Published: 16 March 2016

Appendix A: The STILT model

We use the Stochastic Time Inverted Lagrangian Transport (STILT) model (Lin et al., 2003) to evaluate our running Keeling approach. The STILT model computes the CO_2 mole fraction by time-inverting meteorological fields and tracing particles emitted at the measurement location back in time to identify where the air parcel originated. This so-called footprint area is then multiplied by the surface emissions in the footprint to obtain the CO_2 concentration at the site in question. Photosynthesis and respiration CO_2 fluxes are taken from the vegetation photosynthesis and respiration model (VPRM, Mahadevan et al., 2008). Anthropogenic emissions are taken from EDGARv4.3 emission inventory (EC-JRC/PBL, 2015) for the base year 2010 and further extrapolated to the year 2012 using the BP statistical review of World Energy 2014 (available at: http://www.bp.com/en/global/corporate/about-bp/energy-economics/statistical-review-of-world-energy.html). Additionally, we use seasonal, weekly and daily time factors for different emission categories (Denier van der Gon et al., 2011). Since the EDGAR inventory is separated into different fuel types, we obtain a CO_2 record for each fuel type as well as for respiration and photosynthesis. This allows us, to construct a corresponding $\delta^{13}C(CO_2)$ record by multiplying the isotopic signature of every emission group i to its respective CO_2 mole fraction $\delta^{13}C(CO_2)_i \cdot CO_{2,i}$ (see Tab. 1), adding these to a far-field boundary value of $\delta^{13}C(CO_2) \cdot CO_2$ and dividing it by the total CO_2 at the model site. The CO_2 far-field boundary value for STILT is the concentration at the European domain border (16°W to 36°E and from 32°N to 74°N) at the position where the backwards traced particles leave the domain. The concentration at the domain border is taken from analyzed CO_2 fields generated with TM3 (Heimann and Körner, 2003) based on optimized fluxes (Rödenbeck, 2005). The isotopic boundary value is then constructed artificially by fitting the linear regression between CO_2 and $\delta^{13}C(CO_2)$ in Mace Head (year 2011 from World Data Center for Greenhouse Gases, (Dlugokencky et al., 2015)) and applying the function of the regression to the boundary CO_2 values in the model. Since, in reality, we also have measurement uncertainties of CO_2 and $\delta^{13}C(CO_2)$ we also include a random measurement uncertainty of 0.05 ppm and 0.05 ‰, respectively to the modeled data sets. The CO_2 and $\delta^{13}C(CO_2)$ records are used to calculate the regression-based mean source signature following the running Keeling approach (Sect. 2.2).

A1 Computation of mean modeled source signature

For the reference modeled mean source signature we use a "running" background. In particular, we chose the minimum CO_2 value within 5 hours centered around the measurement point as the background value and all contributions from fuel CO_2 ($c_{F,i}$), respiration (c_{resp}) and from photosynthesis (c_{photo}) are computed as offsets relative to the background (c_{bg}). This is then comparable to the regression-based running Keeling approach as the lowest and highest CO_2 values within five hours span the Keeling plot. We are then able to define and compute the reference modeled mean source signature as:

$$\delta_S^{STILT} = \frac{\sum_i \delta_{F,i}|c_{F,i}| + \delta_{resp}|c_{resp}| + \delta_{photo}|c_{photo}|}{\sum_i |c_{F,i}| + |c_{resp}| + |c_{photo}|} \tag{A1}$$

Note that we use absolute values of all contributions since photosynthetic contributions (c_{photo}) are generally negative while source contributions (c_{resp} and $c_{F,i}$) are generally positive, but both should lead to a negative source signature in a Keeling plot. The calculated source signature δ_S^{STILT} (from Eq. A1) can be seen in Fig. 2a (blue). If we would not take into account

Biogeosciences Discuss., doi:10.5194/bg-2016-93, 2016
Manuscript under review for journal Biogeosciences
Published: 16 March 2016

the different signs of respiration and photosynthesis, we would construct isotopic signatures, which are counter-intuitive and not interpretable as mean source signature (Miller and Tans, 2003) as the denominator could converge against zero. When calculating the isotopic source following Eq. A1, we can interpret δ_S^{STILT} as gross flux weighted mean isotopic signature of sources and sinks.

Appendix B: CO_2 and $\delta^{13}C(CO_2)$ measurements in Heidelberg

A necessary prerequisite of determining the mean source signature correctly at a measurement site is a good quality of CO_2 and $\delta^{13}C(CO_2)$ measurements. Therefore, we briefly describe here the instrumental set-up in Heidelberg, assess the precision of the CO_2 and $\delta^{13}C(CO_2)$ measurements and finally present our four years' ambient air record of CO_2 and $\delta^{13}C(CO_2)$ in Heidelberg.

B1 Instrumental set-up and intermediate measurement precision

Since April 2011, atmospheric trace gas mole fractions are measured with an *in-situ* Fourier Transform-InfraRed (FTIR) spectrometer at three-minute time resolution at the Institut für Umweltphysik in Heidelberg (Germany, 49°25'N, 8°41'E, 116 m a.s.l +30 m a.g.l.) (see Fig. B1 for CO_2 and $\delta^{13}C(CO_2)$. A description of the measurement principle can be found in Esler et al. (2000) and Griffith et al. (2010, 2012). Hammer et al. (2012) describe the Heidelberg-specific instrumental set-up in detail and Vardag et al. (2015a) describe modifications to this set-up and the calibration strategy for the stable isotopologue measurements.

The intermediate measurement precision of the FTIR is about 0.05 ppm for CO_2 and 0.04 ‰ for $\delta^{13}C(CO_2)$ (both 9 minute averages) as determined from the variation of daily target gas measurements (Vardag et al., 2014; Vardag et al., 2015a). In this work, we only use hourly CO_2 and $\delta^{13}C(CO_2)$ values, since simulation runs often have an hourly resolution and thus, observations and simulations can directly be compared. However, from Allan standard deviation tests, we know that the intermediate measurement precision of hourly measurements is only slightly better than for nine-minutely measurements (Vardag et al., 2015a).

B2 Four years of concurrent CO_2 and $\delta^{13}C(CO_2)$ measurements in Heidelberg

The CO_2 concentration in Heidelberg varies over the course of the year and has its maximum in winter and its minimum in summer (Fig. B1). This pattern is mainly driven by larger fossil fuel emissions in winter than in summer. Especially, emissions from residential heating are higher in the cold season. Furthermore, biospheric uptake of CO_2 is lower in winter than in summer. The minimum of the isotopic $\delta^{13}C(CO_2)$ value coincides with the maximum in CO_2 concentration and vice versa. The features are anti-correlated since almost all CO_2 sources in the catchment area of Heidelberg are more $\delta^{13}C$-depleted than the background concentration and therefore a CO_2 increase always leads to a depletion of $\delta^{13}C(CO_2)$ in atmospheric CO_2. Also, the biospheric CO_2 sink, dominating in summer, discriminates against $\delta^{13}C(CO_2)$, leaving the atmosphere enriched in $^{13}C(CO_2)$, while CO_2 decreases. On top of the seasonal cycle, CO_2 in Heidelberg (Fig. B1) slightly increases over the course

Biogeosciences Discuss., doi:10.5194/bg-2016-93, 2016
Manuscript under review for journal Biogeosciences
Published: 16 March 2016

of four years by about 2 ppm year^{-1}. At the same time $\delta^{13}C(CO_2)$ decreases by about 0.04 ‰ year^{-1}. These rates are similar to the CO_2 increase and $\delta^{13}C(CO_2)$ decrease rates in Mauna Loa, Hawaii, USA (Dlugokencky et al., 2015; White et al., 2015) and therefore reflect the global increase of CO_2 from ^{13}C-depleted sources moderated by air-sea gas exchange. It is not visible to the eye, how the degree of depletion in $\delta^{13}C(CO_2)$ varies over the course of the year (see Fig. B1). To analyze this behavior, the mean source signature must be computed (see Sect. 2.2 and Fig. 4).

Author contributions. S. Vardag developed the running Keeling approach in exchange with I. Levin. S.Vardag verified this approach using pseudo data from the STILT model and applied the approach to measured data. The measured data was partly taken by S. Hammer (until Sept. 2011) and mainly by S. Vardag (Sept. 2011 to June 2015). The final discussion and manuscript writing profited from input from all three authors.

Acknowledgements. This work has been funded by the InGOS EU project (284274) and national ICOS project funded by the German Ministry of Education and Research (Contract number: 01LK1225A). We thank NOAA/ESRL and INSTAAR for making their observational data from Mace Head and Mauna Loa available on the WDCGG website. Further, we acknowledge the financial support given by Deutsche Forschungsgemeinschaft and Ruprecht-Karls-Universität Heidelberg within the funding program Open Access Publishing.

Biogeosciences Discuss., doi:10.5194/bg-2016-93, 2016
Manuscript under review for journal Biogeosciences
Published: 16 March 2016

References

Alden, C. B., Miller, B., J., and White, J. W.: Can bottom-up ocean CO_2 fluxes be reconciled with atmospheric ^{13}C observations?, Tellus B, 62, 369–388, doi:doi: 10.1111/j.1600-0889.2010.00481.x, 2010.

Andres, R. J., Marland, G., Boden, T., and Bischof, S.: Carbon Dioxide Emissions from Fossil Fuel Consumption and Cement Manufacture, 1751-1991; and an Estimate of Their Isotopic Composition and Latitudinal Distribution, Environmental Sciences, 1994.

Ballantyne, A. P., Miller, J. B., and Tans, P. P.: Apparent seasonal cycle in isotopic discrimination of carbon in the atmosphere and biosphere due to vapor pressure deficit, Global Biogeochemical Cycles, 24, n/a–n/a, doi:10.1029/2009GB003623, http://dx.doi.org/10.1029/2009GB003623, gB3018, 2010.

Ballantyne, A. P., Miller, J. B., Baker, I. T., Tans, P. P., and White, J. W. C.: Novel applications of carbon isotopes in atmospheric CO2: what can atmospheric measurements teach us about processes in the biosphere?, Biogeosciences, 8, 3093–3106, 2011.

Bastos, A., Janssens, I. A., Gouveia, C. M., Trigo, R. M., Ciais, P., Chevallier, F., Peñuelas, J., Rödenbeck, C., Piao, S., Friedlingstein, P., and Running, S. W.: European land CO_2 sink influenced by NAO and East-Atlantic Pattern coupling, Nature communications, 7, 2016.

Bowling, D. R., Sargent, S. D., Tanner, B. D., and Ehleringer, J. R.: Tunable diode laser absorption spectroscopy for stable isotope studies of ecosystem–atmosphere CO_2 exchange, Agricultural and Forest Meteorology, 118, 1 – 19, doi:http://dx.doi.org/10.1016/S0168-1923(03)00074-1, http://www.sciencedirect.com/science/article/pii/S0168192303000741, 2003.

Bush, S., Pataki, D., and Ehleringer, J.: Sources of variation in $\delta^{13}C$ of fossil fuel emissions in Salt Lake City, USA, Applied geochemistry, 22, 715–723, 2007.

Ciais, P., Tans, P. P., Trolier, M., White, J. W. C., and Francey, R.: A large Northern Hemisphere terrestrial CO_2 sink indicated by the $^{13}C/^{12}C$ ratio of atmospheric CO_2, Science, 269, 1098–1102, 1995.

Ciais, P., Reichstein, M., Viovy, N., Granier, A., Ogee, J., Allard, V., Aubinet, M., Buchmann, N., Bernhofer, C., Carrara, A., Chevalier, F., De Noblet, N., Friend, A. D., Friedlingstein, P., Grunwald, T., Heinesch, B., Keronen, P., Knohl, A., Krinner, G., Loustau, D., Manca, G., Matteucci, G., Miglietta, F., Ourcival, J. M., Papale, D., Pilegaard, K., Rambal, S., Seufert, G., Soussana, J. F., Sanz, M. J., Schulze, E. D., Vesala, T., and Valentini, R.: Europe-wide reduction in primary productivity caused by the heat and drought in 2003 , Nature, 437, 529–533, 2005.

Denier van der Gon, H., Hendriks, C., Kuenen, J., Segers, A., and Visschedijk, A.: Description of current temporal emission patterns and sensitivity of predicted AQ for temporal emission patterns, TNP Report, EU FP7 MACC deliverable report, https://gmes-atmosphere.eu/documents/deliverables/d-emis/MACC_TNO_del_1_3_v2.pdf, 2011.

Dlugokencky, E., Lang, P., Masarie, K., Crotwell, A., and Crotwell, M.: Atmospheric Carbon Dioxide Dry Air Mole Fractions from the NOAA ESRL Carbon Cycle Cooperative Global Air Sampling Network Sampling Network, 1968-2014, ftp://aftp.cmdl.noaa.gov/data/trace_gases/co2/flask/surface/., 2015.

Esler, M. B., Griffith, D. W., Wilson, S. R., and Steele, L. P.: Precision trace gas analysis by FT-IR spectroscopy. 2. The $^{13}C/^{12}C$ isotope ratio of CO_2., Analytical chemistry, 72, 216–21, 2000.

Eyer, S., Tuzson, B., Popa, M. E., van der Veen, C., Röckmann, T., Rothe, M., Brand, W. A., Fisher, R., Lowry, D., Nisbet, E. G., Brennwald, M. S., Harris, E., Zellweger, C., Emmenegger, L., Fischer, H., and Mohn, J.: Real-time analysis of $\delta^{13}C$- and δD-CH_4 in ambient air with laser spectroscopy: method development and first intercomparison results, Atmospheric Measurement Techniques, 9, 263–280, doi:10.5194/amt-9-263-2016, http://www.atmos-meas-tech.net/9/263/2016/, 2016.

Biogeosciences Discuss., doi:10.5194/bg-2016-93, 2016
Manuscript under review for journal Biogeosciences
Published: 16 March 2016

Griffith, D., Deutscher, N., Krummel, P., Fraser, P., Schoot, M., and Allison, C.: The UoW FTIR trace gas analyser: Comparison with LoFlo, AGAGE and tank measurements at Cape Grim and GASLAB, Baseline atmospheric program (Australia), 2010, 2010.

Griffith, D. W. T., Deutscher, N. M., Caldow, C., Kettlewell, G., Riggenbach, M., and Hammer, S.: A Fourier transform infrared trace gas and isotope analyser for atmospheric applications, Atmospheric Measurement Techniques, 5, 2481–2498, doi:10.5194/amt-5-2481-2012, http://www.atmos-meas-tech.net/5/2481/2012/, 2012.

Gurney, K. R., Mendoza, D. L., Zhou, Y., Fischer, M. L., Miller, C. C., Geethakumar, S., and de la Rue du Can, S.: High resolution fossil fuel combustion CO_2 emission fluxes for the United States, Environmental Science & Technology, 43, 5535–5541, 2009.

Hammer, S., Griffith, D. W. T., Konrad, G., Vardag, S., Caldow, C., and Levin, I.: Assessment of a multi-species in-situ FTIR for precise atmospheric greenhouse gas observations, AMTD, pp. 3645–3692, 2012.

Heimann, M. and Körner, S.: The global atmospheric tracer model TM3, in: Technical Report, edited by Biogeochemie, M.-P.-I. F., vol. 5, p. 131, Max-Planck-Institut für Biogeochemie, Jena, 2003.

Karlsson, J., Jansson, M., and Jonsson, A.: Respiration of allochthonous organic carbon in unproductive forest lakes determined by the Keeling plot method, Limnology and Oceanography, 52, 603–608, doi:10.4319/lo.2007.52.2.0603, http://dx.doi.org/10.4319/lo.2007.52.2.0603, 2007.

Keeling, C. D.: The concentration and isotopic abundances of atmospheric carbon dioxide in rural areas, Geochimica et Cosmochimica Acta, 13, 322–224, 1958.

Keeling, C. D.: The concentrations and isotopic abundances of atmospheric carbon dioxide in rural and marine air., Geochim Cosmochim Acta,, 24, 277–298, 1961.

Knohl, A., Werner, R. A., Brand, W. A., and Buchmann, N.: Short-term variations in $\delta^{13}C$ of ecosystem respiration reveals link between assimilation and respiration in a deciduous forest., Oecologia, 142, 70–82, doi:10.1007/s00442-004-1702-4, http://www.springerlink.com/content/q9qebq8u3674n2pw/, 2005.

Lai, C.-T., Ehleringer, J. R., Tans, P., Wofsy, S. C., Urbanski, S. P., and Hollinger, D. Y.: Estimating photosynthetic ^{13}C discrimination in terrestrial CO_2 exchange from canopy to regional scales, Global Biogeochemical Cycles, 18, n/a–n/a, doi:10.1029/2003GB002148, http://dx.doi.org/10.1029/2003GB002148, gB1041, 2004.

Levin, I., Bergamaschi, P., Dörr, H., and Trapp, D.: Stable isotopic signature of methane from major sources in Germany, Chemosphere, 26, 161 – 177, doi:http://dx.doi.org/10.1016/0045-6535(93)90419-6, http://www.sciencedirect.com/science/article/pii/0045653593904196, proceedings of the {NATO} advanced research workshop, 1993.

Lin, J., Gerbig, C., Wofsy, S. C., Andrews, A. E., Daube, B. C., Davis, K. J., and Grainger, C. A.: A near-field tool for simulating the upstream influence of atmospheric observations: The Stochastic Time-Inverted Lagrangian Transport (STILT) model, Journal of Geophysical Research, 108, 17pp, doi:10.1029/2002JD003161, 2003.

Lloyd, J. and Farquhar, G. D.: ^{13}C discrimination during CO_2 assimilation by the terrestrial biosphere, Oecologia, 99, 201–215, 1994.

Lopez, M., Schmidt, M., Delmotte, M., Colomb, A., Gros, V., Janssen, C., Lehman, S. J., Mondelain, D., Perrussel, O., Ramonet, M., Xueref-Remy, I., and Bousquet, P.: CO, NO_x and $^{13}CO_2$ as tracers for fossil fuel CO_2: results from a pilot study in Paris during winter 2010, Atmospheric Chemistry and Physics, 13, 7343–7358, doi:10.5194/acp-13-7343-2013, http://www.atmos-chem-phys.net/13/7343/2013/, 2013.

Mahadevan, P., Wofsy, S. C., Matross, D. M., Xiao, X., Dunn, A. L., Lin, J. C., Gerbig, C., Munger, J. W., Chow, V. Y., and Gottlieb, E. W.: A satellite-based biosphere parameterization for net ecosystem CO_2 exchange: Vegetation Photosynthesis and Respiration Model (VPRM), Global Biogeochemical Cycles, 22, 2008.

Marland, G., Sr., R. A. P., Apps, M., Avissar, R., Betts, R. A., Davis, K. J., Frumhoff, P. C., Jackson, S. T., Joyce, L. A., Kauppi, P., Katzenberger, J., MacDicken, K. G., Neilson, R. P., Niles, J. O., dutta S. Niyogi, D., Norby, R. J., Pena, N., Sampson, N., and Xue, Y.: The climatic impacts of land surface change and carbon management, and the implications for climate-change mitigation policy, Climate Policy, 3, 149–157, doi:10.3763/cpol.2003.0318, http://www.tandfonline.com/doi/abs/10.3763/cpol.2003.0318, 2003.

McManus, J. B., Nelson, D. D., and Zahniser, M. S.: Long-term continuous sampling of $^{12}CO_2$, $^{13}CO_2$ and $^{12}C^{18}O^{16}O$ in ambient air with a quantum cascade laser spectrometer, Isotopes in Environmental and Health Studies, 46, 49–63, doi:10.1080/10256011003661326, http://dx.doi.org/10.1080/10256011003661326, pMID: 20229384, 2010.

Miller, J. B. and Tans, P. P.: Calculating isotopic fractionation from atmospheric measurements at various scales, Tellus, pp. 207–214, 2003.

Mook, W. G.: Environmental isotopes in the hydrological cycle - Principles and applications, Technical Documents in Hydrology, I, 2000.

Mook, W. G., Koopmans, M., Carter, A. F., and Keeling, C. D.: Seasonal, latitudinal, and secular variations in the abundance and isotopic ratios of atmospheric carbon dioxide: 1. Results from land stations, Journal of Geophysical Research, 88, 10 915–10 933, doi:doi:10.1029/JC088iC15p10915, 1983.

Newman, S., Xu, X., Gurney, K. R., Hsu, Y.-K., Li, K.-F., Jiang, X., Keeling, R., Feng, S., O'Keefe, D., Patarasuk, R., Wong, K. W., Rao, P., Fischer, M. L., and Yung, Y. L.: Toward consistency between bottom-up CO_2 emissions trends and top-down atmospheric measurements in the Los Angeles megacity, Atmospheric Chemistry and Physics Discussions, 15, 29 591–29 638, doi:10.5194/acpd-15-29591-2015, http://www.atmos-chem-phys-discuss.net/15/29591/2015/, 2015.

Ogée, J., Peylin, P., Cuntz, M., Bariac, T., Brunet, Y., Berbigier, P., Richard, P., and Ciais, P.: Partitioning net ecosystem carbon exchange into net assimilation and respiration with canopy-scale isotopic measurements: An error propagation analysis with $^{13}CO_2$ and $CO^{18}O$ data, Global Biogeochemical Cycles, 18, n/a–n/a, doi:10.1029/2003GB002166, http://dx.doi.org/10.1029/2003GB002166, gB2019, 2004.

Pataki, D. E.: The application and interpretation of Keeling plots in terrestrial carbon cycle research, Global Biogeochemical Cycles, 17, 1022, 2003.

Röckmann, T., Eyer, S., van der Veen, C., Popa, M. E., Tuzson, B., Monteil, G., Houweling, S., Harris, E., Brunner, D., Fischer, H., Zazzeri, G., Lowry, D., Nisbet, E. G., Brand, W. A., Necki, J. M., Emmenegger, L., and Mohn, J.: In-situ observations of the isotopic composition of methane at the Cabauw tall tower site, Atmospheric Chemistry and Physics Discussions, 2016, 1–43, doi:10.5194/acp-2016-60, http://www.atmos-chem-phys-discuss.net/acp-2016-60/, 2016.

Rödenbeck, C.: Estimating CO_2 sources and sinks from atmospheric mixing ratio measurements using a global inversion of atmospheric transport, http://www.bgc-jena.mpg.de/bgc-systems/pmwiki2/uploads/Publications/6.pdf, 2005.

Salmon, Y., Buchmann, N., and Barnard, R. L.: Response of $\delta^{13}C$ in plant and soil respiration to a water pulse, Biogeosciences Discussions, 8, 4493–4527, doi:10.5194/bgd-8-4493-2011, http://www.biogeosciences-discuss.net/8/4493/2011/, 2011.

Schumacher, M., Werner, R. a., Meijer, H. a. J., Jansen, H. G., Brand, W. a., Geilmann, H., and Neubert, R. E. M.: Oxygen isotopic signature of CO_2 from combustion processes, Atmospheric Chemistry and Physics, 11, 1473–1490, doi:10.5194/acp-11-1473-2011, http://www.atmos-chem-phys.net/11/1473/2011/, 2011.

Still, C. J., Berry, J. A., Collatz, G. J., and DeFries, R. S.: Global distribution of C3 and C4 vegetation: Carbon cycle implications, Global Biogeochemical Cycles, 17, 1–14, doi:10.1029/2001GB001807, http://dx.doi.org/10.1029/2001GB001807, 1006, 2003.

Torn, M. S., Biraud, S. C., Still, C. J., Riley, W. J., and Berry, J. A.: Seasonal and interannual variability in ^{13}C composition of ecosystem carbon fluxes in the U.S. Southern Great Plains, Tellus B, 63, 181–195, doi:10.1111/j.1600-0889.2010.00519.x, http://dx.doi.org/10.1111/j.1600-0889.2010.00519.x, 2011.

Biogeosciences Discuss., doi:10.5194/bg-2016-93, 2016
Manuscript under review for journal Biogeosciences
Published: 16 March 2016

Tuzson, B., Zeeman, M., Zahniser, M., and Emmenegger, L.: Quantum cascade laser based spectrometer for in situ stable carbon dioxide isotope measurements, Infrared Physics and Technology, 51, 198–206, doi:http://dx.doi.org/10.1016/j.infrared.2007.05.006, http://www.sciencedirect.com/science/article/pii/S135044950700059X, 2008.

Vardag, S. N., Hammer, S., O'Doherty, S., Spain, T. G., Wastine, B., Jordan, A., and Levin, I.: Comparisons of continuous atmospheric CH_4, CO_2 and N_2O measurements – results from a travelling instrument campaign at Mace Head, Atmospheric Chemistry and Physics, 14, 8403–8418, doi:10.5194/acp-14-8403-2014, http://www.atmos-chem-phys.net/14/8403/2014/, 2014.

Vardag, S. N., Hammer, S., Sabasch, M., Griffith, D. W. T., and Levin, I.: First continuous measurements of $\delta^{18}O-CO_2$ in air with a Fourier transform infrared spectrometer, Atmospheric Measurement Techniques, 8, 579–592, doi:10.5194/amt-8-579-2015, http://www.atmos-meas-tech.net/8/579/2015/, 2015a.

Vardag, S. N., Gerbig, C., Janssens-Maenhout, G., and Levin, I.: Estimation of continuous anthropogenic CO_2: model-based evaluation of CO_2, CO, $\delta^{13}C(CO_2)$ and $\Delta^{14}C(CO_2)$ tracer methods, Atmospheric Chemistry and Physics, 15, 12 705–12 729, doi:10.5194/acp-15-12705-2015, http://www.atmos-chem-phys.net/15/12705/2015/, 2015b.

Vogel, F. R., Hammer, S., Steinhof, A., Kromer, B., and Levin, I.: Implication of weekly and diurnal ^{14}C calibration on hourly estimates of CO-based fossil fuel CO_2 at a moderately polluted site in southwestern Germany, Tellus B, 62, 512–520, doi:10.1111/j.1600-0889.2010.00477.x, http://doi.wiley.com/10.1111/j.1600-0889.2010.00477.x, 2010.

Vogel, F. R., Huang, L., Ernst, D., Giroux, L., Racki, S., and Worthy, D.: Evaluation of a cavity ring-down spectrometer for in situ observations of $^{13}CO_2$, Atmospheric Measurement Techniques, 6, 301–308, 2013.

White, J., Vaughn, B., and Michel, S.: Stable Isotopic Composition of Atmospheric Carbon Dioxide (^{13}C and ^{18}O) from the NOAA ESRL Carbon Cycle Cooperative Global Air Sampling Network, 1990-2014, ftp://aftp.cmdl.noaa.gov/data/trace_gases/co2c13/flask/, 2015.

Widory, D., Proust, E., Bellenfant, G., and Bour, O.: Assessing methane oxidation under landfill covers and its contribution to the above atmospheric CO_2 levels: The added value of the isotope ($\delta^{13}C$- and $\delta^{18}O$-CO_2; $\delta^{13}C$- and δD-CH_4) approach, Waste management, 32, 1685–1692, 2012.

Zobitz, J., Keener, J., Schnyder, H., and Bowling, D.: Sensitivity analysis and quantification of uncertainty for isotopic mixing relationships in carbon cycle research, Esevier-Agricultural and Forest Meteorology, 136, 2006.

Biogeosciences Discuss., doi:10.5194/bg-2016-93, 2016
Manuscript under review for journal Biogeosciences
Published: 16 March 2016

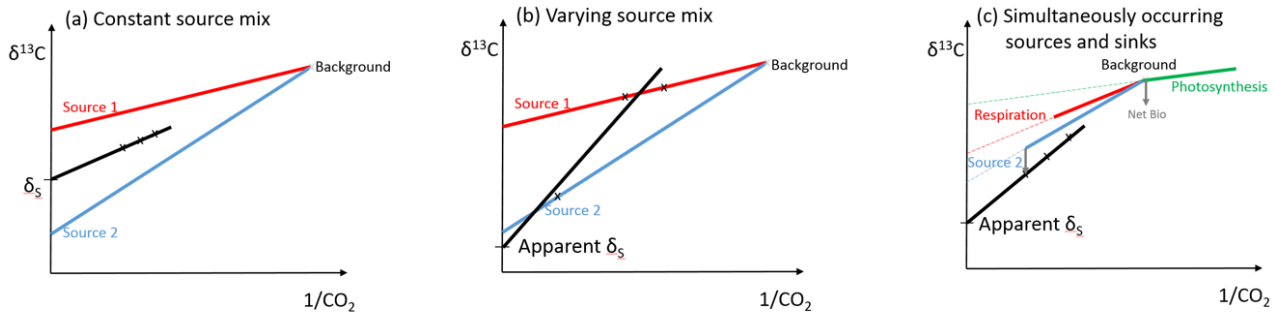

Figure 1. Regression-based determination of source signature using a Keeling plot. For clarity of illustration, we only draw three data points instead of five, which we use for our computation. a) Constant source mix during the time of source signature determination leads to the correct isotopic signature, δ_S. b) Change of source mix during the period of determination of a Keeling plot due to either a temporal change of emission characteristics or a wind direction change leads to a biased result. These situations can be usually identified by a large error of the intercept, δ_S (we choose an error >2 ‰ to reject these results) c) Sources and sinks with different isotopic signatures or sink fractionation occur at the same time and lead to a wrong apparent source signature. Strong biases are prevented by choosing a minimum net CO_2 concentration range of 5 ppm and demanding a monotonous increase of CO_2 during the five hours (see text for more details). Note that the background value is displayed for illustration, but it is not used in the running Keeling plot approach.

Biogeosciences Discuss., doi:10.5194/bg-2016-93, 2016
Manuscript under review for journal Biogeosciences
Published: 16 March 2016

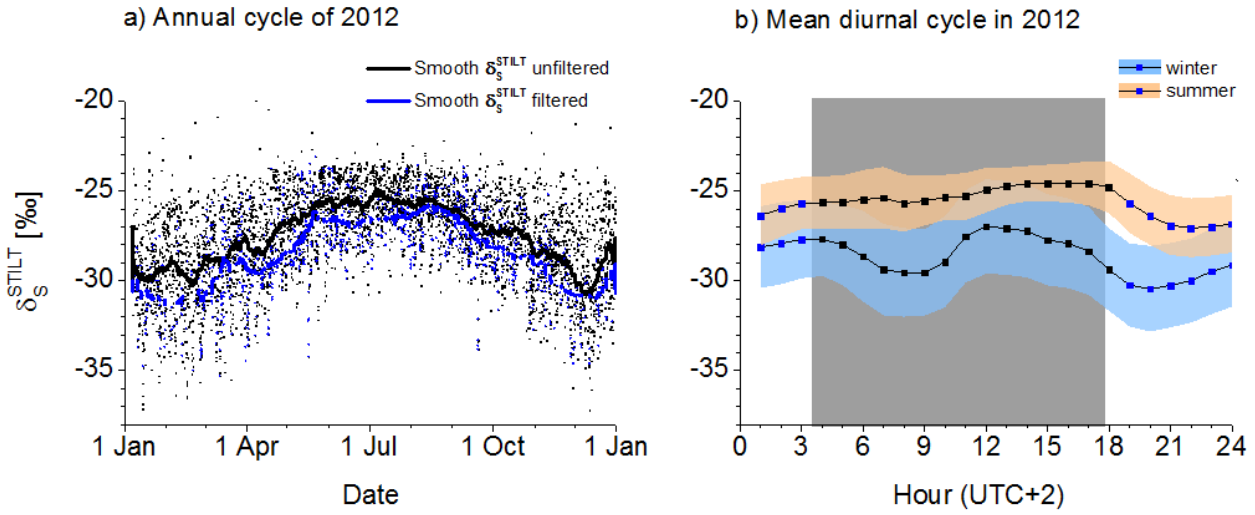

Figure 2. Source signature as calculated with the STILT model following equation A1. a) Unfiltered in black and filtered (for monotonous increase and minimal range) in blue. Only about 15% of all data points fulfill our strict criteria. However, they are distributed approximately evenly throughout the year. b) Diurnal cycle of modeled mean source signature due to diurnally varying mean source mix. Gray areas denote times when source signature is usually filtered out.

Biogeosciences Discuss., doi:10.5194/bg-2016-93, 2016
Manuscript under review for journal Biogeosciences
Published: 16 March 2016

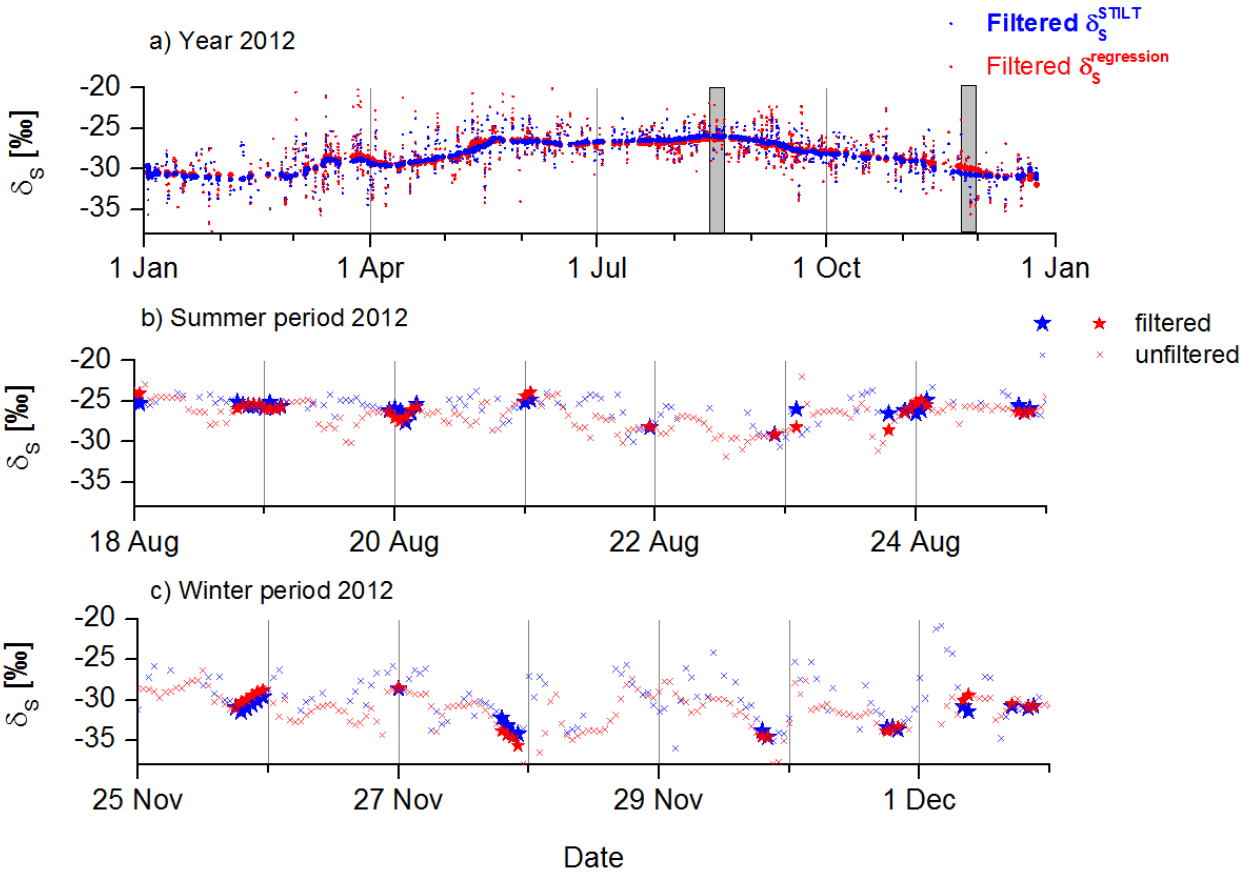

Figure 3. Comparison between modeled reference source signature (blue) and the running Keeling intercept (red), which is regression-based using the modeled CO_2 and $\delta^{13}C(CO_2)$ records. a) Long term comparison for the year 2012. The smoothed lines of window size 100 are also shown in the respective colors. b) Summer excerpt and c) winter excerpt (grey areas in a) of both reference and regression-based source signature. The crosses denote unfiltered data and bold stars denote filtered data.

Biogeosciences Discuss., doi:10.5194/bg-2016-93, 2016
Manuscript under review for journal Biogeosciences
Published: 16 March 2016

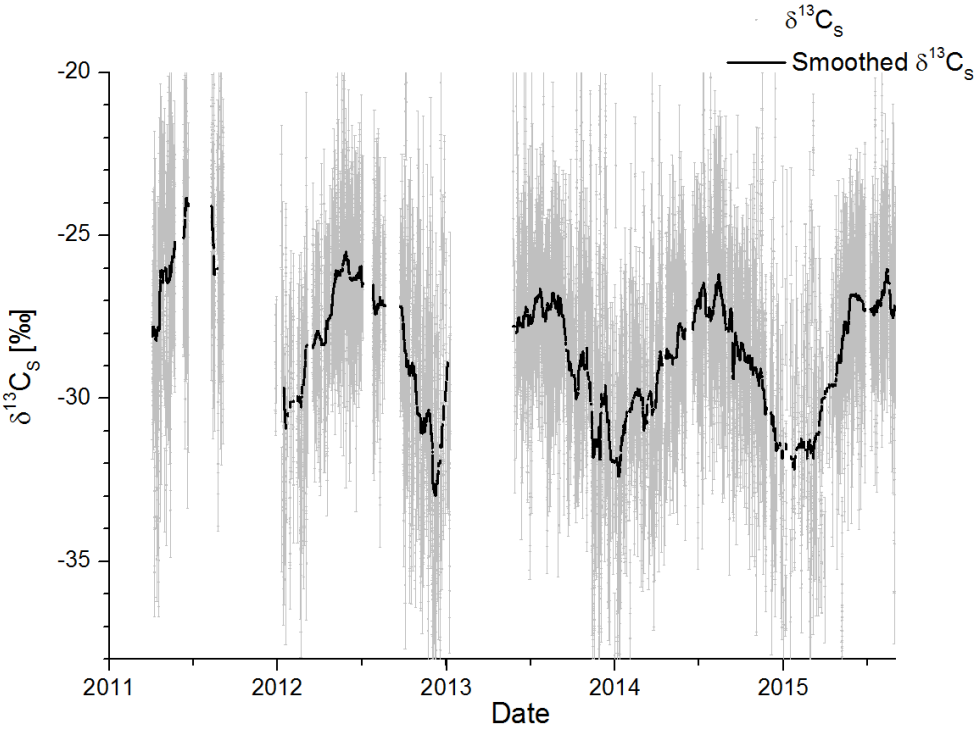

Figure 4. Running Keeling approach-based source signature in Heidelberg from 2011 until mid of 2015. The black line is the smoothed running Keeling signature (50%-percentile filter with window size=100 hours). Half a window size before the beginning of a large data gap the data is not further smoothed to prevent smoothing artifacts.

Biogeosciences Discuss., doi:10.5194/bg-2016-93, 2016
Manuscript under review for journal Biogeosciences
Published: 16 March 2016

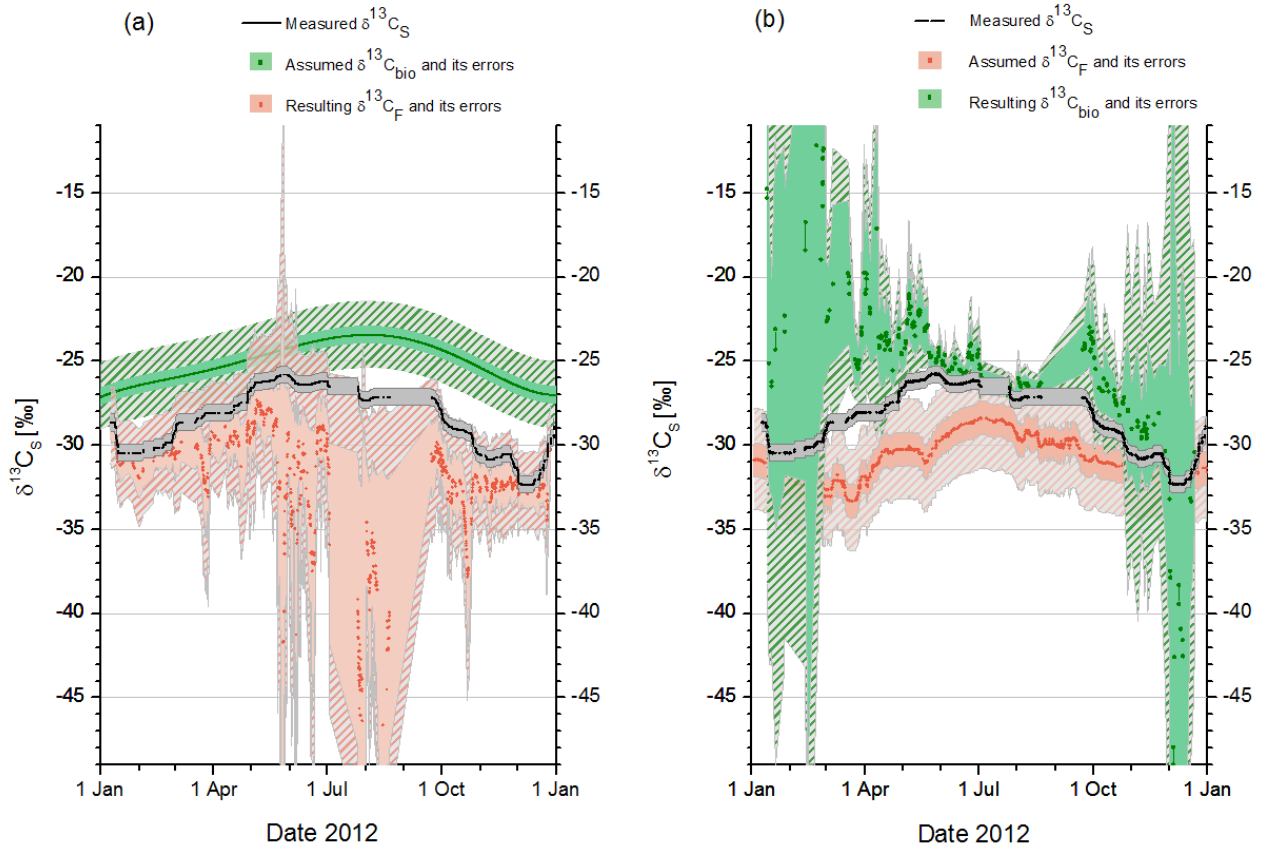

Figure 5. a) A fixed isotopic end member of the biosphere (green, ± uncertainty of 0.5 ‰ (light green area) and 2 ‰ (crosshatched green)) together with the measured source signature (black) results in δ_F (red, ± its uncertainty). b) A fixed isotopic end member of the fuel mix (red, ± uncertainty of 1 ‰ (salmon pink) and 2 ‰ (crosshatched gray-pink)) together with the measured source signature (black) results in δ_{bio} (green, ± its uncertainty). In both cases, also the fuel CO_2 share (or biospheric CO_2 share) is required. We here use the share calculated with STILT on the basis of EDGAR v4.3 and assume an absolute uncertainty of 10%.

Biogeosciences Discuss., doi:10.5194/bg-2016-93, 2016
Manuscript under review for journal Biogeosciences
Published: 16 March 2016

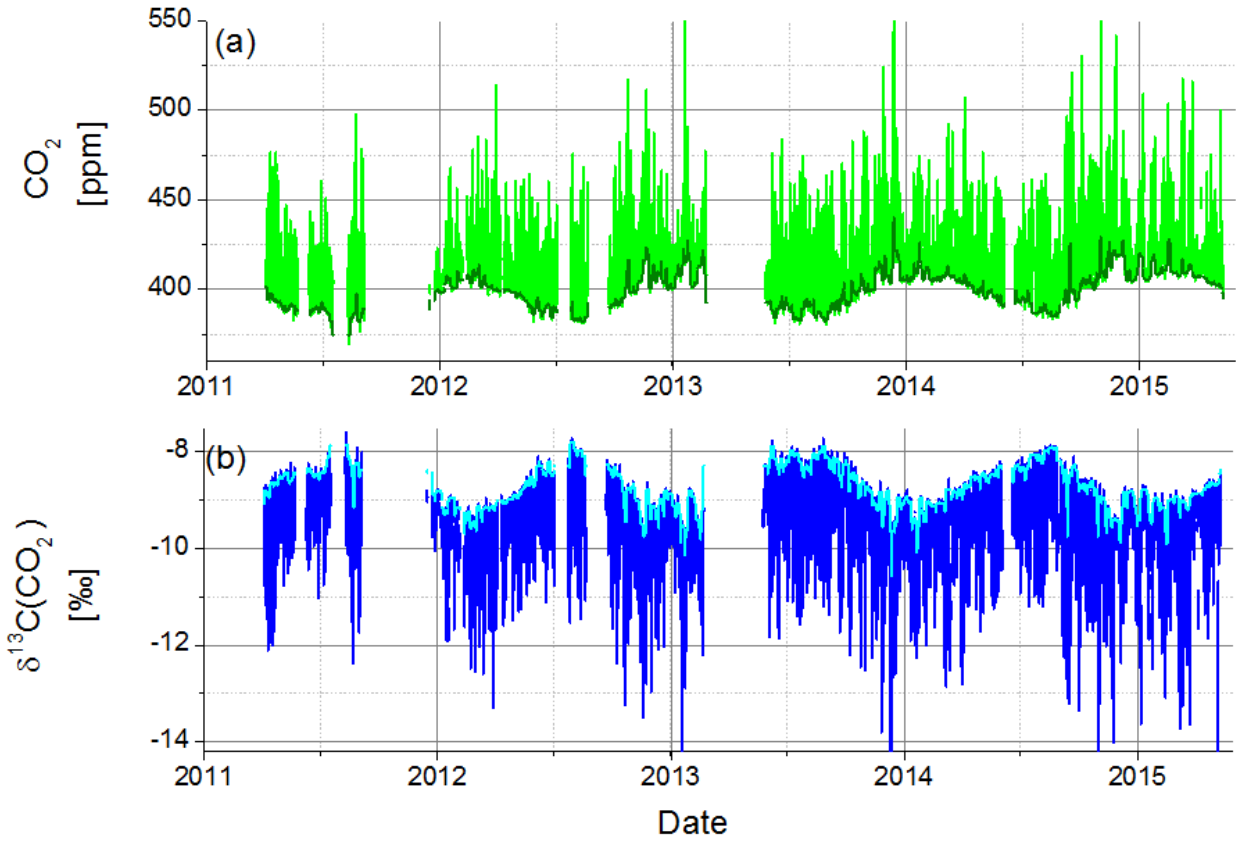

Figure B1. Continuous Heidelberg hourly FTIR record of (a) CO_2 and (b) $\delta^{13}C(CO_2)$ from April 2011- June 2015. Data gaps occur when the instrument was away during a measurement campaign or when instrumental problems occurred. The lower (and upper) 5% envelope is drawn for CO_2 and $\delta^{13}C(CO_2)$ in dark green and light blue, respectively.

Biogeosciences Discuss., doi:10.5194/bg-2016-93, 2016
Manuscript under review for journal Biogeosciences
Published: 16 March 2016

Table 1. $\delta^{13}C(CO_2)$ source signature of fuel types and biosphere as used in the model and the range of literature values. Note, that for a specified region, the range of possible isotopic signature can often be narrowed down, if the origin and/or production process of the fuel type is known.

Emission source	Used $\delta_{F,i}$ or δ_{bio} [‰]	Range of literature values $\delta_{F,i}$ or δ_{bio} [‰]	Reference
Fuel types			
Coal		-23 to -27	Mook, 2000
- Hard Coal	-25		
- Brown coal	-27		
Peat	-28	-22 to -29	Mook, 2000; Schumacher et al., 2011
Oil	-29	-19 to -35	Andres et al., 1994; Mook, 2000; Schumacher et al., 2011
Gas			
-Natural gas	-46	-20 to -100	Andres et al., 1994
-Derived gas	-28	-26 to -29	Bush et al., 2007
Solid waste	-28	-20 to -30	typical range of C3 and C4 plant mixes (Mook, 2000)
Solid biomass	-27	-20 to -30	typical range of C3 and C4 plant mixes (Mook, 2000)
Bio liquid	-29	-20 to -30	typical range of C3 and C4 plant mixes (Mook, 2000)
Biogas	-11	0 to -16	Widory et al., 2012; Levin et al., 1993
Biosphere		-20 to -30	Lloyd and Farquhar, 1994; Mook, 2000
Photosynthesis	-23	-20 to -30	typical range of C3 and C4 plant mixes Mook, 2000
Respiration	-25	-20 to -30	typical range of C3 and C4 plant mixes (Mook, 2000)

Part 3

Discussion

Anthropogenic emissions of greenhouse gases are mainly responsible for the global mean temperature increase since 1880 driving climate change (IPCC, 2014a). Understanding the relevant processes of ecosystems is vital to project how ecosystems will respond to changes in elevated CO_2 levels, drought, heat etc.. Further, initiation and validation of emission mitigation strategies require a quantification of anthropogenic greenhouse gas emissions.

In order to study these greenhouse gas fluxes, high quality greenhouse gas measurements are required. If the greenhouse gas measurements are sufficiently accurate and precise and if different data sets of greenhouse gases from a measurement network are compatible to each other, the joint data can be used to obtain a regional estimate of total net greenhouse gas fluxes. Further, a separation of total greenhouse gas fluxes into net ecosystem fluxes from different reservoirs such as from fossil fuel CO_2 and biospheric CO_2 is vital to study ecosystem fluxes and anthropogenic emissions independently from each other. Finally, for a comprehensive understanding of ecosystem processes, it is essential to separate between gross fluxes such as photosynthesis and respiration as these two opposed fluxes may respond differently to climatic changes.

In this discussion, the contributions of this thesis to improving the European greenhouse gas measurement network are listed and elaborated and limitations and further steps for an improvement of regional flux estimates are pointed out.

I) Providing a long-term greenhouse gas record

Within this work, an accurate and precise greenhouse gas data set has been generated for Heidelberg spanning a time range from April 2011 up to now. For this purpose, it was necessary to optimize the FTIR measurement technique and further develop a robust correction and calibration procedure. The data is partly presented in the publications and the CO_2 and $\delta^{13}C(CO_2)$ record is freely available at: `http://www.iup.uni-heidelberg.de/institut/forschung/groups/kk/Data_html`. It is also displayed in the appendix A together with its accuracy, compatibility and intermediate measurement precision. The precision and stability of the measurements are such that the WMO recommendations can be met for CO_2, CH_4, N_2O and CO. The entire data set can now be used in top-down approaches to calculate greenhouse gas fluxes in the catchment area of Heidelberg for the years 2011 to 2016. It is desirable to

continue the long-term measurements in the future so that changes in regional emission patterns can be detected.

II) Comparing greenhouse gas measurements to assess current compatibility

During a "travelling instrument" campaign from March to May 2013 to the AGAGE and WMO Global Atmosphere Watch (GAW) station Mace Head, Ireland, the Heidelberg FTIR (see appendix A) continuously measured CO_2, CH_4 and N_2O (on the WMO CO_2 X2007 scale, the WMO CH_4 X2004 scale and the WMO N_2O X2006a scale, respectively) in parallel to the station instrumentation (Sect. 2.1). At Mace Head, a GC-MultiDetector (GC-MD) system routinely measures CH_4 and N_2O. The GC-MD performs measurements every 20 minutes, which are on the Tohoku University scale for CH_4 and on the SIO-1998 scale for N_2O. A cavity ring-down spectrometry (CRDS) system continuously measures CO_2 and CH_4 (WMO CO_2 X2007 scale and WMO CH_4 X2004 scale, respectively). During the measurement campaign it was possible to identify the magnitude of differences for CO_2, CH_4 and N_2O measurements between these different instruments and narrow down the origin of the differences. The differences are summarized and evaluated here point by point.

CO_2

For CO_2, the mean differences between the CRDS and the travelling campaign instrument (TCI) is (0.14 ± 0.04) ppb (mean ± standard deviation), which is not seen in cross-cylinder measurements. This highlights the importance of the travelling instrument approach, which compares measurements of different instruments under routine ambient air measurement protocol, thus including a check of the ambient air sample intake line. The reason for the difference cannot be resolved uniquely, but may originate from the water correction of the CRDS instrument. Similar differences in CO_2 (but of opposite sign) have been observed during travelling instrument campaigns by Hammer et al. (2013b). It seems that, unfortunately, the WMO ILC targets for CO_2 are often not met for measurements from different laboratories. Pinning down the reason for the discrepancies and maintaining a good stability will be important to meet the WMO recommendation in the future and to improve the quality of the data.

CH_4

For CH_4, meeting the WMO ILC targets is less challenging because the signal to noise ratio is large. All instruments (CRDS, GC and FTIR) meet the WMO ILC targets. The travelling instrument campaign therefore confirms that already today CH_4 measurements from different networks can be merged and used in inverse model approaches (e.g. Bergamaschi et al., 2010).

N_2O

For N_2O, the mean difference between ambient air measurements of the station instrumentation (GC) and of the TCI is (0.37 $\pm$ 0.22) ppb. This difference is a considerable fraction of the continental N_2O gradient, which is typically about 0.5 ppb. Cylinder as well as ambient air comparisons show the same difference suggesting that the difference originates from a calibration offset. Assessing the magnitude of possible calibration transfer uncertainties (ca. $\pm$ 0.15 ppb) and including results of flask comparisons between both networks (pers. communication, P. Krummel, 2013) into consideration, it appears that the difference can be partly (0.1 to 0.4 ppb) attributed to a discrepancy between calibration scales of the WMO X2006a and the SIO-1998 scale. It is possible that the scale difference is due to a non-linearity of the Electron Capture Detectors (ECD) of the GCs, as both networks derive their N_2O scales from ECD measurements (pers. communication, B. Hall, 2016). Furthermore, the difference may partly be due to specific errors of the station instrumentation (e.g. non-linearity effects), which could not be investigated in the scope of the TCI campaign. Thompson et al. (2014) stated that for N_2O it is valuable to introduce prior values for calibration offsets into inverse models as large biases will distort resulting N_2O fluxes, if not taken into account. Therefore, the estimated calibration scale bias and its uncertainty found in this work (Sect. 2.1) can now be used in top-down approaches for an improvement of N_2O surface fluxes of recent years.

Limiting factors of studying the greenhouse gas cycle

In the first publication (Sect. 2.1), it was shown that the precision of CO_2 and CH_4 measurements of the new optical instruments is already sufficient to detect small vertical gradients and thus, to detect small greenhouse gas fluxes. However, problems

with the accuracy and compatibility within and across measurement networks need to be overcome for CO_2 to effectively use the greenhouse gas measurements from different stations in top-down approaches. At present, the lacking compatibility between different instruments still limits the benefit of a joint data set.

Recommendation for future repetition of travelling instrument campaigns

Especially now, as many new optical instruments are emerging and can contribute to a much denser network of continuous greenhouse gas measurements, systematic problems of instruments (e.g. water corrections) need to be detected and analyzed. As contamination, drifts in calibration cylinders and hardware problems can occur slowly or suddenly and are thus time-dependent, it is important to perform routine quality control checks. Comprehensive comparison campaigns are therefore advisable on a regular basis in the future and were explicitly demanded in Vardag et al. (2014) (first publication, Sect. 2.1). Following the travelling instrument campaigns by Hammer et al. (2013b) and Vardag et al. (2014), the importance of the travelling instrument campaigns has been recently recognized by the ICOS community (ICOS, 2015). It was decided that for every ICOS station, one dedicated sampling intake line must be installed for the TCI for occasional station visits. It was further recognized that the travelling instrument approach is the only approach able to pinpoint individual problems. The routine implementation of the travelling instrument approach into the quality control of the ICOS measurement network is therefore a huge success of this work and will contribute to a homogenized data set for Europe.

III) Establishing $\delta^{18}O(CO_2)$ measurements with the FTIR

Technical implementation

$\delta^{18}O(CO_2)$ measurements were implemented in the FTIR analysis and the compatibility with isotope ratio mass spectrometry (IRMS) as well as the precision of these measurements were assessed. The technical feasibility of measuring this tracer is remarkable as the abundance of $^{18}O(CO_2)$ is small and its absorption band overlaps with that of $^{12}C(CO_2)$. It was shown that an analysis is feasible with a precision of about 0.3 ‰ and compatible to the Heidelberg IRMS if large cross-sensitivity effects

are corrected. Even though the precision does not meet the WMO ILC recommendations, it is sufficient to detect $\delta^{18}O(CO_2)$ signals in ambient CO_2 in Heidelberg and to qualitatively attribute these signals to different exchange processes.

As the FTIR spectra are routinely stored, it is now possible to derive the $\delta^{18}O(CO_2)$ signal from the stored spectra in retrospective. Therefore, also the $\delta^{18}O(CO_2)$ measurements from other FTIR instruments could be analyzed retrospectively to obtain long-term continuous $\delta^{18}O(CO_2)$ data sets at many stations. This is, however, only true if the calibration gases span the atmospheric $\delta^{18}O(CO_2)$ signal and if cross-sensitivities have been determined.

Interpretation of the $\delta^{18}O(CO_2)$ record

The unique property of $\delta^{18}O(CO_2)$ to distinguish between photosynthesis and respiration opens the door to studying regional gross fluxes of CO_2. This is fundamental to understand how photosynthesis and respiration fluxes may respond to future environmental changes (e.g. global warming, droughts or elevated CO_2 levels) (Ciais et al., 2005). In this work, it was demonstrated that strong variations of local $\delta^{18}O(CO_2)$ occur and can be interpreted as changes in the isotopic value of soil water or as anthropogenic signals. In a case study, a qualitative understanding of dominant processes could already be obtained (Sect. 2.2, Vardag et al., 2015a). However, to quantify CO_2 fluxes using atmospheric $\delta^{18}O(CO_2)$ measurements, the $\delta^{18}O(CO_2)$ values of soil and plant fluxes and of anthropogenic CO_2 fluxes must be determined accurately. As the $\delta^{18}O(CO_2)$ values of photosynthesis and respiration are strongly coupled to the water cycle, they can vary on time scales of hours. Therefore, the isotopic composition of precipitation and water vapor needs to be measured as well, also on high temporal resolution. Furthermore, processes such as evapotranspiration and soil invasion influence the atmospheric $\delta^{18}O(CO_2)$ signal and their effect on the $\delta^{18}O(CO_2)$ signal must be estimated to quantify CO_2 gross fluxes correctly from the atmospheric $\delta^{18}O(CO_2)$ record.

Therefore, in order to quantitatively separate net ecosystem fluxes into gross fluxes using atmospheric $\delta^{18}O(CO_2)$, a coupled water-carbon model (Langendörfer et al., 2002) is required, which is fed with explicit boundary conditions such as $\delta^{18}O$ values of precipitation and water vapor, relative humidity, radiation and temperature (Langendörfer et al., 2002; Riley, 2013).

Future perspective of $\delta^{18}O(CO_2)$ measurements

As $\delta^{18}O(CO_2)$ is a unique tracer for biospheric gross fluxes, in the future, the interpretation of the $\delta^{18}O(CO_2)$ signal will remain desirable for the ecosystem community despite its complex behavior. In order to determine the isotopic end members of the water cycle, continuous water isotopologue measurements are currently being built up at the Institute of Environmental Physics in Heidelberg and will soon be complementing atmospheric $\delta^{18}O(CO_2)$, $\delta^{13}C(CO_2)$ and CO_2 measurements, paving the way for successfully implementing a local H_2O-CO_2 model as e.g. described by Langendörfer et al. (2002), Riley et al. (2003) or Riley (2013).

IV) Separating fuel and biogenic CO_2

In order to study ecosystem fluxes, oceanic fluxes and fuel emissions independently of each other, it is necessary to separate between these contributions. Measurements of tracers such as $\delta^{13}C(CO_2)$ offer the prospect of separating between different CO_2 source components. For example, at continental stations, $\delta^{13}C(CO_2)$ could be used to separate between biogenic and fuel contributions (see Sect. 1.5.5 and 2.3) due to the different isotopic signatures of fuels and the biosphere. The continuous measurement of $\delta^{13}C(CO_2)$ is still rather novel, but many continuously measuring $\delta^{13}C(CO_2)$ instruments have been installed globally in the last decade as new optical instruments have been emerging (e.g. Esler et al., 2000; Wahl et al., 2006; Tuzson et al., 2011; Hammer et al., 2013a; Vogel et al., 2013; Griffis, 2013). This opens the door to a separation of fuel and biogenic CO_2 on a continuous basis, which is needed to understand biospheric processes on sub-diurnal scales and to study the emissions of different time-dependent catchment areas. However, the actual benefit of the continuous isotope measurements for understanding the ecosystem and monitoring anthropogenic fuel emissions has not been quantitatively evaluated yet.

In this work an equation for continuous fuel CO_2 estimates based on $^{13}C(CO_2)$ and CO_2 is formulated. This so-called "$\delta^{13}C(CO_2)$ method" can be used to continuously separate biogenic CO_2 from fuel CO_2. There are alternative approaches to estimate fuel CO_2 continuously, such as continuous measurements of CO (together with CO_2), CO_2 alone or hypothetical continuous $^{14}C(CO_2)$ measurements (together with CO_2) if the latter become available in the future. All of them exhibit their own advantages and

disadvantages. In the third publication (Sect. 2.3, Vardag et al., 2015b), the different tracers are introduced and compared in a model setting. The STILT model (Sect. 1.6.1) is used to generate a "pseudo-data set" of all tracer records as well as of fuel CO_2 for three different measurement sites. The great advantage of using a model is that, in the model, the fuel CO_2 is already known. Therefore, when the modeled tracer records are used to estimate fuel CO_2, the resulting fuel CO_2 can be compared with the known reference model fuel CO_2. A quantification of the accuracy and precision of the tracer-based estimations of fuel CO_2 is therefore possible. Here, the findings of the third publication (the advantages, shortcomings and future perspectives of the different tracer methods) are summarized to support the decision which tracer to establish at which station within a measurement network.

$\delta^{13}C(CO_2)$ and CO method

At the moment, $\delta^{13}C(CO_2)$ and CO are the most promising tracers to estimate fuel CO_2 continuously. The **precision** of fuel CO_2 when using the $\delta^{13}C(CO_2)$ and CO method is about 3-4 ppm, which in the Heidelberg model setting corresponds to an uncertainty of about 25 %. While the CO method is mainly limited by the variation of natural CO fluxes, $\delta^{13}C(CO_2)$ is, to a large degree, limited by the measurement precision of $\delta^{13}C(CO_2)$ and CO_2. The technical development of more precise $\delta^{13}C(CO_2)$ measurements will therefore lead to an improvement of the precision of the $\delta^{13}C(CO_2)$ method by up to 2-3 ppm. This is very encouraging as the optical instruments are developing quickly and are expected to further improve their precision in near future, meliorating the precision of the $\delta^{13}C(CO_2)$ method and advocating an implementation of routine continuous $\delta^{13}C(CO_2)$ measurements.

Further, the **accuracy** of the fuel CO_2 estimate is assessed. $\delta^{13}C(CO_2)$ and CO can both accurately estimate fuel CO_2 continuously, but only if the main sources and sinks are well characterized with respect to the isotopic signature δ_F and the CO/CO_2 ratio of fuel emissions, respectively. A determination of δ_F and CO/CO_2 ratio requires either extensive source sampling campaigns in the catchment area of the measurement site, or a calibration using precise $^{14}C(CO_2)$ samples from Accelerator Mass Spectrometry (AMS) measurements or conventional counting.

At present, it is recommended within the ICOS community to take integrated ^{14}C samples. This work (Sect. 2.3) reveals that when using (e.g. monthly) integrated $^{14}C(CO_2)$

samples to analytically calibrate δ_F and the CO/CO_2 ratio of fuel emissions, directional biases are introduced into the fuel CO_2 estimate. An alternative approach is to take grab samples for calibration. In this case, errors are introduced due to the non-representativeness of selected grab samples. These errors are bidirectional, which is preferable over systematic biases, and decrease with number of available $^{14}C(CO_2)$ grab samples. It is shown that even though δ_F and CO/CO_2 ratio of fuel emissions change over the course of one year, it is best to calibrate an annual mean value for δ_F and CO/CO_2 ratio of fuel emissions using all $^{14}C(CO_2)$ grab samples taken in that year to increase the number of grab samples per calibration. When calibrating the annual mean value of δ_F and CO/CO_2 using 24 grab samples, the mean error will be about $\pm$ 1.3 ppm of fuel CO_2 at an urban site such as Heidelberg. It is demonstrated that it is advisable to take (as many as possible) grab samples in addition to the within ICOS recommended integrated samples of ^{14}C for a comprehensive estimate of fuel CO_2 contribution.

Jointly using CO and $\delta^{13}C(CO_2)$ as tracers does not improve the fuel CO_2 estimate as the different emission sectors do not complement each other well in the European model setting. This is an important finding as either one of the tracer measurements are therefore encouraged in European networks.

$^{14}C(CO_2)$ method

Continuous $\Delta^{14}C(CO_2)$ measurements are presently not technically feasible. However, there are some efforts to actually establish such measurements with reduced precision compared to that of AMS measurements or conventional counting (McIntyre et al., 2013). Hypothetical future continuous $\Delta^{14}C(CO_2)$ measurements with reduced precision of 5 ‰ are found to be a good continuous tracer for fuel CO_2 and would be even more precise than CO or $\delta^{13}C(CO_2)$. Thus, it is advisable to invest in these continuous measurements for the future. However, one should remark that $\Delta^{14}C(CO_2)$ measurements bare an important disadvantage as they cannot detect any biofuel contribution. Biofuel CO_2 contributions are therefore attributed to biospheric contributions, which hinder a study of the biospheric fluxes and feedbacks, especially in the future, as biofuel contributions are expected to increase.

CO_2 only method

Turnbull et al. (2015) suggested that one could use CO_2 alone to estimate fuel CO_2 at urban sites in the winter time, if a local background directly upwind of urban areas is used. However, this work shows that the biospheric contribution to the total CO_2 offset is generally still too large, even at polluted sites during winter, to neglect it. Only in selected situations CO_2 only will contain hardly any biogenic CO_2. Therefore, CO_2 should not be used to estimate fuel CO_2, at least not in Europe.

Fuel CO_2 at rural areas

One very important conclusion of this work is that a continuous estimate of fuel CO_2 is not feasible at rural sites no matter which tracer is used. This conclusion follows from the finding that the tracers for fuel CO_2 yield a typical uncertainty of about 3-4 ppm at rural, urban and polluted sites at the most. At rural sites, this is more than 100% of the mean signal. Therefore, it would be better to actually use emission inventories (with typical uncertainties of about 70%) for separation of fuel CO_2 and biogenic CO_2 at rural sites instead of a fuel CO_2 tracer. This finding is especially relevant for network designs. Within the ICOS network, measurement sites are located preferentially far away ($\geq$ 40 km) from strong anthropogenic sources so that ecosystem processes can be studied in an undisturbed way. Polluted sites are not part of the ICOS network at all. In the ICOS network, measurement sites are further separated into class 1 and class 2 sites according to the set of parameters measured. Class 2 sites measure CO_2 and CH_4 and class 1 sites additionally measure CO continuously, N_2O, SF_6, H_2, $\delta^{18}O(CO_2)$ and $\delta^{13}C(CO_2)$ periodically and integrated $\Delta^{14}C(CO_2)$. The findings within this work suggest that continuous measurements of $\delta^{13}C(CO_2)$ and CO do not provide additional information on anthropogenic emissions at clean reference air sites due to the low signal to noise ratio and should rather be conducted at more polluted measurement stations as the fuel CO_2 signals are larger there. At urban or polluted sites the contribution of fuel CO_2 can be determined with a much higher relative precision. Consequently, emission inventories can be better validated or constraint at more polluted sites. In turn, this will be also advantageous for studying ecosystem fluxes as the fuel CO_2 can be better separated from biospheric CO_2. An extension of the ICOS network to urban sites and the additional measurements of $\delta^{13}C(CO_2)$ and $\Delta^{14}C(CO_2)$ at the more polluted stations is therefore recommended.

Transferring the results to other regions and networks

In this work, the best tracer configuration in a network such as in ICOS research infrastructure were investigated. Therefore, the study is based on three representative stations for the European ICOS network, one rural, one urban and one polluted. Worldwide there are large areas without atmospheric measurements stations. Especially in South America, Africa and over Siberia the measurement network is very sparse. In the future, hopefully new measurement networks will be designed also in these regions so that fluxes can be studied there as well. Even though the results presented in the third publication (Sect. 2.3) may be a good indicator of which tracers to consider and which calibration strategies to apply to the tracer methods, the tracers will perform slightly different in different catchment areas. For example, in North America, CO_2 emissions are accompanied by much more CO emissions meliorating the CO-based method. On the other hand, in e.g. Russia, natural gas is very depleted in $\delta^{13}C(CO_2)$, which meliorates the $\delta^{13}C(CO_2)$-based method. An individual preceding analysis of the emission characteristics in the catchment area is therefore important to find the best tracer method for each setting. Therefore, it is advisable to perform a pseudo-data experiment, which was introduced in this work, as preceding analysis before designing atmospheric measurement networks on-site.

V) Determining the source signature routinely in Heidelberg

Concurrent $\delta^{13}C(CO_2)$ and CO_2 records can be used to determine the isotopic source signature of the mean source mix in the catchment area of the measurement site. In the last decade, many continuous measurements of $\delta^{13}C(CO_2)$ and CO_2 have been emerging, offering the prospect of actually studying the CO_2 contributions and their isotopic signature on high temporal resolution in the catchment area of the measurement sites.

As the mean source signature is frequently computed without checking the underlying assumptions and thus, introducing biases in the resulting mean source signature, a routine way of determining the source signature bias-free from continuous $\delta^{13}C(CO_2)$ and CO_2 was developed (Sect. 2.4). It was shown that with the so-called "running Keeling" approach, it is possible to routinely estimate the $\delta^{13}C(CO_2)$ source signature correctly within (0.2 ± 1.2) ‰ (median and inter-quartile range) on hourly basis. The smoothed long-term trend can be estimated within (0.0 ± 0.4) ‰. This is sufficient

to detect long-term changes and mean diurnal and seasonal variations of the source signature at rural as well as urban areas and opens the door to studying emission patterns on all time scales.

When applying the running Keeling approach to the Heidelberg data set of CO_2 and $\delta^{13}C(CO_2)$, the source signature shows a distinct seasonal cycle with more depleted values (-32 ‰) in winter and more enriched values (-26 ‰) in summer as one would expect from a higher share of more depleted fuel CO_2 in winter. However, the origin of the seasonal cycle cannot be uniquely identified if the isotopic end members δ_{bio} and δ_F are not known. From the source signature record itself, it is possible to estimate the isotopic end member δ_F in winter (when the biospheric CO_2 contribution is small) within an uncertainty of ± 2.5 ‰ and the isotopic end member δ_{bio} in summer (when the fuel CO_2 contribution is small) within an uncertainty of ± 1 ‰. But, as the isotopic end members are likely to change throughout one year, the fuel CO_2 share cannot be determined from the mean source signature record only. Even though no determination of the isotopic end members is possible throughout the year from the mean source signature record, it was possible to falsify the reference value of δ_{bio} in the summer time.

Finally, one can conclude that the source signature itself may provide a qualitative understanding of the magnitude of different CO_2 contributions, but will not provide a quantitative estimate unless accompanied with $\Delta^{14}C(CO_2)$ measurements, extensive sampling campaigns and/or good bottom-up estimates to determine the isotopic end members.

Part 4

Summary

In the introduction, the question was raised, how present and future emissions of anthropogenic greenhouse gases might influence environmental processes and drive climate changes.

"If you cannot measure it, you cannot improve it."

- Lord Kelvin

As Lord Kelvin has correctly put it more than 100 years ago and as the World Meteorological Organization recognizes in their regular reports (e.g. GGMT, 2013), measurements are the basis of scientific advancement. To improve and validate the understanding of ecosystem processes or the predictions of climate change, accurate and precise measurements must be performed.

This thesis offers a guideline for acquiring measurement records of highest possible quality. High quality here refers to the actual measurement quality, such as accuracy, precision and compatibility, but also to the usefulness of the various tracers and data sets. The usefulness is evaluated in terms of additional benefit for separating gross and net fluxes, optimization of measurement location and measurement protocol as well as necessity of accompanying measurements or models. The outcomes of this work may provide a scientific basis for further studying environmental processes and climate change in the future and could also support political decisions on emission mitigation.

A fundamental step in studying greenhouse gas fluxes is to measure their atmospheric concentration accurately, precisely and compatibly to other instruments. Therefore, the **accuracy and precision** of greenhouse gas measurements with the FTIR were assessed. It was shown that CO_2, CH_4 and N_2O measurements are accurate and precise enough to meet the WMO target recommendations. During a travelling instrument campaign, the **compatibility** of ambient air greenhouse gas measurements was assessed, which is vital for a bias-free determination of fluxes in top-down approaches. It was further shown that CO_2 ambient air measurements from different instruments encounter significant discrepancies on the order of about 0.15 ppm between each other, which are not seen in cylinder gas measurements. The reason for the discrepancy could not be clarified with certainty, but may be due to the water correction of the CRDS systems and should be investigated in future work in more detail. CH_4 measurements

of three independent instruments agree within the WMO target recommendations. For N_2O, discrepancies are ca. 0.4 ppb. Taking into consideration scale transfer uncertainties as well as flask comparisons between both networks, it appears that differences of calibration scales may exist and may be on the order of 0.1 to 0.4 ppb. The scale difference may be due to non-linearity of the ECDs as both networks derive their scales from ECD measurements (pers. communication, B. Hall, 2016). It has been further demonstrated that at present, the precision of CO_2 and CH_4 measurements is sufficient to detect small greenhouse gas fluxes. However, for CO_2, an insufficient compatibility between instruments limits the accuracy of CO_2 flux estimates. Therefore, a routine implementation of quality control assessments and measurement campaigns is recommended in order to assess and improve the compatibility of different instruments and laboratories. The uniqueness and comprehensiveness of information obtained during travelling instrument campaigns compared to other quality controls is highlighted.

High quality greenhouse gas measurements from a joint network can be used in top-down inversions to study the total net greenhouse gas fluxes (Sect. 1.4). The next step to a comprehensive understanding of greenhouse gas fluxes is a separation of gross fluxes (e.g. respiration and photosynthesis) as well as between net fluxes from different reservoirs (e.g. biosphere, ocean and fossil fuels).

Measurements of $\delta^{18}O(CO_2)$ offer the prospect of disentangling **carbon gross fluxes**. This thesis proves that the continuous measurement of $\delta^{18}O(CO_2)$ is possible with an FTIR analyzer. The precision and compatibility of $\delta^{18}O(CO_2)$ measurements (and $\delta^{13}C(CO_2)$ measurements) were assessed and it was found that although the compatibility recommendations from the WMO are not met, the precision and compatibility are sufficient to detect and interpret $\delta^{18}O(CO_2)$ signals in an urban area such as Heidelberg, Germany. This novel finding opens the door to quantifying different CO_2 gross fluxes. However, due to the complex coupling of $^{18}O(CO_2)$ and $^{18}O(H_2O)$, a quantification of CO_2 gross fluxes using $\delta^{18}O(CO_2)$ requires the determination of isotopic H_2O and CO_2 values of ecosystem and fuel CO_2 fluxes as well as the implementation of a coupled water-carbon model. Thus, the implementation of regional coupled models together with installation of routine water and carbon isotopologue measurements are highly recommended, so that a profound understanding of the regional carbon cycle can be achieved.

The separation of oceanic, biospheric and anthropogenic **net CO_2 fluxes** requires the use of additional tracers, which are characteristic for the reservoir that should

be separated. In the continental European atmosphere, the influence of oceanic fluxes are usually negligible, but a separation of biospheric and fuel CO_2 contributions is desirable for studying the continental carbon cycle. Tracers, which allow separating between biospheric and fuel CO_2 contributions continuously are e.g. CO, $\delta^{13}C(CO_2)$ or hypothetical future $\Delta^{14}C(CO_2)$ measurements. In this work, specific equations for the different tracer-based estimates of continuous fuel CO_2 were formulated and the tracers were compared at different measurement stations using a model pseudo data set (see Sect. 1.6.1). At present, $\delta^{13}C(CO_2)$ and CO based estimates of fuel CO_2 are the most precise tracers for fuel CO_2 estimation at rural, urban and polluted measurement sites. The precision of fuel CO_2 estimates is mainly limited by the variation of natural CO fluxes in the case of the CO-based approach, and by the measurement precision of $\delta^{13}C(CO_2)$ and CO_2 in the case of $\delta^{13}C(CO_2)$-based approaches. In the prospect of further technical development of $\delta^{13}C(CO_2)$ measurements, the precision of the $\delta^{13}C(CO_2)$-based approach is likely to further improve. The accuracy of the CO and $\delta^{13}C(CO_2)$-based approach depends on the accuracy of the emission ratio CO/CO_2 of fuels in the case of CO, and on the accuracy of the assumed isotopic end members, δ_{bio} and δ_F, in the case of $\delta^{13}C(CO_2)$. For an accurate estimation of continuous fuel CO_2, it is possible to calibrate the source characteristics, δ_F and CO/CO_2, using precise $^{14}C(CO_2)$ measurements. The best calibration strategy is to take as many as possible (typically more than 20) $^{14}C(CO_2)$ grab samples per year and use them to calibrate an annual mean value of the isotopic signature δ_F or of the CO/CO_2 emission ratio of fuel CO_2, respectively. A high number of $^{14}C(CO_2)$ grab samples is desirable as the accuracy of δ_F and CO/CO_2 emission ratio improves with increasing number of grab samples. In the future, continuous $^{14}C(CO_2)$ measurements with improved precision of 5 ‰ may become available. It was shown that these measurements could further improve the precision of the separation of anthropogenic and biospheric CO_2 if no nuclear facilities lie in the catchment area and if biofuel CO_2 can be approximated independently. Continuous $^{14}C(CO_2)$ measurements are therefore worth further developing.

Another relevant finding of this work for the network design is that the continuous measurements of fuel CO_2 tracers is not useful at rural sites as the CO_2 signals are so small that the tracer-based fuel CO_2 uncertainties are larger than the uncertainties of emission inventories. An improvement of emission inventories based on atmospheric observations is therefore only possible at urban or polluted sites, which is why it is advisable to build measurement stations at urban and polluted sites if all relevant European emissions are to be monitored.

Finally, in many studies, $\delta^{13}C(CO_2)$ measurements are used to determine the isotopic **source signature** using Keeling plots. Using a pseudo data experiment, a procedure for determining the isotopic signature from continuous CO_2 and $\delta^{13}C(CO_2)$ correctly is suggested and finally the technique is applied to a real CO_2 and $\delta^{13}C(CO_2)$ data set from Heidelberg. The annual pattern of the source signature in Heidelberg shows more enriched values in summer and more depleted values in winter as expected from a larger fraction of more depleted fuel CO_2 in winter due to burning of depleted natural gas. From the source signature record it is possible to determine the end members δ_F in winter and δ_{bio} in summer, allowing a falsification of end member reference values in these periods. However, as the isotopic end members of fuel CO_2 and of the biosphere, δ_F and δ_{bio}, vary throughout the year, the fuel share cannot be quantified unambiguously from the mean source signature record alone and should be supported by additional point measurements and ^{14}C measurements, if possible.

In this thesis, it was investigated which parameters affect the improvement of greenhouse gas flux estimates. The quality of the measurements (accuracy, precision, compatibility), the meteorological trajectories, but also the choice of additional tracers measured (e.g. $\delta^{18}O$, $\delta^{13}C$, CO, $\Delta^{14}C$, etc.) at different stations substantially influence the degree of information, which can be derived from the measurements. A variety of these parameters have been assessed and optimized in this work. In the future, the final goal of improving greenhouse gas flux estimates will profit from a permanent information exchange and collaboration of modellers, experimentalists, technicians and network designers.

References

Alden, C. B., Miller, B., J., and White, J. W. (2010). Can bottom-up ocean CO_2 fluxes be reconciled with atmospheric ^{13}C observations? *Tellus B*, 62:369–388.

Andres, R. J., Marland, G., Boden, T., and Bischof, S. (1994). Carbon Dioxide Emissions from Fossil Fuel Consumption and Cement Manufacture, 1751-1991; and an Estimate of Their Isotopic Composition and Latitudinal Distribution. *Environmental Sciences*.

Bastos, A., Janssens, I. A., Gouveia, C. M., Trigo, R. M., Ciais, P., Chevallier, F., Peñuelas, J., Rödenbeck, C., Piao, S., Friedlingstein, P., and Running, S. W. (2016). European land CO_2 sink influenced by NAO and East-Atlantic Pattern coupling. *Nature communications*, 7.

Bergamaschi, P., Krol, M., Meirink, J. F., Dentener, F., Segers, A., van Aardenne, J., Monni, S., Vermeulen, A. T., Schmidt, M., Ramonet, M., Yver, C., Meinhardt, F., Nisbet, E. G., Fisher, R. E., O'Doherty, S., and Dlugokencky, E. J. (2010). Inverse modeling of European CH_4 emissions 2001-2006. *Journal of Geophysical Research: Atmospheres*, 115(D22). D22309.

Broquet, G., Chevallier, F., Bréon, F.-M., Kadygrov, N., Alemanno, M., Apadula, F., Hammer, S., Haszpra, L., Meinhardt, F., Morguí, J. A., Necki, J., Piacentino, S., Ramonet, M., Schmidt, M., Thompson, R. L., Vermeulen, A. T., Yver, C., and Ciais, P. (2013). Regional inversion of CO_2 ecosystem fluxes from atmospheric measurements: reliability of the uncertainty estimates . *Atmospheric Chemistry and Physics*, 13:9039–9056.

Canadell, J., Mooney, H. A., Baldocchi, D. D., Berry, J. A., Ehleringer, J. R., Field, C. B., Gower, S. T., Hollinger, D. Y., Hunt, J. E., Jackson, R. B., Running, S. W., Shaver, G. R., Steffen, W., Trumbore, S. E., Valentini, R., and Bond, B. Y. (2000). A Global Terrestrial Monitoring NetworkIntegrating Tower Fluxes, Flask Sampling, Ecosystem Modeling and EOS Satellite Data. *Ecosystems*, 3:115–130.

Ciais, P., Crisp, D., Denier van der Gon, H., Engelen, R., Janssens-Maenhout, G., Heiman, M., Rayner, P., and Scholze, M. (2015). Towards a European Operational Observing System to Monitor Fossil CO_2 Emissions, Study report. Technical report, Copernicus.

Ciais, P., Reichstein, M., Viovy, N., Granier, A., Ogee, J., Allard, V., Aubinet, M., Buchmann, N., Bernhofer, C., Carrara, A., Chevalier, F., De Noblet, N., Friend, A. D., Friedlingstein, P., Grunwald, T., Heinesch, B., Keronen, P., Knohl, A., Krinner, G., Loustau, D., Manca, G., Matteucci, G., Miglietta, F., Ourcival, J. M., Papale, D., Pilegaard, K., Rambal, S., Seufert, G., Soussana, J. F., Sanz, M. J., Schulze, E. D., Vesala, T., and Valentini, R. (2005). Europe-wide reduction in primary productivity caused by the heat and drought in 2003 . *Nature*, 437:529–533.

Ciais, P., Tans, P. P., Trolier, M., White, J. W. C., and Francey, R. (1995). A large Northern Hemisphere terrestrial CO_2 sink indicated by the $^{13}C/^{12}C$ ratio of atmospheric CO_2. *Science*, 269:1098–1102.

Cramer, W., Bondeau, A., Woodward, F. I., Prentice, I. C., Betts, R. A., Brovkin, V., Cox, P. M., Fisher, V., Foley, J. A., Friend, A. D., Kucharik, C., Lomas, M. R., Ramankutty, N., Sitch, S., Smith, B., White, A., and Young-Molling, C. (2001). Global response of terrestrial ecosystem structure and function to CO_2 and climate change: results from six dynamic global vegetation models. *Global Change Biology*, 7(4):357–373.

Cuntz, M., Ciais, P., Hoffmann, G., , and Knorr, W. (2003a). A comprehensive global three-dimensional model of $\delta^{18}O$ in atmospheric CO_2: 1. Validation of surface processes. *Journal of Geophysical Research*, 108:4527.

Cuntz, M., Ciais, P., Hoffmann, G., Allison, C. E., Francey, R. J., Knorr, W., Tans, P. P., White, J. W. C., , and Levin, I. (2003b). A comprehensive global three-dimensional model of $\delta^{18}O$ in atmospheric CO_2: 2. Mapping the atmospheric signal. *Journal of Geophysical Research*, 108:4528.

Daansgard, W. (1953). The Abundance of O^{18} in Atmospheric Water and Water Vapour. *Tellus*, 5(4):461 – 469.

Esler, M. B., Griffith, D. W., Wilson, S. R., and Steele, L. P. (2000). Precision trace gas analysis by FT-IR spectroscopy. 2. The $^{13}C/^{12}C$ isotope ratio of CO_2. *Analytical chemistry*, 72(1):216–21.

Farquhar, G. D., Lloyd, J., Taylor, J. A., Flanagan, L. B., Syvertsen, J. P., Hubick, K. T., Wong, S. C., , and Ehleringer, J. R. (1993). Vegetation effects on the isotope composition of oxygen in atmospheric CO_2. *Nature*, 363:439–443.

Feng, L., Palmer, P. I., Parker, R. J., Deutscher, N. M., Feist, D. G., Kivi, R., Morino, I., and Sussmann, R. (2016). Estimates of european uptake of co2 inferred from gosat xco2 retrievals: sensitivity to measurement bias inside and outside europe. *Atmospheric Chemistry and Physics*, 16(3):1289–1302.

Francey, R. J. and Tans, P. P. (1997). Latitudinal variation in oxygen-18 of atmospheric CO_2. *Nature*, 327:495–497.

Gamnitzer, U., Karstens, U., Kromer, B., Neubert, R. E. M., Meijer, H. a. J., Schroeder, H., and Levin, I. (2006). Carbon monoxide: A quantitative tracer for fossil fuel CO_2? *Journal of Geophysical Research*, 111(D22):1–19.

Gavrichkova, O., Proietti, S., Moscatello, S., Portarena, S., Battistelli, A., Matteucci, G., and Brugnoli, E. (2011). Short-term natural $\delta^{13}C$ and $\delta^{18}O$ variations in pools and fluxes in a beech forest: the transfer of isotopic signal from recent photosynthates to soil respired CO_2. *Biogeosciences*, 8(10):2833–2846.

Gerbig, C., Dolman, A. J., and Heimann, M. (2009). On observational and modelling strategies targeted at regional carbon exchange over continents. *Biogeosciences*, 6(10):1949–1959.

Gerbig, C., Körner, S., and Lin, J. C. (2008). Vertical mixing in atmospheric tracer transport models: error characterization and propagation. *Atmospheric Chemistry and Physics*, 8(3):591–602.

GGMT (2013). 17th WMO/IAEA Meeting on Carbon Dioxide, Other Greenhouse Gases and Related Tracers Measurement Techniques (GGMT-2013), Beijing, China, 10-13 June 2013. In Tans, P. and Zellweger, C., editors, *GAW Report 213*.

Ghashghaie, J. and Badeck, F. W. (2014). Opposite carbon isotope discrimination during dark respiration in leaves versus roots - a review. *New Phytologist*, 201(3):751–769. 2013-15744.

Griffis, T. (2013). Tracing the flow of carbon dioxide and water vapor between the biosphere and atmosphere: A review of optical isotope techniques and their application. *Agricultural and Forest Meteorology*, 174 - 175:85 – 109.

Griffith, D. W. T. (1996). Synthetic Calibration and Quantitative Analysis of Gas-Phase FT-IR Spectra. *Applied Spectroscopy*, 50(1):59–70.

Griffith, D. W. T., Deutscher, N. M., Caldow, C., Kettlewell, G., Riggenbach, M., and Hammer, S. (2012). A Fourier transform infrared trace gas and isotope analyser for atmospheric applications. *Atmospheric Measurement Techniques*, 5(10):2481–2498.

Griffith, P. and de Haseth, J. (2007). *Fourier Transform Infrared Spectrometry*, volume 171. John Wiley & Sons.

Guha, T. and Ghosh, P. (2010). Diurnal variation of atmospheric CO_2 concentration and $\delta^{13}C$ in an urban atmosphere during winter - role of the Nocturnal Boundary Layer. *Journal of Atmospheric Chemistry*, 65(1):1–12.

Hammer, S., Griffith, D. W. T., Konrad, G., Vardag, S., Caldow, C., and Levin, I. (2013a). Assessment of a multi-species in situ FTIR for precise atmospheric greenhouse gas observations. *Atmospheric Measurement Techniques*, 6:1153–1170.

Hammer, S., Konrad, G., Vermeulen, A. T., Laurent, O., Delmotte, M., Jordan, A., Hazan, L., Conil, S., and Levin, I. (2013b). Feasibility study of using a "travelling" CO_2 and CH_4 instrument to validate continuous in situ measurement stations. *Atmospheric Measurement Techniques*, 6(5):1201–1216.

Hesterberg, R. and Siegenthaler, U. (1991). Production and stable isotopic composition of CO_2 in a soil near Bern, Switzerland. . *Tellus B*, 43:197–205.

ICOS (2015). ICOS Atmospheric Station Specifications. `https://icos-atc.lsce.ipsl.fr/?q=filebrowser/download/8681`. [Online; accessed 04-February 2016].

IPCC (2013). *Climate Change 2013: The Physical Science Basis. Contribution of Working Group I to the Fifth Assessment Report of the Intergovernmental Panel on Climate Change*. Cambridge University Press, Cambridge, United Kingdom and New York, NY, USA.

IPCC (2014a). Climate Change 2014: Synthesis Report. Contribution of Working Groups I, II and III to the Fifth Assessment Report of the Intergovernmental Panel on Climate Change [Core Writing Team, R.K. Pachauri and L.A. Meyer (eds.)]. *IPCC, Geneva, Switzerland*, page 151 pp.

IPCC (2014b). *Climate Change 2014:Impacts, Adaptation, and Vulnerability. Part A: Global and Sectoral Aspects. Contribution of Working Group II to the Fifth Assessment Report of the Intergovernmental Panel on Climate Change*. Cambridge University Press, Cambridge, United Kingdom and New York, NY, USA.

Joint Committee for Guides in Metrology (JCGM-WG2) (2012). International Vocabulary of Metrology - Basic and General Concepts and Associated Terms (VIM). http://www.bipm.org/en/publications/guides/vim.html. Last access: 22.02.2015.

Keeling, C. D. (1958). The concentration and isotopic abundances of atmospheric carbon dioxide in rural areas. *Geochimica et Cosmochimica Acta*, 13(4):322–224.

Keeling, C. D. (1960). The Concentration and Isotopic Abundances of Carbon Dioxide in the Atmosphere. *Tellus*, 12:200 – 203.

Keeling, C. D. (1961). The concentrations and isotopic abundances of atmospheric carbon dioxide in rural and marine air. *Geochim Cosmochim Acta,*, 24:277–298.

Kodama, N., Ferrio, J. P., Brüggemann, N., and Gessler, A. (2011). Short-term dynamics of the carbon isotope composition of CO_2 emitted from a wheat agroecosystem - physiological and environmental controls. *Plant Biology*, 13(1):115–125.

Körner, C., Asshoff, R., Bignucolo, O., Hättenschwiler, S., Keel, S. G., Peláez-Riedl, S., Pepin, S., Siegwolf, R. T., and Zotz, G. (2005). Carbon flux and growth in mature deciduous forest trees exposed to elevated CO_2. *Science*, 309(5739):1360–1362.

Krevor, S., Perrin, J.-C., Esposito, A., Rella, C., and Benson, S. (2010). Rapid detection and characterization of surface CO_2 leakage through the real-time measurement of C signatures in CO_2 flux from the ground . *International Journal of Greenhouse Gas Control*, 4(5):811 – 815.

Langendörfer, U., Cuntz, M., Ciais, P., Peylin, P., Bariac, T., Milykova, I., Kolle, O., Naegler, T., and Levin, I. (2002). Modelling of biospheric CO_2 gross fluxes via oxygen isotopes in a spruce forest canopy: a ^{222}Rn calibrated box model approach. *Tellus B*, 54(5):476–496.

Lauvaux, T., Uliasz, M., Sarrat, C., Chevallier, F., Bousquet, P., Lac, C., Davis, K. J., Ciais, P., Denning, A. S., , and Rayner, P. J. (2008). Mesoscale inversion: first results from the CERES campaign with synthetic data . *Atmospheric Chemistry and Physics*, 8:3459–3471.

Le Quéré, C., Moriarty, R., Andrew, R. M., Canadell, J. G., Sitch, S., Korsbakken, J. I., Friedlingstein, P., Peters, G. P., Andres, R. J., Boden, T. A., Houghton, R. A., House, J. I., Keeling, R. F., Tans, P., Arneth, A., Bakker, D. C. E., Barbero, L., Bopp, L., Chang, J., Chevallier, F., Chini, L. P., Ciais, P., Fader, M., Feely, R. A., Gkritzalis, T., Harris, I., Hauck, J., Ilyina, T., Jain, A. K., Kato, E., Kitidis, V., Klein Goldewijk, K., Koven, C., Landschützer, P., Lauvset, S. K., Lefèvre, N., Lenton, A., Lima, I. D., Metzl, N., Millero, F., Munro, D. R., Murata, A., Nabel, J. E. M. S., Nakaoka, S., Nojiri, Y., O'Brien, K., Olsen, A., Ono, T., Pérez, F. F., Pfeil, B., Pierrot, D., Poulter, B., Rehder, G., Rödenbeck, C., Saito, S., Schuster, U., Schwinger, J., Séférian, R., Steinhoff, T., Stocker, B. D., Sutton, A. J., Takahashi, T., Tilbrook, B., van der Laan-Luijkx, I. T., van der Werf, G. R., van Heuven, S., Vandemark, D., Viovy, N., Wiltshire, A., Zaehle, S., and Zeng, N. (2015). Global Carbon Budget 2015. *Earth System Science Data*, 7(2):349–396.

Levin, I. and Karstens, U. (2007). Inferring high-resolution fossil fuel CO_2 records at continental sites from combined $^{14}CO_2$ and CO observations . *TellusB*, 59:245–250.

Levin, I., Kromer, B., Schmidt, M., and Sartorius, H. (2003). A novel approach for independent budgeting of fossil fuel CO_2 over Europe by $^{14}CO_2$ observations. *Geophysical Research Letters*, 30(23).

Lin, J. and Gerbig, C. (2005). Accounting for the effect of transport errors on tracer inversions. *Geophysical research letters*, 32(1).

Lin, J., Gerbig, C., Wofsy, S. C., Andrews, A. E., Daube, B. C., Davis, K. J., and Grainger, C. A. (2003). A near-field tool for simulating the upstream influence of atmospheric observations: The Stochastic Time-Inverted Lagrangian Transport (STILT) model. *Journal of Geophysical Research*, 108:17pp.

Lopez, M., Schmidt, M., Delmotte, M., Colomb, A., Gros, V., Janssen, C., Lehman, S. J., Mondelain, D., Perrussel, O., Ramonet, M., Xueref-Remy, I., and Bousquet, P. (2013). CO, NO_x and $^{13}CO_2$ as tracers for fossil fuel CO_2: results from a pilot study in Paris during winter 2010. *Atmospheric Chemistry and Physics*, 13(15):7343–7358.

Masarie, K. A., Pétron, G., Andrews, A., Bruhwiler, L., Conway, T. J., Jacobson, A. R., Miller, J., Tans, P., Worthy, D., and Peters, W. (2011). Impact of CO_2 measurement bias on CarbonTracker surface flux estimates. Journal of Geophysical Research: Atmospheres (1984-2012). *Journal of Geophysical Research*, 116:D17.

McIntyre, C. P., McNichol, A. P., Roberts, M. L., Seewald, J. S., von Reden, K. F., and Jenkins, W. J. (2013). Improved precision of 14c measurements for ch4 and co2 using gc and continuous-flow ams achieved by summation of repeated injections. *Radiocarbon*, 55(2–3):677–685.

Miller, J. B., Lehman, S. J., Montzka, S. A., Sweeney, C., Miller, B. R., Karion, A., Wolak, C., Dlugokencky, E. J., Southon, J., Turnbull, J. C., and Tans, P. P. (2012). Linking emissions of fossil fuel CO_2 and other anthropogenic trace gases using atmospheric $^{14}CO_2$. *Journal of Geophysical Research*, 117:D08302.

Miller, J. B. and Tans, P. P. (2003). Calculating isotopic fractionation from atmospheric measurements at various scales. *Tellus*, pages 207–214.

Mook, W. G. (2000). Environmental isotopes in the hydrological cycle - Principles and applications. *Technical Documents in Hydrology*, I.

Mook, W. G., Koopmans, M., Carter, A. F., and Keeling, C. D. (1983). Seasonal, latitudinal, and secular variations in the abundance and isotopic ratios of atmospheric carbon dioxide: 1. Results from land stations. *Journal of Geophysical Research*, 88:10915–10933.

Newman, S., Xu, X., Gurney, K. R., Hsu, Y.-K., Li, K.-F., Jiang, X., Keeling, R., Feng, S., O'Keefe, D., Patarasuk, R., Wong, K. W., Rao, P., Fischer, M. L., and Yung, Y. L. (2015). Toward consistency between bottom-up CO_2 emissions trends and top-down atmospheric measurements in the Los Angeles megacity. *Atmospheric Chemistry and Physics Discussions*, 15(20):29591–29638.

Norby, R. J. and Iversen, C. M. (2006). Nitrogen uptake, distribution, turnover, and efficiency of use in a CO_2-enriched sweetgum forest. *Ecology*, 87(1):5–14.

Norman, J. M., Kucharik, C. J., Gower, S. T., Baldocchi, D. D., Crill, P. M., Rayment, M., Savage, K., and Striegl, R. G. (1997). A comparison of six methods for measuring soil-surface carbon dioxide fluxes. *Journal of Geophysical Research*, 102:28771–28777.

Oren, R., Ellsworth, D. S., Johnsen, K. H., Phillips, N., Ewers, B. E., Maier, C., Schäfer, K. V., McCarthy, H., Hendrey, G., McNulty, S. G., et al. (2001). Soil fertility limits carbon sequestration by forest ecosystems in a CO_2-enriched atmosphere. *Nature*, 411(6836):469–472.

Pataki, D. E. (2003). The application and interpretation of Keeling plots in terrestrial carbon cycle research. *Global Biogeochemical Cycles*, 17(1):1022.

Riley, W. J. (2013). Using model reduction to predict the soil-surface $C^{18}OO$ flux: an example of representing complex biogeochemical dynamics in a computationally efficient manner. *Geoscientific Model Development*, 6(2):345–352.

Riley, W. J., Still, C. J., Helliker, B. R., Ribas-Carbo, M., and Berry, J. A. (2003). ^{18}O composition of CO_2 and H_2O ecosystem pools and fluxes in a tallgrass prairie: Simulations and comparisons to measurements. *Global Change Biology*, 9(11):1567–1581.

Rizzo, A., Liuzzo, M., Ancellin, M., and Jost, H. (2015). Real-time measurements of $\delta^{13}C$, CO_2 concentration, and CO_2/SO_2 in volcanic plume gases at Mount Etna, Italy, over 5 consecutive days. *Chemical Geology*, 411:182 – 191.

Roberts, M. and Southon, J. (2007). A preliminary determination of the absolute $^{14}C/^{12}C$ ratio of OX-I. *Radiocarbon*, 49(2):441–445.

Roedel, W. and Wagner, T. (2000). *Physik unserer Umwelt*. Springer Verlag.

Rothman, L., Rinsland, C., Goldman, A., Massie, S., Edwards, D., Flaud, J.-M., Perrin, A., Camy-Peyret, C., Dana, V., Mandin, J.-Y., Schroeder, J., McCann, A., Gamache, R., Wattson, R., Yoshino, K., Chance, K., Jucks, K., Brown, L., Nemtchinov, V., and Varanasi, P. (1998). The HITRAN molecular spectroscopic database and HAWKS (HITRAN atmospheric workstation). *Journal of Quantitative Spectroscopy and Radiative Transfer*.

Running, S., Baldocchi, D., Turner, D., Gower, S., Bakwin, P., and Hibbard, K. (1999). A Global Terrestrial Monitoring NetworkIntegrating Tower Fluxes, Flask Sampling, Ecosystem Modeling and EOS Satellite Data. *Remote Sensing of Environment*, 70:108–127.

Schulze, E., Luyssaert, S., Ciais, P., Freibauer, A., Janssens, I., Soussana, J., Smith, P., Grace, J., Levin, I., Thiruchittampalam, B., et al. (2009). Importance of methane and nitrous oxide for Europe's terrestrial greenhouse-gas balance. *Nature Geoscience*, 2(12):842–850.

Stuiver, M. and Polach, H. A. (1977). Reporting of C-14 data. *Radiocarbon*, 19(3):355–363.

Thompson, R. L., Ishijima, K., Saikawa, E., Corazza, M., Karstens, U., Patra, P. K., Bergamaschi, P., Chevallier, F., Dlugokencky, E., Prinn, R. G., Weiss, R. F., O'Doherty, S., Fraser, P. J., Steele, L. P., Krummel, P. B., Vermeulen, A., Tohjima, Y., Jordan, A., Haszpra, L., Steinbacher, M., Van der Laan, S., Aalto, T., Meinhardt, F., Popa, M. E., Moncrieff, J., and Bousquet, P. (2014). TransCom N_2O model inter-comparison − Part 2: Atmospheric inversion estimates of N_2O emissions. *Atmospheric Chemistry and Physics*, 14(12):6177–6194.

Turnbull, J. C., Karion, A., Fischer, M. L., Faloona, I., Guilderson, T., Lehman, S. J., Miller, B. R., Miller, J. B., Montzka, S., Sherwood, T., Saripalli, S., Sweeney, C., and Tans, P. P. (2011). Assessment of fossil fuel carbon dioxide and other anthropogenic trace gas emissions from airborne measurements over Sacramento, California in spring 2009. *Atmospheric Chemistry and Physics*, 11(2):705–721.

Turnbull, J. C., Sweeney, C., Karion, A., Newberger, T., Lehman, S. J., Tans, P. P., Davis, K. J., Lauvaux, T., Miles, N. L., Richardson, S. J., Cambaliza, M. O., Shepson, P. B., Gurney, K., Patarasuk, R., , and Razlivanov, I. (2015). Toward quantification and source sector identification of fossil fuel CO_2 emissions from an urban area: Results from the INFLUX experiment. *Journal of Geophysical Research - Atmosphere*, 120:292–312.

Tuzson, B., Henne, S., Brunner, D., Steinbacher, M., Mohn, J., Buchmann, B., and Emmenegger, L. (2011). Continuous isotopic composition measurements of tropospheric CO_2 at Jungfraujoch (3580 m a.s.l.), Switzerland: real-time observation of regional pollution events. *Atmospheric Chemistry and Physics*, 11(4):1685–1696.

UNFCCC (2015). Historic Paris Agreement on Climate Change. *Press release*, last access: 19.01.2015, http://newsroom.unfccc.int/unfccc-newsroom/finale-cop21/.

Vardag, S. N. (2012). *CO_2 source apportionment in the Heidelberg region using continuous $^{13}CO_2$ measurements*. Master's thesis, Ruprecht-Karls-Universität.

Vardag, S. N., Hammer, S., O'Doherty, S., Spain, T. G., Wastine, B., Jordan, A., and Levin, I. (2014). Comparisons of continuous atmospheric CH_4, CO_2 and N_2O measurements − results from a travelling instrument campaign at Mace Head. *Atmospheric Chemistry and Physics*, 14(16):8403–8418.

Vardag, S. N., Hammer, S., Sabasch, M., Griffith, D. W. T., and Levin, I. (2015a). First continuous measurements of $\delta^{18}O-CO_2$ in air with a Fourier transform infrared spectrometer. *Atmospheric Measurement Techniques*, 8(2):579–592.

Vardag, S. N., Gerbig, C., Janssens-Maenhout, G., and Levin, I. (2015b). Estimation of continuous anthropogenic CO_2: model-based evaluation of CO_2, CO, $\delta^{13}C(CO_2)$ and $\Delta^{14}C(CO_2)$ tracer methods. *Atmospheric Chemistry and Physics*, 15(22):12705–12729.

Vogel, F. R. (2010). *$^{14}CO_2$-calibrated carbon monoxide as proxy to estimate the regional fossil fuel CO_2 component at hourly resolution*. PhD thesis, Universität Heidelberg, Heidelberg.

Vogel, F. R., Hammer, S., Steinhof, A., Kromer, B., and Levin, I. (2010). Implication of weekly and diurnal ^{14}C calibration on hourly estimates of CO-based fossil fuel CO_2 at a moderately polluted site in southwestern Germany. *Tellus B*, 62(5):512–520.

Vogel, F. R., Huang, L., Ernst, D., Giroux, L., Racki, S., and Worthy, D. (2013). Evaluation of a cavity ring-down spectrometer for in situ observations of $^{13}CO_2$. *Atmospheric Measurement Techniques*, 6(2):301–308.

Wahl, E. H., Fidric, B., Rella, C. W., Koulikov, S., Kharlamov, B., Tan, S., Kachanov, A. A., Richman, B. A., Crosson, E. R., Paldus, B. A., Kalaskar, S., and Bowling, D. R. (2006). Applications of cavity ring-down spectroscopy to high precision isotope ratio measurement of $^{13}C/^{12}C$ in carbon dioxide. *Isotopes in Environmental and Health Studies*, 42(1):21–35. PMID: 16500752.

Wang, R., Tao, S., Ciais, P., Shen, H. Z., Huang, Y., Chen, H., Shen, G. F., Wang, B., Li, W., Zhang, Y. Y., Lu, Y., Zhu, D., Chen, Y. C., Liu, X. P., Wang, W. T., Wang, X. L., Liu, W. X., Li, B. G., , and Piao, S. L. (2013). High-resolution mapping of combustion processes and implications for CO_2 emissions. *Atmosheric Chemistry and Physics*, 13:5189–5203.

Acronyms

AMS Accelerator Mass Spectrometry

AGAGE Advances Global Atmospheric Gases Experiment

CRDS Cavity Ring-Down Spectroscopy

CCL Central Calibration Laboratory

ECD Electron Capture Detector

EDGAR Emissions Database for Global Atmospheric Research

FTIR Fourier Transform InfraRed (analyzer)

GC Gas Chromatograph

GC-MD Gas Chromatograph MultiDetector

HITRAN High resolution transmission molecular absorption database

ICOS Integrated Carbon Observation system

ILC Inter-Laboratory Compatibility

IPCC Intergovernmental Panel of Climate Change

IRMS Isotope Ratio Mass Spectrometer

LSCE Laboratoire des Sciences du Climat et de l'Environnment

MALT Multiple atmospheric layer transmission

MPI Max-Planck Institute

NOAA National Oceanic and Atmospheric Administration

STILT Stochastic Time-Inverted Lagrangian Particle model

TCI Travelling Comparison Instrument

WMO World Meteorological Organization

List of Figures

List of Tables

Part 5

Appendix

A

The Fourier Transform Infrared (FTIR) analyzer

A Fourier Transform Infrared analyzer measures the molecular absorption spectrum of a sample of air. The light beam of a broad-banded infrared source is directed into an air sample, where the intensity of the spectrum is reduced due to molecular absorption of the gas molecules in the air sample. From the absorption spectrum the greenhouse gas concentration of CO_2, CH_4, N_2O, CO, $^{13}C(CO_2)$ and $^{18}O(CO_2)$ in the sample is calculated. The FTIR has been routinely measuring the trace gases in Heidelberg since April 2011 in parallel to a gas chromatograph (GC) and a cavity ring-down spectroscopy (CRDS) system. Here the instrumental set-up, the sample handling and calibration strategy of the FTIR analyzer are explained. Its intermediate measurements precision, accuracy and compatibility are summarized. Further the duration and reason for down times are named. Finally, the long-term FTIR ambient air measurements is presented.

A1 Brief description of set-up and measurement principle of the FTIR

Instrumental set-up

The in-situ FTIR analyzer has been running routinely in Heidelberg since April 2011. A detailed description of the FTIR can be found in Griffith et al. (2012) and Hammer et al. (2013a). Modifications to this set-up have been described by Vardag et al. (2015a). This latest set-up of the FTIR can be seen in Fig. A.1 and is described briefly here. Older configurations are also described in Hammer et al. (2013a).

The FTIR has four inlets for gaseous samples. One of these inlets is typically used as ambient air intake. It is possible to additionally connect multi-position valves to these

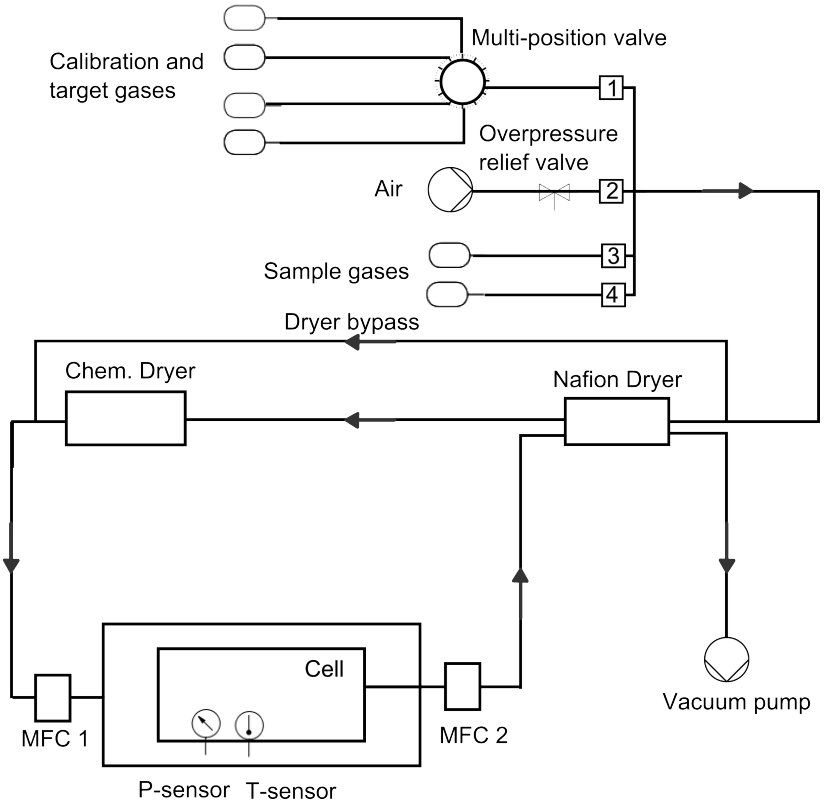

Fig. A.1: Schematic set-up of the FTIR.

inlets in order to permanently connect more cylinders (e.g. standard and target gases) to the instrument. In the Heidelberg set-up, one multi-position valve (MWSD16 selection valve, Valco, USA) was installed to which cylinders are permanently connected. An oil-free vacuum pump (model MV2NT, Vacuubrand, Germany) located at the outlet of the instrument draws the samples through the instrument. First, the sample is optionally directed into a drying unit consisting of a 24 inch (0.6 m) Nafion Dryer (Permapure, Toms River, NJ, USA) operated in counter-flow mode and followed by a chemical Magnesium perchlorate dryer. The drying unit reaches a dew point of -65 °C. It can be bypassed if desired. The sample is then led through a temperature controlled and nitrogen purged enclosure, in which a White cell (model 24 PA, IR analysis Inc., Anaheim, CA) and the interferometer are located. The interferometer is an IRcube (Bruker Optics, Germany) and the detector is a thermoelectrically-cooled Mercury Cadmium Telluride (MCT). The multi-pass cell holds 3.5 L and has 24 m optical path length. It is temperature stabilized at 30 °C within ± 0.01°C. The cell and the interferometer are flushed with high-purity nitrogen class 5.0 to avoid contamination in the optical path with air. The cell flow is regulated at 1 ± 0.05 standard liter per minute (SLPM) using a mass-flow controller (MFC 1) located in front of the cell, whereas a

second MFC (MFC 2) behind the cell regulates the cell pressure to within ± 0.1 hPa. The measurements are typically performed at slight overpressure (1100 hPa).

The Interferometer

The underlying principle of the FTIR is similar to a Michelson interferometer. A light source emits on to a semitransparent mirror. The reflected as well as the emitted beam are then reflected by outer mirrors and joined after passing the semi-transparent mirror again (see Fig. A.2). The beams then pass the cell (typically filled with a sample) and are detected. One of the outer mirrors can be moved and thus the optical path length of one beam can be changed. The full path length difference can be scanned 80 times in one minute. For three minutely averaged measurements, about 240 scans are co-added. When using a laser beam as light source, one would detect a typical cosine interference pattern as function of the optical path difference, which is called interferogram. By Fourier transformation and with known mirror position, the interferogram (i.e. intensity as function of path length difference) can be transformed to a spectrum (i.e. intensity as function of wavelength) (Griffith and de Haseth, 2007). In case of the laser source, this would result in one intensity peak at the laser wavelength. For a broadband infrared source many interference patterns of different wavelengths overlap and together form a characteristic source interferogram. The characteristic source interferogram can be transformed to the characteristic source spectrum by Fourier transformation. The covered wavelength range of the spectrum depends on the maximal path length difference. The interferometer in Heidelberg covers a range from about 0 to 7899 cm^{-1}. If there are absorbers in the optical path of the infrared beam, they absorb the infrared light at molecule specific wavelengths and therewith reduce the intensity spectrum at these wavelengths. The infrared spectrum of a sample therefore shows absorption lines at different wavelengths. The depth of the absorption lines is dependent on the concentration of the different greenhouse gases according to Beer-Lambert law:

$$T = \frac{I}{I_0} = e^{-\epsilon l c} \tag{A.1}$$

with

T= transmittance

I, I_0 = intensity [$W \cdot m^{-2}$] of transmitted and incident radiation

ϵ= molar absorptivity [$m^2 \cdot mol^{-1}$]

l= optical pathlength [m]
c= molar concentration [mol·l^{-1}]

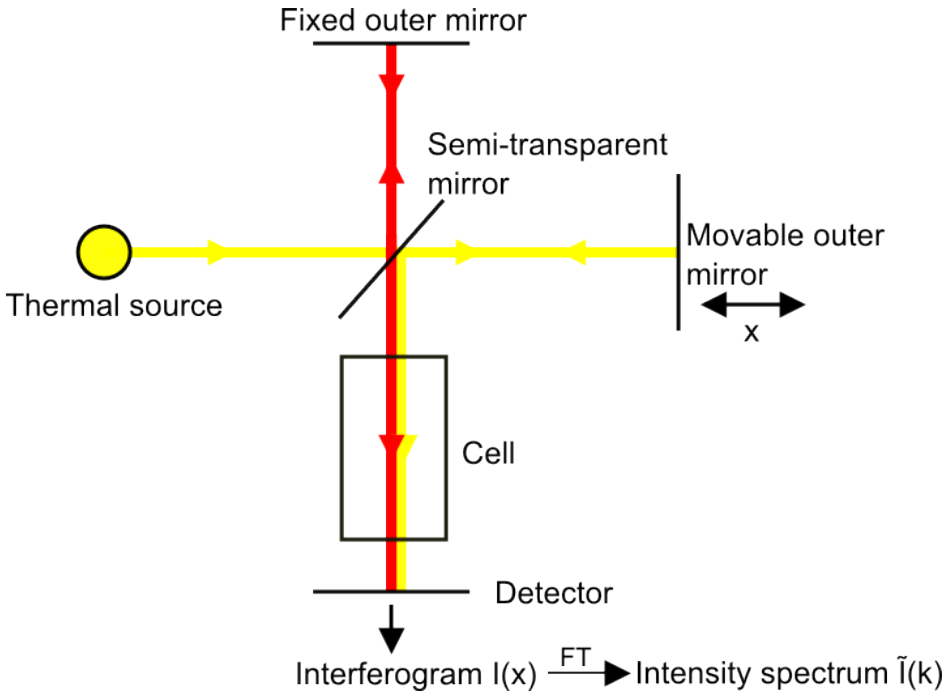

Fig. A.2: Sketch of the measurement principle of the FTIR. Picture is taken from Vardag (2012).

From spectra to concentration

The intensity spectrum (as function of wavelength) is measured with and without (evacuated cell) air sample in the optical cell. A transmittance spectrum is then calculated (see Fig. 1.6) as the relative difference of the two spectra, thereby canceling all deficits of light source and optical set-up. The intensity of the transmittance spectrum will be reduced at the wavelength at which absorption takes place. Infrared absorption processes include changes in rotational and vibrational states of the molecules. The specific wavelengths at which these transition states are excited are specific for each molecule. As the amount of absorption is dependent on the concentration of molecules, pressure and temperature following Beer-Lambert's law, the concentration can be derived by fitting a theoretical spectrum calculated by the Multiple Atmospheric Layer Transmission (MALT) model to the measured transmittance spectrum by a non-linear least square fitting algorithm to obtain the concentration (Griffith, 1996). The theoretical absorption coefficients are listed in the HIgh resolution TRANsmission molecular

absorption database (HITRAN) (Rothman et al., 1998). Since the different molecules (and isotopologues) absorb at different wavelengths (see Fig. 1.6), a simultaneous analysis of the different greenhouse gas concentrations is possible.

Correction and Calibration procedure

The retrieved concentration is still uncorrected and uncalibrated. However, corrections are necessary as absorption spectra of different species can overlap and as the absorption spectra in HITRAN are accurate only within 2 % (Griffith, 1996). Additionally, inaccuracies of measured parameters such as temperature or pressure distort the conversion from transmittance spectra to mole fraction. Tests with varying pressure, flow, temperature and CO_2 concentration, but same sample air composition were therefore performed to quantify these cross-sensitivities. These tests are described in Hammer et al. (2013a) and Vardag et al. (2015a) in more detail. The corrections are listed in Table A.1 and are routinely used to correct the data. The data is then calibrated with a linear regression of the three standard gases, which are measured weekly. The three standard gases are measured under the same conditions as the ambient air and corrected according to Table A.1, respectively. These corrected standard measurements together with the assigned reference values of the cylinders (assigned by the ICOS Calibration Laboratory, Jena) are then used to determine the linear instrument response function. The weekly determined instrument response functions are then linearly interpolated to obtain a instrument response function for all measurement times, which is then used to calibrate the actual measurements. The calibration scales are also listed in Table A.1.

A2 Performance indicators

Down-times of the instrument

Three reference gases spanning the ambient mole fraction range of every species are measured once a week. The cell is evacuated twice prior to each new sample in order to eliminate memory effects. Additionally, a weekly measured long-term target, a daily measured short-term target and a working standard for smoothed $\delta^{18}O$ correction (see Vardag et al., 2015a) are analyzed. One cylinder measurement uses about 25 liters of gas and takes about 35 minutes. This means that typically 8 hours a week are spent for

Table A.1: Cross sensitivity correction and calibration scales

Species	Pressure sensitivity [$mbar^{-1}$]	CO_2 sensitivity [ppm^{-1}]	Flow sensitivity [$slpm^{-1}$]	Temperature sensitivity [K^{-1}]	Calibration scale
CO_2 [ppm]	0.0085	–	-0.3383	0.06	WMO CO_2 X2007
$\delta^{13}C(CO_2)$ [‰]	0.00249	see Vardag et al. (2015a)	-0.9142	0.127	VPDB-CO_2
CO [ppb]	0.0083	0.01366	-1.0389	-0.12	WMO CO X2004
N_2O [ppb]	0.0067	0.0008	-0.2696	0.316	WMO N_2O X2006a
CH_4 [ppb]	0.0298	-0.00276	-2.1962	-0.159	WMO CH_4 X2004
$\delta^{18}O(CO_2)$ [‰]	-0.18694	see Vardag et al. (2015a)	-2.9217	4.256	VPDB-CO_2

calibration gas or target gas measurements. When switching from one suite of reference gases to the next, additional measurements of the new and old reference gases are necessary to guarantee a smooth transition. Therefore, effectively about 10 hours a week are used for these control samples, which is about 3 % of the measurement time. During the last four years the data set has been interrupted due to installation of new software (twice, in total about 2 weeks), instrumental improvements (2 weeks), exchanging broken laser (1 week), exchanging weakening MIR source (1 day), operator-related issues such as closed cylinders, two simultaneous opened ports or wrong temperature, pressure or flow (2 months). This is about 7 % of the total measurement time. Further interruptions in the Heidelberg record are due to measurement campaigns, which took place in Cabauw, OPE and Mace Head and in total covered a period of about 5 months. This is about 10 % of the total measurement time.

Intermediate measurement precision - Target tanks

Over the course of four years the intermediate measurement precision was monitored by measuring a so-called target cylinder on daily basis. As one expects the intermediate measurement precision to be the same for ambient air and cylinder measurements, this target cylinder quality control is used to estimate the precision of the ambient air

measurements and contributes to a comprehensive uncertainty budget for the instrument.

Fig. A.3 shows the results of the target measurements since 2011. The last 9 minutes of a 35-minutely measurement were averaged to obtain a single target value. When measuring a 50 L cylinder every day with the FTIR, the target cylinder lasts about one year. Therefore, more than one target cylinder are needed for tracking the intermediate measurement precision over the course of four years. In Fig. A.3, the deviation of the daily measured value to the averaged value of each cylinder gas is shown. Even though some small, but distinct structures remain (especially for CO and CO_2), no long-term drifts or worrying features are observed.

In Table A.2, the intermediate measurement precision is summarized over the course of four years and compared to the WMO recommendations for all trace gases. One can see that all trace gases, except $\delta^{13}C(CO_2)$ and $\delta^{18}O(CO_2)$ meet the WMO compatibility goals in terms of precision. Altogether, a good intermediate stability of the FTIR instrument can be confirmed.

Table A.2: Intermediate measurement precision (as determined from repeated daily target gas measurements) and WMO recommended compatibility targets of the different trace gases.

Species	Intermediate measurement precision	WMO ILC target GGMT (2013)	WMO extended compatibility goal GGMT (2013)
CO_2 [ppm]	0.06	0.1 (Northern hemisphere)	0.2
$\delta^{13}C(CO_2)$ [‰]	0.06	0.01	0.1
CO [ppb]	0.38	2	5
N_2O [ppb]	0.09	0.1	0.3
CH_4 [ppb]	0.27	2	5
$\delta^{18}O(CO_2)$ [‰]	0.35	0.05	0.1

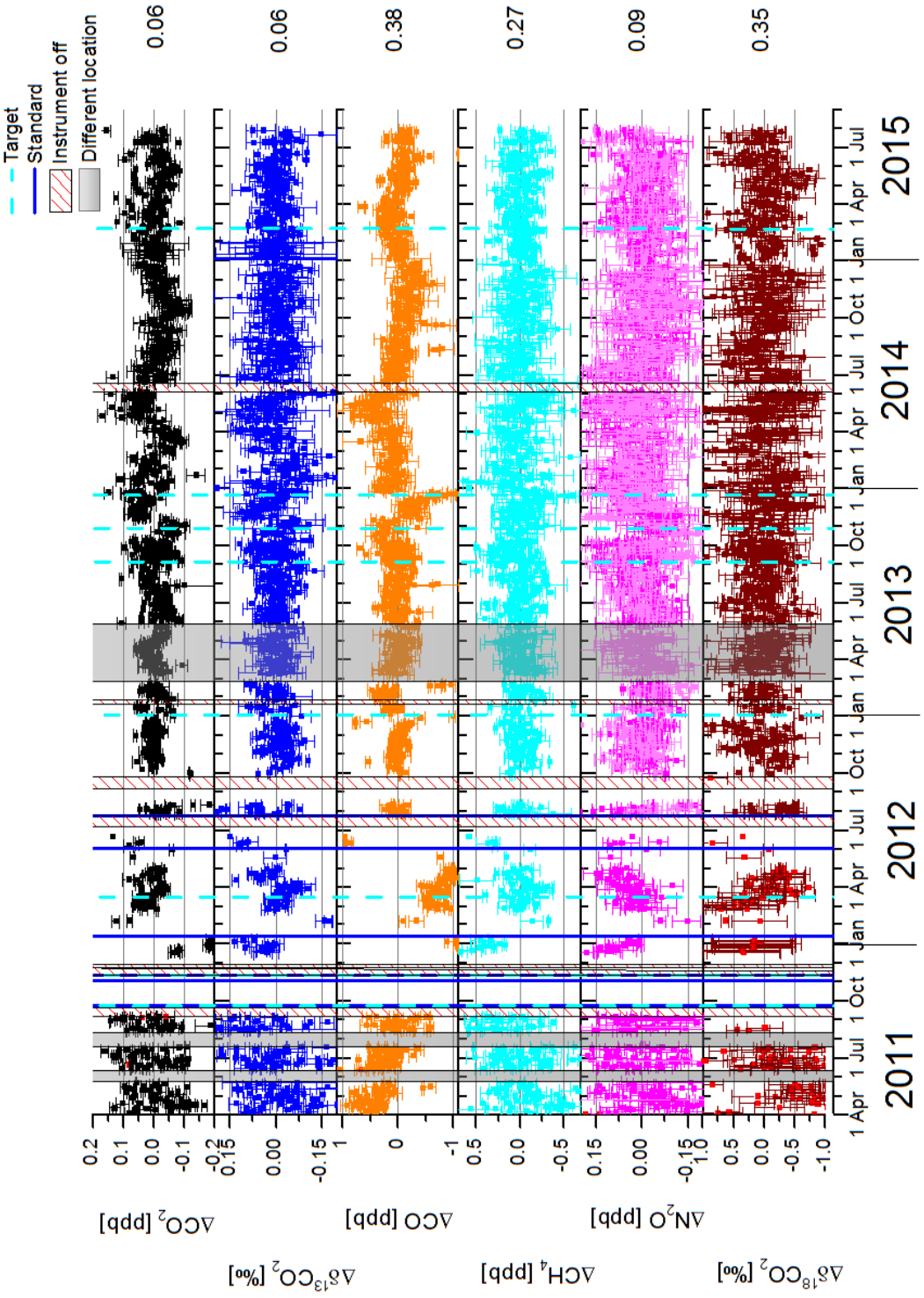

Fig. A.3: Repeated target measurements for the trace gases CO_2, $\delta^{13}C(CO_2)$, CO, N_2O, CH_4 and $\delta^{18}O(CO_2)$. The deviation between the daily measured value and the averaged value of the cylinder gas is plotted. The standard deviation of the difference is given on the right. Note, that $\delta^{18}O(CO_2)$ can only be usefully analyzed since July 2012, since $\delta^{18}O(CO_2)$ values of calibration gases were too close to each other for a good calibration. Before, they are therefore flagged and marked with red dots here.

Accuracy and compatibility

Vardag et al. (2015a) assessed the accuracy of the FTIR by replicate measurement of the laboratory primary cylinders on the FTIR. The laboratory primary cylinders are, at the same time, National Oceanic and Atmospheric Administration (NOAA) calibrated tertiary cylinders. They were directly calibrated and remeasured at the NOAA Institute, Boulder, Colorado for CO_2, CH_4 and N_2O, . Differences between the assigned reference values and the measured values provide a measure for the accuracy of the system for the specific species. For the isotopologues $\delta^{13}C(CO_2)$ as well as $\delta^{18}O(CO_2)$, a central calibration laboratory exists at the MPI Jena. The working standards were directly calibrated by the MPI Jena, but the NOAA calibration tertiary cylinders have not been calibrated for $\delta^{13}C(CO_2)$ and $\delta^{18}O(CO_2)$ yet and therefore the accuracy of the isotopologues cannot be assessed sufficiently well. Therefore, the assessment of compatibility is especially vital. Vardag et al. (2014) assessed and discussed the compatibility of CO_2, CH_4 and N_2O measurements of the FTIR to the Heidelberg GC and Vardag et al. (2015a) as well as the compatibility of $\delta^{13}C(CO_2)$ and $\delta^{18}O(CO_2)$ measurements of the FTIR to the Heidelberg IRMS. The results for accuracy and compatibility are summarized in Table A.3 and are discussed in more details in Vardag et al. (2014) and Vardag et al. (2015a).

Table A.3: Accuracy and compatibility of the FTIR as taken from Vardag et al. (2014) and Vardag et al. (2015a). The accuracy is given as difference of the FTIR measurement of tertiary cylinders to their assigned values by the WMO Central Calibration Laboratory (CCL). The compatibility is given as difference of the FTIR measurement to a reference instruments (GC or IRMS).

Species	Accuracy (FTIR − WMO CCL)	Compatibility (reference instrument − FTIR)
CO_2 [ppm]	-0.03 ± 0.04	0.04 ± 0.2
$\delta^{13}C(CO_2)$ [‰]	–	0.01 ± 0.02
N_2O [ppb]	0.00 ± 0.03	0.01 ± 0.12
CH_4 [ppb]	0.04 ± 0.01	-0.25 ± 2.2
$\delta^{18}O(CO_2)$ [‰]	–	0.08 ± 0.14

Note, that the accuracy and compatibility of CO has not been carefully assessed yet as it is in question that the CO cylinders are stable and as the GC is not stable in CO. The future plan is to also assess the CO accuracy and compatibility.

A3 Complete ambient air record

The ambient air measurements were evaluated in Heidelberg for the last four years. Figure A.4 shows the entire record for all trace gases. The CO_2 and $\delta^{13}C(CO_2)$ data is available at `http://www.iup.uni-heidelberg.de/institut/forschung/groups/kk/Data_html` and can be used. However, prior to publication, the data owners need to be contacted. One can see a distinct seasonal cycle in CO_2, $\delta^{13}C(CO_2)$, CO, CH_4 and $\delta^{18}O(CO_2)$. This originates partly from the seasonal variation of the planetary boundary layer height, which suppresses vertical mixing with the free troposphere and partly from the season dependent emission characteristics, e.g. fossil fuel CO_2 emissions are largest in winter and photosynthetic CO_2 uptake reaches its maximum in summer. The $\delta^{18}O$ record starts only in June 2012 as before June 2012 the calibration standards were too close to each other for a solid calibration. After that, $\delta^{18}O(CO_2)$ shows a repeating seasonal cycle.

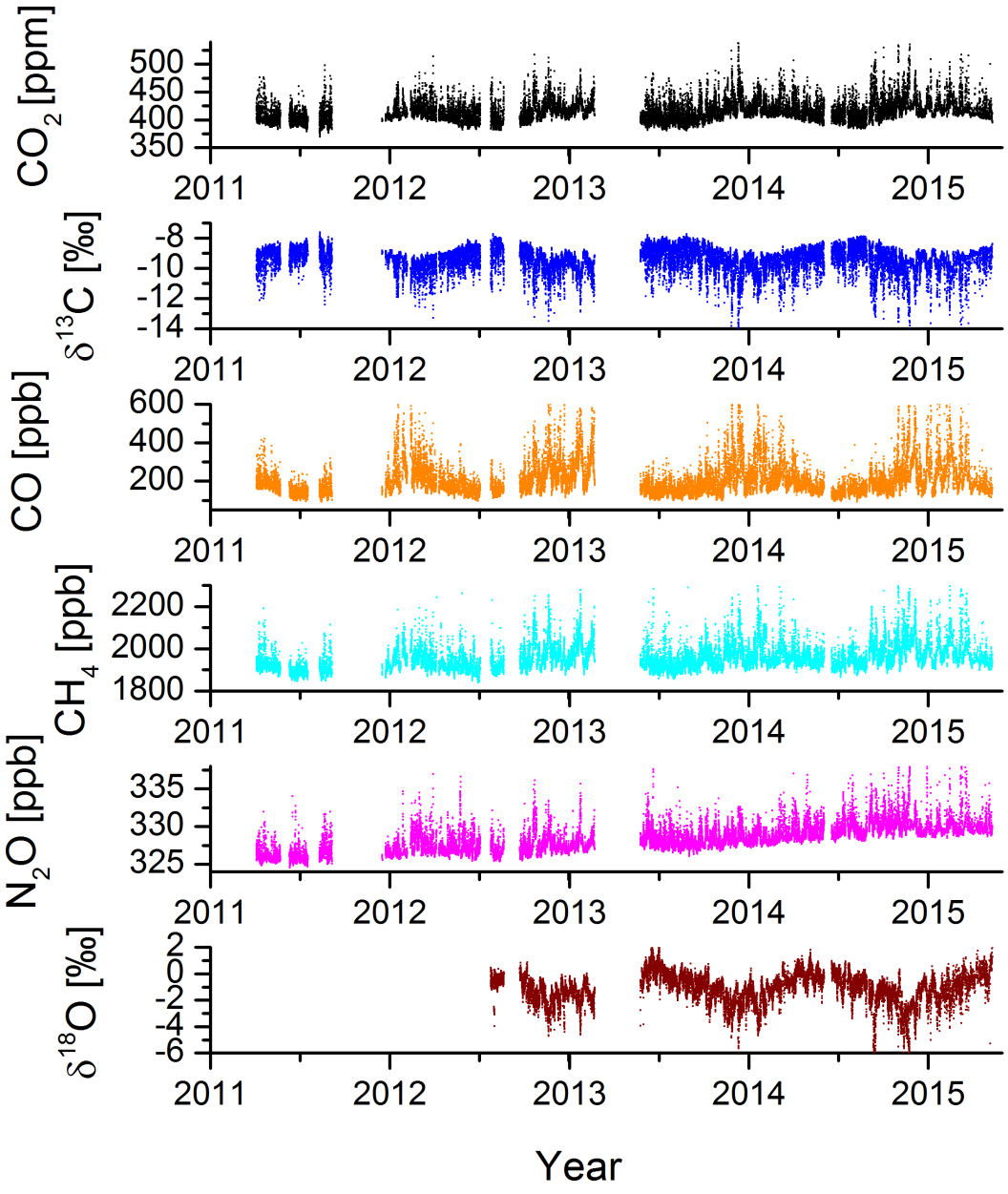

Fig. A.4: Ambient air record of the FTIR from 2011 to 2015. The $\delta^{18}O$ record starts only in June 2012 as before that calibration standards were too close to each other for a solid calibration.

B

Vocabulary of Metrology (VIM)

The metrological terms used in this work are defined uniquely by the Joint Committee for Guides in Metrology (JCGM) (Joint Committee for Guides in Metrology (JCGM-WG2) (2012)) and a full list can be found here: http://jcgm.bipm.org/vim/en/alphaindex.html. The definitions relevant for this work are listed here:

Accuracy - closeness of agreement between a measured quantity value and a true quantity value of a measurand
Bias - estimate of a systematic measurement error
Error - measured quantity value minus a reference quantity value
Intermediate precision - measurement precision under a set of intermediate precision conditions of measurement
Intermediate precision condition of measurement - condition of measurement, out of a set of conditions that includes the same measurement procedure, same location, and replicate measurements on the same or similar objects over an extended period of time, but may include other conditions involving changes
Metrological comparability - comparability of measurement results, for quantities of a given kind, that are metrologically traceable to the same reference
Metrological compatibility - property of a set of measurement results for a specified measurand, such that the absolute value of the difference of any pair of measured quantity values from two different measurement results is smaller than some chosen multiple of the standard measurement uncertainty of that difference
Precision - closeness of agreement between indications or measured quantity values obtained by replicate measurements on the same or similar objects under specified conditions

Repeatability - measurement precision under a set of repeatability conditions of measurement

Repeatability condition of measurement - condition of measurement, out of a set of conditions that includes the same measurement procedure, same operators, same measuring system, same operating conditions and same location, and replicate measurements on the same or similar objects over a short period of time

Reproducibility - measurement precision under reproducibility conditions of measurement

Reproducibility condition of measurement - condition of measurement, out of a set of conditions that includes different locations, operators, measuring systems, and replicate measurements on the same or similar objects

Systematic measurement error- component of measurement error that in replicate measurements remains constant or varies in a predictable manner

Uncertainty - non-negative parameter characterizing the dispersion of the quantity values being attributed to a measurand, based on the information used

Giving of thanks

First and foremost, I am deeply grateful to Ingeborg Levin for giving me the opportunity to work in an exciting research area, which lies close to my heart. In our many discussions I have learned so much about environmental physics and scientific work, which I will hopefully always remember. I am thankful that I was given the confidence to freely study and work on my own, but guidance whenever I needed it.

I want to thank Werner Aeschbach for accepting the review of my dissertation in his sabbatical year.

It was a pleasure to work in the supportive environment of the carbon cycle group. I especially want to thank Michael Sabasch for helping me many times in the lab and for his daily portion of positivity. Thanks also to Martina Schmidt who motivated and supported me to continue my way in science. And thanks to Samuel Hammer for good ideas when I needed them.

I am grateful to Christoph Gerbig, Ute Karstens and Thomas Koch, who supported me with the STILT model. Further, I am thankful for various discussion with David Griffith and for his technical support with the FTIR.

My dear friends Patrick Blaser, Stefan Schmitt and Felix Vogel, thanks for proofreading parts of my dissertation! I also appreciate the many fun adventures and lively conversations on science and non-science.

Finally, I want to thank my family for their support and belief in me. Marian, Shirin, Mama and Papa, I am the luckiest girl in the world because you are my family.